Investigation into mitochondrial DNA, mitochondrial function and nerve activity in oxaliplatin-induced peripheral neuropathy

Trecarichi, Annalisa

Awarding institution:
King's College London

Investigation into mitochondrial DNA, mitochondrial function and nerve activity in oxaliplatin-induced peripheral neuropathy

Thesis submitted to King's College London for the degree of

Doctor of Philosophy in Neuroscience

Annalisa Trecarichi

Wolfson Centre for Age-Related Diseases

Institute of Psychiatry, Psychology & Neuroscience

King's College London

2017 – 2020

Abstract

Chemotherapy-induced peripheral neuropathy (CIPN) is the major dose-limiting side effect of several first-line chemotherapeutic agents, including oxaliplatin. Symptoms can be very detrimental to the patients' quality of life. They can occur at any time during and after treatment and can endure for months or years after treatment cessation. No treatment is currently available to prevent or reverse CIPN and there is no tool to identify those at risk. Moreover, the causal mechanisms of CIPN are still under investigation. This thesis aimed to explore the feasibility of a blood biomarker for oxaliplatin-induced peripheral neuropathy (OIPN) and to get a deeper understanding of the mechanisms involved in its development and maintenance.

Mitochondrial DNA (MtDNA) content in blood and other bodily fluid has already been used as biomarker for several diseases. Here, we recruited > 50 colorectal cancer patients undergoing an oxaliplatin treatment. Blood was collected prior to, during and after treatment completion, and MtDNA content in whole blood was measured using real-time quantitative PCR. We found that MtDNA content varied among patients and time points. By comparing MtDNA content in patients who developed OIPN to that of patients who did not, we will understand whether MtDNA is a feasible predictive biomarker for OIPN.

A rat model of OIPN was generated by the systemic (intraperitoneal) administration of 2 mg/kg clinically formulated oxaliplatin on four alternate days. The model displayed a persistent mechanical hypersensitivity, but other symptoms observed in the clinic, including cold allodynia, numbness and spontaneous pain, could not be replicated. Studies focused on two key time points: day 7, 24 hours after treatment cessation, when animals did not display symptoms of pain-like behaviour, and peak pain, when the nociceptive behaviour reached its maximal severity. The electric properties of the saphenous nerve were evaluated in terms of compound action potentials (CAPs) of A- and C-fibres. In oxaliplatin-treated animals, CAPs were altered at day 7, but not at peak pain. Mitochondrial dysfunction is a key factor in the development and the maintenance of OIPN. Systemic exposure to oxaliplatin did not affect parameters of mitochondrial respiration or glycolytic function in DRG neurons at day 7. Similarly, *in vitro* exposure to oxaliplatin for an hour did not affect the bioenergetic status of DRG neurons. The expression levels of mitochondrial Ca^{2+} channels were evaluated in the DRG, sciatic and saphenous nerves. In particular, the expression of the $Na^{+}/Ca^{2+}/Li^{+}$ exchanger (NCLX) and of the mitochondrial calcium uniporter (MCU) was altered after oxaliplatin administration, thus potentially affecting mitochondrial functionality. These studies provided a further insight on mitochondrial dysfunction and altered nerve conduction in the pathophysiology of OIPN.

Table of contents

Table of figures

Table of tables

Acknowledgements

Firstly, I would like to thank my supervisors: thanks to Sarah Flatters for giving me the opportunity to work on this project for the past three years. Thanks to Stuart Bevan for sharing his expertise and offering his assistance. I am very thankful to Nicola Hamilton-Whitaker for the constant support and the words of encouragement she offered in times of need. I am thankful to the MRC Doctoral Training Partnership Programme for allowing me to do a PhD in the first place, and to the Guy's and St Thomas' Charity for funding my project.

I am most grateful to Natalie Duggett for introducing me to the lab and sharing her infinite knowledge and wisdom with me. She has been the kindest and most patient mentor in all aspects of science and life. Thanks to Larissa de Clauser for being my bench buddy in the last months of my PhD and for helping with the initial set-up of qPCR experiments. I am very thankful to Martyn Jones and Thomas Sears for sharing their knowledge of electrophysiology with me. I am grateful to the BSU staff for taking care of animals. Special thanks go to Claire Pearce and Garry Fulcher for always listening to my rants and for giving me my very first birthday trifle. I am thankful to the pharmacy staff in the Chemotherapy Village at Guy's Cancer Centre for providing oxaliplatin.

I am deeply grateful to all the friends I made during this PhD. To Christina, I cannot imagine what the past three years would have been without you. You brought an unexpected, chaotic energy into my life and challenged my quietness with your fierceness and liveliness. I am grateful to call you a dear friend. To Yaz, your unwavering support, your hugs and your (irritatingly) good mood in the morning turned you into the little brother I never had. To Elisa, thank you for all the advice you offered and for the long chats about life, Italy and (mostly) food. To Joana, Naomi, Nur, Tilly, Nisha and Vin, thank you for all the lunches and the laughs we shared and for the help inside and outside of the lab. And to Valeria, we have been in this together since the very beginning and being your flatmate for the past four years has gifted me with some of my most treasured memories. I will miss the little family we have created here in London.

I am thankful to my friends back home, who have cheered me on from afar for the past three years. Thank you to my family for their never-ending encouragement. Mum and dad, thank you for always believing in me and for helping me to achieve my dreams. Lastly, Davide, you have been by my side through thick and thin for the past eleven years. I would not be where I am today without your love and your support and my biggest thanks go to you, always.

Publications and abstracts

Trecarichi A, Duggett NA, Granat L, Lo S, Malik AN, Zuliani-Álvarez L and Flatters SJL (2020). Preclinical evidence for mitochondrial DNA as a potential blood biomarker for chemotherapy-induced peripheral neuropathy. *Mitochondrion.* Under review.

Trecarichi A and Flatters SJL (2019). Mitochondrial dysfunction in the pathogenesis of chemotherapy-induced peripheral neuropathy. *Int Rev Neurobiol.* 145: 83-126.

Trecarichi A, Duggett NA, Zuliani-Alvarez L, Granat L and Flatters SJL (2019) Mitochondrial DNA and activity in whole blood during the timecourse of chemotherapy-induced peripheral neuropathy. *Presented at the International Association for the Study of Pain – 7th International Congress on Neuropathic Pain, London, UK.*

Abbreviations

$[Ca^{2+}]_i$	Intracellular calcium concentration
$[Ca^{2+}]_m$	Mitochondrial calcium concentration
3-NP	3-Acetylphenyl N-(P-Tolyl) carbamate
5-FU	5-fluorouracil
5-HD	5-hydroxydecanoate
5-HT	Serotonin
ABC	Adenosine triphosphate-binding cassette
A-CAP	A-fibres compound action potential
Actb	β-actin
ADP	Adenosine diphosphate
ALC	Acetyl-L-carnitine
ANCOVA	Analysis of covariance
ANOVA	Analysis of variance
APS	Ammonium persulfate
AraC	Cytosine arabinoside
ASCO	American society of clinical oncology
ASIC	Acid-sensing ion channel
ATP	Adenosine triphosphate
AU	Arbitrary units
AUC	Area under the curve
BAPTA	1,2-bis(o-aminophenoxy)ethane-N,N,N′,N′-tetraacetic acid
BCA	Bicinchoninic acid
BL	Baseline
BPI	Brief pain inventory
BSA	Bovine serum albumin
Calb1	Calbindin 1
CAP	Compound action potential
C-CAP	C-fibres compound action potential
CGRP	Calcitonin gene-related peptide
CI-V	Complex I-V
CIPN	Chemotherapy-induced peripheral neuropathy
C_{max}	Peak plasma concentration
CNS	Central nervous system
CoA	Coenzyme-A
CRC	Colorectal cancer
CS	Citrate synthase

Ct	Cycle threshold
Ctrl	Control
CuZnSOD	Copper-zinc superoxide dismutase
CV	Conduction velocity
CypD	Cyclophilin D
Cyt c	Cytochrome c
DACH	Diaminocyclohexane
DAPI	4',6-diamidino-2-phenylindole
dH_2O	Distilled water
DMSO	Dimethyl sulfoxide
DNA	Deoxyribonucleic acid
dNTP	Deoxyribonucleotide triphosphate
DPD	Dihydropyrimidine dehydrogenase
DPYD	Dihydropyrimidine dehydrogenase (gene)
DRG	Dorsal root ganglia
Drp1	Dynamin-related protein 1
DTT	1,4-dithiothreitol
EB	Elution buffer
ECAR	Extracellular acidification rate
ECOG	Eastern cooperative oncology group
EDTA	Ethylenediaminetetraacetic acid
EMRE	Essential mitochondrial calcium uniporter regulator
EORT QLQ-CIPN20	European organisation for research and treatment of cancer quality of life questionnaire–chemotherapy-induced peripheral neuropathy
EORTC QLQ-C30	European organisation for research and treatment of cancer quality of life questionnaire
ETC	Electron transport chain
FA	Folinic acid
Fact/GOG-Ntx	Functional assessment of cancer therapy/gynecologic oncology group–neurotoxicity
$FAD(H_2)$	Flavin adenine dinucleotide
FBS	Foetal bovine serum
FCCP	Carbonyl cyanide-4 (trifluoromethoxy) phenylhydrazone
FDA	Food and drug administration
FOLFOX	Oxaliplatin + 5-fluorouracil + leucovorin
FOLFOXIRI	Oxaliplatin + irinotecan + 5-fluorouracil + leucovorin
GABA	Gamma-aminobutyric acid
GDNF	Glial cell-derived neurotrophic factor

GFRα-1	GDNF family receptor alpha 1
GPx	Glutathione peroxidase
GSH	Glutathione
GWA	Genome-wide association
H_2O_2	Hydrogen peroxide
hB2M	Human β2-microglobulin
HDAC6	Histone deacetylase 6
HIV	Human immunodeficiency virus
hMito	Human mitochondrial fragment
IASP	International association for the study of pain
IB4	Isolectin B4
ICD	International Classification of Diseases
IENF	Intraepidermal nerve fibre
IM	Inner membrane
IP	Intraperitoneal
IV	Intravenous
K2P	Two-pore domain potassium channel
K_v	Voltage-gated potassium channel
LC	Locus coeruleus
LEMT1	Leucine zipper and EF-hand containing transmembrane protein 1
LV	Leucovorin
M1R	Muscarinic acetylcholine type 1 receptor
MeCbl	Methylcobalamin
MCU	Mitochondrial calcium uniporter
MCUb	Mitochondrial calcium uniporter dominant negative beta
MCUR1	Mitochondrial calcium uniporter regulator 1
MEM	Minimum essential media
MICU	Mitochondrial calcium uptake protein
MnSOD	Manganese-dependent superoxide dismutase
MPQ	McGill pain questionnaire
mPTP	Mitochondrial permeability transition pore
Mrgprd	Mas-related G-protein-coupled receptor D
mRNA	Messenger RNA
MtDNA	Mitochondrial DNA
N/A	Not available
NA	Noradrenaline
NADH	Nicotinamide adenine dinucleotide
NADPH	Nicotinamide adenine dinucleotide phosphate

NAMPT	Nicotinamide phosphoribosyltransferase
Na_v	Voltage-gated sodium channel
NCI-CTC	National cancer institute – common toxicity criteria
NCLX	$Na^+/Ca^{2+}/Li^+$ exchanger
NCS	Nerve conduction studies
NCX	Na^+/Ca^{2+} exchanger
nDNA	Nuclear DNA
NeuN	Neuronal nuclei antibody
NGF	Nerve growth factor
NMDA	N-methyl-D-aspartate
NO	Nitric oxide
NOS	Nitric oxidase synthase
NP	Neuropathic pain
Ntrk1,2,3	Neurotrophic receptor tyrosine kinase 1,2,3
$O_2^{\bullet-}$	Superoxide
OCR	Oxygen consumption rate
OIPN	Oxaliplatin-induced peripheral neuropathy
OM	Outer membrane
OXPHOS	Oxidative phosphorylation
P/S	Penicillin/streptomycin
PAG	Periaqueductal grey
PBN	Phenyl N-tert-butylnitrone
PBS	Phosphate buffered saline
PCR	Polymerase chain reaction
PFA	Paraformaldehyde
PFT-μ	Pifithrin-mu
Pi	Inorganic phosphate
Piezo2	Piezo-Type Mechanosensitive Ion Channel Component 2
PNQ	Patient neurotoxicity questionnaire
PNS	Peripheral nervous system
PPAR-γ	Peroxisome proliferator-activated receptor gamma
Pt	Platinum
PVDF	Polyvinylidene difluoride
Q	Coenzyme Q
qPCR	Quantitative polymerase chain reaction
QST	Quantitative sensory testing
Redox	Reduction–oxidation
Ret	RET receptor tyrosine kinase

RIPA	Radioimmunoprecipitation assay
RM	Repeated measures
RNA	Ribonucleic acid
RNS	Reactive nitrogen species
ROS	Reactive oxygen species
Rpm	Revolutions per minute
rRNA	Ribosomal RNA
RVM	Rostroventromedial medulla
SD	Standard deviation
SDS	Sodium dodecyl sulphate
SDS-PAGE	SDS polyacrylamide gel electrophoresis
SEM	Standard error of the mean
SH	Seahorse
SLC	Solute carrier
SNP	Single nucleotide polymorphism
SOD	Superoxide dismutase
TBS	Tris buffered saline
TEMED	N,N,N',N'-Tetramethylethylenediamine
TEMPOL	4-Hydroxy-2,2,6,6-tetramethylpiperidine-1-oxyl
TENS	Transcutaneous electrical nerve stimulation
TNS	Total neuropathy score
TrkA	Tropomyosin receptor kinase A
tRNA	Transfer RNA
TRP	Transient receptor potential channel
TRPA	Transient receptor potential ankyrin channel
TRPM	Transient receptor potential melastatin channel
TRPV	Transient receptor potential vanilloid channel
TrxR	Thioredoxin reductase
VDAC	Voltage-dependent anion-selective channel protein
Vglut3	Vesicular glutamate transporter 3
V_m	Resting membrane potential
WCIC	Wohl cellular imaging centre
WHO	World health organisation
Ywhaz	Tyrosine 3-Monooxygenase/Tryptophan 5-Monooxygenase Activation Protein Zeta
β-tb	Beta-tubulin
$\Delta\psi_m$	Mitochondrial membrane potential
σ1R	Sigma-1 receptor

Chapter 1 General introduction

1.1 Somatosensory pathways and nociception

1.1.1 Neuron and nerve structure

All neurons share a typical structural organisation, although their actual morphology varies among different neuronal cells based on their function. The cell body (or soma) contains the nucleus and most of the organelles. Most neurons contain dendrites, processes that branch out of the cell body to form synapses with neighbouring neurons and receive information in the form of neurotransmitters. Lastly, an axon (or fibre) extends from the cell body, from a region named the axon hillock, and conducts nerve impulses towards the axon terminals, which synapse on target cells. Axons can be myelinated or unmyelinated. Myelinated axons are surrounded by a lipid-rich myelin sheath generated by supporting glial cells (oligodendrocytes in the central nervous system (CNS) and Schwann cells in the peripheral nervous system (PNS)). Unmyelinated axons from different neurons are surrounded by a non-myelinating Schwann cell in structures known as Remak bundles. Nerves can be described as bundles of axons; their structural organisation is illustrated in Figure 1-1.

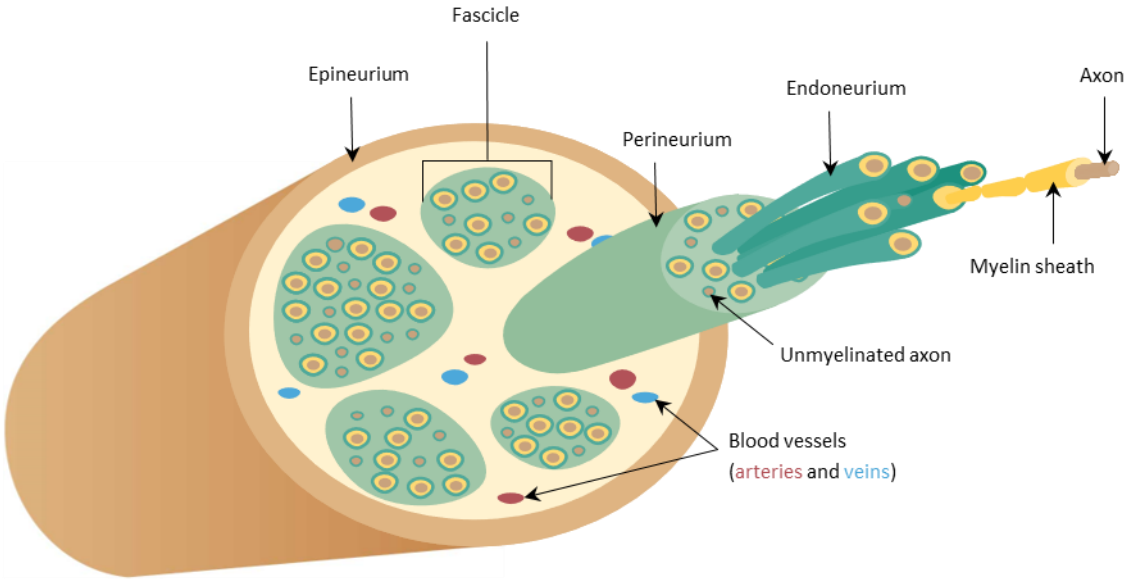

Figure 1-1 Schematic representation of the nerve structural organisation

Each axon is surrounded by the endoneurium, a layer of fibrous connective tissue. Multiple axons are bundled together in fascicles, which are wrapped by concentric layers of fibroblasts and connective tissue (perineurium). Lastly, fascicles are enclosed within the epineurium, the outermost connective layer of the nerve. The nerve functionality is supported by blood vessels that are encapsulated within the epineurium as well.

Based on their morphology, neurons can be classified into: pseudo-unipolar cells (only sensory neurons), which have one axon that splits in two, where one branch reaches the periphery to receive information and the other synapses into the spinal cord; bipolar cells, which possess one axon and one dendrite and are only found in the olfactory epithelium and the retina; and multipolar cells (all other neurons), which have one axon and numerous dendrites. Alternatively, neurons can be classified by function:

- Sensory (or afferent) neurons are activated by various stimuli at the periphery and relay sensory information back to the CNS. Sensory neurons will be discussed further in section 1.1.3.
- Motor (or efferent) neurons control voluntary and involuntary movements. Their cell bodies are located in the CNS, either in the cerebral cortex (upper motor neurons) or in the brainstem and spinal cord (lower motor neurons). Upper motor neurons synapse with lower motor ones, which in turn innervate muscles and organs.
- Interneurons are only located in the CNS, where they transmit information from one neuron to the other.

1.1.2 Action potential

The propagation of nervous signals occurs through electrical impulses, or action potentials. Hodgkin and Huxley recorded the first ever action potential from the squid giant axon in 1939 (Hodgkin and Huxley 1939). In 1952, they published their mathematical model of the action potential, which was the first quantitative description of nerve cell excitability (Hodgkin and Huxley 1952), gaining them the Nobel prize in 1963. Their model provided the basis for electrophysiology investigations and paved the way for many more experiments that allowed to understand how nerve impulses are generated and transmitted.

The driving force behind action potential generation and propagation is the electrochemical gradient between the intra and extracellular environment: ions are unequally distributed on the two sides of the membrane and their flow across it is what generates the electrical signalling. The two main ions involved in action potentials are Na^+ and K^+. Na^+ concentration is approximately 10 times higher in the extracellular compartment, whereas K^+ concentration is approximately 10 times higher on the intracellular side. When nerves are at rest, the intracellular side of the membrane is more negative than the outside. Therefore, under physiological conditions, neurons possess a negative resting membrane potential (V_m) ranging between -40 and -90 mV. V_m is maintained by a fine control over the ion flow across the membrane. The membrane is highly permeable to K^+ ions. They can move across the membrane

through ‘leak’ channels (K2P, a family of 2-pore domain channels) and flow towards the outside compartment. By contrast, some Na^+ ions can move inside, but membrane permeability to Na^+ ions is much lower compared with that of K^+. For this reason, V_m is closer to the equilibrium potential of K^+ of ~ -90 mV than to that of Na^+ (~ +60 mV) [reviewed in (Chrysafides et al. 2020)]. The Na^+/K^+ ATPase constantly restores the V_m by moving Na^+ and K^+ against their concentration gradients: it actively pumps 3 Na^+ ions outside the cells and simultaneously moves 2 K^+ ions back inside for each adenosine triphosphate (ATP) molecule consumed [reviewed in (Pivovarov et al. 2018)]. Several stimuli, such as the activation of ligand-gated channels by the binding of a neurotransmitter in the synaptic cleft or the activation of sensory receptors in the periphery, can lead to changes in V_m, which in turn trigger an action potential. Pivotal to this event are voltage-gated Na^+ (Na_v) and K^+ (K_v) ion channels, which open and close in response to voltage changes across the membrane. Several isoforms of Na_v and K_v have been identified: the Na_v family comprises 9 isoforms [reviewed in (Bennett et al. 2019a)], whereas the K_v family comprises 40 channels, further classified in 12 sub-families [reviewed in (Ranjan et al. 2019)]. A low-intensity depolarising stimulus (subthreshold) causes the aperture of few Na_v channels and the influx of Na^+ ions within the cell. The response to these stimulations is graded, as the change in V_m is proportional to the intensity of the stimulus. Once the stimulus intensity exceeds a threshold value of approximately -50 mV (suprathreshold stimulus), the membrane undergoes a rapid depolarising phase. Depolarisation is driven by a positive feedback loop known as the ‘Hodgkin cycle’: the influx of Na^+ inside the cells activates even more Na_v channels to open, thus depolarising the membrane further. During this depolarising phase, the V_m becomes positive and approaches the equilibrium potential for Na^+ (~ +60 mV) but never reaches it, peaking at approximately +40-50 mV [reviewed in (Raghavan et al. 2019)]. Once the action potential reaches its peak, Na_v channels are inactivated and K_v channels are activated, thus allowing the membrane to become repolarised through an efflux of K^+. K^+ efflux causes a rapid drop in V_m, which returns to negative values. As K^+ reaches its potential equilibrium around -90 mV and K_v channel are slightly delayed in their closing, the V_m drops to lower voltages for a few milliseconds (hyperpolarisation phase), until K_v channels close again and the V_m returns to its baseline values [reviewed in (Raghavan et al. 2019)]. As soon as the action potential is initiated, and briefly after the repolarisation phase starts, Na_v channels are inactivated and the neuron cannot generate a second action potential, regardless of the intensity of the stimulus received. This is known as the absolute refractory phase. A relative refractory period follows, when some Na_v channels can be activated again, provided that the cell is exposed to a stimulus of strong intensity (> initial suprathreshold stimulus) (Hodgkin and Huxley 1952). Unlike the graded responses triggered by subthreshold stimulations, action potentials are an all-or-none type of response, which means

that once the stimulus is suprathreshold, the amplitude of the response is independent from the strength of the stimulus itself and remains constant in its amplitude and duration. However, it is worth mentioning that the shape of the action potential varies among different neuronal types (Bean 2007). Once the action potential reaches the axon terminal (pre-synaptic terminal), voltage-gated Ca^{2+} channels open and lead to an influx of Ca^{2+} into the cell. The increase in Ca^{2+} in the cytoplasm promotes the release of neurotransmitter vesicles into the synaptic area, and the subsequent binding of neurotransmitters onto post-synaptic neurons (Katz and Miledi 1967).

The velocity at which action potentials are conducted along the axon (conduction velocity) is directly proportional to the axon diameter. Therefore, myelinated axons conduct at faster velocities than unmyelinated ones, in what is known as saltatory conduction (Tasaki 1939, Huxley and Stämpfli 1949). The myelin sheath is not a contiguous layer, but rather presents small (1 µm) gaps for the entire axonal length, called nodes or Ranvier, which are rich in Na_v channels (Caldwell et al. 2000). The myelin sheath acts an insulator and prevents current leakage across the membrane, so that the action potential can travel along it until it reaches a node of Ranvier, where another action potential is generated.

1.1.3 Sensory neurons

The somatosensory system is responsible for the perception of various information from the external and internal environment, such as touch, vibration, pressure, temperature, movement and position. Sensory neurons are pseudo-unipolar and their cell bodies cluster together in structures known as ganglia, which are visible as swellings of the nerves. Two types of ganglia can be distinguished in the somatosensory pathways: cell bodies of neurons in the spinal nerves cluster together in the dorsal root ganglia (DRG), which are located alongside the spinal cord. Likewise, cell bodies of the trigeminal nerve, which innervates the face, cluster together in the trigeminal ganglia. In humans, there is a total of 31 pairs of spinal nerves, which innervate the entire body except for the face. They can be further distinguished as 8 cervical (C1-8), 12 thoracic (T1-12), 5 lumbar (L1-5), 5 sacral (S1-5) and 1 coccygeal nerve pairs. Mammalian species share a similar organisation of the spinal cord, with some differences in the number of segments; for instance, rats possess a sixth lumbar nerve (Rigaud et al. 2008).

Different subtypes of sensory neurons are responsible for the detection of different stimuli:

- Low-threshold mechanoreceptors are located both in the hairy and glabrous skin, where they detect mechanical stimuli, thus being responsible for the perception of touch, pressure and vibration. They comprise complex structures of specialised epithelial cells, connective tissue and/or Schwann cells, which encapsulate a single large myelinated nerve fibre. They

can be classified as rapidly adapting, which adapt quickly to changing stimuli but whose activity decreases if the stimulus remains constant (i.e. they detect movement and vibration), and slowly adapting, which respond continuously to a persistent stimulus and can therefore detect static stimulations (i.e. pressure and stretch). Meissner's corpuscles, located just below the epidermis, are rapidly adapting and possess a small receptive field, hence they detect low-frequency vibrations. Pacinian corpuscles, also rapidly adapting, reside deep in the dermis, are characterised by a large receptive field, and detect high-frequency vibrations. Ruffini's endings in the dermis are slowly adapting, with a large receptive field, and detect skin stretch and touch-pressure. Lastly, Merkel's disks, located in the upper layer of the dermis, represent the only unencapsulated complexes, formed by Merkel's cells associated with a nerve ending. They are slowly adapting and have a small receptive field, which allows them to detect light touch [reviewed in (Goodwin and Wheat 2020, Iheanacho and Vellipuram 2020)]. Additionally, free nerve endings from small myelinated and unmyelinated fibres, known as intraepidermal nerve fibres (IENFs), extend into the epidermis and contribute to the detection of tactile stimuli.

- Thermoreceptors have been identified as non-specialised free nerve endings that are able to detect changes in temperature. They can be differentiated into cold thermoreceptors, which possess small myelinated axons, and warm thermoreceptors, with unmyelinated axons.
- Proprioceptors innervate muscles, joints and tendons and are involved in the perception of body position and movement.
- Nociceptors are high-threshold non-specialised free nerve endings that are "*capable of transducing and encoding noxious stimuli"* ("IASP Terminology" 2011) (i.e. stimuli that are damaging, or have the potential to be, to tissues.

These different types of sensory neurons express a variety of ion channels that are specifically activated by innocuous or noxious mechanical, thermal and/or chemical inputs, and are therefore responsible for the transduction (i.e. conversion of sensory stimulation into an action potential) of these sensations. Activation of these channels results in an inward cationic current leading to depolarisation, which facilitates the generation of an action potential. Transient receptor potential channels (TRP) are a family of non-selective cation-permeable channels that are highly permeable to Ca^{2+} and, to a lesser extent, to Na^{+}. The TRP family comprises six members; of these, TRP vanilloid receptors (TRPV), TRP melastatin (TRPM) and TRP ankyrin (TRPA) have been associated with nociceptive signalling [reviewed in (Aromolaran and Goldstein 2017)]. Many of these channels are thermo-sensitive. In particular, TRPV1 is activate by noxious

temperatures (approximately > 43°C), while TRPV2 is activated at even higher temperatures (approximately > 52°C). TRPV3 and TRPV4 are activated by innocuous warm stimuli between 25 and 35°C. TRPM8 is activated by innocuous cool temperatures (< 25°C). Lastly, TRPA1 is activated by noxious cold (< 15°C). In addition, TRP channels can be activated by natural and synthetic ligands, like capsaicin (TRPV1), menthol (TRPM8) and mustard oil (TRPA1), and appear to be involved in mechanotransduction as well [reviewed in (Basbaum et al. 2009, Gomis 2015)]. Acid-sensing ion channels (ASICs) are proton-gated Na^+ channels, thus being activated by extracellular acidification, and may also participate in mechanotransduction [reviewed in (Basbaum et al. 2009)]. Transducers for mechanical stimuli have not been completely identified. Piezo-type mechanosensitive ion channel component 2 (Piezo2), a mechanically-gated non-selective cation-permeable channel, has been suggested as the major transducer of light touch [reviewed in (Geng et al. 2017)].

1.1.4 Sensory fibres classification

Nerve fibres responsible for somatosensory signalling are typically classified based on their myelination status, and therefore conduction velocity, and type of sensation they detect, as summarised in Table 1-1 (Parker et al. 2018). Aα- and Aβ-fibres are thickly myelinated and possess very fast conduction velocities (40-120 m/s). Aα-fibres are involved in proprioception, while Aβ-fibres detect low-threshold (non-noxious) mechanical stimuli (i.e. light touch and vibration). Nociceptive transduction relies on Aδ- and C-fibres. Aδ-fibres are wrapped in a thin layer of myelin and therefore their conduction velocity is reduced compared with other A-fibres (5-15 m/s). Lastly, C-fibres are the predominant fibre type, comprising up to ~ 50% of all the fibres (Baraniuk 2012). They are unmyelinated and conduct at the slowest velocity in the somatosensory system (0.2-2.0 m/s). C-fibres detect a variety of noxious stimuli, including hot and cold temperatures, mechanical stimuli, chemical agents and pruritogens. Most fibres are polymodal and can respond to both thermal and mechanical stimuli, some can detect only one of those sensations and a small proportion of them respond to pruritogens and mediate itch sensations (Benarroch 2015). Additionally, a small subset of low-threshold C-fibres is involved in the detection of innocuous tactile stimuli (Vallbo et al. 1999) and have been associated with the perception of weak, pleasant touch (Olausson et al. 2008). Nociceptive C-fibres have historically been divided in two categories: peptidergic C-fibres synthesise neuropeptides such as substance P and calcitonin gene-related peptide (CGRP) and respond to nerve growth factor (NGF) through tropomyosin receptor kinase A (TrkA). By contrast, non-peptidergic neurons do not contain neuropeptides and bind the isolectin B4 (IB4), express the ATP-gated ion channel $P2X_3$ and respond to glial cell-derived neurotrophic factor (GDNF) through the GDNF family receptor alpha 1 (GFRα-1) [reviewed in (Hunt and Mantyh 2001)]. Non-peptidergic fibres innervate the stratum

granulosum of the epidermis, whereas peptidergic fibres terminate in a deeper epidermal layer (stratum spinosum) (Zylka et al. 2005). These differences suggest that peptidergic and non-peptidergic neurons may have different functions in the somatosensory pathways. Given the different conduction velocities of Aδ- and C-fibres, they are responsible for two different pain sensations: initial pain is conducted by Aδ-fibres and is sensed as a brief, well-localised and sharp pain, whereas delayed pain is conducted by the slower C-fibres and is sensed as a long-lasting, less localised, dull and burning sensation.

Table 1-1 Classification of sensory fibres according to myelination status, axon diameter, conduction velocity and sensory information

Fibre type	Myelination status	Fibre diameter	Conduction velocity	Sensation
Aα	Thickly myelinated	13-22 µm	70-120 m/s	Proprioception
Aβ	Thickly myelinated	8-13 µm	40-70 m/s	Innocuous mechanical stimuli
Aδ	Thinly myelinated	1-4 µm	5-15 m/s	Noxious stimuli
C	Unmyelinated	0.1-1.0 µm	0.2-2.0 m/s	Noxious stimuli

In the last decade, the advancements made in single-cell RNA sequencing allowed for a more accurate classification of sensory neurons based on their gene expression profiles. Single-cell RNA sequencing of murine lumbar DRG neurons identified 11 classes of sensory neurons, NF1-NF5 (neurofilament-containing), NP1-NP3 (non-peptidergic nociceptors), PEP1, PEP2 (peptidergic nociceptors) and TH (tyrosine hydroxylase-containing) (Usoskin et al. 2015). Investigating the expression of genetic markers that had previously been associated with classes of sensory neurons, the authors of this study proposed distinct functionalities for these classes:

- NF1-NF5 are myelinated neurons. In particular:
  - NF1-NF3 neurons express *Ntrk2* (neurotrophic receptor tyrosine kinase 2, ot TrkB), *Ret* (RET receptor tyrosine kinase), *Calb1* (calbindin 1) and *Ntrk3* (neurotrophic receptor tyrosine kinase 3, or TrkC), suggesting that they act as low-threshold mechanoreceptors.
  - NF4 and NF5 neurons express *Ntrk3* and parvalbumin, suggesting that they are limb proprioceptive neurons.
- NP1-NP3 are unmyelinated, non-peptidergic neurons characterised by the expression of *Mrgprd* (Mas-related G-protein-coupled receptor D) and of the ATP-gated ion channel $P2x_3$, and may act as pruriceptors. Additionally,
  - NP1 neurons seem to have a role in neuropathic pain.

- NP3 neurons may transduce inflammatory itch.

- PEP1 and PEP2 represent peptidergic neurons, with a typical expression of *TrkA* and release of CGRP.
  - PEP1 neurons, which are unmyelinated, express substance P and are proposed as thermoreceptors.
  - PEP2 neurons, express *Ntrk1* (neurotrophic receptor tyrosine kinase 1, or *Trka*) and *Nefh* (neurofilament heavy chain) and are suggested as Aδ nociceptors.
- Lastly, TH are myelinated neurons, characterised by high expression of *Piezo2* and *Vglut3* (vesicular glutamate transporter 3), which suggest their function as C-fibre low-threshold mechanoreceptors.

Using a high-coverage single-cell RNA sequencing, Li and colleagues identified a larger number of representative genes of murine DRG neurons. Combining the transcriptomics approach with patch clamp recordings and single-cell PCR in mouse lumbar DRG, they described 10 different classes (C1 to C10) and 14 subclasses of sensory neurons with distinct transcriptomic, functional and morphological features (Li et al. 2016). In addition, the authors were able to show that different neuron subtypes share common genetic markers, and suggested that most nociceptors are polymodal, with only few of them specialised to respond to just one stimulus modality (Li et al. 2016) (Table 1-2).

Interestingly, single-cell RNA sequencing of primate DRG neurons showed that the majority of molecular neuronal classes described above (Usoskin et al. 2015) are conserved between mice and primates, and NP1 and NP2 are the two most divergent neuronal types between species (Kupari et al. 2021). Even more importantly, transcriptomic analyses in human DRG have revealed that the majority of genes identified in the mouse are conserved in humans, thus supporting the translational value of murine models (Ray et al. 2018).

Table 1-2 Functional probability and proposed framework of sensory neurons

Types and subtypes		Functional phenotypes						Proposed functionality
		Nociceptors			Mechanoreceptors		Pruriceptors	
		Thermal		Mechanical	Pressure	Brush		
		Cold	Heat					
Small neurons	**C1** ***C1-1*** ***C1-2***	Undetected *Undetected* *Undetected*	Medium *Undetected* *High*	Medium *Medium* *High*	Medium *Medium* *Medium*	Low *Medium* *Low*	Undetected *Undetected* *Undetected*	Mechanoheat nociceptor
	C2 ***C2-1*** ***C2-2***	Low *Low* *Undetected*	Medium *Medium* *Medium*	Medium *Medium* *Medium*	Undetected *Undetected* *Undetected*	Low *Low* *Undetected*	High *High* *High*	Mechanoheat nociceptor (mechanically insensitive, itch-sensitive)
	C3	Undetected	Undetected	Medium	Medium	High	Undetected	C-fibre low-threshold mechanoreceptor
	C4 ***C4-1*** ***C4-2***	Low *Low* *Undetected*	Medium *Medium* *Medium*	High *High* *High*	Medium *Medium* *Medium*	Low *Medium* *Low*	High *High* *High*	Mechanoheat nociceptor (itch-sensitive)
	C5 ***C5-1*** ***C5-2***	Low	Medium	Medium	Medium	Low	High	Mechanoheat nociceptor (itch-sensitive)
	C6 ***C6-1*** ***C6-2***	Low	Medium	High	Medium	Medium	Undetected	Mechanoheat nociceptor
Large neurons	**C7**	Undetected	Medium	High	High	Low	Undetected	Mechanoheat nociceptor (mechanically sensitive)
	C8 ***C8-1*** ***C8-2***	N/A	N/A	N/A	N/A	N/A	N/A	Mechanoreceptor
	C9 ***C9-1*** ***C9-2***	Undetected	Low	High	Medium	Undetected	Undetected	Mechanical nociceptor
	C10	N/A	N/A	N/A	N/A	N/A	N/A	Mechanoreceptor and/or proprioceptor

N/A: not available. Adapted from (Li et al. 2016).

1.1.5 Dorsal horn projections

Once primary afferent neurons are activated by a stimulus, the action potential propagates along the axon until it reaches the axonal terminal in the dorsal horn of the spinal cord, where neurotransmitters are released. Hence, the sensory information from the periphery is transmitted onto second-order neurons (see below). The grey matter of the spinal cord is organised into ten Rexed laminae (I to X), which are named after Bror Rexed who first identified them in the cat spinal cord (Rexed 1952). Figure 1-2 shows a schematic representation of the spinal cord structural organisation. Sensory processing involves the dorsal horn, which comprises laminae I to VI, whereas laminae VII to IX of the ventral horn are mainly involved in motor processing. Investigations in the spinal cord of cats, rodents and monkeys in the '70s and '80s have shown that nociceptive signals target mainly the superficial dorsal horn (laminae I and II), while non-noxious stimuli are transmitted to deeper laminae. Aδ-fibres project to lamina I (or marginal zone) and V (Light and Perl 1979), while C-fibres terminate in laminae I and II (or substantia gelatinosa) (Sugiura et al. 1986). In particular, peptidergic neurons terminate in lamina I and in the outer part of lamina II (II_o), while non-peptidergic neurons terminate in the inner portion of lamina II (II_i) (Hunt and Rossi 1985). Lastly, Aβ-fibres project to laminae III-VI (Brown et al. 1981, Woolf and Fitzgerald 1986) and are most abundant in lamina III and IV compared with lamina V and VI (Brown et al. 1981).

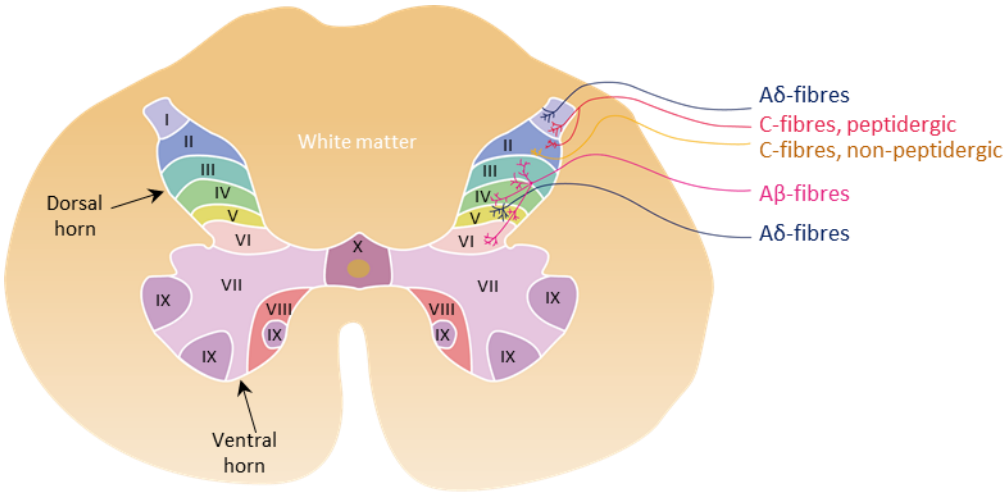

Figure 1-2 Rexed laminae organisation in the spinal cord

Sensory fibres terminate in the dorsal horn (laminae I to VI), while motor processing terminate in the ventral horn (laminae VII to IX). Aβ-fibres project to laminae III-VI, Aδ-fibres project to lamina I and V, and C-fibres project to laminae I and II (peptidergic neurons terminate in lamina I and in the outer part of lamina II, whereas non-peptidergic neurons terminate in the inner portion of lamina II).

As mentioned above, primary sensory neurons project onto second-order neurons in the dorsal horn laminae. These second-order neurons can either be interneurons, which only project within the spinal cord, or they can be projection neurons that terminate in the brain via ascending tracts (see section 1.1.6). Interneurons represent the most abundant type of second-order neurons in the spinal cord and can be distinguished in excitatory or inhibitory neurons, based on whether they release glutamate (excitatory) or gamma-aminobutyric acid (GABA) and/or glycine (inhibitory). Interneurons modulate the somatosensory signals from the periphery before they reach the brain through a complex organisation of neuronal interactions. However, a 'simpler' explanation of how interneurons modulate pain signalling is the gate control theory proposed by Melzack and Wall (Melzack and Wall 1965) (Figure 1-3). According to the theory, in the absence of an input from the periphery, an inhibitory interneuron in the dorsal horn inhibits project neurons to conduct signals to higher centres in the CNS (= gate closed). Similarly, when large myelinated fibres are activated by non-noxious stimuli and transmit this information to the spinal cord, they activate an inhibitory interneuron, which in turn impairs the ascending transmission. Conversely, when nociceptive fibres are activated, they prevent the inhibitory function of the interneuron, thus allowing projection fibres to send signals to the brain (= gate open). Additionally, the simultaneous detection of innocuous and noxious stimuli also has a 'gate closing' effect. Hence, applying pressure/rubbing or applying mild electrical impulses (transcutaneous electrical nerve stimulation, TENS) to an injured area can provide a temporary pain relief.

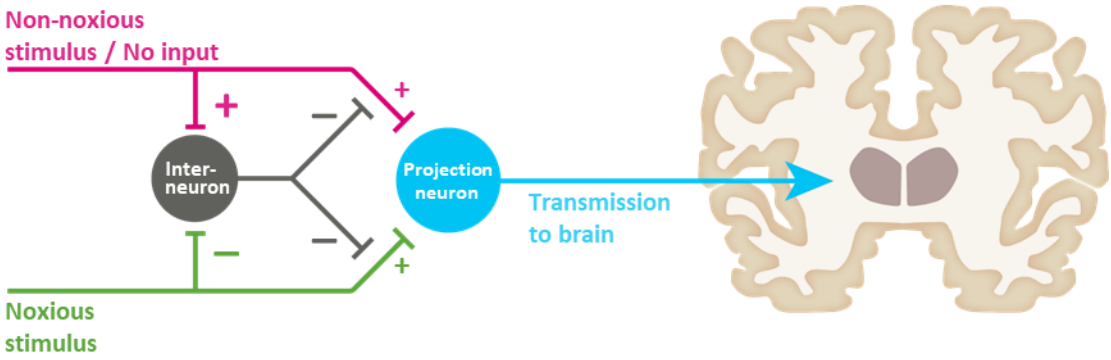

Figure 1-3 Gate control theory

The gate is closed when large myelinated fibres are activated by non-noxious stimuli (or in the absence of a sensory input altogether), and in turn activate an interneuron that inhibits the transmission of sensory information to higher centres. The gate is open when small and unmyelinated fibres are activated by noxious stimuli and inhibit the interneuron, thus allowing transmission of signals to higher centres.

Furthermore, the spinal cord is the site of the withdrawal reflex. Upon contact with a painful stimulus, an immediate limb withdrawal takes place without the involvement of the higher centres in the brain, in order to avoid additional damage to the body. This reflex is mediated by a polysynaptic circuitry: the activated afferent fibre synapses onto an interneuron, which in turn activates a motor neuron in the ventral horn. The motor neuron stimulates the contraction of the flexor muscle in the ipsilateral limb, whilst an interneuron inhibits the extensors muscles in the same limb, thus resulting in limb withdrawal.

1.1.6 Ascending pathways

Sensory inputs of different nature are transmitted to the brain via different ascending tracts. One of these pathways is the dorsal column medial lemniscus pathway [reviewed in (Al-Chalabi et al. 2021)]. Upon entering the spinal cord, most primary afferent neurons belonging to it do not synapse in the grey matter but enter the dorsal funiculus in the white matter and project to medullary nuclei. In particular, inputs from the upper limbs are transmitted through the fasciculus cuneatus, while axons from the lower limbs form the fasciculus gracilis. Second-order neurons in the medulla decussate and terminate in the ventral posterolateral nucleus of the thalamus, which represents the main integration site of sensory information from the periphery. Lastly, neurons in the thalamus project to the somatosensory cortex of the postcentral gyrus, where sensations of touch, vibration and proprioception are perceived [reviewed in (Al-Chalabi et al. 2021)]. The other ascending pathways are located in the ventrolateral funiculus; in these tracts, first-order neurons synapse with projection neurons in the dorsal horn laminae, which decussate before ascending to higher centres. One of the major pathways is the spinothalamic tract, which originates mainly from laminae I, IV and V [reviewed in (Basbaum et al. 2008)] and relays sensory information from the spinal cord to nuclei in the thalamus [reviewed in (Westlund 2008)]. Signals arising from the same area of the body converge on the same third-order neurons in the thalamus, thus allowing to localise the sensory input [reviewed in (Westlund 2008)]. The spinothalamic tract comprises a ventral and a lateral pathway. The former is located in the anterior funiculus in the white matter of the spinal cord and relays information about crude touch and pressure; the latter is located in the lateral funiculus and transmits information about noxious stimuli and temperature [reviewed in (Sengul and Watson 2015)]. In the thalamus, the spinothalamic tract terminates in the ventroposterior nuclei, the intralaminar nuclei, the posterior complex and the central lateral nucleus. Third-order neurons in the thalamus convey information to multiple areas in the brain [reviewed in (Basbaum et al. 2009)], including the sensory cortex, involved in the discriminatory aspect of pain perception (e.g. location, intensity and duration), and the anterior cingulate gyrus and insular cortex, key components of the limbic system that have a major role in modulating emotional and motivational responses to pain (e.g. fear, anxiety and escape and avoidance behaviours) [reviewed in (Bushnell et al. 2013)]. Additionally, the spinothalamic tract possesses collateral branches that terminate in the rostroventromedial medulla (RVM) and the periaqueductal grey (PAG) [reviewed in (Sengul and Watson 2015)], which participate to the descending pain modulation. The spinoreticular tract, parallel to the spinothalamic one, ascends from the ventrolateral funiculus in the spinal cord and synapses onto third-order neurons in the reticular formation of the medulla and the pons [reviewed in (Sengul and Watson 2015)]. Projections from the reticular formation reach thalamic

nuclei, which then synapse onto various regions of the sensory cortex. The main function of the spinoreticular tract is to generate arousal/alertness in response to diffuse noxious and innocuous mechanical stimuli and noxious heat [reviewed in (Mendoza 2011)]. The spinomesencephalic system, also closely associated with the spinothalamic tract, collects different pathways, the main ones being the spinotectal and spinoparabrachial tracts [reviewed in (Yezierski 2013)], and relays information about both noxious and innocuous stimuli [reviewed in (Sengul and Watson 2015)]. The spinotectal tract terminates in the superior colliculus in the midbrain and is responsible for the integration of visual and sensory information (i.e. spinovisual reflexes) [reviewed in (Kayalioglu 2009)]. The spinoparabrachial tract projects to parabrachial nuclei in the brainstem, which in turn relay information to various other regions, including the hypothalamus, involved in the autonomic and endocrine response to pain; the amygdala, involved in the affective response to pain (e.g. anxiety and fear); and the PAG [reviewed in (Sengul and Watson 2015)]. Given its vast reciprocal connections to various nuclei in the brain, the PAG is involved in decision making, emotional coping strategies and aversive and defensive behaviours (through its interaction with the amygdala and medial prefrontal cortex); reward circuits and motivational responses (through its interaction with the ventral tegmental area); and homeostatic responses (through its interaction with the hypothalamus and parabrachial nuclei) [reviewed in (Motta et al. 2017, Tryon and Mizumori 2018)].

1.1.7 Descending pathways

Different structures within the brainstem are involved in the descending modulation of pain, both in an inhibitory and excitatory direction [reviewed in (Ossipov et al. 2014)]. The PAG in the midbrain plays a key role in this modulation, which was first demonstrated by the observation that morphine microinjections (Tsou and Jang 1964) and electrical stimulation (Reynolds 1969) of this region produced an analgesic effect in animals. A similar analgesic effect was also observed by electrical stimulation of the PAG in humans (Hosobuchi et al. 1977, Richardson and Akil 1977). The PAG carries out its modulatory action specifically through its interaction with the RVM (in the medulla oblungata) and the locus coeruleus (LC; in the pons). The thalamus, parabrachial region and LC also project onto the RVM, which represents the final relay centre in the descending pathways, as it then terminates in the dorsal horn [reviewed in (Ossipov et al. 2014)]. The main neurotransmitters involved in the descending pathways are serotonin and noradrenaline, which can have an inhibitory or excitatory effect, depending on the receptors they bind to. Serotonin (5-HT) has an inhibitory effect when interacting with 5-HT1 and 5-HT2 receptors, whereas it exerts an excitatory action when binding 5-HT3 receptors. Likewise, noradrenaline (NA) inhibits neuronal activity by binding α-2A and α-2B/C receptors, while binding to α-1A receptor has an excitatory function [reviewed in (Boadas-Vaello et al. 2016)]. Figure 1-4 summarises the main ascending and descending pathways.

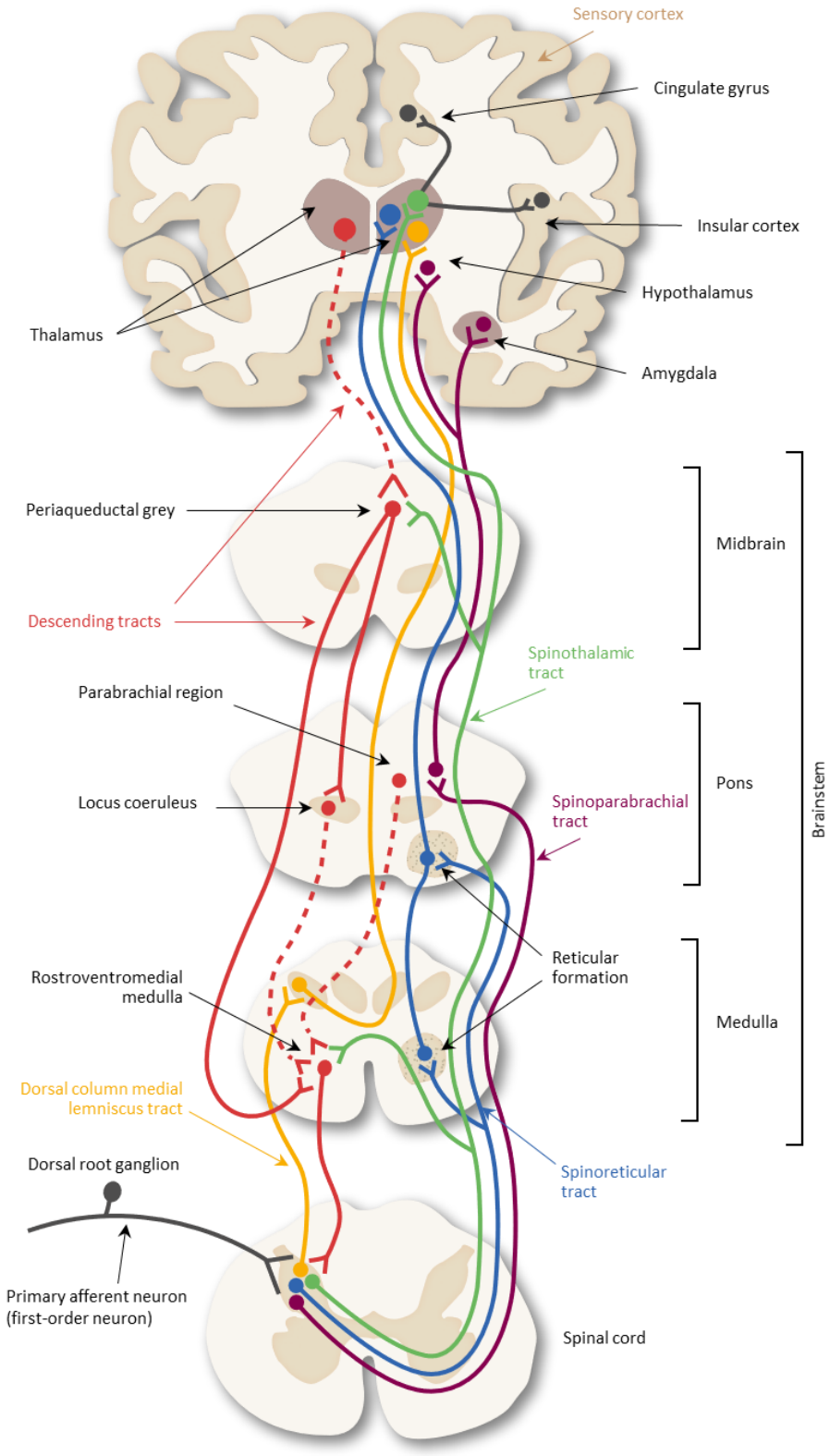

Figure 1-4 Schematic representation of ascending and descending sensory pathways

Signals from the periphery terminate onto a second-order projection neuron in the spinal cord, which in turn projects to higher centres in the brain and the brainstem via different ascending pathways, including the dorsal column medial lemniscus (in yellow), spinothalamic (in green), spinoreticular (in blue) and spinoparabrachial (in purple) tracts. Pain modulation is carried out by descending tracts from the higher centres to the spinal cord (in red).

1.1.8 Nociception and pain

Nociception and pain should not be confused and used as interchangeable terms. The International Association for the Study of Pain (IASP) defines nociception as "*the neural process of encoding noxious stimuli*" and does not imply that pain is associated with it ("IASP Terminology" 2011). Indeed, nociception is an objective and quantifiable response to a noxious stimulus. By contrast, pain is always subjective and defined as *"an unpleasant sensory and emotional experience associated with, or resembling that associated with, actual or potential tissue damage"* (Raja et al. 2020). This definition stresses the fact that pain comprises an emotional state. As such, pain cannot be quantified by an external observer, but rather can only be experienced individually.

Pain can be distinguished into acute or chronic manifestations. Acute pain appears rapidly after an injury or disease but typically lasts for a short period of time. Conversely, any persistent or recurring pain lasting more than three months is classified as chronic (Treede et al. 2015). A task force of the IASP recently developed a systematic classification of chronic pain that was implemented in the 11th edition of the International Classification of Diseases (ICD-11) (Treede et al. 2019). Chronic primary pain "*is associated with significant emotional distress and/or significant functional disability (interference in activities of daily life and participation in social roles) and the symptoms are not better accounted for by another diagnosis*" (Nicholas et al. 2019). Conversely, chronic secondary pain is the consequence of other underlying conditions. In particular, the task force identified six subgroups of secondary pain (Treede et al. 2019): chronic cancer-related pain; chronic neuropathic pain; chronic posttraumatic and postsurgical pain; chronic secondary visceral pain; chronic secondary headache and orofacial pain; and chronic secondary musculoskeletal pain.

1.1.9 Neuropathic pain

The IASP defines neuropathic pain (NP) as "*pain caused by a lesion or disease of the somatosensory nervous system*" (Jensen et al. 2011). The prevalence of chronic pain with neuropathic characteristics in the general population has been estimated at 7-10% (Torrance et al. 2006, Bouhassira et al. 2008, Yawn et al. 2009, de Moraes Vieira et al. 2012). Lesions or diseases affecting the central somatosensory nervous system may evoke central NP, whereas lesions/diseases of the peripheral nerves may evoke peripheral NP. The reclassification of chronic pain for ICD-11 identified four different manifestations of chronic central NP: chronic central NP associated with spinal cord injury; chronic central NP associated with brain injury; chronic central poststroke pain; and chronic central NP caused by multiple sclerosis (Scholz et al. 2019). Chronic peripheral NP was also classified in five subgroups (Scholz et al. 2019):

- trigeminal neuralgia affects the trigeminal nerve and therefore manifests as orofacial pan.
- chronic NP after nerve injury is caused by a lesion to peripheral nerves and can also be classified as peripheral chronic posttraumatic and postsurgical pain (Schug et al. 2019).
- painful polyneuropathy is associated with metabolic (e.g. diabetes) and autoimmune (e.g. rheumatoid arthritis and Guillain-Barré syndrome) diseases, and exposure to environmental toxins and neurotoxic treatments (e.g. chemotherapy). In particular, chemotherapy-induced peripheral neuropathy can also be classified as chronic cancer-related pain, which comprises pain caused by cancer or metastases or by cancer treatment (Bennett et al. 2019b).
- postherpetic neuralgia is caused by varicella-zoster virus.
- painful radiculopathy is caused by a lesion of the cervical, thoracic, lumbar, or sacral nerve roots.

NP can be a consequence of a peripheral neuropathy but does not develop in all patients affected by it [reviewed in (Colloca et al. 2017)]. NP symptoms can be both positive and negative, thus reflecting a gain or loss of somatosensory function, respectively. Positive symptoms include spontaneous abnormal sensations like paresthesia and/or dysesthesia (e.g. tingling and pricking), burning and/or paroxysmal pain and evoked pain in response to mechanical or thermal stimuli [reviewed by (Gierthmühlen and Baron 2016)]. In particular, responses to stimuli are defined allodynic when evoked by stimuli that are not normally painful, whereas hyperalgesia defines increased pain to painful stimuli. Conversely, negative symptoms comprise mechanical and thermal hypoalgesia (reduced pain in response to a stimulus that normally provokes pain) and hypoesthesia (reduced sensitivity to stimuli) [reviewed by (Gierthmühlen and Baron 2016)].

Given the high degree of heterogeneity in its causes and symptoms, understanding the pathophysiology of NP, and subsequently investigating new therapeutic targets, is challenging. Several preclinical models have been developed to get a better understanding of its causal mechanisms. Rodents are the predominant species used in these preclinical investigations. The most common model for the study of NP involves a surgical procedure to generate a physical nerve injury (e.g. sciatic nerve ligation). However, other models have also been employed to mimic neuropathy induced by diseases or pharmacological agents, such as models of diabetic, HIV-associated and chemotherapy-induced neuropathy [reviewed in (Burma et al. 2017)].

1.2 Chemotherapy-induced peripheral neuropathy

Chemotherapy-induced peripheral neuropathy (CIPN) is the major dose-limiting side effect of several chemotherapeutic agents. Drugs associated with CIPN are used as first line treatment and combination therapy in a wide a variety of solid and haematological tumours and differ in their anti-cancer actions. As a result, it is still not clear whether their neurotoxic actions rely on similar mechanisms or not. Table 1-3 summarises the main chemotherapeutic compounds associated with CIPN and their mechanisms of action.

Table 1-3 Commonly used chemotherapeutic compounds associated with CIPN and their mechanisms of action

Chemotherapy agent	Mechanism of action
Platinum analogues Cisplatin Carboplatin Oxaliplatin	DNA cross-linking
Taxanes Paclitaxel Docetaxel	Microtubule stabilisation
Epothilones Ixabepilone	Microtubule stabilisation
Vinka alkaloids Vincristine Vinblastine	Microtubule destabilisation
Monoclonal antibodies Brentuximab	Microtubule destabilisation
Eribulin	Microtubule destabilisation
Bortezomib	Proteasome inhibitor
Thalidomide	Immunomodulation/anti-angiogenesis

Adapted from (Staff et al. 2017)

1.2.1 Clinical presentation of CIPN

Patients affected by CIPN report mostly sensory symptoms, that typically appear in a stocking-and-glove distribution in both feet and hands. Symptoms include paresthesias, dysesthesias, hypersensitivity to mechanical and/or thermal stimuli, numbness and spontaneous, ongoing pain, which may impair daily life activities greatly. (Flatters et al. 2017). These symptoms have a profound effect on the patients' quality of life. For instance, patients report difficulty in picking up objects and buttoning up clothing or putting on jewellery, due to numbness and impaired fine finger movement; inability to remove items from the fridge and to endure winter weather,

due to cold hypersensitivity; and loss of balance and pain on walking because of mechanical hypersensitivity and numbness in the feet. The emotional and social functions are also impacted and patients describe feelings of isolation, loss of independence, altered social and family relationships and inability to perform certain work tasks (Bakitas 2007, Speck et al. 2012). CIPN can appear at any time during the treatment, even after the treatment has been stopped, and symptoms can endure for months or years after the chemotherapy regimen has been ceased, which is a phenomenon known as 'coasting' (Farquhar-Smith 2011, Han and Smith 2013). The time course of CIPN is dependent on the chemotherapy and on the duration of the treatment. Typically, CIPN is dose-dependent and symptoms develop after cumulative doses of chemotherapy, generally after the 3rd or 4th cycle (Grisold et al. 2012). A recent systematic review and meta-analysis reviewed data from 31 studies on over 4 000 patients administered with oxaliplatin, cisplatin, carboplatin, paclitaxel, vincristine, thalidomide and bortezomib, either alone or in combination, to calculate the average CIPN prevalence (Seretny et al. 2014). The study revealed that 68.1% of patients suffered from CIPN within the first month following the cessation of chemotherapy, 60% at 3 months and 30% at 6 months or later. However, the authors reported a high degree of heterogeneity among studies, which was related to the time and method of assessment, dose received and chemotherapy type (Seretny et al. 2014).

1.2.2 CIPN treatment and prevention

Despite several clinical trials that tested the efficacy of various agents, many of which were selected after positive results in other chronic pain conditions (e.g. diabetic neuropathy), no treatment is currently available to prevent or treat CIPN completely (Hershman et al. 2014). The American Society of Clinical Oncology (ASCO) published clinical practice guidelines based on 48 randomised controlled trials for CIPN treatment identified in a systematic literature search (Hershman et al. 2014). 42 trials tested the efficacy of chemoprotectants, anticonvulsants, antidepressants, vitamins, minerals and dietary supplements in the prevention of CIPN, but no agent was recommended as preventative treatment, due to a lack of significant benefits when compared with placebo controls. The remaining 6 trials investigated tricyclic antidepressants, anticonvulsants and a topical gel for the treatment of established CIPN. The only agent receiving a moderate recommendation was duloxetine (Hershman et al. 2014), which had already shown a beneficial effect in diabetic neuropathy (Goldstein et al. 2005), fibromyalgia (Russell et al. 2008) and osteoarthritis (Chappell et al. 2011). Duloxetine showed efficacy in reducing pain severity in a large randomised Phase III placebo-controlled trial in oxaliplatin- and paclitaxel-treated patients (Smith et al. 2013). However, further exploratory analyses showed that patients receiving oxaliplatin benefited more from duloxetine treatment than those administered with paclitaxel (Smith et al. 2013). Given the lack of meaningful preventive or analgesic treatment

options, the appearance of CIPN symptoms is often associated with dose reduction or cessation of treatment, which may potentially affect patient survival (Bhatnagar et al. 2014, Seretny et al. 2014).

1.2.3 CIPN diagnosis and assessment

Currently, there is no reliable and standardised diagnostic tool for CIPN. A clinical examination and assessment of medical history are required to initially diagnose the neuropathy (Gordon-Williams and Farquhar-Smith 2020). Many clinical grading scales are used in clinical practice to describe the severity of the neuropathy (Table 1-4). However, a significant interobserver variation has been reported between scales (Postma et al. 1998). Furthermore, these scales do not allow to assess pain thoroughly, and clinicians typically underscore the severity of the neuropathy when compared with direct patient reports (Shimozuma et al. 2009). A more composite grading tool, the Total Neuropathy Score (TNS), assesses the neuropathy by combining patient reports on their symptoms with physical assessments and electrophysiological investigations (Cornblath et al. 1999). However, it lacks an adequate assessment of pain (Smith et al. 2008). Currently, there's no general consensus on the use of one grading tool over another (Farquhar-Smith 2011). Further self-report grading tools have been developed to evaluate the impact of CIPN on the quality of life. The Functional Assessment of Cancer Therapy/Gynecologic Oncology Group–Neurotoxicity (Fact/GOG-Ntx) is a comprehensive 11-item questionnaire that assesses CIPN symptoms and their impact on quality of life in oncology patients, with a focus on four different aspects of well-being: physical, social, emotional and functional (Calhoun et al. 2003). The Patient Neurotoxicity Questionnaire (PNQ) is a self-report questionnaire developed to assess sensory and motor symptoms and their effect on daily activities typically affected by CIPN, like buttoning clothes, putting on jewellery, tying shoelaces etcetera (Shimozuma et al. 2009). The McGill Pain Questionnaire (MPQ) allows to describe the location, quality and severity of pain, together with describing factors that alleviate or worsen it (Melzack 1975). Similarly, the Brief Pain Inventory (BPI) addresses the location and severity of pain and its impact on function (e.g. social relationships, mood and sleep) (Cleeland and Ryan 1994). Lastly, two questionnaires have been developed to evaluate quality of life. The European Organization for Research and Treatment of Cancer quality of life questionnaire (EORTC QLQ-C30) is not specific to CIPN but allows to assess the impact of cancer on various functions, including the physical, emotional and social ones, as well as the overall impact on general health and financial economic situation. The EORT QLQ-CIPN20 has been later developed to assess the specific impact of CIPN on quality of life (Postma et al. 2005).

Table 1-4 Clinical grading scales for CIPN assessment

	Grade 0	Grade 1	Grade 2	Grade 3	Grade 4
WHO	None	Paresthesias and/or decreased tendon reflexes	Severe paresthesias and/or light weakness	Intolerable paresthesias and/or pronounced motor loss	Paralysis
Ajani *sensory*	None	Decreased deep tendon reflexes and/or paresthesias	Loss of deep tendon reflexes, mild to moderate function impairment	Severe paresthesias, severe function impairment	Complete sensory loss, loss of function
motor		Mild or temporary muscle weakness	Constant moderate weakness	Unable to walk	Complete paralysis
NCI-CTC *sensory*	None or no change	Mild paresthesias and/or loss of deep tendon reflexes	Mild or moderate sensory loss and/or moderate paresthesias	Severe sensory loss or paresthesias with function impairment	
motor	None or no change	Subjective weakness	Mild weakness, no impairment of function	Weakness and impairment of function	Paralysis
ECOG *sensory*	None or no change	Loss of deep tendon reflexes, mild paresthesias	Moderate paresthesias, mild or moderate sensory loss	Severe sensory loss, and impairment of function	
motor	None or no change	Subjective weakness	Mild weakness, no impairment of function	Severe weakness and impairment of function	Paralysis

WHO: World Health Organisation; NCI-CTC: National Cancer Institute – Common Toxicity Criteria; ECOG: Eastern Cooperative Oncology Group (Postma et al. 1998, Kaplow and Iyere 2017).

Quantitative sensory testing (QST) comprises several non-invasive psychological and physiological tests to assess which afferent nerve fibre is associated with the neuropathy: large myelinated Aβ-fibres are evaluated through touch detection, Aδ-fibres with sharp pain detection and C-fibres function is assessed through thermal testing (Dougherty et al. 2004, Dougherty et al. 2007). Therefore, they may provide a useful tool to characterise the neuropathy. For instance, deficits in tactile and vibration threshold were associated with moderate to severe CIPN in breast cancer survivors who had received taxanes, alone or in combination with platinum agents. (Zhi et al. 2019). Oxaliplatin- and docetaxel-treated patients who presented symptoms of the neuropathy after treatment completion showed abnormal QST measurements (Krøigård et al. 2014). Altered QSTs have also been identified following treatment with most of the other neuropathy-inducing chemotherapeutic agents and results from a variety of studies have been comprehensively reviewed by Argyriou and colleagues

(Argyriou et al. 2019). Despite much evidence of abnormal QSTs in CIPN, performance of a complete set of QSTs is time-consuming and necessitates of specialised equipment and staff. Additionally, patient-related factors like attention level, boredom or confusion may affect QST performance and results (Siao and Cros 2003). For these reasons, QSTs are not routinely performed during the clinical evaluation of CIPN.

Nerve conduction studies (NCS) involve the stimulation of peripheral nerves with small electrical impulses to assess the functionality of large myelinated fibres by measuring the amplitude and conduction velocity of sensory and motor action potentials. Using NCS, abnormal electrophysiological findings have been reported in various nerves (sural, median, ulnar, radial and peroneal) of patients exposed to different chemotherapeutic compounds, including cisplatin (Krarup-Hansen et al. 2007), oxaliplatin (Argyriou et al. 2007), paclitaxel (Chen et al. 2013), docetaxel (Chen et al. 2013) and bortezomib (Velasco et al. 2010). Therefore, NCS provide a good complementary tool to the clinical assessment for the diagnosis of peripheral neuropathies. Nevertheless, they have a few limitations. First of all, they do not provide any information on Aδ- or C-fibres, so NCS may be normal in the presence of small fibre nerve damage. In addition, performance of NCS relies on specialised equipment and trained personnel and may be discomforting for the patients. Therefore, they are not routinely employed in clinical practice [reviewed in (Matsuoka et al. 2016)]. Nerve excitability studies allow to obtain a deeper understanding of the degree and type of the electrophysiological deficit evoked by chemotherapy, as they provide information regarding ion channel function and membrane potential [reviewed in (Huynh and Kiernan 2015)]. Using this technique, sensory abnormalities were identified in oxaliplatin-treated patients before the observation of NCS deficits and the development of a severe neuropathy (Park et al. 2009a, Park et al. 2015).

Nerve biopsies would provide an optimal tool to diagnose CIPN, but they are rarely employed for this scope. An investigation on the usefulness of sural nerve biopsy in neuropathy patients revealed that the biopsy itself changed the neuropathy diagnosis and was a source of increased pain (Gabriel et al. 2000). The only reports of sural nerve biopsies in CIPN patients showed severe fibre loss following paclitaxel (Sahenk et al. 1994) and docetaxel regimens (Fazio et al. 1999). A skin punch biopsy can be performed to evaluate loss of IENFs, which would be a downstream effect of damage to Aδ- and C-fibres (Mangus et al. 2020). Indeed, loss of IENF density has been associated with CIPN, but results were often conflicting among studies [reviewed in (Argyriou et al. 2019)]. Moreover, IENFs are typically affected after the patients display clinical symptoms of the neuropathy. Additionally, the technique is expensive, time-consuming and relatively invasive. Therefore, skin biopsies are not often used in the diagnosis of CIPN, nor are recommended for this scope (Gordon-Williams and Farquhar-Smith 2020).

1.3 Oxaliplatin-induced peripheral neuropathy

1.3.1 Clinical presentation

Oxaliplatin is the first-line treatment for colorectal cancer (CRC). As of 2018, CRC represents the third most common cancer and the second most common cause of cancer-related death worldwide. It accounted for 10.2% of all new cancer cases, with > 1.8 million new cases diagnosed that year (Bray et al. 2018). In the UK alone, CRC was the fourth most common cancer and affected > 42 000 people, as of 2017 ("Bowel cancer incidence statistics" Cancer Research UK 2020). Oxaliplatin-induced peripheral neuropathy (OIPN) manifests as two different clinical syndromes. Acute neurotoxicity appears during chemotherapy administration or hours/days after the first infusion cycles and affects the majority (68-98%) of patients treated with different combinations of regimens (85-130 mg/m^2 oxaliplatin) (Díaz-Rubio et al. 1998, Land et al. 2007, Park et al. 2009a, Storey et al. 2010, Argyriou et al. 2012, Alejandro et al. 2013, Argyriou et al. 2013a, Argyriou et al. 2013b, Soveri et al. 2019). Patients report cold-triggered perioral and pharyngolaryngeal dysesthesias, jaw tightness, difficulty with swallowing, muscle cramps and hand dysesthesias (Attal et al. 2009, Argyriou et al. 2013b). Nevertheless, acute OIPN is transient and often resolves between infusion cycles. A recent examination of patients receiving adjuvant oxaliplatin treatment showed that OIPN symptoms peaked around day 3 after the first chemotherapy administration, then improved but did not resolve completely before the second infusion cycle (Pachman et al. 2016). In case of severe acute neuropathy, patients did not require dose reductions/treatment discontinuation, but only a prolonged infusion time (Argyriou et al. 2012, Argyriou et al. 2013b). By contrast, chronic OIPN manifests after cumulative doses of oxaliplatin and tends to worsen over time, as the treatment progresses. Moreover, the neurotoxicity can keep worsening even after treatment completion and can last for several months (Pachman et al. 2016). Therefore, patients often require dose reduction or discontinuation of the chemotherapy regimen. Patients display spontaneous paresthesias or dysesthesias in the hands and feet, deficits to thermal and/or mechanical stimuli, loss of tendon reflexes, vibration deficit, proprioceptive ataxia, weakness, numbness and tingling (Land et al. 2007, Attal et al. 2009, Pachman et al. 2016). A large prospective, multicentre study showed that 72.5% of patients (145/200) were affected by chronic OIPN after treatment discontinuation, with most patients (75.1%) experiencing grade1-2 neuropathy compared with grade 3 (24.8%) (Argyriou et al. 2013a). Chronic OIPN symptoms suggest that the chronic neurotoxicity is a continuation of the acute one. This hypothesis is supported by evidence that patients experiencing more severe acute OIPN would then develop more severe chronic neuropathy (Park et al. 2009a, Argyriou et al. 2013b, Pachman et al. 2016). Chronic symptoms are partly reversible in approximately 80% of patients, and in 40% of cases resolve completely after 6-8

months after treatment discontinuation [reviewed in (Argyriou et al. 2008)]. Nevertheless, after a median follow-up time of 4.2 years after treatment cessation, 69% of patients who received an adjuvant oxaliplatin treatment still experienced sensory neuropathy (grade 1 to 4) (Soveri et al. 2019). Additionally, a prospective study on 91 CRC patients reported that chronic OIPN symptoms were still present in 84% of patients 2 years after oxaliplatin treatment had been stopped, although the neuropathy severity was significantly reduced (Briani et al. 2014). Moreover, coasting has been reported in a patient that did not display any symptoms of acute or chronic OIPN for the entirety of the chemotherapy treatment, but started showing a quick progression of typical OIPN symptoms such as numbness and tingling in the upper and lower limbs, difficulty with balance and loss of fine movement once the treatment was over (Choi et al. 2006). Symptoms improved with time but still persisted for 7.5 months (Choi et al. 2006). A potential explanation for these persistent manifestations of oxaliplatin-induced neurotoxicity is that oxaliplatin may be accumulating in the DRG, as observed both *in vitro* and *in vivo* in preclinical models of OIPN (see section 1.3.4).

1.3.2 Discovery and development of platinum analogue compounds

The discovery of the anti-tumour effect of platinum compounds dates back to the '60s, when Rosenberg and colleagues stumbled upon the inhibitory effect of platinum (Pt) on E. coli cell division whilst investigating the effects of an electric field on bacterial growth (Rosenberg et al. 1965). Further experiments from the same authors described a variety of different ionic species of Pt complexes that could be formed in solution. In particular, *cis*-platinum (II) diamminodichloride (*cis*-Pt(II)$(NH_3)_2Cl_2$), later named cisplatin (Figure 1-5 A), was identified as one of the specific complexes responsible for cell division inhibition (Rosenberg et al. 1967). A potential inhibitory effect on cancer growth was conjectured and the jump from bacteria to mammal models followed quickly.

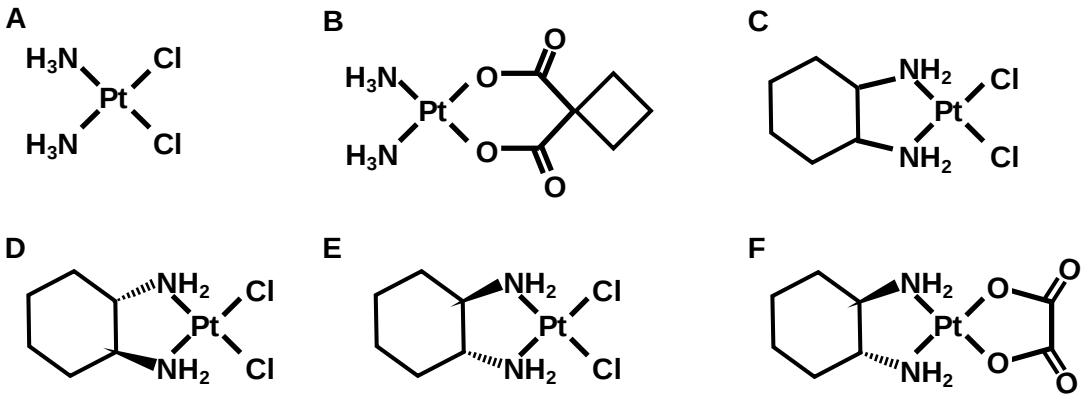

Figure 1-5 Chemical structure of the platinum analogues developed throughout the years

(A) Cisplatin, whose fortuitous discovery dates back to 1965, was the first anti-tumour compound belonging to the platinum (Pt) analogue family. (B) In an attempt to reduce cisplatin nephrotoxicity, the second-generation Pt analogue carboplatin was synthesised. Carboplatin was obtained by the substitution of the chlorine atoms of cisplatin with a bidentate group. (C-E) The amine groups in cisplatin were replaced with a diaminocyclohexane (DACH) group to further overcome cisplatin and carboplatin limitations. Nevertheless, DACH compounds were not soluble in water. The DACH group was a mixture of *cis* and *trans* isomeric forms: (C) *cis*-DACH Pt(II), the least potent of the isomers; (D) *trans*-d-DACH Pt(II) and (E) *trans*-l-DACH Pt(II), the most potent of the isomers. (F) Oxaliplatin, a third-generation compound, was developed by retaining the *trans*-l-DACH group and replacing the chloride groups with oxalate. Oxaliplatin was both an effective anti-tumour compound and easily soluble in water, thus becoming a good candidate for clinical trials.

Since then, the anti-tumour effect of Pt was rapidly demonstrated. Cisplatin was able to inhibit tumour growth in sarcoma 180 and leukaemia L1210 mice models (Rosenberg et al. 1969) and to induce regression of solid sarcoma 180 tumours in mice (Rosenberg and VanCamp 1970). Following the first preclinical investigations, cisplatin was found to be effective in a wide variety of cancers in different animal models [reviewed in (Rosenberg 1985)]. Positive results were also obtained with experimental tumour systems at the National Cancer Institute, which eventually led to the first clinical trials of cisplatin in cancer patients in 1972. Cisplatin was clinically successful in the treatment of various solid tumours and in 1978 received the Food and Drug Administration (FDA) approval for treating advanced testicular, ovarian and bladder cancer. Early trials were impaired by a severe and dose-limiting nephrotoxicity, in addition to significant emesis, oto-, myelo- and neurotoxicity [reviewed in (McKeage 1995)]. Several cisplatin analogues were synthesised trying to maintain its broad anti-tumour activity and to overcome its toxic side effects. Over 300 compounds were tested at the Institute of Cancer Research (London, UK). The most successful compound was carboplatin (*cis*-diamino-1,1-cyclobutane dicarboxylato platinum II), which was synthesised by replacing the two chloride groups of cisplatin with a bidentate cyclobutene dicarboxylate ligand (Figure 1-5 B). The substitution of

chlorine with a bidentate group increased carboplatin water solubility by 17 times compared with cisplatin. Carboplatin did not evoke any significant nephrotoxicity and produced a less severe emesis than cisplatin. However, it was associated with a dose-limiting myelosuppression (Calvert et al. 1982). Further attempts were made to overcome cisplatin and carboplatin limitations. The substitution of the amine groups in cisplatin with diaminocyclohexane (DACH) groups allowed retaining a good anti-tumour activity but no cross-resistance with cisplatin [reviewed in (Di Francesco et al. 2002)] (Figure 1-5 C-E). Nevertheless, DACH complexes were not soluble in water and therefore not suitable for clinical development. Improved water solubility was obtained by maintaining the most active DACH group, the *trans*-l-DACH, and substituting the chloride groups with more anionic groups. Finally, the substitution of chloride with oxalate led to the development of the third-generation Pt compound oxalate *trans*-l-DACH Pt(II), later named oxaliplatin (Figure 1-5 F). Oxaliplatin was 8 times more water soluble (Mathe et al. 1989) and presented similar or greater efficacy than cisplatin in several mouse models of haematologic and solid tumours (Kidani et al. 1980, Mathe et al. 1985, Tashiro et al. 1989), without displaying the marked nephrotoxicity associated with cisplatin (Mathe et al. 1985). Oxaliplatin was also reported to not produce cross-resistance to cisplatin in cisplatin-resistant cells, both *in vitro* (Kraker and Moore 1988, Tashiro et al. 1989, Rixe et al. 1996) and *in vivo* (Tashiro et al. 1989). The effectiveness of oxaliplatin was further highlighted by an investigation on the activity of Pt analogues *in vitro* on the National Cancer Institute's Anticancer Drug Screen Panel, which showed that colon cancer cell lines were particularly sensitive to oxaliplatin, whilst they displayed resistance to both cisplatin and carboplatin (Rixe et al. 1996). Oxaliplatin underwent its first Phase I clinical trial in 1986. No nephrotoxicity was reported, whilst nausea and emesis remained the most significant side effects (Mathe et al. 1986). A Phase II clinical trial reported the effectiveness of the combination of oxaliplatin and 5-fluorouracil (5-FU) and folinic acid (FA, also known as leucovorin) on metastatic colorectal cancer (in 58% of cases) (Levi et al. 1992). The most frequent side effects of oxaliplatin treatment remained nausea and emesis, whilst nephrotoxicity and myelotoxicity were not as frequent as in case of cisplatin and carboplatin, respectively. However, neurotoxicity was identified as a marked side effect of oxaliplatin (Mathe et al. 1989). The abundance of positive preclinical and clinical results led to oxaliplatin approval in France in 1996 and in Europe in 1999 as first-line treatment for metastatic CRC, together with 5-FU and leucovorin (LV). FDA approval to treat patients with recurring CRC after initial therapy followed in 2002. Finally, in 2004, it received FDA approval as initial treatment for CRC as well (Graham et al. 2004, Ibrahim et al. 2004).

1.3.3 Mechanism of action of platinum analogues

Oxaliplatin, like any other member of the Pt analogue family, is believed to carry out its cytotoxic action mainly through DNA damage. Downstream of DNA damage, the major effect of Pt compounds is the inhibition of DNA replication, which in turn leads to cell cycle arrest and eventually cell death via apoptosis and/or necrosis [reviewed in (Martinez-Balibrea et al. 2015)]. To carry out their cytotoxic action, all Pt analogues first undergo a biotransformation that produces the active form of the compound. Oxaliplatin non-enzymatic biotransformation comprises the displacement of the inactive oxalate group and the formation of several transient reactive species, such as dichloro-, monochloro-, and diaquo-platin, which in turn can bind to amino acids, plasma proteins and DNA, thus exerting their cytotoxic activity (Alcindor and Beauger 2011). The Pt-DNA interaction was first reported in 1970. Harder and Rosenberg observed that DNA synthesis, measured as ^{3}H-thymidine incorporation, in human AV_3 cells exposed to cisplatin was rapidly and irreversibly inhibited by cisplatin in a dose-dependent manner. A secondary inhibitory effect on RNA and protein synthesis was also observed, but only at higher concentrations and after longer exposure periods (Harder and Rosenberg 1970). The Pt-DNA interaction has been the object of extensive research ever since. Examination of the cisplatin-DNA adducts showed that Pt was bound to the N7 atoms of guanine and adenine, thus forming intrastrand cross-links preferably at guanine clusters, d(GpG) and d(ApG) (Fichtinger-Schepman et al. 1985). Intrastrand cross-links are the most common adducts formed by cisplatin (Eastman 1983). Interstrand cross-links have been identified, but only accounted for 1% of the total Pt-DNA adducts, and a small fraction of DNA-protein cross-links have been observed as well (Eastman 1983). The chemical structure of cisplatin-derived Pt analogues, and in particular their leaving group, was thought to affect drug-binding sites and partly explains their different degrees of anti-tumour activity. For instance, Micetich and colleagues observed that carboplatin was 45 times less potent than cisplatin on L1210 cells. Carboplatin was also associated with a 12-hour delay in the formation of DNA interstrand cross-links and a 6-hour delay in the formation of DNA-protein cross-links, compared with cisplatin (Micetich et al. 1985). The authors hypothesised that such a delay was due to the stability of the bidentate cyclobutene dicarboxylate ligand, which makes carboplatin more resistant to hydrolysis and therefore more slowly activated than cisplatin, whose chloride groups can be easily displaced. By contrast, oxaliplatin formed the same intra- and interstrand and DNA-protein cross-links as cisplatin (Woynarowski et al. 1998, Woynarowski et al. 2000), but was less reactive on naked SV40 DNA (Woynarowski et al. 1998), calf thymus DNA (Saris et al. 1996) and on intracellular DNA in human ovarian carcinoma A2780 cells. Despite its reduced reactivity, oxaliplatin was four times more cytotoxic in the same A2780 cells than cisplatin (Woynarowski et al. 1998). A potential

explanation for the difference in cytotoxicity between oxaliplatin and other Pt compounds is the existence of different cellular mechanisms of drug resistance. Several mechanisms of cellular drug uptake and efflux have been identified and associated with oxaliplatin, cisplatin and carboplatin resistance, including the copper solute carrier (SLC) and the ATP-binding cassette (ABC) transporters and the glutathione (GSH) system [reviewed in (Martinez-Balibrea et al. 2015)]. However, no significant difference in drug uptake and/or efflux, nor in its intracellular inactivation, was observed among Pt compounds, thus suggesting that different mechanisms of DNA repair may be responsible for the different anti-tumour activities of these agents [reviewed in (Di Francesco et al. 2002)].

1.3.4 Platinum accumulation in the peripheral nervous system

It is generally believed that CIPN is a direct consequence of chemotherapeutic compounds accumulation in the PNS. Indeed, clinical and preclinical investigations have identified Pt accumulation in different peripheral neuronal tissues. Conversely, the blood-brain barrier provides an effective protection against drug accumulation in the CNS, and delivery of anti-tumour agents to the brain and spinal cord is therefore challenging. An early examination of three patients treated with cisplatin reported accumulation of Pt in the DRG (mean levels: 3.8 µg/g) and, to a lesser extent, in the peripheral nerves (sural, tibial, femoral and median; mean levels: 2.3 to 3.5 µg/g) up to 4 months after cisplatin treatment. On the other hand, Pt levels in the brain and spinal cord were 10 to 20 times lower, with mean levels of 0.17 and 0.36 µg/g, respectively (Thompson et al. 1984). A further investigation in 21 cisplatin-treated patients revealed that DRG were characterised by the highest accumulation of Pt, followed by peripheral nerves, with mean levels of 1.68 and 1.30 µg/g, respectively. The lowest Pt concentration was detected within the brain and spinal cord, with mean levels of 0.37 and 0.24 µg/g, respectively (Gregg et al. 1992). Furthermore, patients who displayed clinical evidence of neurotoxicity showed the highest levels of Pt accumulation in the DRG and peripheral nerves (Gregg et al. 1992). To our knowledge, Pt accumulation in the peripheral tissues has not been investigated in a clinical setting following oxaliplatin administration. However, a lot of *in vitro* and *in vivo* evidence is present in the literature. Pt accumulated in DRG neurons after *in vitro* exposure to oxaliplatin (Luo et al. 1999, Ta et al. 2006, Liu et al. 2013). Repeated systemic administration of oxaliplatin in rat models (cumulative dose 29.6 to 48 mg/kg) resulted in Pt accumulation in the DRG (Holmes et al. 1998, Cavaletti et al. 2001, Ip et al. 2013, Fujita et al. 2019) and sciatic nerve (Cavaletti et al. 2001, Ip et al. 2013) immediately after treatment cessation. Pt accumulation was also observed in the DRG of oxaliplatin-treated mice (Park et al. 2015). Pt levels in both tissues were still detectable after a follow-up period of 5-8 weeks, but were decreased compared with the previous time point (Holmes et al. 1998, Cavaletti et al. 2001). Accumulation of Pt within

nervous tissues is dose-dependent: Pt levels in the neuronal population of the DRG and sciatic nerve increased with cumulative doses of oxaliplatin (4 mg/kg administered twice a week for 2, 4 or 6 weeks), and accumulation was evident in the mitochondrial fraction of both tissues (Nishida et al. 2018). Conversely, plasma levels of Pt were approximately 10-fold lower than those in neuronal tissues, thus supporting the evidence that Pt accumulates within sensory neurons (Nishida et al. 2018). In rats administered bi-weekly with oxaliplatin, Pt accumulated increasingly within the DRG, sural and sciatic nerves in a time- and dose-dependent manner over the course of eight weeks (Screnci et al. 2000). Additionally, Pt levels in the brain and spinal cord were at least 10-fold lower than in the peripheral tissues (Screnci et al. 2000, Ip et al. 2013).

1.3.5 Preclinical models of OIPN

Many animal models of OIPN have been described in the literature. Models differ in treatment schedule, administration route, cumulative dose and species used. Most studies are conducted in male rats and mice, and oxaliplatin is administered through the intraperitoneal (IP) or intravenous (IV) route, for a systemic exposure to the compound [reviewed in (Hopkins et al. 2016)]. Typically, animal models do not involve the induction or implantation of tumour loads in the animals. It might be argued that the incorporation of the tumour environment in these models would be more clinically relevant and would provide more translational results. However, animal welfare needs to be taken into account and causing excessive stress and/or pain needs to be avoided. Additionally, evaluation of chemotherapy-induced pain-like behaviours would be hindered if the animals displayed signs of pain and/or ill health non-related to chemotherapy administration. OIPN animal models can be broadly divided into acute and chronic models. Acute models rely on the administration of a single dose (1-12 mg/kg) of oxaliplatin, which results in the rapid development of both cold and mechanical allodynia [reviewed in (Hopkins et al. 2016)]. By contrast, chronic models comprise the repeated administration of oxaliplatin, typically with an intermittent regimen to mimic the clinical administration schedule. Chronic models are highly heterogeneous across studies from different research groups, both in terms of length of treatment and of final cumulative dose [reviewed in (Hopkins et al. 2016)]. Mechanical and/or cold hypersensitivity are commonly observed after chronic doses of oxaliplatin, although the duration and severity of pain-like behaviours vary among investigations, depending on the methodological approach used.

A few studies have employed primates, which are phylogenetically closer and display similar neuroanatomical characteristics to humans [reviewed in (Hama et al. 2018)]. Hence, they would provide a more translational tool in the investigation of new analgesic therapies for CIPN. Oxaliplatin-induced cold hypersensitivity was observed in a study comparing the efficacy of

three different analgesic compounds (duloxetine, pregabalin and tramadol) in cynomolgus macaques and rats, although primates displayed an earlier onset compared with rats (Shidahara et al. 2016). In primates, only duloxetine displayed an analgesic effect, whereas all three compounds were effective in the rat model, thus suggesting that OIPN pathophysiology and symptoms may be species-specific. Nevertheless, differences in methodology (i.e. administration route and schedule and behavioural tests employed) may also have contributed to such differences between models (Shidahara et al. 2016). Cold hypersensitivity was also observed in another macaque model of OIPN, where duloxetine was also able to relieve oxaliplatin-induced pain-like behaviour (Nagasaka et al. 2017). Another advantage of primate models is the possibility to infuse oxaliplatin IV, following clinical instructions (Shidahara et al. 2016, Nagasaka et al. 2017). Nevertheless, the use of primates for research is associated with more complex ethical implications and concerns compared with rodent models. Moreover, the practical feasibility of using primate models is limited by the amount of care necessary to maintain and develop them. For these reasons, rodents remain the predominant model used in preclinical CIPN research, despite their limitations.

1.3.5.1 Behavioural assessments in animal models

The intrinsic limitation of preclinical models in the study of pain is the fact that animals cannot self-report pain. Therefore, pain evaluation relies on the observation of pain-like behaviours evoked by noxious stimuli, while symptoms like spontaneous pain, paresthesias/dysesthesias and numbness are more challenging to investigate. Furthermore, the usefulness of these models in the investigation of new potential treatments for CIPN (and pain in general) has been questioned, after many failed clinical trials on analgesic compounds that were effective in the preclinical phase [reviewed in (Percie du Sert and Rice 2014)].

Mechanical-evoked responses were first assessed with the Randall-Selitto (or paw pressure) test (Randall and Selitto 1957): animals are physically restrained to apply a progressively increasing mechanical pressure to the paw or tail, until the nociceptive threshold is reached (withdrawal or vocalisation). More commonly, mechanical hypersensitivity (either allodynic or hyperalgesic response) is evaluated with von Frey filaments, which are nylon monofilaments that allow application of a reproducible, specific force upon bending. Animals are placed in individual cages that allow to access the paws and the filament is gently applied to the plantar surface. Paw withdrawal, flicking and/or licking are registered as pain-like responses. Less commonly, other body surfaces can be assessed, including the snout for the evaluation of orofacial pain or the abdomen for the assessment of visceral pain. Von Frey testing can be performed with different protocols. The most common approach is the up-down method, which involves the repeated

application of filaments to identify the 50% withdrawal threshold, i.e. the force necessary to induce a response in 50% of the animals. If no response is observed after application of the first filament, the test proceeds with the application of another one with increasing force; conversely, if animals do respond to the filament, a new one with lower force is tested. According to the presence or lack of response to the different forces, the test is repeated between four and nine times on each paw (Chaplan et al. 1994). Therefore, limitations of this technique comprise the variability in the number of stimulations among animals and the potential sensitisation that may occur after repeated stimulations. The frequency (or percent) method consists in the repeated application of filaments (usually 5-10 times for every animal) with increasing forces and the number of pain-like responses is counted (Kim and Chung 1992). In this case, withdrawal threshold cannot be identified. Risk of sensitisation is a caveat of this approach as well but, unlike the up-down technique, it allows all the animals to be exposed to the same amount of stimulations. Electronic von Frey apparatuses can also be employed for the automated application of increasing forces (Martinov et al. 2013), although a trained experimenter is still required to evaluate the animals' responses.

Pain-like behaviour in response to thermal stimuli can be measured through a variety of tests. In the tail flick test (D'amour and Smith 1941), animals' tails are exposed to a hot stimulus (i.e. hot water or radiant heat) and the withdrawal latency is measured. Alternatively, the hot plate test (Woolfe and Macdonald 1944) allows to measure the heat threshold in the hind paws, as animals are placed on a hot surface and latency to response (i.e. paw withdrawal, licking and jumping) is recorded. The plate can be kept at a constant noxious temperature (> 50°C) or can be set to progressively increase the temperature, starting from non-noxious ones (42°C), until a response is observed (Ogren and Berge 1984). The cold plate works in a similar way: animals are placed on a cooled surface that can be set to specific noxious and innocuous temperatures (-5°C to 25°C) and latency to withdrawal is measured to identify the cold pain threshold (Allchorne et al. 2005). Sensitivity to cool temperatures can also be measured with the acetone test (Yoon et al. 1994), although this test does not allow to expose the animals to specific temperatures. Animals are placed in individual cages with mesh floor and a small amount of acetone is applied to the hind paws. The cold stimulus is provided by the evaporation of the acetone, which creates a cooling sensation. Cold sensitivity can be assessed either by counting the number of withdrawal responses (Yoon et al. 1994) or by scoring the severity of the responses (Flatters and Bennett 2004). Lastly, the thermal place preference allows to monitor animals as they move freely on two contiguous plates set at fixed temperatures, and to measure the amount of time spent on both surfaces. One plate is set at an innocuous temperature while the other is set at a specific noxious one (Moqrich et al. 2005).

In recent years, behavioural tests that do not rely on evoked pain-like responses have been developed in attempt to investigate spontaneous pain and better mimic the clinical syndrome. In this context, deficits in natural behaviours like wheel running and burrowing may be regarded as signs of spontaneous pain. Wheel running behaviour has been observed in laboratory rodents since the end of the 19th century (Stewart et al. 1985) and has been widely used ever since. To perform the test, animals are singly caged and are given free access to a wheel apparatus. Running activity can be measured via a software connected to the wheel itself, thus allowing experimenters to monitor the behaviour over long periods of time. In the burrowing test (Deacon 2006), animals are placed in individual cages and have access to a burrowing tube filled with a burrowing substrate for a set amount of time. The amount of material left in the tube at the end of the test is weighed to assess potential alterations in burrowing behaviour compared with baseline or control animals.

1.4 Mitochondria

Mitochondria are commonly known as the 'powerhouse of the cell', as they sustain the functionality of every cell, except for erythrocytes, through energy production in form of ATP via oxidative phosphorylation (OXPHOS). They are also involved in other essential functions, including reactive oxygen species (ROS) generation and intracellular calcium homeostasis. First observations of cellular components that were later identified as mitochondria date back to the 1840s. The development of better staining and imaging techniques by 1890s allowed Altmann to properly observe structures, which he named bioblasts, within all cells (Altmann 1890). Bioblasts were later renamed mitochondria by Benda in 1898 (Benda 1898). The development of electron microscopy allowed to obtain the first high-resolution images of mitochondria in 1953, thus allowing to understand the internal structure of the organelles (Palade 1953, Sjostrand 1953). Figure 1-6 illustrates the main features of mitochondrial structure. Mitochondria are encapsulated within two separate membranes. The outer membrane (OM) separates mitochondria from the cell cytoplasm but is selectively permeable to ions and small molecules that can cross the membrane through porins. Conversely, the inner membrane (IM) is impermeable to all ions and molecules, which can only cross it via specific transporters. The IM encapsulates the innermost mitochondrial matrix, which contains mitochondria's own DNA, ribosomes for protein synthesis and granules, which are rich in calcium and phosphorus (Wolf et al. 2017). The IM is characterised by deep invaginations, named cristae, where the complexes of OXPHOS reside. The tiny gap between the two membranes (approximately 20 nm) represents the intermembrane space (Kühlbrandt 2015). The structure of mitochondria is strikingly similar to that of prokaryotic cells. In 1967 Lynn Margulis proposed that mitochondria and other eukaryotic organelles like plant chloroplasts originated from a bacterium engulfed by an ancient eukaryotic cell, thus living in endosymbiosis (Sagan 1967). Further studies in the '70s and '80s identified homologous oligonucleotide sequences between mitochondrial and prokaryotic ribosomal RNAs (Bonen et al. 1977, Yang et al. 1985), thus supporting the endosymbiotic hypothesis.

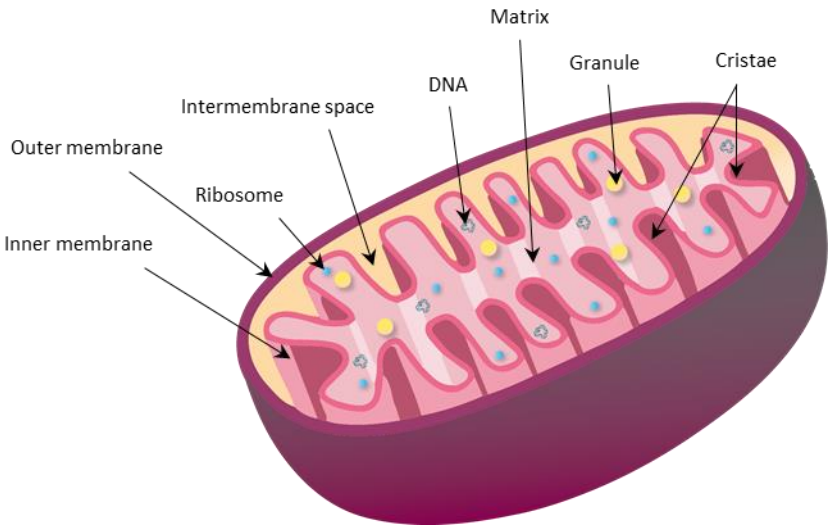

Figure 1-6 Structural organisation of a mitochondrion

The outer and inner membranes generate two distinct areas within a mitochondrion: the intermembrane space, between the two membranes, and the mitochondrial matrix, encapsulated within the inner membrane, and containing DNA, ribosomes and granules. Part of this figure was created with BioRender.com.

1.4.1 Oxidative phosphorylation

Cellular respiration begins in the cytoplasm with the conversion of one molecule of glucose into two molecules of pyruvate and ATP during anaerobic glycolysis. Pyruvate is converted to acetyl-Coenzyme A (CoA) in the mitochondrial matrix and enters the citric acid cycle for the production of nicotinamide adenine dinucleotide (NADH) and flavin adenine dinucleotide ($FADH_2$). NADH and $FADH_2$ act as electron carriers in OXPHOS, which is the main source of energy production for the cell. Indeed, the final yield of one OXPHOS reaction is 30-38 molecules of ATP. The role of mitochondria in the aerobic metabolism through OXPHOS has been known since 1940s, when isolation of intact mitochondrial fractions allowed to demonstrate the mitochondrial-specific distribution of enzymes involved in ATP production [reviewed in (Pagliarini and Rutter 2013)]. It wasn't until 1961 that scientists finally understood the principles of OXPHOS, with Mitchell's theory of chemiosmotic coupling (Mitchell 1961). Mitchell proposed that ATP generation was driven by a proton motive force, where the pumping of protons across the IM is coupled with electron transfer across complexes of the electron transport chain (Mitchell 1961). The validity of Mitchell's theory was debated for many years, until supporting evidence emerged and Mitchell was awarded with the Nobel Prize in Chemistry in 1978.

OXPHOS takes place in five protein complexes located in the cristae of the IM. Complex I to IV make up the electron transport chain (ETC) system and are responsible for the transfer of electrons through a series of redox reactions, which eventually lead to the reduction of O_2 into water. Downstream of the ETC, Complex V converts adenosine diphosphate (ADP) to ATP. The abundance of cristae within the mitochondria reflects the energy demand of the tissue they are supplying: high-energy demand-tissues, like skeletal muscles and the heart, are characterised by dense, closely stacked cristae, where OXPHOS complexes can accumulate. By contrast, tissues that require less energy are characterised by less dense cristae (Kühlbrandt 2015). OXPHOS reactions are described below [reviewed in (Papa et al. 2012)] and illustrated in Figure 1-7:

- Complex I (NADH dehydrogenase) is the largest complex in the ETC, comprising 45 different subunits, and represents the first point of entry for electrons. Complex I oxidises NADH to NAD^+ by transferring two electrons to ubiquinone (or coenzyme Q), which is reduced to ubiquinol. At the same time, four protons are pumped from the matrix to the intermembrane space.
- Complex II (succinate dehydrogenase) consists of only 4 subunits and represents the second point of entry for electrons. It is the only complex shared between the ETC and the citric acid cycle, from which it receives electrons via succinate. Succinate is oxidised to fumarate and two electrons are transferred to flavin adenine dinucleotide (FAD), which is reduced to $FADH_2$. $FADH_2$ is oxidised back to FAD by transferring two electrons to ubiquinone. No protons are pumped into the intermembrane space through Complex II.
- Complex III (coenzyme Q: cytochrome c-oxidoreductase) comprises 11 subunits. Ubiquinol transports electrons from Complex I and II to Complex III, where it donates its electrons to two molecules of cytochrome c. At the same time, four protons are released into the intermembrane space.
- Complex IV (cytochrome c oxidase), composed of 13 subunits, catalyses the oxidation of cytochrome c, whose electrons are transferred to O_2, thus reducing it to H_2O. Four more protons are pumped into the intermembrane space. The result of these ETC reactions is the generation of a proton gradient across the IM. This gradient generates both a difference in pH (ΔpH_m; matrix pH $\sim$ 8 and intermembrane space pH $\sim$ 7) and a mitochondrial membrane potential ($\Delta\psi_m$) across the IM, with the matrix being characterised by a negative voltage.
- Complex V (ATP synthase) comprises two distinct functional units, which are connected by a central stalk: F_0, embedded in the IM, and F_1, in the matrix. Complex V exploits the electrochemical gradient generated by the accumulation of protons in the intermembrane space to convert ADP and inorganic phosphate (Pi) to ATP. In particular, protons flow back

into the matrix passing through F_0 and cause the rotation of F_1, thus modifying its conformation and allowing it to bind ADP and Pi for ATP synthesis. Complex V is the only reversible complex, therefore it can either synthesise ATP from ADP and Pi or act as an ATPase and hydrolyse ATP back to ADP and Pi, based on the cell energy demand.

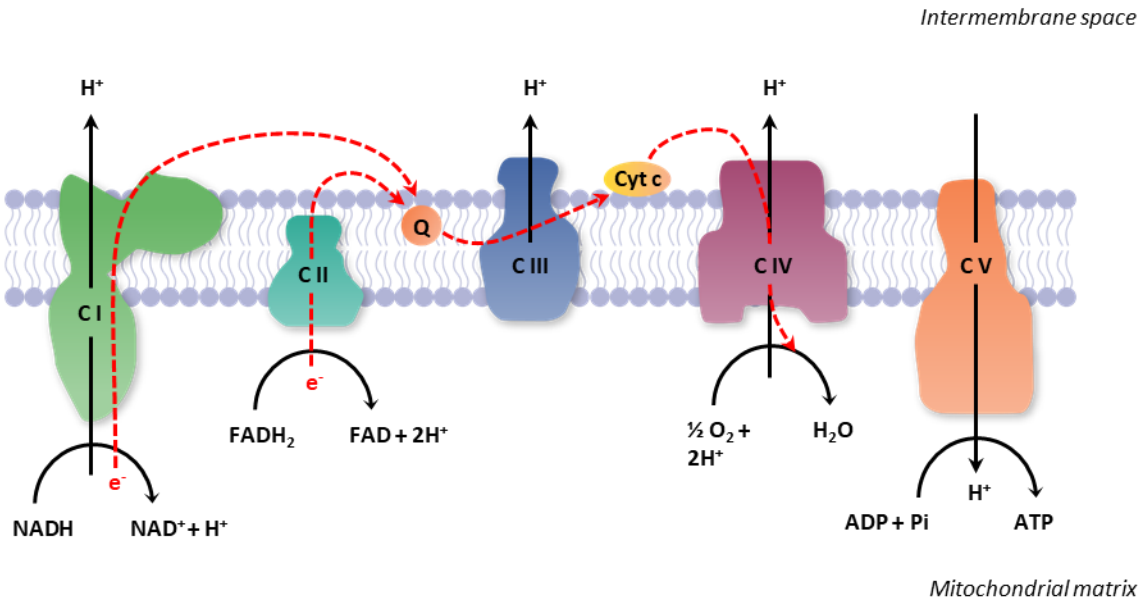

Figure 1-7 Mitochondrial complexes responsible for oxidative phosphorylation

In the electron transport chain (Complex I to IV) electrons are transferred across complexes while protons are pumped into the intermembrane space, thus generating a proton motive force. As protons flow back into the mitochondrial matrix through Complex V, ADP is converted to ATP. CI-V: Complex I-V; Q: coenzyme Q; Cyt c: cytochrome c; Pi: inorganic phosphate.

1.4.2 Reactive oxygen species production

Mitochondria are the main source of ROS production inside the cell. During OXPHOS, electrons may leak from the ETC, especially from Complex I and III, and reduce molecular oxygen to superoxide ($O_2^{\bullet -}$), a highly reactive ROS. $O_2^{\bullet -}$ is normally dismutated to the more stable hydrogen peroxide (H_2O_2) by superoxide dismutase (SOD) enzymes, including manganese-dependent SOD (MnSOD or SOD2), in the mitochondrial matrix, and copper-zinc SOD (CuZnSOD or SOD1), in the intermembrane space [reviewed in (Kowaltowski et al. 2009)]. $O_2^{\bullet -}$ scavenging is pivotal for cell functionality and survival. For instance, MnSOD knockout mice displayed reduced growth rates, CNS and cardiac injuries, motor deficits and survived only up to 18 days after birth (Lebovitz et al. 1996). CuZnSOD knockout mice were also characterised by decreased growth rates and progressive loss of skeletal muscle mass, which was associated with motor deficits compared with wild-type animals (Muller et al. 2006). H_2O_2 can then be transported to the cytoplasm and scavenged by cytosolic antioxidant enzymes, including catalase, glutathione peroxidase (GPx),

and thioredoxin reductase (TrxR) [reviewed in (Kowaltowski et al. 2009)]. Together with ROS, mitochondria also produce reactive nitrogen species (RNS) by reducing nitrite to nitric oxide (NO) after electron leakage from Complex III and IV [reviewed in (Gupta and Igamberdiev 2016)]. NO can interact with $O_2^{\cdot -}$ and generate peroxynitrite (Radi et al. 2002).

1.4.3 Intracellular calcium homeostasis

Intracellular Ca^{2+} is involved in many essential cellular functions, including cell proliferation, cell death, gene transcription and neurotransmitter exocytosis, and its concentration ($[Ca^{2+}]_i$) is finely regulated by different systems. Mitochondria contribute to the maintenance of $[Ca^{2+}]_i$ through the accumulation of Ca^{2+} within their matrix or its extrusion into the cytoplasm via different channels in the mitochondrial membranes (Figure 1-8).

The driving force for Ca^{2+} uptake is the $\Delta\psi_m$ generated by OXPHOS across the IM. To be able to reach the mitochondrial matrix, Ca^{2+} has to move across both the OM and the IM. The OM is highly permeable to Ca^{2+}, thanks to the expression of voltage-dependent anion-selective channel proteins (VDACs). Three VDAC isoforms have been identified so far (VDAC1, VDAC2 and VDAC3) [reviewed in (Shoshan-Barmatz et al. 2017)] and overexpression of any of the three isoforms resulted in increased mitochondrial Ca^{2+} uptake in HeLa cells (De Stefani et al. 2012). An excessive uptake of Ca^{2+} within the mitochondria triggers the release of pro-apoptotic molecules and VDACs are involved in the regulation of these apoptotic signals. For instance, silencing of VDAC1 expression in HeLa cells reduced cell apoptosis induced by H_2O_2 or ceramide. VDAC2 silencing had the opposite effect, thus suggesting that VDAC1 has a pro-apoptotic role, whereas VDAC2 promotes cell survival (De Stefani et al. 2012). The movement of Ca^{2+} ions across the IM is mediated mainly by the mitochondrial calcium uniporter (MCU). Indeed, overexpression of MCU in HeLa cells significantly increased mitochondrial Ca^{2+} uptake, whereas MCU silencing inhibited Ca^{2+} accumulation within the mitochondria (De Stefani et al. 2011). Surprisingly, MCU knockout mice did not display any deficit in basal metabolism, physiological function or mitochondrial number/morphology compared with wild-type mice, despite the lack of mitochondrial Ca^{2+} uptake (Pan et al. 2013). However, viability was only maintained in mixed genetic backgrounds, as demonstrated by MCU deletion in inbred strains of C57BL/6 mice that died at embryonic stages (Murphy et al. 2014). MCU forms the actual pore in the IM but is associated with many other proteins that modulate its activity. In fact, the MCU multiprotein complex comprises different proteins other than MCU: MCUb, the essential MCU regulator (EMRE) and the mitochondrial calcium uniporter regulator 1 (MCUR1) localise across the membrane; and the associated regulatory subunits mitochondrial calcium uptake 1, 2 and 3 proteins (MICU1, MICU2 and MICU3) reside in the intermembrane space [reviewed in (Mishra

et al. 2017)]. MCU has a low affinity for Ca^{2+} and therefore requires high $[Ca^{2+}]_i$ to mediate Ca^{2+} uptake. In case of low $[Ca^{2+}]_i$, the leucine zipper and EF-hand containing transmembrane protein 1 (LEMT1), a Ca^{2+}/H^+ antiporter (Jiang et al. 2009), may provide an alternative Ca^{2+} uptake route (Waldeck-Weiermair et al. 2011).

Ca^{2+} efflux from the mitochondria is mediated principally by the $Na^+/Ca^{2+}/Li^+$ exchanger (NCLX), which extrudes Ca^{2+} in exchange for Na^+ or Li^+ ions (Palty et al. 2004). NCLX silencing in a cell line inhibited Ca^{2+} efflux and conditional NCLX knockout in mice resulted in rapid animal death, which was associated with cardiac dysfunction (Luongo et al. 2017). Another Ca^{2+} efflux mechanism involves the mitochondrial permeability transition pore (mPTP). Different proteins, including VDAC, have been suggested as components of the mPTP, but only the role of cyclophilin D (CypD) has been confirmed in the opening of mPTP. In pathological conditions, mPTP is involved in cell death regulation, as its irreversible opening leads to $\Delta\psi_m$ loss, swelling and eventually cell death via necrosis [reviewed in (Tsujimoto and Shimizu 2007)]. However, transient opening of mPTP has a role in Ca^{2+} efflux. Indeed, CypD deletion in a mouse model resulted in increased heart dysfunction and mortality, which were associated with Ca^{2+} overload within the mitochondrial matrix of cardiomyocytes (Elrod et al. 2010). LEMT1 may also mediate Ca^{2+} efflux, however its exact role still needs to be elucidated after many conflicting results following LEMT1 silencing *in vitro* [reviewed in (Giorgi et al. 2018)].

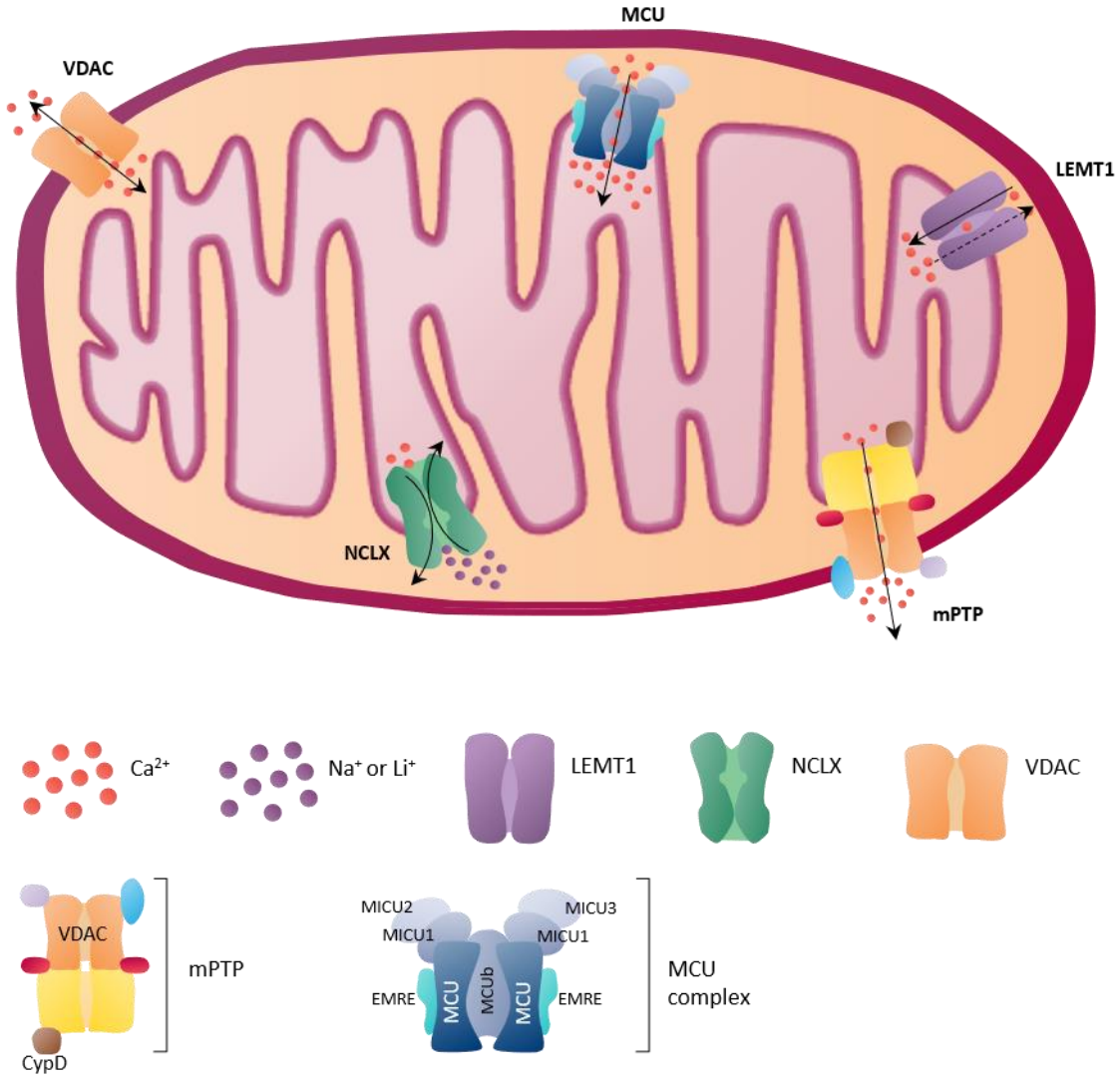

Figure 1-8 Ca^{2+} channels in the mitochondrial membranes

The voltage-dependent anion-selective channel proteins (VDACs) on the outer membrane are highly permeable to Ca^{2+}. The mitochondrial calcium uniporter (MCU) and the leucine zipper and EF-hand containing transmembrane protein 1 (LEMT1), located in the inner membrane, mediate calcium influx into the mitochondrial matrix. The $Na^{+}/Ca^{2+}/Li^{+}$ exchanger (NCLX) in the inner membrane extrudes calcium ions whilst simultaneously pumping sodium or lithium ions into the matrix. LEMT1 may also be involved in Ca^{2+} efflux. The mitochondrial permeability transition pore (mPTP), a multiprotein complex that may be associated with VDAC, contributes to the extrusion of calcium ions from the mitochondrion.

1.4.4 Mitochondrial DNA

Mitochondria are peculiar organelles, as they contain their own DNA, which is derived from the α-proteobacterium engulfed by the ancient eukaryotic cell. Mitochondrial DNA (MtDNA) is completely maternally inherited (Giles et al. 1980, Pyle et al. 2015), as paternal MtDNA is removed during embryogenesis after ubiquitination of sperm mitochondria (Sutovsky et al. 1999). MtDNA is a 16.6 kb circular molecule made of two strands, a heavy-strand, rich in guanine, and a light-strand, rich in cytosine, and does not contain intronic regions [reviewed in (Chinnery and Hudson 2013, Wallace 2013). Unlike genomic DNA, MtDNA is not packaged with histones into chromatin, but is still assembled into DNA-protein complexes named nucleoids. Nucleoids contain proteins for MtDNA replication and transcription, as well as other proteins involved in RNA stability, protein quality control and lipid metabolism [reviewed in (Bogenhagen 2012)]. MtDNA comprises 37 genes:

- 13 genes encode for OXPHOS proteins: 7 subunits of Complex I; 1 subunit of Complex III; 3 subunits of Complex IV; and 2 subunits of Complex V. Therefore, Complex II is the only ETC complex that is entirely encoded by nuclear DNA.
- 24 genes encode for RNA products necessary for mitochondrial protein synthesis: 22 transfer RNA (tRNA) and 2 ribosomal RNA (rRNA) products.

Nuclear DNA encodes for the rest of the 79-80 subunits of the OXPHOS system and for proteins required for their assembly, it regulates MtDNA replication and transcription and mitochondrial fusion and fission.

The number of mitochondria per cell varies depending on the energy demand. For instance, erythrocytes do not contain mitochondria at all, while liver and neuronal cells contain over thousands. Moreover, the amount of MtDNA within each mitochondrion is variable as well, and each organelle can contain 0-10 MtDNA molecules. Consequently, MtDNA copy number can vary between 10 and 10 000 per cell [reviewed in (Chinnery and Hudson 2013, Wallace 2013)].

1.4.5 Mitochondrial dysfunction in CIPN

Mitochondrial dysfunction has been accepted has a major contributor to the development and maintenance of CIPN, and evidence supporting this hypothesis has been extensively reviewed by Trecarichi and Flatters (2019). Given the multiple roles of mitochondria in maintaining cell functionality, their dysfunction can manifest in various forms, including altered mitochondrial morphology, bioenergetics and ROS generation.

1.4.5.1 Morphological changes

The first evidence of mitochondrial dysfunction in CIPN came from an extensive electron microscopy investigation of the saphenous nerves in paclitaxel-treated rats (Flatters and Bennett 2006). The authors observed that myelinated and unmyelinated fibres from both vehicle- and paclitaxel-treated rats contained normal and atypical (vacuolated for more than 50% and/or swollen) mitochondria. However, the incidence of atypical organelles was significantly increased by paclitaxel treatment. The investigation was conducted at three key time points: day 7, 24 hours after the last paclitaxel injection and prior to the development of pain-like behaviour (assessed in terms of mechanical hypersensitivity); day 27, when the pain-like behaviour reached its maximum severity; and day 160, when pain-like behaviour had resolved. The paclitaxel-induced increase in the incidence of atypical mitochondria in A- and C-fibres was observed at day 7 and 27, but not at day 160, thus suggesting a role for atypical mitochondria in the development and maintenance of the neuropathy (Flatters and Bennett 2006). Further studies in rat and mouse models of paclitaxel-induced neuropathy confirmed these findings and atypical mitochondria were observed in the DRG (Barrière et al. 2012, Krukowski et al. 2015), dorsal root (Xiao et al. 2011), saphenous (Jin et al. 2008, Xiao et al. 2011, Janes et al. 2013, Nieto et al. 2014), sciatic (Barrière et al. 2012, Wu et al. 2014, Bobylev et al. 2015, Krukowski et al. 2015, Chen et al. 2017, Jia et al. 2017) and tibial nerve (Bobylev et al. 2015). Abnormal mitochondria appeared only in sensory axons. By contrast, myelinated motor axons and Schwann cells in the ventral and dorsal root and in the saphenous nerve displayed no difference in atypical mitochondria incidence between paclitaxel- and vehicle-treated rats (Xiao et al. 2011). Reports of atypical mitochondria were not limited to models of paclitaxel-induced neuropathy. Vincristine-treated rats showed significantly more atypical mitochondria in A- and C-fibres of the sciatic nerve compared with saline-treated controls 19 days after treatment initiation, when animals displayed mechanical and thermal hypersensitivity (Xu et al. 2016). Abnormal mitochondria were observed in the saphenous nerve of oxaliplatin-, bortezomib- and vehicle-treated rats (Xiao et al. 2012, Zheng et al. 2012). However, at day 35, when chemotherapy-treated animals reached the peak of pain-like behaviour severity, the incidence

of vacuolated/swollen mitochondria in A- and C-fibres from oxaliplatin- and bortezomib-treated animals was significantly increased compared with vehicle-treated controls (Xiao et al. 2012, Zheng et al. 2012). As reported for paclitaxel (Xiao et al. 2011), the incidence of abnormal mitochondria in Schwann cells was very low and no difference relative to the control group could be detected after oxaliplatin (Xiao et al. 2012) or bortezomib treatment (Zheng et al. 2012). Maj and colleagues reported similar findings in a cisplatin-induced mouse model. They observed a significantly increased incidence of atypical mitochondria, characterised by disorganised cristae and membranes, in the DRG and sciatic nerves of cisplatin-treated mice 3 weeks after cisplatin administration compared with saline-treated controls (Maj et al. 2017).

Mitochondrial morphological abnormalities have been observed in a few clinical studies as well. Skin punches from the distal leg were collected from seven advanced breast cancer patients receiving ixabepilone. The number and structure of mitochondria in Remak Schwann cells was assessed to generate the following grading scale: grade 0 = normal; grade 1 = distortion of cristae; grade 2 = loss of cristae and homogenous matrix; grade 3 = electron dense matrix and distorted OM; and grade 4 = electron dense matrix, vacuolation and fragmentation (Ebenezer et al. 2014). Increasing cumulative doses of ixabepilone were associated with a progressive loss of mitochondria and an increased incidence of abnormal organelles (grade 3 or 4), coupled with a parallel decrease in the incidence of normal mitochondria (grade 0 or 1) (Ebenezer et al. 2014). Additionally, swollen and vacuolated mitochondria were visible in the electron micrographs of myelinated and unmyelinated axons in the sural nerve of a pancreatic carcinoma patient following three cycles of docetaxel (Fazio et al. 1999) and of a lung adenocarcinoma patient after 17 courses of paclitaxel (Sahenk et al. 1994).

1.4.5.2 Altered bioenergetics

Assays of mitochondrial functionality allow to identify specific aspects of mitochondrial function that are impaired by chemotherapy regimens. *In vitro* exposure of immortalised DRG neurons to increasing concentration of paclitaxel (0, 1, 5, 10 and 100 µM) for 24 hours resulted in a dose-dependent reduction in metabolic activity and $\Delta\psi_m$, which was concomitant with a progressive increase in mitochondrial volume (McCormick et al. 2016, Galley et al. 2017). By contrast, one hour exposure of primary cultures of naïve rat DRG to 10 nM or 10 µM paclitaxel in our lab resulted in no change in mitochondrial or glycolytic functionality, nor in ATP or ADP levels compared with vehicle-treated controls; this suggested that prolonged *in vivo* exposure to paclitaxel is necessary to observe a metabolic deficit in DRG neurons (Duggett et al. 2017). However, it is worth mentioning that the differences in experimental settings between the two research groups may be responsible for the contrasting results. Mouse DRG neurons exposed to

10 µM cisplatin for 24 hours presented deficits in OXPHOS function as well (Gorgun et al. 2017). Additionally, exposure of the neuroblastoma Neuro-2a cell line to 50 µmol oxaliplatin for 24 hours resulted in loss of $\Delta\psi_m$ compared with control cells (Areti et al. 2017a).

The effects of *in vivo* exposure to chemotherapy on bioenergetics have also been widely investigated. In *ex vivo* preparations of teased rat sciatic nerves, Complex I and Complex II-mediated respiration, ATP production and O_2 consumption rates were significantly impaired by paclitaxel, oxaliplatin and bortezomib compared with the vehicle-treated group (Zheng et al. 2011, Zheng et al. 2012). Impaired ATP production was also reported in the saphenous nerve of rats treated with paclitaxel, oxaliplatin and bortezomib (Janes et al. 2013). Isolated mitochondria from the sciatic nerve of oxaliplatin-treated rats displayed a significant reduction in Complex I and II, and to a lesser extent, of Complex III and IV activity, in mitochondrial $\Delta\psi_m$ and in ATP production compared with control animals (Areti et al. 2017a, Areti et al. 2017b, Areti et al. 2018). Deficits in Complex I, II, III and V activity were also observed in isolated brain mitochondria from oxaliplatin-treated rats (Waseem and Parvez 2016). Using the Seahorse XF Analyzer (see section 2.4.1), which allows to simultaneously measure OXPHOS and glycolytic function in intact cells, our research group investigated mitochondrial function in intact DRG neurons from paclitaxel-treated rats prior to (day 7), during (day 24 to 44) and at the resolution of pain-like behaviour (day 170-218) (Duggett et al. 2017). At day 7, but not at the peak pain or resolution time points, maximal respiration and spare reserve capacity (ability of mitochondria to respond to stress) were significantly decreased in DRG neurons from paclitaxel-treated animals compared with vehicle-treated controls. Basal glycolysis and glycolytic capacity were significantly increased at the peak pain time point in DRG neurons of paclitaxel-treated rats, thus suggesting an increased tendency to switch to glycolysis, which may be an adaptive and protective response of DRG neurons to avoid producing excessive ROS. Additionally, ATP levels at day 7 and peak pain were significantly lower in DRG neurons form paclitaxel-treated rats, while ADP levels and the ATP:ADP ratio were unaltered by paclitaxel, thus suggesting that the compound does not induce a reversal in Complex V activity (Duggett and Flatters 2017). Another research group has employed the Seahorse XF Analyzer to investigate mitochondrial functionality following *in vivo* exposure to cisplatin. Tibial nerves and DRG neurons from cisplatin-treated mice displayed a significant reduction in basal respiration, ATP turnover-linked respiration, maximal respiration capacity (Krukowski et al. 2017, Maj et al. 2017) and spare reserve capacity (Maj et al. 2017) compared with saline-treated controls. Additionally, the authors reported a cisplatin-induced deficit in $\Delta\psi_m$ in DRG neurons (Maj et al. 2017). However, a different study from the same investigators only reported a cisplatin-induced deficit in

maximal respiration capacity in DRG neurons, whilst other OXPHOS parameters remained unaffected (Krukowski et al. 2017).

1.4.5.3 Uncontrolled oxidative stress

An extensive body of evidence is present in the literature about chemotherapy-induced uncontrolled ROS generation, both after *in vitro* and *in vivo* exposure to chemotherapy. Most investigations on CIPN-related oxidative stress have focused on paclitaxel. Several studies have demonstrated a significant paclitaxel-induced increase in ROS/RNS generation, measured as production of H_2O_2, peroxynitrite, NO, 8-isoprostane F2α (end product of the peroxidation of arachidonic acid) or malondialdehyde (end product of lipid peroxidation) in plasma (Ishii et al. 2018), isolated DRG mitochondria (Barrière et al. 2012), sciatic (Galley et al. 2017) and saphenous nerve (Galley et al. 2017), compared with control animals. Additionally, paclitaxel inhibited MnSOD activity, but stimulated the activation of nitric oxide synthase (NOS) and of nicotinamide adenine dinucleotide phosphate (NADPH) oxidase in the spinal cord, which would translate into increased production on NO and $O_2^{\bullet-}$, respectively. (Doyle et al. 2012). Our group measured ROS levels in the DRG and spinal cord *in situ* during the time course of paclitaxel-induced neuropathy (Duggett et al. 2016). Paclitaxel significantly increased ROS levels in IB4+ DRG and spinal cord neurons prior to the development of paclitaxel-induced pain-like behaviour and, to a lesser extent, at the peak of pain severity. Moreover, at the peak of pain severity, MnSOD, CuZnSOD and GPx activities were increased in the DRG and saphenous nerves of paclitaxel-treated animals compared with vehicle-treated controls (Duggett et al. 2016). By contrast, there was no difference in antioxidant activity prior to the development of pain-like behaviour, with the exception of paclitaxel-increased CuZnSOD activity, thus suggesting that the endogenous antioxidant response was insufficient and led to excessive ROS accumulation. Chronic oxaliplatin administration was responsible for an increased incidence of ROS and RNS in the DRG (Toyama et al. 2014, Areti et al. 2017a, Areti et al. 2017b) and sciatic nerve (Areti et al. 2017a, Areti et al. 2017b, Areti et al. 2018) compared with vehicle-treated animals. At the same time, the activity of antioxidant enzymes was inhibited by oxaliplatin: in oxaliplatin-treated animals, MnSOD activity was decreased in the DRG (Areti et al. 2017a, Areti et al. 2017b, Areti et al. 2018), sciatic (Areti et al. 2017a, Areti et al. 2017b, Areti et al. 2018) and saphenous nerve (Janes et al. 2013), while GSH activity was significantly decreased in isolated brain mitochondria (Waseem et al. 2016). Oxidative stress was also evaluated in terms of lipid, protein and DNA oxidation, whose levels were increased in the plasma, sciatic nerve and spinal cord (Di Cesare Mannelli et al. 2012) and brain mitochondria (Waseem et al. 2016) of oxaliplatin-treated rats. In a bortezomib-induced neuropathy rat model, MnSOD activity in the saphenous nerve was significantly inhibited at the peak of bortezomib-induced mechanical hypersensitivity (Janes et

al. 2013). In addition, vincristine stimulated NADPH oxidase activity in the spinal dorsal horn, which would then lead to increased ROS production (Xu et al. 2016).

1.4.5.4 Pharmacological modulation of mitochondria in CIPN

Over the years, several compounds that affect one or more aspects of mitochondrial functionality have been tested *in vivo* for their potential prophylactic or analgesic effects in CIPN [reviewed in (Trecarichi and Flatters 2019)]. Compounds can be broadly classified in three categories and are summarised in Table 1-5:

- Known mitochondrial modulators, which selectively modulate ETC complexes.
- ROS scavengers and antioxidant compounds.
- Other compounds that ameliorate mitotoxicity via mechanisms non-related to the ETC or ROS production.

Each complex of the ETC can be specifically inhibited by a selective inhibitor. In particular, rotenone inhibits Complex I, 3-Acetylphenyl N-(P-Tolyl) carbamate (3-NP) inhibits Complex II, antimycin A inhibits Complex III, sodium cyanide inhibits Complex IV and oligomycin inhibits Complex V**.** A single injection of any of these inhibitors was able to produce a moderate reduction in vincristine-induced mechanical hyperalgesia, particularly within the first 30 minutes post-administration (Joseph and Levine 2006). In our lab, a single injection of rotenone attenuated established paclitaxel-induced mechanical hypersensitivity, although it caused deficits in the normal motor function (Griffiths and Flatters 2015). In the same animal model, antimycin A was able to reverse established pain-like behaviour and to inhibit its development when administered prophylactically (Griffiths and Flatters 2015). However, contrary to these findings of anti-nociceptive effect of ETC complexes inhibitors, Xiao and Bennett reported that both rotenone and oligomycin significantly exacerbated the mechano-allodynia and hyperalgesia induced by paclitaxel and oxaliplatin regimens (Xiao and Bennett 2012).

The efficacy of many ROS scavenging and antioxidant compounds has confirmed the hypothesis that ROS play an important role in the development and maintenance of CIPN. Phenyl N-tert-butylnitrone (PBN), a non-specific ROS scavenger, was able to prevent the development and to reverse established mechanical hypersensitivity and cold allodynia in paclitaxel-treated rats (Kim et al. 2010, Fidanboylu et al. 2011, Jia et al. 2017). A single bolus of 4-Hydroxy-2,2,6,6-tetramethylpiperidine-1-oxyl (TEMPOL), a SOD-2 mimetic, alleviated paclitaxel-induced mechanical hypersensitivity in a dose-dependent manner, whereas a week-long TEMPOL prophylactic treatment was able to prevent its development (Kim et al. 2017). However, our group observed that TEMPOL had an ameliorating effect on established paclitaxel-induced

nociceptive behaviour only at high dose (250 mg/kg), which was not well-tolerated by the animals (Fidanboylu et al. 2011). Peroxynitrite decomposition catalysts ($FeTMPyP^{5+}$, MnTE-2-PyP^{5+}, SRI6 and SRI110), which convert peroxynitrite to nitrate, alleviated established paclitaxel-induced mechanical hypersensitivity (Doyle et al. 2012) and prevented the development of mechanical allodynia and hyperalgesia following paclitaxel (Doyle et al. 2012, Janes et al. 2013), oxaliplatin and bortezomib administration (Janes et al. 2013). Concomitant administration of mitochondria-targeted antioxidants like SS-31 and SS-20 during an oxaliplatin regimen alleviated oxaliplatin-induced mechanical and cold hypersensitivities (Toyama et al. 2014, Toyama et al. 2018). Acutely, only SS-31 was able to ameliorate established cold hypersensitivity (Toyama et al. 2014). MitoVitE and melatonin can accumulate within mitochondria and act as antioxidants, and their administration in a prophylactic paradigm limited the development of paclitaxel- (McCormick et al. 2016, Galley et al. 2017) and oxaliplatin-induced cold, mechanical and hot hypersensitivities (Waseem and Parvez 2016, Areti et al. 2017a). Carvedilol, a non-selective beta-adrenergic receptor blocker, and rosmarinic acid, a natural phenol, alleviated cold and mechanical hypersensitivity in oxaliplatin-treated rats (Areti et al. 2017b, Areti et al. 2018). Prophylactic administration of alpha-tocopherol, a form of vitamin E, and silibinin, a natural flavonoid, alleviated mechanical and cold hypersensitivity to oxaliplatin (Di Cesare Mannelli et al. 2012). Lastly, prophylactic administration of acetyl-L-carnitine (ALC) completely prevented the development of paclitaxel- (Ghirardi et al. 2005b, Flatters et al. 2006, Jin et al. 2008, Zheng et al. 2011), oxaliplatin- (Ghirardi et al. 2005a, Zheng et al. 2011), cisplatin- (Ghirardi et al. 2005b), vincristine- (Ghirardi et al. 2005b) and bortezomib-induced mechanical hypersensitivity (Zheng et al. 2012). ALC administration after the establishment of pain-like behaviour attenuated, and in some cases reversed, mechanical hypersensitivity following paclitaxel (Ghirardi et al. 2005a, Ghirardi et al. 2005b, Flatters et al. 2006), cisplatin (Ghirardi et al. 2005b) and vincristine (Ghirardi et al. 2005b) treatments, but its analgesic effect was lost after treatment discontinuation (Flatters et al. 2006). Nevertheless, a 24-week randomised double-blind clinical trial in breast cancer patients undergoing a paclitaxel- or docetaxel-based adjuvant treatment failed to demonstrate a beneficial effect of ALC on neuropathy scores (Hershman et al. 2013). In fact, ALC treatment was associated with worsened neuropathy scores by the end of the treatment (Hershman et al. 2013). For these reasons, the ASCO guidelines (see section 1.2.2) recommend avoiding the use of ALC for the prevention of CIPN (Hershman et al. 2014). Like ALC, other antioxidant compounds, like vitamin E and glutathione, did not produce consistent/conclusive results in clinical trials against placebo controls (Hershman et al. 2014); therefore, the clinical significance of ROS scavengers/antioxidant compounds in CIPN treatment and prevention still needs to be validated.

Several other compounds have shown efficacy in alleviating or preventing nociceptive behaviours and mitochondrial dysfunction in preclinical models of paclitaxel-, vincristine-, oxaliplatin- and cisplatin-induced peripheral neuropathy [reviewed in (Trecarichi and Flatters 2019)]. The variety in their mechanism of action is summarised in Table 1-5. A few of these novel compounds have been selected for clinical trials, following promising preclinical results. For instance, prophylactic administration of nicotinamide riboside, a form of vitamin B3 and NAD precursor, prevented the development of paclitaxel-induced tactile hypersensitivity in rats (M. V. Hamity et al. 2017). Patients are currently being recruited for two Phase II clinical trials assessing nicotinamide riboside analgesic potential (NCT04112641) and its prophylactic efficacy (NCT03642990) in CIPN. Selective antagonism of the sigma-1 receptor (σ1R), which is involved in Ca^{2+} homeostasis at the mitochondrion-associated endoplasmic reticulum membrane (Hayashi and Su 2007), prevented the development of paclitaxel-induced cold and mechanical allodynia (Nieto et al. 2012, Nieto et al. 2014). A novel σ1R antagonist, MR309, has been recently investigated in a Phase II, randomised, double-blind, placebo-controlled clinical trial for its concomitant administration with oxaliplatin in chemotherapy-naïve CRC patients (Bruna et al. 2018). MR309 reduced symptoms of acute OIPN and significantly reduced the incidence of grade 3 neuropathy after cumulative doses of oxaliplatin (Bruna et al. 2018), thus suggesting its potential efficacy in preventing and treating OIPN. However, further studies are required to confirm these findings. Lastly, ACY-1215, a histone deacetylase 6 (HDAC6) inhibitor, reversed established cisplatin-induced mechanical allodynia in mice (Krukowski et al. 2017) and is currently being evaluated in a Phase I clinical trial in combination with Nab-paclitaxel in metastatic breast cancer patients (NCT02632071).

Table 1-5 List of pharmacological modulators that alleviated or prevented CIPN *in vivo*

Compound	Mechanism of action	Treatment paradigm	Behavioural effects	Reference
Known mitochondrial modulators				
Rotenone	Inhibition of Complex I	Single intraplantar administration	↓ Mechanical threshold in vincristine-induced hyperalgesia model	(Joseph and Levine 2006)
Rotenone	Inhibition of Complex I	Single bolus	↑ Paclitaxel- and oxaliplatin-induced mechanical hypersensitivity	(Xiao and Bennett 2012)
Rotenone	Inhibition of Complex I	Single bolus	↓ Paclitaxel-induced mechanical hypersensitivity	(Griffiths and Flatters 2015)
3-Acetylphenyl N-(P-Tolyl) carbamate (3-NP)	Inhibition of Complex II	Single intraplantar administration	↓ Mechanical threshold in vincristine-induced hyperalgesia model	(Joseph and Levine 2006)
Antimycin A	Inhibition of Complex III	Single intraplantar administration	↓ Mechanical threshold in vincristine-induced hyperalgesia model	(Joseph and Levine 2006)
Antimycin A	Inhibition of Complex III	Single bolus/Prophylactic	↓ Paclitaxel-induced mechanical hypersensitivity	(Griffiths and Flatters 2015)
Sodium Cyanide	Inhibition of Complex IV	Single intraplantar administration	↓ Mechanical threshold in vincristine-induced hyperalgesia model	(Joseph and Levine 2006)
Oligomycin	Inhibition of Complex V	Single intraplantar administration	↓ Mechanical threshold in vincristine-induced hyperalgesia model	(Joseph and Levine 2006)
Oligomycin	Inhibition of Complex V	Single bolus	↑ Paclitaxel- and oxaliplatin-induced mechanical hypersensitivity	(Xiao and Bennett 2012)
ROS scavengers/antioxidant compounds				
Auranofin	Inhibitor of mitochondrial TrxR	Single bolus	↑ Paclitaxel- and oxaliplatin-induced mechanical hypersensitivity	(Xiao and Bennett 2012)
Phenyl N-tert-butylnitrone (PBN)	Non-specific ROS scavenger	Repeated administration/Single bolus/Prophylactic	↓ Paclitaxel-induced mechanical hypersensitivity	(Kim et al. 2010, Fidanboylu et al. 2011, Jia et al. 2017)
4-hydroxy-2,2,6,6-tetramethylpiperidine-1-oxyl (TEMPOL)	Superoxide dismutase mimetic	Single bolus/Repeated administration	↓ Paclitaxel-induced mechanical hypersensitivity	(Fidanboylu et al. 2011, Kim et al. 2017)

FeTMPyP^{5+}	Peroxynitrite decomposition catalyst	Single bolus/Prophylactic	↓ Paclitaxel-induced mechano-hyperalgesia and mechano-allodynia	(Doyle et al. 2012)
MnTE-2-PyP^{5+}	Peroxynitrite decomposition catalyst	Single bolus/Prophylactic	↓ Paclitaxel-induced mechano-hyperalgesia and mechano-allodynia	(Doyle et al. 2012)
MnTE-2-PyP^{5+}	Peroxynitrite decomposition catalyst	Prophylactic	↓ Paclitaxel-, oxaliplatin- and bortezomib-induced mechano-hyperalgesia and mechano-allodynia	(Janes et al. 2013)
SRI110	Superoxide-sparing peroxynitrite decomposition catalyst	Prophylactic	↓ Paclitaxel-induced mechano-hyperalgesia and mechano-allodynia	(Doyle et al. 2012)
SRI6	Superoxide-sparing peroxynitrite decomposition catalyst	Prophylactic	↓ Paclitaxel-induced mechano-hyperalgesia and mechano-allodynia	(Doyle et al. 2012)
SS-31	Mitochondria-targeted antioxidant	Prophylactic/Single bolus	↓ Oxaliplatin-induced cold and mechanical hypersensitivity	(Toyama et al. 2014)
SS-20	Analogue of SS-31 but no ROS scavenging-active	Prophylactic	↓ Oxaliplatin-induced cold and mechanical hypersensitivity	(Toyama et al. 2018)
MitoVitE	Mitochondria-targeted antioxidant	Prophylactic	↓ Oxaliplatin-induced mechanical hypersensitivity	(McCormick et al. 2016)
Melatonin	Antioxidant properties	Prophylactic	↓ Paclitaxel-induced cold and mechanical hypersensitivity	(Galley et al. 2017)
Melatonin	Antioxidant properties	Prophylactic	↓ Oxaliplatin-induced mechanical and cold hypersensitivity and thermal hyperalgesia	(Waseem and Parvez 2016, Areti et al. 2017a)
Carvedilol	Antioxidant properties	Not described	↓ Oxaliplatin-induced cold and mechanical hypersensitivity	(Areti et al. 2017b)
Rosmarinic acid	Antioxidant properties	Not described	↓ Oxaliplatin-induced cold and mechanical hypersensitivity	(Areti et al. 2018)
Alpha-tocopherol	Antioxidant properties	Prophylactic	↓ Oxaliplatin-induced mechanical and thermal hypersensitivity	(Di Cesare Mannelli et al. 2012)
Silibinin	Antioxidant properties	Prophylactic	↓ Oxaliplatin-induced mechanical and	(Di Cesare Mannelli et al. 2012)

			thermal hypersensitivity	
Acetyl-L-carnitine (ALC)	Free fatty acids oxidation and ROS scavenger	Prophylactic/ Repeated administration	↓ Paclitaxel-, oxaliplatin-, cisplatin-, and vincristine-induced mechanical hypersensitivity	(Pisano et al. 2003, Ghirardi et al. 2005a, Ghirardi et al. 2005b, Flatters et al. 2006, Jin et al. 2008, Zheng et al. 2011, Zheng et al. 2012)
Other compounds				
Cholest-4-en-3-one,oxime (Olesoxime)	Binding to mitochondrial permeability transition pore	Repeated administration/ Prophylactic	↓ Paclitaxel- and vincristine-induced mechanical hypersensitivity	(Bordet et al. 2008, Xiao et al. 2009)
Dynamin-related protein 1 (Drp1)	Catalyst of mitochondrial fission	Single bolus	↓ Oxaliplatin-induced mechanical hyperalgesia	(Ferrari et al. 2011)
Pifithrin-μ (PFT-μ)	Inhibition of p53 mitochondrial accumulation	Prophylactic	↓ Inhibition of paclitaxel- and cisplatin-induced mechanical allodynia	(Krukowski et al. 2015, Maj et al. 2017)
P7C3-A20	NAMPT stimulator	Prophylactic	↓ Paclitaxel-induced mechanical allodynia, heat hypoalgesia and cold allodynia	(LoCoco et al. 2017)
Nicotinamide riboside	NAD^+ precursor	Prophylactic	↓ Paclitaxel-induced tactile hypersensitivity	(Hamity et al. 2017)
Methylcobalamin (MeCbl)	Not known	Prophylactic	↓ Vincristine-induced mechanical allodynia and thermal hyperalgesia development	(Xu et al. 2016)
BD-1063	Selective antagonism of sigma-1 receptor	Prophylactic/Single bolus	↓ Paclitaxel-induced cold and mechanical allodynia	(Nieto et al. 2012, Nieto et al. 2014)
S1RA	Selective antagonism of sigma-1 receptor	Prophylactic/Single bolus	↓ Paclitaxel-induced cold and mechanical allodynia	(Nieto et al. 2012)
5-hydroxydecanoate (5-HD)	Mitochondrial ATP-sensitive K^+ channel antagonist	Prophylactic	↓ Paclitaxel-induced thermal insensitivity and mechanical allodynia	(Chen et al. 2015)
Minoxidil	Not known	Prophylactic	↓ Paclitaxel-induced thermal insensitivity and mechanical allodynia	(Chen et al. 2017)
Ghrelin	Not known	Prophylactic	↓ Cisplatin-induced mechanical hyperalgesia	(Garcia et al. 2008)

Ghrelin	Not known	Prophylactic	↓ Paclitaxel-induced mechanical and thermal hypersensitivity	(Ishii et al. 2018)
Pirenzepine	Selective muscarinic acetylcholine type 1 receptor (M1R) antagonist	Repeated administration	↓ DCA- and paclitaxel-induced mechano-allodynia and thermal hyperalgesia	(Calcutt et al. 2017)
ACY-1083	Selective histone deacetylase 6 (HDAC6) inhibitor	Repeated administration/ Prophylactic	↓ Cisplatin-induced mechanical allodynia and spontaneous pain'-like behaviour	(Krukowski et al. 2017)
ACY-1083	Selective HDAC6 inhibitor	Repeated administration	↓ Paclitaxel-induced mechanical hypersensitivity	(Krukowski et al. 2017)
ACY-1215	Selective HDAC6 inhibitor	Repeated administration	↓ Cisplatin-induced mechanical allodynia	(Krukowski et al. 2017)
ACY-738	Selective HDAC6 inhibitor	Prophylactic	↓ Vincristine-induced mechanical hypersensitivity	(Van Helleputte et al. 2018)
Tubastatin A	Selective HDAC6 inhibitor	Prophylactic	↓ Vincristine-induced mechanical hypersensitivity	(Van Helleputte et al. 2018)
Evodiamine	Multiple actions	Single bolus	↓ Paclitaxel-induced mechanical and thermal hypersensitivity	(Wu and Chen 2019)
Pioglitazone	Peroxisome proliferator-activated receptor (PPAR)-γ agonist	Prophylactic/Single bolus	↓ Cisplatin-induced mechanical and cold hyperalgesia	(Khasabova et al. 2019)

Single bolus refers to systemic administration. Adapted from (Trecarichi and Flatters 2019).

1.5 Aims

The two main aims of this thesis were to investigate a potential blood biomarker for OIPN and to gather a deeper understanding of the mechanisms involved in the neuropathy. Using various techniques, including electrophysiology, mitochondrial stress assays, western blot and quantitative PCR, we investigated the hypothesis that altered mitochondrial function and nerve conduction are pivotal factors in the development and maintenance of OIPN.

Chapter 3 investigates the feasibility of MtDNA content in the whole blood as predictive biomarker for OIPN in colorectal cancer patients.

In chapter 4, we aim to characterise a chronic rat model of OIPN in terms of mechanical and cold sensitivity, ongoing pain and numbness.

In chapter 5, we test the hypothesis that oxaliplatin affects the electrical properties of sensory nerves through the characterisation of various electrophysiological characteristics of the saphenous nerve.

Lastly, chapter 6 investigates the hypothesis that oxaliplatin determines a bioenergetic dysfunction in neuronal mitochondria and alters their ability to regulate the intracellular Ca^{2+} homeostasis.

Chapter 2 Materials and methods

2.1 Clinical investigation

2.1.1 Patient selection

57 colorectal cancer (CRC) patients about to start an oxaliplatin regimen were recruited by our collaborators at the Royal Marsden Hospital, London. Patients were a mix of males and females diagnosed with CRC and the exclusion criteria was metastatic cases. All participants provided written informed consent prior to enrolment in the study. Approval for the study was obtained by the London - Riverside Research Ethics Committee (REC reference 15/LO/0174).

2.1.2 Blood samples collection

3-5 ml of blood were harvested from each patient and collected in BD Vacutainer Blood Collection tubes containing K2-EDTA (ethylenediaminetetraacetic acid) as an anticoagulant. Tubes were labelled with a unique, patient-specific code to ensure anonymity. To prevent degradation, blood samples were immediately divided in 200 µl aliquots and frozen at -80°C upon arrival from the clinic. Blood samples storage and records keeping complied with the Human Tissue Act 2004 regulations. Patient blood was collected at different time points, as outlined in Figure 2-1: T0 – prior to initiation of the oxaliplatin regimen; T1 - after completion of the first cycle of chemotherapy and prior to the administration of the second one; T2 – approximately 3 months after chemotherapy initiation. When a dose reduction was required due to neuropathy, blood was harvested after the last infusion cycle; T3 – approximately 6 months after chemotherapy initiation. When a dose reduction was required due to neuropathy, blood was harvested after the last infusion cycle; T4 – approximately 3 months after completion of the oxaliplatin regimen, to help identify patients with coasting. At each time point, patients were asked to complete a self-report questionnaire to identify the presence of the neuropathy: they completed the Functional Assessment of Cancer Therapy/Gynecologic Oncology Group–Neurotoxicity (Fact/GOG-Ntx), a comprehensive questionnaire that assesses quality of life in oncology patients implemented with questions about chemotherapy-induced peripheral neuropathy (CIPN) symptoms and their impact on life. Neuropathy was classified as painful or non-painful with the Brief Pain Inventory (BPI) and the McGill Pain Questionnaire (MPQ), which provide scores and scales to evaluate the nature and intensity of pain.

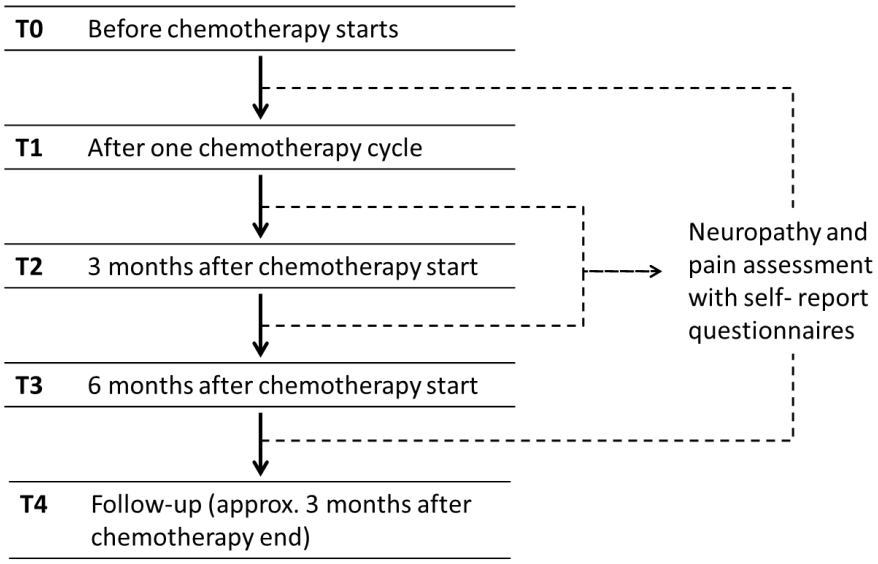

Figure 2-1 Flowchart of blood samples collection from CRC patients undergoing oxaliplatin treatment
Blood was collected from patients before the initiation of the oxaliplatin treatment, at various time points during it and, where possible, after treatment cessation. At each time point, patients were asked to complete self-report questionnaires to describe the state of the neuropathy and pain.

2.1.3 DNA extraction

DNA was extracted from whole blood samples as described in (Ajaz et al. 2015) using silica-based columns, following the manufacturer's protocol (DNeasy Blood & Tissue Kit; Qiagen, UK). Samples were used either fresh (immediately after samples reception/aliquoting) or after being stored at -80°C. Frozen blood was allowed time to thaw in ice before use. Maximum DNA yield was obtained using a starting volume of 100 µl of blood. 20 µl of proteinase K, 100 µl of phosphate buffered saline (PBS) and 200 µl of lysis buffer were added to the blood. Samples were mixed thoroughly by vortexing and incubated at 56°C for 10 minutes, to allow lysis. Following the lysis step, 200 µl of ethanol (95-99.9%; Sigma, UK) were added to each sample and vortexed thoroughly. The solution was then transferred to a DNeasy Mini spin column in a 2 ml collection tube and samples were centrifuged at 8 000 rpm for 1 minute. The spin column was placed into a new 2 ml collection tube and 500 µl of buffer AW1 were added to wash the membrane inside the column. Samples were centrifuged at 8 000 rpm for 1 minute, collection tubes were discarded, and spin columns placed into new 2 ml collection tubes. 500 µl of buffer AW2 were added and columns were centrifuged at 14 000 rpm for 3 minutes. To elute DNA, spin columns were transferred to sterile tubes and 50 µl of elution buffer were added to the column membrane. Columns were incubated at room temperature for 1 minute and centrifuged at 8 000 rpm for 1 minute. To increase DNA yield, the eluted 50 µl were re-added to the column membrane to repeat the elution step once more. Eluted DNA was sonicated for 10 minutes using a water bath sonicator (Ultrawave, UK). DNA quantity and quality were assessed using a

NanoDrop ND-1000 spectrophotometer (ThermoFisher, UK). Final DNA concentrations were adjusted to 10 ng/µl using nuclease-free water (Qiagen, UK).

2.1.4 Mitochondrial DNA quantification

Real-time quantitative polymerase chain reaction (qPCR) was used to measure MtDNA content in DNA isolated from patient samples. Primers for the mitochondrial genome, which do not amplify nuclear pseudogenes, were used to quantify a unique mitochondrial fragment (hMito) relative to a single-copy region of the housekeeping gene β-2-microglobulin (hB2M) (Malik et al. 2011). The oligonucleotide sequences (Sigma, UK) for MtDNA and nuclear DNA (nDNA) are shown in Table 2-1.

Table 2-1 Oligonucleotide sequences for Mt/nDNA determination using real-time qPCR

Primer name	Sequence (5'→ 3')	Amplicon length (bp)
hMito Forward	CACTTTCCACACAGACATCA	129
hMito Reverse	TGGTTAGGCTGGTGTTAGGG	
hB2M Forward	TGTTCCTGCTGGGTAGCTCT	187
hB2M Reverse	CCTCCATGATGCTGCTTACA	

2.1.4.1 DNA standards preparation

Absolute qPCR was used to measure Mt/nDNA content in whole blood relatively to a standard curve for hMito and hB2M products, as previously described (Ajaz et al. 2015). To generate a standard curve, the hMito and hB2M PCR products were amplified using DNA isolated from blood samples from healthy donors. The PCR master mix was prepared with 5 µl of Green GoTaq Reaction Buffer (5x stock; Promega, UK), 1.5 µl of $MgCl_2$ (25 mM stock; Promega, UK), 0.5 µl of deoxyribonucleotide triphosphates (dNTPs; 10 mM stock; Promega, UK), 0.3 µl of GoTaq Polymerase (5 units/µl; Promega, UK), 0.5 µl of each forward and reverse primer (10 µM; Sigma, UK) and 15.7 µl of RNase-free water (Qiagen, UK). The final reaction volume of 25 µl was obtained by adding 1 µl of DNA template (10 ng/µl stock). PCR was performed using a Thermal Cycler (Applied Biosystems, Thermofisher, UK) with the following protocol: hot start at 95°C for 15 min; 30 cycles of denaturation at 94°C for 30 s, annealing at 60°C for 30 s and extension at 72°C for 1 min and 30 s; and a final extension at 72°C for 7 min. To verify the success of the PCR, PCR products were separated by electrophoresis on a 1.5% (w/v) agarose (Sigma, UK) gel, alongside a DNA ladder (Promega, UK), as a reference for base pair sizes. hMito and hB2M bands were visualised under UV light and excised from the gel with a gel extraction tool (x-tracta Gel Extraction Tool; Starlab, UK) to be purified with the QIAquick Gel Extraction Kit (Qiagen,UK), as per manufacturer's instructions. Excised bands were weighed and 3 volumes of Buffer QG were added per 1 volume of gel, according to its weight (e.g. 100 mg of gels = approximately 300 µl

of buffer). Bands were left to dissolve at 50°C for 10 minutes, with the help of regular vortexing every 2-3 minutes. If needed, the solution pH was adjusted to 7.5 with 10 µl of 3 M sodium acetate, pH 5, to yield a yellow colour (rather than orange or violet, indicative of a higher pH). 1 gel volume of isopropanol (Sigma, UK) was added to the mix and the solution was transferred to a QIAquick spin column placed inside a 2 ml collection tube. Columns were centrifuged at 13 000 rpm for 1 minute and the flow-through was discarded. Columns were washed with 750 µl of Buffer PE and centrifuged again at 13 000 rpm for 1 minute. The flow-through was discarded and samples were centrifuged once more at 13 000 rpm for 1 minute. Columns were placed into clean 1.5 ml centrifuge tubes and DNA was eluted in 30 µl of buffer EB after a 2-minute incubation step at room temperature and a final centrifugation at 13 000 rpm for 1 minute. DNA was quantified using a NanoDrop ND-1000 (ThermoFisher, UK) and copy number per µl of purified DNA was calculated as:

$$\frac{\textbf{Concentration of purified DNA in } \frac{\textbf{g}}{\boldsymbol{\mu}\textbf{l}}}{\textbf{Amplicon length in basepairs} \times \textbf{660}} \times \textbf{6.022} \times \textbf{10}^{\textbf{23}}$$

where amplicon length is: hB2M 187 bp; hMito129 bp.

DNA was diluted in nuclease-free water (Qiagen, UK) containing 10 µg/ml transfer RNA (Invitrogen, UK) to yield a 10^{10} molecules/µl standard. Serial dilutions were performed to obtain eight DNA standards within a range of 10^{8}-10^{2} molecules/µl to generate a standard curve for absolute quantification.

2.1.4.2 Real-time qPCR

All reagents required for qPCR were allowed time to thaw in ice. A qPCR reaction mix was prepared using 5 µl of QuantiFast SYBR Green PCR master mix (2x stock; Qiagen, UK), 0.3 µl of each forward and reverse primer (10 µM; Sigma, UK) and 2.4 µl nuclease-free water (Qiagen, UK), for a total volume of 8 µl reaction mix per DNA sample. The reaction mix was loaded in a 384-well plate (Roche, UK) and 2 µl of sample DNA (10 ng/µl stock) or DNA standards were added. Sample DNA and reference DNA standards (10^{8}-10^{2} molecules/µl range) were loaded in triplicate in a single plate. Three different negative controls were loaded in the plate: a no-template control containing all reagents except for DNA, to check for the presence of primer dimers; a reaction mix containing all reagents except for primers, to verify the absence of contamination within the SYBR Green PCR master mix; and nuclease-free water (same water used to prepare the reaction mix), to verify the absence of contamination in it. All negative controls were loaded in triplicate in a single plate as well. Once plates had been loaded, they were sealed with an adhesive sealing foil (Roche, UK) followed by a 1-minute centrifugation at 1 000 rpm to ensure all reagents were at the bottom of the wells. Real-time qPCR was performed

using the LightCycler 480 (Roche, Switzerland) with the following conditions: preincubation at 95°C for 5 min (1 cycle); denaturation at 95°C for 10 s, annealing and extension at 60°C for 30 s (repeat denaturation and extension steps for 40 cycles); melting at 95°C for 5 s, 65°C for 60 s, and 95°C continues (melt curve analysis, 1 cycle); and lastly, cooling at 40°C for 30 s. To ensure technical reproducibility, qPCR reactions were prepared fresh and run on three independent occasions (i.e. three separate days). Data analysis was performed using the LightCycler 480 software 1.5.1 (Roche, UK). Ct values (cycle threshold) for mitochondrial and nuclear genome were interpolated to their respective standard curves, in order to obtain copy numbers for MtDNA and nDNA. As plating was done in triplicate, the three copy numbers for each DNA sample were averaged to provide a final copy number value. MtDNA levels were then measured as MtDNA/nDNA ratio in each plate. The final MtDNA/nDNA ratio was obtained by averaging the three ratios obtained from the three independent technical replicates.

2.2 Oxaliplatin-induced peripheral neuropathy animal model

2.2.1 Animals

Adult male Sprague-Dawley rats with an average starting weight of 180-220 g (Envigo, UK and Netherlands colonies) were housed in groups of 3-4 in plastic cages held in a climate-controlled environment with a 12-hour light/dark cycle. Cages were lined with sawdust bedding and environmental enrichment materials and animals had access to food and water *ad libitum.* All procedures were conducted in compliance with the UK Animals (Scientific Procedures) Act, 1986 and the IASP ethical guidelines (Zimmermann 1983). The procedures were approved by the Ethical Review Panel of King's College London and conducted under project licenses 70/8015, PABEF3413 and PBA346803.

2.2.2 Chemotherapy administration

Clinical formulation of oxaliplatin 5 mg/ml concentrate for Solution for Infusion (Accord Healthcare Ltd) was provided by Guy's Hospital Cancer Centre pharmacy. Oxaliplatin was diluted with 0.9% sterile saline (Fresenius Kabi, UK) to a final concentration of 2 mg/ml. Control animals received an equivalent amount of vehicle solution made of 0.9% sterile saline. Animals received 2 mg/kg oxaliplatin or an equal volume of vehicle solution intraperitoneally (IP) on four alternate days (0, 2, 4, 6) and were dosed according to their weight (i.e. 1ml/kg). To perform the IP injection, animals were restrained gently on the experimenter's side: the rat's body was placed along the arm, with its head facing the crook of the elbow. Animals were turned to a supine position to expose their abdomen and identify the midline, and their head and body were then tilted downwards. A 25-gauge needle was inserted at an ~ 45° angle in the right lower quadrant of the abdomen to avoid perforation of internal organs, and the entire drug volume was

administered. A new needle and syringe were used for each animal. Upon completion of drug administration, animals were placed in their cages and observed for 5-10 minutes to ensure their health and that no complication had arisen. Fresh oxaliplatin and vehicle solutions were prepared on each day of the treatment regimen.

2.2.3 Randomisation and blinding

In order to avoid bias when assigning animals to saline or oxaliplatin treatment, treatment allocation was randomised. Upon completing baseline testing, animals were split into two groups, keeping the average baseline scores of the two as equal as possible. This allowed to equally distribute animals across the two treatment cohorts and avoid baseline imbalance, which would make interpretation of results harder. For instance, if all the animals with high baseline responses to von Frey stimulation (see section 2.2.4.1) were randomly allocated to receive oxaliplatin, it would not be possible to evaluate the true effect of oxaliplatin on mechanical sensitivity, as these animals would have already reached the maximum score achievable (or scores close to that) before oxaliplatin administration.

One animal group was then allocated to receive treatment A, while the second group received treatment B, or vice versa. At the beginning of each study, a third party anonymised oxaliplatin and saline vials (as A or B) and the same blinding code was applied throughout the dosing regimen. To avoid any potential bias when performing behavioural assessments, all tests were performed blindly (i.e. without knowing the identity of the treatment administered) until the end of the study, when data analysis was performed.

2.2.4 Behavioural assessments

Animals were regularly checked for weight gain and health status and no animal had to be excluded due to weight loss or ill health. Two key time points were investigated in this oxaliplatin-induced peripheral neuropathy (OIPN) model: day 7, 24 hours after the last treatment administration, and peak pain, when animals reached the peak of pain-like behaviour (day 28-34). The peak pain time point occurred over a period of seven days, as behavioural responses were different among animals and were dependent on individual responses compared to baseline. A total of 96 animals were used in the studies described in this thesis (saline n = 48, oxaliplatin n = 48). Allocation of animals to different behavioural tests is summarised in Table 2-2.

Table 2-2 Allocation of saline- and oxaliplatin-treated animals to behavioural tests

Saline		Oxaliplatin	
Mechanical hypersensitivity			
Total	**n = 31**	**Total**	**n = 31**
of which reached peak pain	n = 8	of which reached peak pain	n = 9

Saline n = 17					**Oxaliplatin n = 17**				
#	**Cold allodynia**	**Wheel running**	**Adhesive removal test 1**	**Adhesive removal test 2**	**#**	**Cold allodynia**	**Wheel running**	**Adhesive removal test 1**	**Adhesive removal test 2**
1	✓	✓		✓	1	✓	✓		✓
2	✓	✓		✓	2	✓	✓		✓
3	✓	✓		✓	3	✓	✓		✓
4	✓	✓		✓	4	✓	✓		✓
5	✓	✓		✓	5	✓	✓		✓
6	✓	✓			6	✓	✓		
7	✓	✓			7	✓	✓		
8	✓	✓			8	✓	✓		
9	✓	✓			9	✓	✓		
10	✓	✓			10	✓	✓		
11	✓	✓			11	✓	✓		
12	✓		✓		12	✓		✓	
13	✓		✓		13	✓		✓	
14	✓		✓		14	✓		✓	
15	✓		✓		15	✓		✓	
16	✓		✓		16	✓		✓	
17	✓		✓		17	✓		✓	

2.2.4.1 Mechanical hypersensitivity to von Frey filaments

Behavioural tests were performed in a rig made of 12 elevated, clear Perspex boxes (15 cm x 16 cm x 21 cm) with a wire-rung floor that allowed access to the animals' paws. Animals were habituated to the testing environment for 30 minutes on two separate occasions the day before starting baseline assessment. Prior to each behavioural test, animals were left to acclimatise in the boxes for an additional 5-10 minutes, or until they quieted. Mechanical hypersensitivity was assessed by withdrawal responses to 4 g, 8 g and 15 g von Frey filaments (Touch-Test Sensory Evaluators, Linton Instrumentation, UK), as previously described (Duggett and Flatters 2017, Griffiths et al. 2018). Filaments were applied to the midplantar region of the left and right hind paw, starting from the lower force filament. All animals were tested using one von Frey filament on one hind paw before moving to the other hind paw with the same bending force filament. Each filament was applied 5 consecutive times, for 5 seconds each. Each paw withdrawal from the filament was counted as a positive response. The maximum score per filament force was 10, obtained by the summation of left and right paw scores for each filament. Prior to oxaliplatin or saline administration, animals were assessed on three days for baseline scores and the results of the three assessments were averaged to obtain the final baseline score. Animals were split in two groups of nearly equal baseline scores and randomised to either saline or oxaliplatin treatment. Mechanical hypersensitivity was then measured at day 7 or weekly until the peak

pain endpoint was reached. Testing was always performed between 8 and 11 am and under blind conditions. Testing was carried out on animals there were awake, not grooming and with all four paws in contact with the wired floor.

A total of 76 animals (saline n = 38, oxaliplatin n = 38) were tested for mechanical hypersensitivity in order to be allocated to further investigations. Of those, 14 animals (saline n = 7, oxaliplatin n = 7) were excluded because their behavioural responses were considered unreliable, and therefore their behaviour is not displayed in this thesis. Reasons to exclude these animals comprise: animals were falling asleep repeatedly whilst being tested, and so resulted insensitive to von Frey stimulation at different time points during the behavioural investigation; and animals were constantly grooming and/or moving in the testing apparatus, thus making it challenging to test them with their four paws in contact with the wired floor and to discern actual withdrawal responses to mechanical stimulation from other spontaneous behaviours. In both cases, withdrawal responses, or lack thereof, were not considered an accurate measurement of mechanical sensitivity, as they were not deemed to be solely due to stimulation with von Frey filaments. Hence, their inclusion in the study was considered inappropriate. The remaining 62 animals tested for mechanical hypersensitivity (saline n = 31, oxaliplatin n = 31) were allocated to further experimental procedures to investigate electrophysiological and mitochondrial properties (see Figure 4-1). Animals tested for mechanical hypersensitivity were not used for other behavioural investigations.

2.2.4.2 Cold allodynia

Animals were tested in the rig described above following the same habituation paradigm. 50 µl of acetone (Fisher Scientific, UK) were applied to the midplantar region of the hind paw with a P200 pipette (Eppendorf, UK). Acetone was carefully applied to the paw surface only, in order to avoid wetting the rats' fur, as animals would start grooming and pain-like responses would be difficult to assess. A stopwatch was started at the time of acetone application and animals were observed for 20 seconds. If no response occurred, the trial was interrupted; if animals did respond to the stimulus, their responses were recorded for additional 20 seconds, for a total trial run of 40 seconds. Pain-like behaviour was evaluated using a cold scoring system, as previously described (Flatters and Bennett 2004): 0 = no response; 1 = one to three responses (paw withdrawal or flicking); 2 = three or more responses; 3 = three or more responses plus licking of the plantar surface/pulling at the nails. Acetone was applied to both left and right hind paw and the test was repeated three times. Each time, all animals were tested on one hind paw before beginning to test the other hind paw. Responses for the three trials were summed and the maximum achievable score was 18. Prior to oxaliplatin or saline administration, animals

were assessed on four days for baseline scores and the results of the four assessments were averaged to obtain the final baseline score. Three different cohorts of animals were tested for cold allodynia. Animals in the first cohort were split into two groups of approximately equal baseline cold scores and randomly assigned to oxaliplatin or saline treatment (saline n = 6, oxaliplatin n = 6). Animals in the second and third cohorts were also tested for spontaneous wheel activity (see section 2.2.4.3) and were split in two groups of approximately equal baseline distances run on wheels, which were then randomised to receive either oxaliplatin or saline (saline n = 11, oxaliplatin n = 11). Cold allodynia was then measured at day 7 or weekly until the peak pain endpoint was reached. Testing was always performed between 8 and 11 am and under blind conditions. Testing was carried out on animals that were awake, not grooming and with all four paws in contact with the wired floor. Results from separate cohorts of animals that were tested at different times in the lab were collated. A total of 34 animals were used for this test (saline n = 17, oxaliplatin n = 17).

2.2.4.3 Spontaneous wheel running

Spontaneous wheel running activity was recorded using Spontaneous Activity Wheels BIO-ACTIVW-R (Bioseb, France). Animals were placed in individual cages (48 cm x 31.5 cm x 47 cm) made of Type III polycarbonate. Within each cage, animals had free access to a stainless-steel wheel (diameter: 34 cm; width: 7 cm) and were able to spin in both clockwise and counterclockwise direction. Cages contained sawdust and animals had access to food and water *ad libitum* and were kept in the same holding room where they were normally housed. Wheels were connected to a computer and wheel activity was recorded through the ACTIVW-SOFT software (Bioseb, France). The software recorded different parameters of wheel activity every 5 minutes, including total distance run, mean and maximum speed, maximum acceleration, time spent on the wheel (active time) and number of times the animal accessed the wheel (access count). Animals were habituated in the wheel-cage for one hour during the morning before each testing. They were then placed in the testing apparatus between 17:00 and 18:00 and activity was recorded overnight until 09:00-10:00 the following morning. To account for rats being nocturnal animals, data were only analysed during the dark phase (19:10 to 6:30). Animals included in this study were also tested for cold allodynia (see section 2.2.4.2). One baseline recording was taken following the last acetone baseline testing. Animals were split in two groups that ran approximately the same average distance during the dark phase and were then randomised to oxaliplatin or saline treatment. Further time points investigated were days 7, 14, 28, and 34. A maximum of six wheel-cages were used at any time. Animals were always placed in the same cage for habituation and activity recording and were returned to their home cages afterwards. Testing was always performed under blind conditions. Results were obtained by

collating recordings from two separate cohorts of animals that were tested at different times in the lab. A total of 22 animals were used in this test (saline n = 11, oxaliplatin n =n 11).

2.2.4.4 Numbness assessment

2.2.4.4.1 Adhesive removal test - trial 1

The adhesive removal test (Schallert et al. 1982) was evaluated for its potential use in assessing numbness in rats following chemotherapy administration. Round adhesive labels (diameter: 13 mm; Ryman, UK) were applied to the dorsal surface of the left and right forepaws, whilst the animal was restrained in one hand (Figure 2-2). Care was taken to limit the stress experienced by the animals whilst restrained. Animals were tested for two different parameters: time needed for them to notice the adhesive label (paw brought to mouth and licked and/or flicking) and time needed to remove it. Animals were allowed a maximum of 5 minutes per trial and the test was conducted in an empty plastic cage, one animal at a time. If animals did not manage to remove the label by the end of trial, their attempt was considered null and the whole time point was excluded from analysis. Animals were trained for three days to habituate to the experimenter's hold and label appliance. Additionally, rats were habituated to the empty cage for one minute before each label appliance. All animals were tested on one forepaw before beginning to test the opposite paw. Animals included in this study were also tested for cold allodynia (see section 2.2.4.2). One baseline recording was taken after the last acetone baseline testing and animals were split into two groups of almost equal baseline cold scores. The wo groups were then randomly allocated to receive saline or oxaliplatin. Animals were tested regularly on days 7, 14, 22, 28 and 31. Testing was always performed between 2 and 4 pm and under blind conditions. A total of 12 animals were used for this test (saline n = 6, oxaliplatin n = 6).

2.2.4.4.2 Adhesive removal test - trial 2

An alternative version of the adhesive removal test was attempted based on the protocol described by (Komotar et al. 2007). A rectangular piece of tape (4 cm x 0.9 cm) was wrapped around the paw, so that the extremities could attach together and covered most of the dorsal and plantar region, with only the fingers sticking out, as illustrated in Figure 2-2. Two different types of tape were tested at first, mask tape and electrical tape; electrical tape was selected to carry out the study, as removing it from the animals' fur was easier. Animals were allowed 20 seconds to settle down once the tape was applied. A stopwatch was started after that and animals were observed for 30 seconds. Time spent attending to the paw (licking and/or biting) was recorded with another stopwatch. Results were calculated as ratio of time spent trying to remove the tape/30 s. The test was carried out by two experimenters, one restraining the animal

and one applying the tape. Animals were trained once to habituate to the experimenter's hold and tape appliance. Additionally, rats were habituated to the empty cage for one minute before each tape appliance. All animals were tested on one forepaw before beginning to test the opposite paw. Animals included in this study were also tested for cold allodynia and spontaneous wheel running (see sections 2.2.4.2 and 2.2.4.3). One baseline recording was taken prior to oxaliplatin or saline administration. Animals were split into two groups of nearly equal baseline distances run on the wheels, and one group was randomly allocated to oxaliplatin, whilst the other received saline. Animals were then tested on day 8, 21 and 29. Testing was always performed between 2 and 4 pm and under blind conditions. A total of 10 animals were used for this test (saline n = 5, oxaliplatin n = 5).

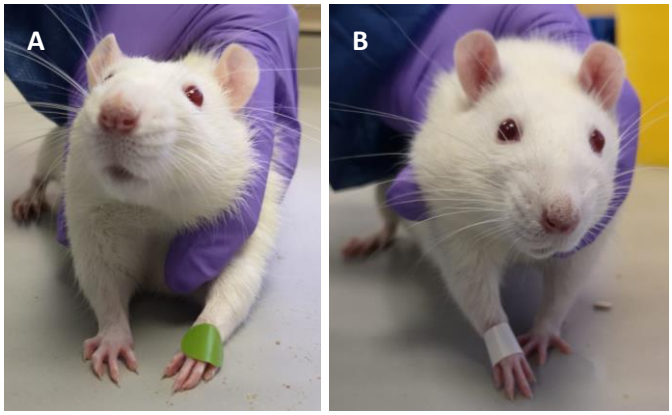

Figure 2-2 Two different methodologies of the adhesive removal test

(A) Trial 1: A round adhesive label was applied to the dorsal surface of the forepaw. The time to sense the label and to remove it were measured. Animals were given a maximum time of 5 minutes to perform the task. (B) Trial 2: a rectangular piece of electrical tape was wrapped around the animal forepaw and the two extremities were attached together. Animals were observed for 30 seconds and the time spent trying to remove the tape was measured.

2.3 Electrophysiological investigation

2.3.1 Saphenous nerve dissection

At the time point of interest, animals were terminally anesthetised with an overdose of pentobarbital sodium (Euthatal; Merial, UK). Depth of anaesthesia was assessed by checking animal reflexes, including pedal withdrawal, blink and righting reflex. Once reflexes had been lost, the skin of the inner thigh was cut open to expose the saphenous nerve and the connective tissue surrounding it was removed. A cut was made at the distal segment of the nerve to free the extremity. Holding the cut end gently, the nerve was carefully freed from the surrounding fascia and blood vessels, until a sufficient nerve length was achieved. A second cut was made at the proximal end to dissect the nerve out completely. The nerve was placed in Hibernate A (Thermo Fisher, UK), a maintenance medium for neuronal tissue, and the second nerve was harvested from the animal. Nerves were kept in Hibernate A for a maximum of 3 hours. As each nerve was an independent unit, sample size for all electrophysiology experiments refers to number of nerves rather than number of animals.

2.3.2 Electrophysiology bath set-up

Nerves were placed in the stimulating/recording apparatus, made of clear Perspex boxes (7.3 cm x 2.9 cm x 1.7 cm) that could be divided into three inner chambers: a stimulating one (2 cm x 1 cm x 1 cm), a recording one (2.6 cm x 1 cm x 1 cm) and a middle chamber for nerve superfusion (0.8 cm x 1 cm x 1 cm). Two plastic bars separated the middle chamber from the stimulating and recording ones (3.5 cm x 0.6 cm x 0.1 cm). High vacuum silicone grease (Dow Corning, UK) was applied to the top of the bars and the nerve was laid over them and across a pair of stimulating and a pair of recording electrodes. Two additional bars were coated with silicone grease and fitted on top of the others, thus isolating the three chambers, as shown in Figure 2-3. The stimulating and recording chambers were filled with mineral oil (Sigma Aldrich, UK), while the nerve section in the central chamber was superfused with oxygenated bicarbonate solution (124 mM NaCl, 26 mM $NaHCO_3$, 1 mM NaH_2PO_4, 2.5 mM KCl, 1 mM $MgCl_2$, 2.5mM $CaCl_2$, 10 mM glucose, pH 7.4 maintained with carbogen 95% O2/5% CO_2; BOC, UK) at a rate of 2 ml/min with a mechanical pump (Ismatec, Germany). Bicarbonate solution was constantly suctioned off the chamber at the same rate. The Perspex boxes were made of hollow walls, in which a constant flow of hot water allowed to maintain the bath temperature constant at 34-35°C. Electrode pairs were placed at a distance of at least 5 mm and were made of chlorided silver wire (99.99% purity, ⌀ 0.75 mm). Chlorination was obtained by placing the silver wire in bleach for 10-15 minutes. Nerves were harvested at a sufficient length (average length ~ 2.8 cm) to place them across the electrodes without excessive stretching, which would impair

nerve integrity and subsequent electrical properties. The nerve extremity on the second recording electrode was gently crushed with a pair of forceps (InterFocus, UK) to allow for a monophasic recoding. Post-dissection nerve electrical activity was tested by stimulating the nerve once with A- and C-fibres compound action potential (CAP) characterising protocols (see section 2.3.4). Whenever electrical stimulation did not generate a CAP, the nerve was repositioned on the electrodes to generate a better nerve/electrode connection. After this initial trial, nerves were left to rest in the bath for 20 -50 minutes before recording. Occasionally (< 10% of all C-CAPs recorded), the C-CAP was no longer present after the resting period and the pre-rest recording was included in the final analysis.

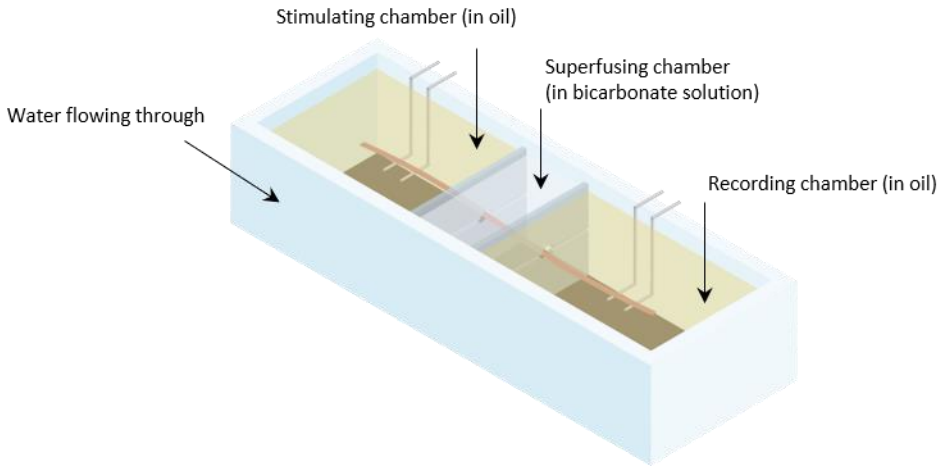

Figure 2-3 Schematic representation of the electrophysiology bath set-up

Electrical stimulation of the saphenous nerve was carried out in a clear Perspex box divided into three isolated inner chambers. The outermost chambers were filled with mineral oil and contained a pair of stimulating and a pair of recording electrodes. The middle chamber contained oxygenated bicarbonate solution that was constantly pumped through and suctioned off at a rate of 2 ml/min. The saphenous nerve (in pink) was laid across the electrodes. Hot water flew through the hollow walls of the Perspex box to maintain a constant temperature of 34-35°C.

2.3.3 Electrophysiology set-up optimisation

2.3.3.1 Effects of substrate supplementation on CAP recordings

A first optimisation attempt aimed to assess the effects of fructose and glucose as sugar supplements in the bicarbonate solution. Nerves (n = 4) were harvested from two naïve animals and placed in Hibernate A (Thermo Fisher, UK) for up to 3 hours, as described in 2.3.1. Nerves rested in the bath for 30-45 minutes before starting recording. The electrophysiology bath was set up as described in section 2.3.2. The bath central chamber was initially filled with oxygenated bicarbonate solution containing 10 mM glucose at a rate of 2 ml/min. After the resting period, nerves were electrically stimulated, as described in section 2.3.4. Upon cessation of the

stimulation protocols, oxygenated bicarbonate solution that did not contain any sugar supplement was pumped into the central chamber for 30 minutes, in order to wash out any trace of glucose. Nerves were then superfused with oxygenated bicarbonate solution supplemented with 20 mM fructose and stimulating protocols were reapplied to the nerves.

2.3.3.2 Effects of nerve crushing on CAP recordings

Nerves were harvested from saline-treated animals and placed in Hibernate A (Thermo Fisher, UK), as described in section 2.3.1. The electrophysiology bath was set up as previously described in 2.3.2. Initial recordings were carried out by laying nerves (n = 10) across the electrodes and simply placing the nerve extremity on the second recording electrode. As nerves were cut at their extremities, recordings were considered monophasic in practice. In order to obtain a truly monophasic recording, further experiments were conducted on nerves whose extremities were gently crushed on the second recording electrode. Results for the crushed set-up were collated from nerves harvested from saline-treated animals at day 7 and day 28-37, for a total of 22 nerves.

2.3.4 Stimulating and recording set-up

Stimulating protocols were set up using Spike2 software 8.13 (Cambridge Electronic Design, UK), which was connected to a CED 1401 interface (Cambridge Electronic Design, UK). A DAC output (digital to analogue converter) in the CED 1401 sent a voltage signal to a DS4 bi-phasic stimulus isolator (Digitimer, UK). The DS4 produced a constant current stimulus that was applied to the nerves via the stimulating electrodes. Nerves were stimulated with square wave pulses at a frequency of 0.2 Hz. A-CAP and C-CAP minimum thresholds were determined through the application of pulses of increasing current:

A-CAP threshold: from 0 to 0.3 mA in 0.01 mA increments (31 stimuli) – 50 µs pulse width

(Day 7: saline n = 13 nerves, oxaliplatin n = 8 nerves. Peak pain: saline n = 9 nerves, oxaliplatin n = 11 nerves)

C-CAP threshold: from 0 to 4 mA in 0.1 mA increments (41 stimuli) – 1 ms pulse width

(Day 7: saline n = 9 nerves, oxaliplatin n = 10 nerves. Peak pain: saline n = 6 nerves, oxaliplatin n = 8 nerves)

A second protocol was applied to both A- and C-fibres to characterise CAPs in terms of amplitude, area under the curve (AUC), duration and conduction velocity:

A-CAP characterisation: from 0 to 0.5 mA in 0.02 mA increments (26 stimuli) - 50 µs pulse width

(Day 7: saline n = 13 nerves, oxaliplatin n = 8 nerves. Peak pain: saline n = 9 nerves, oxaliplatin n = 11 nerves)

C-CAP characterisation: from 0.5 to 10 mA in 0.5 mA increments (20 stimuli) – 1 ms pulse width

(Day 7: saline n = 10 nerves, oxaliplatin n = 11 nerves. Peak pain: saline n = 9 nerves, oxaliplatin n = 12 nerves)

A pair of recording electrodes (A and B) were connected to a NL100AK AC pre-amplifier headstage (Digitimer, UK). The headstage was power-supplied by a NL104 AC pre-amplifier (NeuroLog System, UK) set on the differential recording A-B and the signal output was amplified (x 1000). The output was band-pass filtered (100-1500 Hz, NL125-NL126; NeuroLog System, UK) and 50-60 Hz noise was eliminated by a HumBug Noise Eliminator (Quest Scientific, Digitimer, UK). The signal was sent to an oscilloscope (TDS 3012; Tektronix, UK) that was back-connected to the CED 1401 and allowed the visualisation of action potentials in real-time (Figure 2-4). Recordings were analysed using Spike2 software 8.13 (Cambridge Electronic Design, UK).

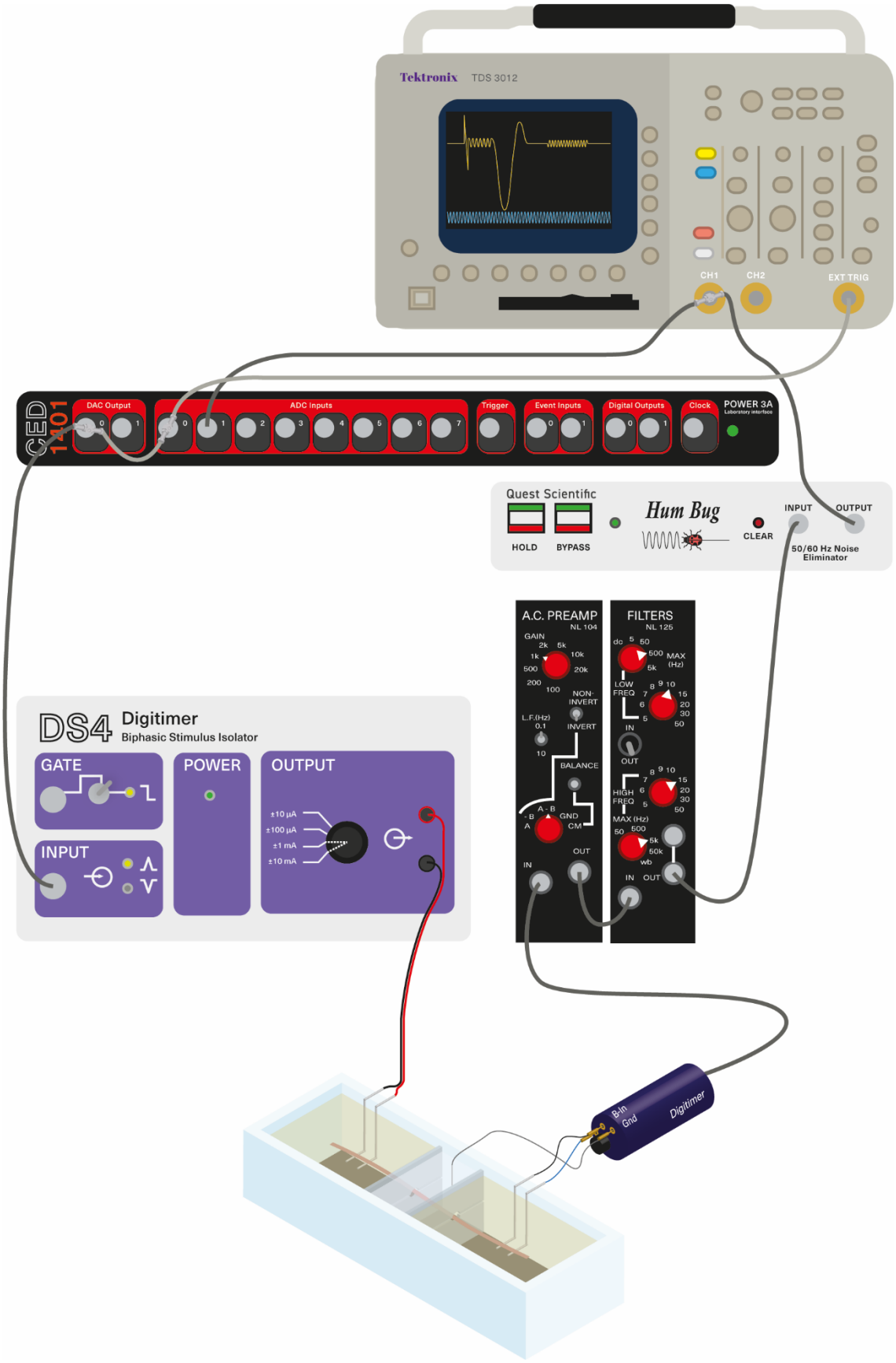

Figure 2-4 Schematic representation of the electrophysiology set-up

The saphenous nerve was electrically stimulated with a constant current stimulus produced by the DS4 bi-phasic stimulus isolator and applied at the two stimulating electrodes. The DS4 received a voltage signal

from a DAC output of the CED 1401 interface, which was directly connected to Spike2 software. The opposite end of the nerve was placed on a pair of recording electrodes connected to a NL100AK AC pre-amplifier headstage. The headstage was powered by an NL104 AC pre-amplifier. The NL104 was set on the differential recording A-B and amplified the signal x1000. The output was band-pass filtered (100-1500 Hz) with an NL125-NL126 filter and 50-60 Hz electrical noise was further eliminated by a HumBug Noise Eliminator. The HumBug sent the final signal to an oscilloscope, where action potential could be observed in real-time.

2.4 Mitochondrial functionality investigation

2.4.1 Assessment of bioenergetic profiles

2.4.1.1 Dissection of dorsal root ganglia (DRG) and isolation of DRG neurons

Animals were terminally anesthetised with an overdose of pentobarbital sodium (Euthatal; Merial, UK). Depth of anaesthesia was assessed by checking animal reflexes, including pedal withdrawal, blink and righting reflex. Once reflexes had been lost, cardiac puncture was performed, and 2-5 ml of blood were extracted to facilitate further dissection. The skin on the rats' back was cut open to expose the spinal column and cuts were made bilaterally in the muscle alongside the spine, starting from the cervical down to the sacral region. The spinal cord was exposed through a laminectomy: the spine was cut transversally at the caudal end and curved scissors were inserted into the spinal canal. Small cuts were made into the bone on both sides, proceeding rostrally, in order to peel away the lamina and access the spinal cord lying underneath. DRG were collected bilaterally, starting at L6/L5 proceeding rostrally until 14 DRG were collected. Immediately after dissection, DRG were placed in Minimum Essential Media (MEM; Sigma, UK) containing 1% penicillin/streptomycin (P/S; Invitrogen, UK) at room temperature. All DRG were additionally trimmed to remove any remaining blood, dura mater, dorsal and ventral roots and placed into 2 ml of fresh, sterile MEM containing 1% P/S and 2.5% collagenase (type IV; Worthington Biochemicals, UK). DRG were incubated at 37°C/5% CO_2 for three hours and triturated hourly through a sterile flame-polished glass pipette, to facilitate their digestion. 0.25% trypsin (Sigma, UK) was added and DRG were incubated at 37°C/5% CO_2 for 10-20 minutes. A single-cell suspension was obtained by additional trituration and warm MEM with 1% P/S and 10% foetal bovine serum (FBS; Sigma, UK) was added to a final volume of 10 ml. The cell suspension was centrifuged at 1 000 rpm for 5 minutes and the supernatant was discarded. The cell pellet was resuspended in 2 ml of warm MEM with 1% P/S, 10% FBS and 0.05% DNase I (Worthington Biochemicals, UK) and gently pipetted on top of a 15% bovine serum albumin (BSA) cushion (2 ml; prepared in MEM with 1% P/S and 10% FBS; Sigma, UK). The suspension was centrifuged at 1 000 rpm for 10 minutes and the layer of debris and myelin that

formed at the interface was removed. BSA and MEM were removed as well and the cell pellet was resuspended in fresh MEM with 1% P/S, 10% FBS and 0.1 % cytosine arabinoside (AraC; Sigma, UK). To ensure a resuspension as homogeneous as possible, cells were triturated 200 times through a 200 µl pipette tip. The cell suspension (100 µl/well) was plated onto XF24 Analyzer multi-well plates (Agilent, UK), leaving 4 empty wells for background correction. Cell plates were incubated overnight at 37°C/5% CO_2 to be used the following day.

2.4.1.2 Bioenergetic profile assay

The Seahorse XF24 Analyzer (Seahorse Bioscience, USA) enables the simultaneous measurement of oxygen consumption and protons production in culture media immediately surrounding adherent cells in a 24-well plate. The readouts of the assay are oxygen consumption rate (OCR), a direct measurement of mitochondrial respiration, and extracellular acidification rate (ECAR), an indicator of glycolytic rate. The Seahorse XF24 FluxPak (Agilent, UK) comprises the XF24 cell culture microplate and a sensor cartridge. The XF24 Analyzer slowly lowers the cartridge into the microplate wells, thus creating a transient microchamber, where optical microsensors at the bottom of the cartridge probe can detect oxygen and proton changes in the culture media. The cartridge also contains four injection ports that allow to add mitochondrial inhibitors directly to the cell wells: oligomycin (Complex V inhibitor); carbonyl cyanide-4 (trifluoromethoxy) phenylhydrazone (FCCP) (uncoupler of oxidative phosphorylation, OXPHOS); and antimycin A and rotenone (Complex III and Complex I inhibitors). The inhibitors are injected in a specific order, to enable the measurement of different parameters of mitochondrial and glycolytic function. OCR measurements following sequential addition of these inhibitors onto DRG neurons allow to assess six parameters of respiratory function: basal respiration; ATP turnover-linked respiration; proton leak; maximal respiration; spare reserve capacity (the ability of cells to respond to stressful conditions); and non-mitochondrial respiration. At the same time, ECAR measurements allow to assess basal glycolysis and glycolytic capacity (the ability of cells to switch from OXPHOS to glycolysis). The morning following DRG neurons isolation, 50 ml of Seahorse (SH) medium were prepared as follows: Seahorse XF base medium containing 2 mM GlutaMAX (Agilent, UK) was supplemented with 5 mM glucose (Sigma, UK) and 1 mM sodium pyruvate (Fisher Scientific, UK), pH was adjusted to 7.4 and the medium was warmed to 37°C. 50 µl of MEM were removed from each cell well of the XF24 Analyzer multi-well plate and DRG neurons were washed with 1 ml of SH medium. 500 µl of SH medium were further added in each well, for a final volume of 550 µl/well. 550 µl of SH medium were added to the background correction wells too. The plate was incubated at 37°C/0% CO_2 for approximately 45 minutes. Mitochondrial inhibitors were dissolved in dimethyl sulfoxide (DMSO; Sigma, UK) to 2.5 mM stock concentration. On the day of the experiment, stock solutions were diluted to their final

working concentration with warm SH medium. Extensive preliminary experiments have been carried out in our lab in the past to identify the optimal concentrations of the compounds on isolated DRG cells. Once diluted to their final concentrations, inhibitors were loaded into injection ports of the XF24 sensor cartridge in the following order: port A contained 55 µl of DMSO, SH medium or oxaliplatin (see sections 2.4.1.3 and 2.4.1.4); port B contained 60 µl of 0.5 µM oligomycin; port C contained 65 µl of 0.2 µM FCCP; and port D contained 70 µl of 0.5 µM antimycin and 0.5 µM rotenone. The cartridge was inserted into the Seahorse XF24 Analyzer for calibration and equilibration. Once these steps were completed, the XF24 multi-well plate was loaded into the Seahorse XF24 Analyzer and the protocol was initiated. A 'mix-wait-measure' cycle was carried out first for 3 times. Each step was carried out as follows: the XF24 Analyzer mixed the wells for 3.5 minutes, paused for 1 minute, mixed the wells for 10 additional seconds and then took OCR/ECAR measurements for 2 minutes. The mitochondrial inhibitors in ports A-D were injected one at a time and 3 cycles of 'mix-wait-measure' were performed in between each port injection. Upon protocol completion, the multi-well plate was ejected from the XF24 Analyzer. Analysis was performed on wells displaying a basal OCR (last measurement before oligomycin addition) between 200 and 900 pMol/min, as seeding densities in this range would ensure a reliable measurement of other OCR parameters by the machine. Therefore, basal OCR values < 200 and > 900 pMol/min were excluded from the final analysis. Final respiration parameters were obtained by subtracting non-mitochondrial respiration from basal respiration, ATP turnover, maximal respiration and proton leak values. 6 to 10 wells were analysed per animal.

2.4.1.3 Bioenergetic profile after exposure to oxaliplatin *in vitro*

DRG were harvested from naïve animals and DRG neurons were isolated as described in section 2.4.1.1. Oxaliplatin (5 mg/ml; Accord Healthcare Ltd) was diluted with fresh SH medium. Different concentrations of oxaliplatin were tested: 50 nM, 5 µM, 10 µM, 100 µM, 250 µM and 500 µM. SH medium was used as a control. Oxaliplatin or SH medium alone were loaded in port A and injected during the bioenergetic profile assay. To ensure sufficient exposure time, the 'mix-wait-measure' step after port A injection was repeated a total of 9 times, for a total exposure time of 1 hour. The rest of the protocol was carried out as described in 2.4.1.2.

2.4.1.4 Bioenergetic profile after exposure to oxaliplatin *in vivo*

Saline- and oxaliplatin-treated animals were tested for mechanical hypersensitivity at day 7 (n = 4 animals/group) and 14 DRG were harvested from each animal (see section 2.4.1.1). Dissociated DRG neurons from one saline- and one oxaliplatin-treated animal were plated onto the same XF24 Analyzer multi-well plate to be assayed simultaneously. The bioenergetic profile

assay was set up as described in section 2.4.1.2. Port A was loaded with 0.8% DMSO as control, as DMSO was used as diluent of compounds in ports B-D.

2.4.1.5 Data normalisation to total protein content

Upon completion of the metabolic assay, 600-700 µl of medium were carefully removed from the wells without disrupting the DRG neurons, ultimately leaving 50-100 µl/well. DRG neurons were fixed in cold 4% (w/v) paraformaldehyde (PFA; Sigma, UK) for 15 minutes and washed in PBS. Cells were fixed in order to be later stained with 4',6-diamidino-2-phenylindole (DAPI; 1: 10 000 in PBS; Sigma, UK) and Neuronal Nuclei antibody (NeuN; 1:5 000 in PBS; Abcam, UK), for the identification of all cell nuclei and neurons, respectively. Stained plates would have then been imaged with the Opera Phenix High Content System in the Wohl Cellular Imaging Centre (WCIC), thus allowing the identification and quantification of neuronal cells (DAPI +ve/NeuN +ve) contributing to the OCR/ECAR profiles generated by the Seahorse XF24 Analyzer. Non-neuronal cells (DAPI +ve/NeuN -ve) would not have been included in the analysis, as a previous investigation in our lab revealed that their contribution to OCR and ECAR profiles is negligible (Duggett et al. 2017). Due to COVID-19, closing of facilities and later social distancing measures meant that training at the WCIC was not feasible and access to use the Opera Phenix was not obtained. Consequently, the normalisation of the XF24 cell culture microplates to neuronal cell number was not possible and was performed based on protein content instead. The PBS volume in each well was transferred to separate 1.5 ml tubes (one tube per well). 50 µl/well of 0.25% trypsin (Sigma, UK) were added and plates were incubated at 37°C for 20 minutes to help cells to detach from the wells. Cells were additionally scraped off the bottom of the wells and transferred to their respective tubes for a centrifugation step at 14 000 rpm for 10 minutes. The supernatant was discarded and 100 µl of lysis buffer were added. The lysis buffer was prepared as follows (Sadick and Darling 2017): 300 mM Tris-HCl, pH 8; 2% (% w/v) sodium dodecyl sulphate (SDS; Sigma, UK); and Protease Inhibitor Cocktail Set III (VWR International, UK), NaF (Sigma, UK) and sodium orthovanadate (Sigma, UK) at 1:100 dilution. Samples were boiled at 100°C for 30 minutes, followed by 2 hours at 60°C. Lysates were centrifuged at 14 000 rpm for 15 minutes at 4°C. Supernatants were transferred to fresh tubes and the protein content in each well was quantified using the BCA (Bicinchoninic acid) Protein Assay Kit (Merck, UK), following the manufacturer's protocol. A standard curve was prepared with BSA references (Merck Millipore, UK) used at the following concentrations: 0, 25, 125, 250, 500 and 1 000 µg/ml. 5 µl of protein homogenates/BSA standards were loaded in triplicate onto a 96-well plate. A BCA working reagent was prepared mixing the BCA solution and 4% cupric sulfate provided in the kit, in a 50:1 ratio, and 100 µl were added per well. Plates were kept in the dark and incubated on a shaker for 45 minutes at room temperature to develop a colorimetric reaction. Absorbance was

read at 562 nm in a SpectraMax 340PC Microplate Reader (Molecular Devices, USA). The absorbance value of the standard references was plotted against their concentration to generate a standard curve. Absorbance values of protein lysates were interpolated to the standard curve to calculate protein concentration. OCR and ECAR parameters were normalised to total protein content.

2.4.2 Protein expression of mitochondrial calcium channels and citrate synthase

At the time point of interest, animals were terminally anesthetised with an overdose of pentobarbital sodium (Euthatal; Merial, UK). Depth of anaesthesia was assessed by checking animal reflexes, including pedal withdrawal, blink and righting reflex. Once reflexes had been lost, DRG were collected as described in section 2.4.1.1. 10-12 DRG were harvested per animal. Saphenous nerves were collected bilaterally as described in section 2.3.1. For sciatic nerve collection, the skin and muscle of the outer thigh were cut longitudinally to expose the nerve lying underneath. The connective tissue surrounding the nerve was removed. Nerve samples of approximately 1-2 cm were obtained cutting the nerve distally, before its branching into sural, tibial and peroneal nerves, and proximally at the sciatic notch region. Both sciatic nerves were dissected. All samples were collected in 1.5 ml tubes. Immediately after dissection, DRG and nerves were flash-frozen in liquid nitrogen and stored at -80°C.

2.4.2.1 Sample homogenisation

DRG samples and saphenous nerves were lysed in 300 µl of RIPA (Radioimmunoprecipitation assay) lysis buffer, whilst sciatic nerves were lysed in 500 µl of the same buffer. The RIPA lysis buffer consisted of 50 mM Tris HCl (pH 7.4), 150 mM NaCl (Fisher Scientific UK), 1% (% v/v) Triton X-100 (Fisher Scientific, UK), 0.5% (% w/v) sodium deoxycholate (Sigma, UK), 0.1% (% w/v) SDS (Sigma, UK), 1 mM EDTA disodium salt (Fisher Scientific, UK) and 10 mM NaF (Sigma, UK). Protease Inhibitor Cocktail Set III (VWR International, UK) and sodium orthovanadate (Sigma, UK) were added fresh to the RIPA lysis buffer (1:100) just before the homogenisation process began. To avoid protein degradation, samples were not allowed to thaw before addition of lysis buffer and were always kept on ice. DRG and lysis buffer were placed inside a glass tube and mechanically homogenised with a PFTE pestle attached to a motor-driven tissue homogeniser (VWR International, UK). Samples underwent two 30-second cycles of homogenisation, with a 10-second break in between. If necessary, a third mechanical burst was applied for 30 additional seconds. The glass tube was constantly kept on ice to avoid sample overheating. Once completely dissolved into solution, samples were moved to their original 1.5 ml tube. The glass tube and pestle were cleaned with ethanol (Sigma, UK) and water before a new DRG sample was homogenised. Samples were centrifuged at 4°C, 12 000 rpm for 20 minutes. Supernatants were

transferred to new 1.5 ml tubes, while the pellets containing cell debris were discarded. Nerves were homogenised with an ultrasonic homogenizer 4710 (Cole-Parmer, USA) and underwent two 30-second cycles of sonication, with a 10-second break in between. If necessary, a third sonication burst was applied for 30 additional seconds. Tubes were kept on ice to avoid overheating during the sonication process. The sonicator was carefully cleaned with Virkon (Lanxess, Germany), ethanol (Sigma, UK) and water before a new sample was homogenised.

2.4.2.2 Protein quantification and sample preparation

Homogenates were kept at -20°C and were allowed time to thaw in ice before protein quantification. Quantification was performed with the BCA Protein Assay Kit (Merck, UK), as described in section 2.4.1.5, using a standard curve of BSA references (Merck Millipore, UK) at the following concentrations: 0, 200, 400, 600, 800, 1 000, 1 200, 1 400, 1 600, 1 800 and 2 000 µg/ml. Protein homogenates were diluted in double distilled water to obtain a solution containing 25 µg of protein. A sample loading buffer made of 30 mM NaH_2PO_4 (Sigma, UK), 30% (% v/v) glycerol (Fisher Scientific, UK), 0.05% (% w/v) bromophenol blue (Sigma, UK) and 7.5% (% w/v) SDS (Sigma, UK) was added to protein samples to facilitate gel loading and sample visualisation. 1,4-Dithiothreitol (DTT, 200 mM stock; Sigma, UK) was added as reducing agent. Protein samples, loading buffer and DTT were mixed in a 10:5:2 ratio. Samples were mixed thoroughly by vortexing and were centrifuged at 2 000 rpm for 10 seconds. Samples used to detect the Mitochondrial Calcium Uniporter (MCU), the Voltage-Dependent Anion Channel 1 (VDAC1) and Citrate Synthase (CS) were boiled at 95°C for 5 minutes. Samples used for the detection of OXPHOS complexes were heated at 37°C and samples for the $Na^+/Ca^{2+}/Li^+$ exchanger (NCLX) detection were left cold, to avoid protein degradation.

2.4.2.3 Western blot

Protein samples were separated through SDS polyacrylamide gel electrophoresis (SDS-PAGE). Gels were hand cast using two glass plates (short plate: 10.1 cm x 7.3 cm; spacer plate: 10.1 cm x 8.2 cm; depth in between: 1.5 mm) locked in place in a Mini-PROTEAN Tetra Cell Casting Stand apparatus (Bio-Rad, UK). Samples for MCU, VDAC, CS and NCLX detection were run onto 10% resolving polyacrylamide gels, whilst samples for OXPHOS complexes were run onto 15% resolving polyacrylamide gels. Gel recipes are displayed in Table 2-3 and Table 2-4. The running gel buffer used in the preparation of resolving gels was made of 1.5 mM TRIS base (FisherScientific, UK), 8 mM EDTA disodium salt (Fisher Scientific, UK), 0.4% (% w/v) SDS (Sigma, UK), and pH was adjusted to 8.8. Resolving gels set for 45-60 minutes. Once the resolving gels were set, 4.8% stacking gels were prepared on top, using the formulation in Table 2-4. Wells were formed placing a 1.5 mm-thick 15-well comb (Bio-Rad, UK) between the two glass plates.

The stacking gel buffer, used in the preparation of stacking gels, was made of 0.5 mM TRIS base (FisherScientific, UK), 8 mM EDTA disodium salt (Fisher Scientific, UK), 0.4% (% w/v) SDS (Sigma, UK) and pH was adjusted to 6.8. Stacking gels set for 15-20 minutes. Resolving and stacking gels were prepared in advance and kept at 4°C for up to 7 days. On the day of the experiment, gels were placed inside a Mini-PROTEAN Tetra Cell 2-gel vertical electrophoresis system (Bio-Rad, UK) and the tank was filled with electrode buffer (50 mM TRIS base, 384 mM glycine, 1.8 mM EDTA disodium salt, 10% SDS (% w/v) and pH adjusted to 8.8). Combs were carefully removed from the gel and wells were washed with dH_2O to remove any excess of acrylamide. 15 µl of each protein sample were loaded into a well with a gel loading tip (Alpha Laboratories, UK). 3 µl of Precision Plus Protein All Blue Prestained Protein Standards (Bio-Rad, UK) were loaded into one well to act as a reference for molecular weights. 5 µl of liver homogenate or rat heart mitochondria (Abcam, UK) were loaded into a well as positive control. Sample loading buffer was added to any empty well to ensure a straight run across the gel. Electrophoresis was performed at 30 mA (constant) until samples run through the stacking gel and reached the resolving gel. At that point, electrophoresis was performed at 40 mA (constant) until the dye front reached the bottom of the glass plate.

Table 2-3 Resolving polyacrylamide gel recipe

	10% gel	**15% gel**
Running gel buffer	3 ml	3 ml
Acrylamide (30% ProtoGel; National Diagnostics, UK)	4 ml	6 ml
Ammonium persulfate 1 mM (APS; Sigma, UK)	60 µl	60 µl
N,N,N',N'-Tetramethylethylenediamine (TEMED; Sigma, UK)	6 µl	6 µl
dH_2O	5 ml	3 ml

Table 2-4 Stacking polyacrylamide gel recipe

Stacking gel buffer	1 ml
Acrylamide (30% ProtoGel; National Diagnostics, UK)	650 µl
APS 1 mM (Sigma, UK)	80 µl
TEMED (Sigma, UK)	5 µl
dH_2O	2.3 ml

At the end of the run, gels were removed from their glass cassette and the stacking gel portion was cut off. Proteins were transferred onto an Immobilon-P polyvinylidene difluoride (PVDF) membrane (pore size 0.45 µm; Merck Millipore, UK) that had been activated in methanol (Fisher Scientific, UK) for 3 minutes before use. A transfer cassette was assembled as: sponge, blotting paper (x2), PVDF membrane, gel, blotting paper (x2) and sponge. Sponges, blotting paper and the PVDF membrane were all soaked in transfer buffer (25 mM TRIS base, 192 mM glycine, 20% (% v/v) methanol) before being assembled into the transfer cassette. The cassette was placed inside a Mini Trans-Blot Electrophoretic Transfer Cell (Bio-Rad, UK) and the tank was filled with transfer buffer. An ice packet was placed inside the tank and the tank itself was kept on ice, to avoid overheating. The transfer was performed at 50 V (constant), 230 mA maximum, for 2.5 hours. The membrane was then incubated in blocking buffer (5% (% w/v) dried skimmed milk, 0.2% (% v/v) Tween-20 (Fisher Scientific, UK) in tris-buffered saline (TBS)) for 1 hour at room temperature. TBS comprised 50 mM TRIS-base, 154 mM NaCl and pH was adjusted to 7.4. After blocking, the membrane was incubated with primary antibodies (listed in Table 2-5) in 5% (% w/v) dried skimmed milk, 0.1% (% v/v) Tween-20 (Fisher Scientific, UK) in TBS overnight at 4°C. The following day, the membrane was washed four times in 10-minute steps in washing buffer (2.5% (% w/v) dried skimmed milk, 0.2% (% v/v) Tween-20 (Fisher Scientific, UK) in TBS). The membrane was incubated with secondary fluorescent antibodies (listed in Table 2-5) for one hour at room temperature and the washing steps were repeated once more. The membrane was left in TBS until imaging. Imaging was performed at the LI-COR Odyssey (LI-COR Biosciences) scanner, that allowed to visualise protein bands in the 700 nm and 800 nm channels at the same time. Images were saved as .tif files for further analysis.

Table 2-5 List of primary and secondary antibodies for western blot

Primary antibody	**Host and dilution**
Anti-MCU (14997, Cell Signaling Technology, UK)	Rabbit; 1:500
Anti-VDAC1 (ab15895, Abcam, UK)	Rabbit; 1:1 000
Anti-CS (16131-1-AP, Proteintech, UK)	Rabbit; 1:2 000
Anti-NCLX (SAB2102181, Sigma, UK)	Rabbit; 1:500
Anti-OXPHOS complexes (ab110413, Abcam, UK)	Mouse; 1:1 000
Anti-β actin (MAB1501, Merck Millipore, UK)	Mouse; 1:5 000
Anti-β tubulin (ab18207, Abcam, UK)	Rabbit; 1:1 000
Secondary antibody	**Host and dilution**
Anti-rabbit Dylight 800 (A23920, Abbkine, China)	Goat; 1:5 000
Anti-mouse Alexa fluor 680 (A21058, Fisher Scientific, UK)	Goat; 1:5 000

2.4.2.4 Semi-quantitative analysis

Analysis was performed using ImageJ software 1.53a. A same-size rectangular box was drawn around each band and pixel intensity was measured. A box of the same size was also drawn above or below each band to measure background pixel intensity. Band intensity was subtracted from the background measurements to obtain the intensity value for each protein band. β-actin or β-tubulin were used as loading controls. Protein intensity of each band was normalized to the loading control in the same protein lane. MCU, VDAC, CS and NCLX were normalized to β-actin expression, whilst protein intensity for the OXPHOS complexes was normalized to β-tubulin expression.

2.4.3 Gene expression of mitochondrial calcium channels and citrate synthase

2.4.3.1 RNA extraction

DRG, saphenous and sciatic nerves were collected as previously described (see section 2.4.2). Samples were placed into gentleMACS M Tubes (Miltenyi Biotec, UK) and kept on ice, to avoid RNA degradation. RNA was extracted from samples using TRIzol Reagent (Invitrogen, UK) and silica-based columns (PureLink RNA Micro Kit, Invitrogen, UK), following the manufacturer's protocols. Samples were homogenised in 1 ml of TRIzol Reagent. 5 ng/µl of PureLink Carrier RNA were added to each tube to increase the final RNA yield. Samples were homogenised using a gentleMACS Dissociator (Miltenyi Biotec, UK) and centrifuged at 12 000 rpm for 1 minute. Lysates were moved into sterile, nuclease-free 1.5 ml tubes and left to rest at room temperature for 5 minutes. 200 µl of chloroform (Invitrogen, UK) were added and tubes were shaken vigorously for 5 minutes and incubated at room temperature for 5 minutes. After a centrifugation step at 14 000 rpm at 4°C for 15 minutes, the lysates separated into a clear, top aqueous layer containing RNA, an interphase and a lower red phenol-chloroform layer, rich in proteins and DNA. The aqueous layer was carefully transferred into new sterile, nuclease-free 1.5 ml tubes and RNA was precipitated by the addition of an equal amount of 70% ethanol (Sigma, UK). Samples were vortexed, moved to PureLink Micro Kit Columns and centrifuged at 14 000 rpm for 1 minute. The flow-through was discarded and spin columns were washed with 350 µl of Wash Buffer I, followed by a centrifugation step at 14 000 rpm for 1 minute. Spin columns were placed into a new collection tube and 20 µl of PureLink DNase solution (10 µl PureLink DNase in 10 µl 2X DNase Buffer) were added. After a 15-minute incubation at room temperature, spin columns were washed again with 350 µl of Wash Buffer I, followed by a centrifugation step at 14 000 rpm for 15 seconds. The flow-through was discarded and spin columns were washed with 500 µl of Wash Buffer II, followed by a centrifugation step at 14 000 rpm for 15 seconds. The flow-through was discarded and the washing step in Wash Buffer II was

repeated once again. To ensure that the column membrane was dry, spin columns were centrifuged at 14 000 rpm for 1 minute. The columns were placed into recovery tubes and the membrane-bound RNA was eluted in 12 µl (nerves) or 22 µl (DRG) of RNAse-free water (Qiagen, UK) after an incubation step at room temperature for 1 minute and a 1-minute centrifugation at 14 000 rpm. RNA quantity and quality were assessed using a NanoDrop ND-1000 spectrophotometer (ThermoFisher, UK).

2.4.3.2 Reverse transcription

Reverse transcription of RNA was performed using the iScript cDNA Synthesis Kit (Bio-Rad, UK). 5 µl of master mix solution (4 µl 5X iScript Reaction Mix plus 1 µl iScript Reverse Transcriptase) were added to a clean, RNAse-free PCR tube. 1 µg of RNA was added to the tube and the reaction volume was brought up to 20 µl with nuclease-free water (Qiagen, UK), thus obtaining a cDNA concentration of 50 ng/µl. cDNA synthesis was carried out in a thermal cycler (Applied Biosystems, Thermofisher, UK) using the following protocol: priming at 25°C for 5 min; reverse transcription at 46°C for 20 min; reverse transcriptase inactivation at 95°C for 1 min; and hold at 4°C. Final cDNA concentrations were adjusted to 5 ng/µl using nuclease-free water (Qiagen, UK).

2.4.3.3 Primer validation

The oligonucleotide sequences (Sigma, UK) for *Mcu*, *Vdac*, *Nclx* and *Cs* amplification are shown in Table 2-6. Differences in gene expression between saline- and oxaliplatin-treated animals were measured through relative quantification by normalisation to two housekeeping genes, β-actin (*Actb*) and Tyrosine 3-Monooxygenase/Tryptophan 5-Monooxygenase Activation Protein Zeta (*Ywhaz*) (Sigma, UK; Table 2-6). Primers for *Actb* and *Ywhaz* had already been validated by Dr L. de Clauser, who kindly provided them for this investigation.

Table 2-6 Oligonucleotide sequences for *Mcu*, *Vdac*, *Nclx*, *Cs, Actb and Ywhaz* amplification

Primer name	Sequence (5'→ 3')	Amplicon length (bp)
Mcu Forward	ATGACGCGCCAGGAATATGT	164
Mcu Reverse	AGCGGGTCTCTCAGTCTCTT	
Vdac1 Forward	GACTGCTGTCAATCTCGCCT	106
Vdac1 Reverse	GTTCACTTTGGCCGAAAAGC	
Nclx Forward	TCCGAGGTGAAGCTGGAAC	175
Nclx Reverse	TGAGGAGGACCACCACAATGA	
Cs Forward	ACCTTACCATCCACAGTGACCAT	145
Cs Reverse	TGGTTTGCTAGTCCATGCAGAG	
Actb Forward	ACCCGCGAGTACAACCTTCTT	208
Actb Reverse	GACCCATACCCACCATCACAC	
Ywhaz Forward	CCACTCCGGACACAGAATATC	127
Ywhaz Reverse	GCTCCTTGCTCAGTGACAGAC	

Primers were designed using Primer-BLAST. Upon reception, primers were dissolved in nuclease-free water to prepare a 100 µM solution. Primer validation was performed to ensure primer specificity and optimal experimental conditions. A qPCR reaction mix was prepared using 5 µl of SsoAdvanced Universal SYBR Green Supermix (2x stock; Bio-Rad, UK), 0.5 µl of each forward and reverse primer, 3.5 µl of nuclease-free water (Qiagen, UK) and 0.5 µl of cDNA/negative control, for a total volume of 10 µl reaction mix. A DRG cDNA sample (5 ng/µl) was used for this validation experiment. Three different negative controls were included: a no-reverse transcriptase control containing all reagents and a reverse transcribed product synthesised without addition of reverse transcriptase, to detect genomic contamination in the RNA products; a no-template control containing all reagents except for cDNA, to detect primer dimers; and a genomic DNA control, to detect primer binding with genomic DNA. The genomic DNA control (5 ng/µl) was obtained from rat muscle tissue and was provided by L. de Clauser. Two reaction mixes were prepared for each cDNA/negative control to test two stock concentrations of primers, 2 µM and 1 µM. The reaction mix was loaded in duplicate in a single 384-well plate (Roche, UK). Plates were sealed with an adhesive sealing foil (Roche, UK) and centrifuged at 1 000 rpm for 1 minute

to ensure all reagents were at the bottom of the wells. Real-time qPCR was performed using the LightCycler 480 (Roche, UK) with the following conditions: preincubation at 95°C for 3 min (1 cycle); denaturation at 95°C for 30 s, annealing at 62°C for 30 s and extension at 72°C for 30 s (repeat denaturation, annealing and extension steps for 40 cycles); melting at 95°C for 5 s, 65°C for 60 s and 95°C continues (melt curve analysis, 1 cycle); and lastly, cooling at 40 °C for 30 s. Data analysis was performed using the LightCycler 480 software 1.5.1 (Roche, UK). At the end of the qPCR run, the sealing foil was removed and 0.5 µl of TriTrack DNA Loading Dye 6X (ThermoFisher, UK) were added to each well for gel electrophoresis. The content of each well was loaded onto a 2% (w/v) agarose (Sigma, UK) gel. Samples were run alongside a GeneRuler 100 bp Plus DNA Ladder (ThermoFisher, UK) at 100 V for 45 minutes. Upon completion of the electrophoretic run, the gel was visualised under a UV transilluminator (Syngene, UK). The size of the qPCR amplicons was assessed to confirm amplification of the correct target. Negative control wells were also evaluated to confirm the lack of amplification. It was concluded that all primers were specific for the target genes and their optimal stock concentration was 2 µM. A further qPCR experiment was performed to assess the optimal concentration of cDNA for DRG and nerve samples. Four total amounts of cDNA were tested: 1, 5, 10 and 20 ng. It was concluded that 5 ng of DRG cDNA were sufficient, whereas saphenous and sciatic nerves required 10 ng of cDNA to amplify all target genes.

2.4.3.4 Real-time qPCR

A qPCR reaction mix was prepared using 5 µl of SsoAdvanced Universal SYBR Green Supermix (2x stock; Bio-Rad, UK), 0.5 µl of each forward and reverse primer (2 µM) and 2-3 µl of nuclease-free water (Qiagen, UK), for a total volume of 8-9 µl reaction mix per cDNA sample. The reaction mix was loaded in a 384-well plate (Roche, UK) and 1 µl (DRG) or 2 µl (nerves)of cDNA (5ng/µl stock) were added into each well. Samples were loaded in triplicate in a single plate. Three different negative controls were included in the plate: a reaction mix containing all reagents except for primers, to detect contamination in the reagents; a no-template control containing all reagents but no cDNA, to detect primer dimers; and a no-reverse transcriptase control, to detect genomic contamination. All negative controls were loaded in triplicate in a single plate as well. DRG, sciatic and saphenous nerve samples were loaded onto different plates. Biological replicates of each tissue from saline and oxaliplatin treatment groups harvested at the same time point (day 7 or peak pain) were loaded onto the same plate. A brain sample from a naïve animal was used as positive control. Upon loading completion, plates were sealed with an adhesive sealing foil (Roche, UK) and centrifuged at 1 000 rpm for 1 minute to ensure all reagents were at the bottom of the wells. Real-time qPCR was performed using the LightCycler 480 (Roche, UK) using the same conditions described in section 2.4.3.3.

As samples were plated in triplicate within a plate, the three Ct values were averaged to provide the final Ct value for each sample. Standard deviation between Ct values for each triplicate was accepted at ≤ 0.3 and Ct values outside this cut-off value were excluded from average. Relative quantification was performed using the $2^{-\Delta\Delta Ct}$ method. *Actb* and *Ywhaz* Ct values were averaged to obtain a mean housekeeping Ct value.

ΔCt was calculated as:

Ct (target gene) - Ct (housekeeping genes average)

A control ΔCt (saline average) was calculated by averaging the ΔCt values of samples from saline-treated animals.

ΔΔCt was then calculated as:

ΔCt (sample) – ΔCt (saline average).

The final $2^{-\Delta\Delta Ct}$ value represents the fold-change in gene expression.

2.5 Statistical analysis

All statistical analyses were performed with GraphPad Prism 8. Patient data are expressed as mean ± standard deviation (SD). All preclinical data are expressed as mean ± standard error of the mean (SEM), except for cold allodynia data, which are expressed as median ± interquartile range. Statistical significance was accepted at $p < 0.05$ and no further distinction was made between $p < 0.01$ or $p < 0.001$.

The sample size for the clinical investigation had been selected prior to the beginning of this PhD project and approved by a research ethics committee. *A priori* power calculations were not performed for the preclinical investigations. In most cases, individual animal cohorts generated to characterise this OIPN model's behaviour or to collect nerve/DRG samples for further experiments consisted of 6 animals per group. This was dictated by the testing equipment available, which only allowed 6 (i.e. wheels for spontaneous running behaviour) or 12 (i.e. rig for mechanical and cold stimulation) animals to be tested at a time. Based on the lab's previous experience with rat models of CIPN, studies including a minimum of 6 animals per group are powered enough to detect a significant difference in behaviour between treatment groups. Additionally, final behavioural analyses were conducted by collating results from animal cohorts tested for the same behavioural response but at different times, thus increasing the sample size, and therefore the power of the tests. Electrophysiology investigations were also more powered, as sample sizes were based on nerves rather than animals. Lastly, the sample size of mitochondrial bioenergetics investigations was limited by COVID-19 restrictions.

As data in our studies are approximately normally distributed, parametric tests were selected to conduct all statistical analyses, except for the evaluation of cold allodynia development where an ordinal scale was employed to score animals, thus requiring a nonparametric test. A repeated measures (RM) two-way ANOVA was employed whenever tests were conducted repeatedly (with the exception of mechanical hypersensitivity data, see below), with treatment as the between-subjects factor. Time was the within-subjects factor for behavioural investigations and OCR/ECAR evaluation, while current intensity was the within-subjects factor for electrophysiology experiments. *Post hoc* corrections were only carried out if the initial test found a significant main effect or interaction between the two factors. Correction for multiple comparisons between saline- and oxaliplatin-treated animals was conducted with Holm-Sidak, as the Bonferroni test was deemed overly conservative, especially in case of the large number of repeats in the electrophysiology data. Dunnett's *post hoc* (or Dunn's, in case of nonparametric test) was employed when saline- and oxaliplatin-treated groups were compared with their respective baselines to assess how the behaviour developed over time. Comparisons across two unrelated group at a single time point were conducted with unpaired t-tests, whereas dependent samples were tested with a paired t-test. When more than two independent groups were compared, a one-way ANOVA was used, and a *post hoc* analysis was conducted in case a significant result was obtained in the first place. Some of the experiments described here had been performed in other CIPN models (i.e. paclitaxel- and bortezomib-induced peripheral neuropathy) previously investigated in the lab by other members of the group. Statistical tests and associated *post hoc* analyses used then were evaluated and only applied when considered the most appropriate ones to analyse the data presented here. The statistical tests used to analyse specific datasets throughout this thesis are summarised below.

To assess the weight gain between saline- and oxaliplatin-treated animals during the study, a repeated measures (RM) two-way ANOVA with Holm-Sidak *post hoc* was performed (Figure 4-2). To assess the development of mechanical hypersensitivity between saline- and oxaliplatin-treated animals at each time point, two-tailed multiple-comparison unpaired t-tests with Holm-Sidak correction were carried out (Figure 4-3, Figure 5-7, Figure 6-1 and Figure 6-7). To assess the development of cold allodynia in saline- and oxaliplatin-treated animals, a Friedman test (nonparametric equivalent to RM one-way ANOVA) was carried out with Dunn's *post hoc* to compare scores to their respective baselines in each group (Figure 4-4, Figure 4-5). To assess spontaneous wheel running (Figure 4-7) and numbness (Figure 4-8) between saline- and oxaliplatin-treated animals, a RM two-way ANOVA with Holm-Sidak *post hoc* was performed. To evaluate the effect of learning on running behaviour, a RM two-way ANOVA with Dunnett's *post hoc* compared to baseline was performed (Figure 4-7).

To assess A-CAP parameters between glucose- and fructose-supplemented bicarbonate, data were analysed as follows: peak to peak amplitude, A-CAP area under the curve (AUC) and duration were analysed with a RM two-way ANOVA with Holm-Sidak *post hoc* (Figure 5-3 A-C). Area under the curve of the traces for peak to peak amplitude, A-CAP AUC and duration, latency, conduction velocity and threshold were analysed with paired two-tailed t-tests (Figure 5-3 D-F and inserts A-C). To assess A-CAP parameters between crushed and uncrushed nerves, and between saline- and oxaliplatin-treated animals, data were analysed as follows: peak to peak amplitude, A-CAP AUC and duration were analysed with a RM two-way ANOVA with Holm-Sidak *post hoc* (Figure 5-5, Figure 5-8 and Figure 5-10 A-C). Area under the curve of the traces for peak to peak amplitude, A-CAP AUC and duration, latency, conduction velocity and threshold were analysed with unpaired two-tailed t-tests; in case of unequal variances between groups, Welch's correction was performed (Figure 5-5, Figure 5-8 and Figure 5-10 D-F and inserts A-C). To assess C-CAP peak amplitude between crushed and uncrushed nerves and between saline- and oxaliplatin-treated animals, data were analysed with a RM two-way ANOVA with Holm-Sidak *post hoc* (Figure 5-6, Figure 5-9 and Figure 5-11 A). C-CAP parameters between crushed and uncrushed nerves and between saline- and oxaliplatin-treated animals at 0.5, 1.0 and 1.5 mA (peak amplitude, C-CAP AUC, duration, latency, conduction velocity and threshold) were analysed with unpaired two-tailed t-tests; in case of unequal variances between groups, Welch's correction was performed (Figure 5-6, Figure 5-9 and Figure 5-11 B-G).

To assess raw OCR and ECAR profiles in dissociated DRG neurons between saline- and oxaliplatin-treated animals and between *in vitro* concentrations of oxaliplatin, data were analysed with a RM two-way ANOVA with Holm-Sidak *post hoc* (Figure 6-2, Figure 6-3, Figure 6-5 and Figure 6-6 A). To assess basal respiration, ATP turnover, maximal respiration, spare reserve capacity, proton leak, basal glycolysis and glycolytic capacity in DRG neurons between saline- and oxaliplatin-treated animals, data were analysed with paired two-tailed t-tests. A pairwise comparison was carried out as DRG neurons from one saline- and one oxaliplatin-treated animal were always plated and assessed in parallel in the same multi-well plate (Figure 6-2, Figure 6-3 B). To assess basal respiration, ATP turnover, maximal respiration, spare reserve capacity, proton leak, basal glycolysis and glycolytic capacity in DRG neurons between *in vitro* concentrations of oxaliplatin, data were analysed with a one-way ANOVA with Dunnett's *post hoc* compared to control (SH medium) (Figure 6-5 B-G and Figure 6-6 B-D). To assess protein expression of OXPHOS complexes, MCU, VDAC, NCLX and CS (Figure 6-4, Figure 6-9, Figure 6-10, Figure 6-11 and Figure 6-12) and mRNA expression of *Mcu*, *Vdac*, *Nclx* and *Cs* (Figure 6-8), data were analysed with unpaired two-tailed t-tests.

Chapter 3 Mitochondrial DNA as predictive biomarker for OIPN

3.1 Introduction

Chemotherapy-induced peripheral neuropathy (CIPN) patients commonly report symptoms of physical and social distress that negatively impact on their daily life (Bakitas 2007, Speck et al. 2012). Therefore, it is imperative to develop easy and accessible techniques to early identify patients at risk of neuropathy, thus potentially changing the chemotherapy regimen or alternatively reducing its dose to alleviate CIPN symptoms. Quantitative sensory testing (QST) might be used as a predictor tool for CIPN. A retrospective analysis revealed that head and neck cancer patients presented sensory deficits, in particular in touch detection, before receiving chemotherapy compared with healthy volunteers (Roldan et al. 2018). Similarly, multiple myeloma patients displayed a high incidence of QST deficits before chemotherapy administration (baseline) compared with healthy controls (Kosturakis et al. 2014) and measures of sharpness and warmth detection at baseline were associated with increased pain and numbness later on during the chemotherapy treatment (Vichaya et al. 2013). Several QST studies have identified sensory deficits in oxaliplatin-treated patients. In a recent prospective study, patients with gastrointestinal malignancies about to start an oxaliplatin treatment were assessed for different QSTs before treatment initiation (baseline); at different times during the chemotherapy regimen; and 1 year after treatment completion (Reddy et al. 2016). Deficits in heat detection and pellet retrieval, the ability to pick up small pellets from adjacent wells, at baseline were associated with grade 2-3 chronic neuropathies at 1 year, thus suggesting a predictive role for these tests. Nevertheless, the study included a small number of patients and its results need to be validated in bigger cohorts (Reddy et al. 2016). Similar subclinical sensory deficits were reported prior to treatment initiation in larger cohorts of colorectal cancer (CRC) patients compared with healthy volunteers (Boyette-Davis et al. 2012, de Carvalho Barbosa et al. 2014, Wang et al. 2016). These deficits predisposed patients to the development of chronic oxaliplatin-induced peripheral neuropathy (OIPN) after cumulative doses of oxaliplatin. Interestingly, it has been suggested that cancer itself might predispose patients to develop more severe neuropathic symptoms after exposure to chemotherapy (de Carvalho Barbosa et al. 2014, Wang et al. 2016). Different studies have employed the Bumps Detection test, a rapid, inexpensive and easy QST, where subjects are asked to detect a small cylinder raised at different heights on a smooth surface; the shortest bump height identified represents the tactile detection threshold (Kennedy et al. 2011). The test has been suggested as a baseline screening tool for the early detection of neuropathy in CRC patients, given the identification of a subclinical

deficit in touch detection prior to oxaliplatin administration (Boyette-Davis et al. 2012, de Carvalho Barbosa et al. 2014, Wang et al. 2016).

A genetic screening approach could provide a useful tool to identify patients at risk. For instance, genetic screening is already in use in the clinic to prevent severe and lethal toxicity to capecitabine in breast cancer patients. The main cause of toxicity is a deficiency in dihydropyrimidine dehydrogenase (DPD), a key enzyme in the catabolism of the drug that is encoded by *DPYD*. Up to 5% of patients have no functional DPD and have a significantly higher risk of developing severe and potentially lethal toxicity to capecitabine. *DPYD* genotyping is therefore used in some centres to predict capecitabine toxicity based on the presence of the most common deleterious polymorphism (Lunenburg et al. 2016, Etienne-Grimaldi et al. 2017). A recent systematic meta-analysis identified 36 studies using a pharmacogenomics approach to investigate potential predictive markers of OIPN (Cliff et al. 2017). Although the mechanism underlying the pathology is not clear yet, most studies have employed a candidate gene approach focusing on genes coding for enzymes involved in drug detoxification, sensitivity to chemotherapy compounds and DNA repair mechanisms. Overall, there is no real evidence that single nucleotide polymorphisms (SNPs) in these genes are actually associated with oxaliplatin neurotoxicity, as most results could not be validated or reproduced in further studies (Cliff et al. 2017). Rather than focusing on a few specific genes, a genome-wide association (GWA) analysis allows investigation of hundreds of SNPs at a time. A Korean GWA study reported 9 novel SNPs in 8 genes putatively associated with chronic OIPN (Won et al. 2012). However, a further retrospective study in a Japanese population showed that only one of the 'Korean' SNPs was significantly linked to severe OIPN (Oguri et al. 2013). Moreover, another study on a Caucasian population aimed at validating the same SNPs failed to confirm their role in chronic OIPN (Terrazzino et al. 2015). The inconsistency of results obtained so far highlights the need to improve the methodology of pharmacogenomic studies before a genetic screening approach can be introduced in the clinic to stratify patients at risk of developing OIPN.

Mitochondria play many pivotal roles within the cell and alterations to their functionality are often associated with pathological states and disorders, including CIPN [reviewed in (Trecarichi and Flatters 2019)]. Mitochondrial functionality is regulated for the most part by nuclear genes. However, mitochondria possess their own genome, which encodes for 37 essential genes for mitochondrial function (see section 1.4.4). Mitochondrial mass, shape and mitochondrial DNA (MtDNA) copy number vary among cell types and physiological and/or pathological states. Additionally, transcription of mitochondrial genes, and therefore mitochondrial activity, is often proportional to MtDNA copy number [reviewed in (Hock and Kralli 2009)]. The mitochondrial network is highly dynamic and mitochondrial mass is maintained by the balance between

mitochondrial formation (biogenesis) and degradation (mitophagy) and processes of fusion and fission (division) [reviewed in (Dominy and Puigserver 2013)]. In particular, biogenesis can be induced in states of long-term high-energy demand (i.e. stressful conditions), through a finely regulated machinery involving transcription of nuclear and mitochondrial genes, MtDNA replication and proteins import within the organelles [reviewed in (Dominy and Puigserver 2013)]. For instance, *in vitro* exposure of different cell lines to chemotherapy agents, including etoposide, paclitaxel and other microtubule modulators (Arany et al. 2008, Fu et al. 2008, Wagner et al. 2008), and oxidative stress (Lee et al. 2000) resulted in increased mitochondrial biogenesis. As MtDNA levels can vary in stressful conditions, MtDNA content has been suggested as biomarker of mitochondrial dysfunction (Malik and Czajka 2013).

As the mitochondrial genome is independent of the nuclear one, MtDNA can be quantified by assessing the ratio of MtDNA to nuclear DNA (nDNA) through real-time quantitative PCR (qPCR). Preclinical evidence generated in our lab using qPCR showed that MtDNA levels were increased by 64% in the whole blood of oxaliplatin-treated animals compared with saline-treated controls 24 hours after treatment cessation and before the appearance of pain-like symptoms [under review (Trecarichi et al. 2020)]. This finding suggested that altered MtDNA levels might be involved in OIPN development. Conversely, MtDNA levels did not differ from saline-treated animals when pain-like behaviour reached the peak of its severity. We did not observe any change in Complex I expression or activity between treatment groups at either time point investigated. Our hypothesis is that mitochondrial biogenesis and/or MtDNA replication were increased to compensate for the oxaliplatin-induced mitochondrial dysfunction. As a result, Complex I expression/activity could be restored as well. By comparison, MtDNA levels in the blood of paclitaxel- and bortezomib-treated animals did not differ from vehicle-treated controls before the appearance of pain-like behaviour and were only increased at the peak pain time point. Overall, our results suggested a potential role for MtDNA as blood biomarker for OIPN.

3.2 Aims

The aim of this investigation was to assess the feasibility of using MtDNA as blood biomarker to predict the susceptibility to OIPN in CRC patients. Whole blood samples were collected from oxaliplatin-naïve patients prior to treatment initiation, at different time points during infusion cycles and after treatment cessation. DNA was extracted from blood samples and MtDNA levels were quantified as MtDNA/nDNA ratio.

3.3 Results

3.3.1 Primers specifically amplify regions in the mitochondrial and nuclear genome

More than 95% of MtDNA is duplicated in the nuclear genome. Therefore, it is pivotal to select primers that avoid the co-amplification of nuclear pseudogenes to accurately quantify MtDNA content. Melting curves were checked to ensure specific amplification of the nuclear and mitochondrial DNA regions. Both hB2M and hMito primers amplified specific and distinguishable regions of DNA, as shown by the two single peaks at approximately 79°C and 83°C in Figure 3-1.

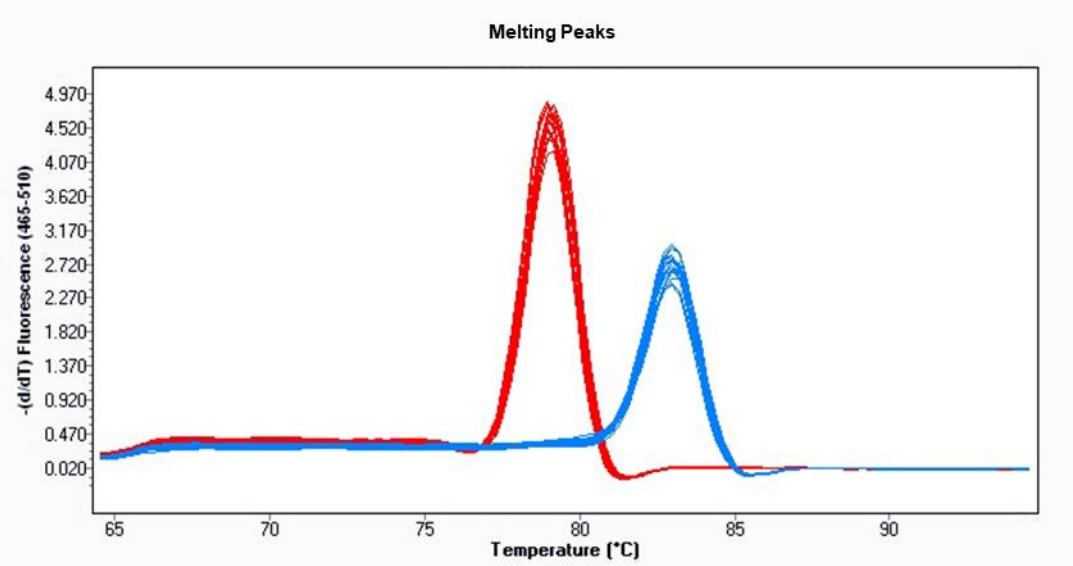

Figure 3-1 Representative melting curves for MtDNA and nDNA products

Typical melting curves of nuclear amplicons (in red) show a peak at approximately 79°C, while mitochondrial amplicons (in blue) appear as a single peak at approximately 83°C.

3.3.2 MtDNA levels are heterogenous among patients and time points

A total of 57 patients were recruited in the study and blood was harvested before treatment initiation (T0). Blood was then collected at regular intervals throughout the chemotherapy cycles: T1 = after the first cycle of chemotherapy; T2 = approximately after 3 months from the beginning of chemotherapy; T3 = approximately after 6 months from the beginning of chemotherapy; and T4 = approximately after 3 months from completion of chemotherapy (see section 2.1.2). Collection of blood at these later time points was not always feasible and the final sample sizes for data analysis were as follows: T1 n = 51; T2 n = 37; T3 n = 20; and T4 n = 11. Figure 3-2 A illustrates the distribution of MtDNA levels (expressed as MtDNA/nDNA ratio) across the different time points investigated. Mean MtDNA content was similar at all time points, as shown in Table 3-1.

Table 3-1 Mean MtDNA content at different time points in the study

Time point	MtDNA content (mean ± SD)
T0	30.01 ± 24.46
T1	28.33 ± 18.03
T2	25.67 ± 15.61
T3	27.76 ± 18.00
T4	27.64 ± 18.47

However, results showed a high level of heterogeneity among patients, with MtDNA copy numbers ranging from values close to 0 to a maximum of 146.3 (at T0). Figure 3-2 B represents individual MtDNA contents over time. Whilst in some cases MtDNA levels were relatively stable across time points, some patients displayed highly variable MtDNA levels from one time point to the other, thus suggesting that MtDNA copy number might be altered after treatment. However, access to patient data is required in order to confirm this hypothesis.

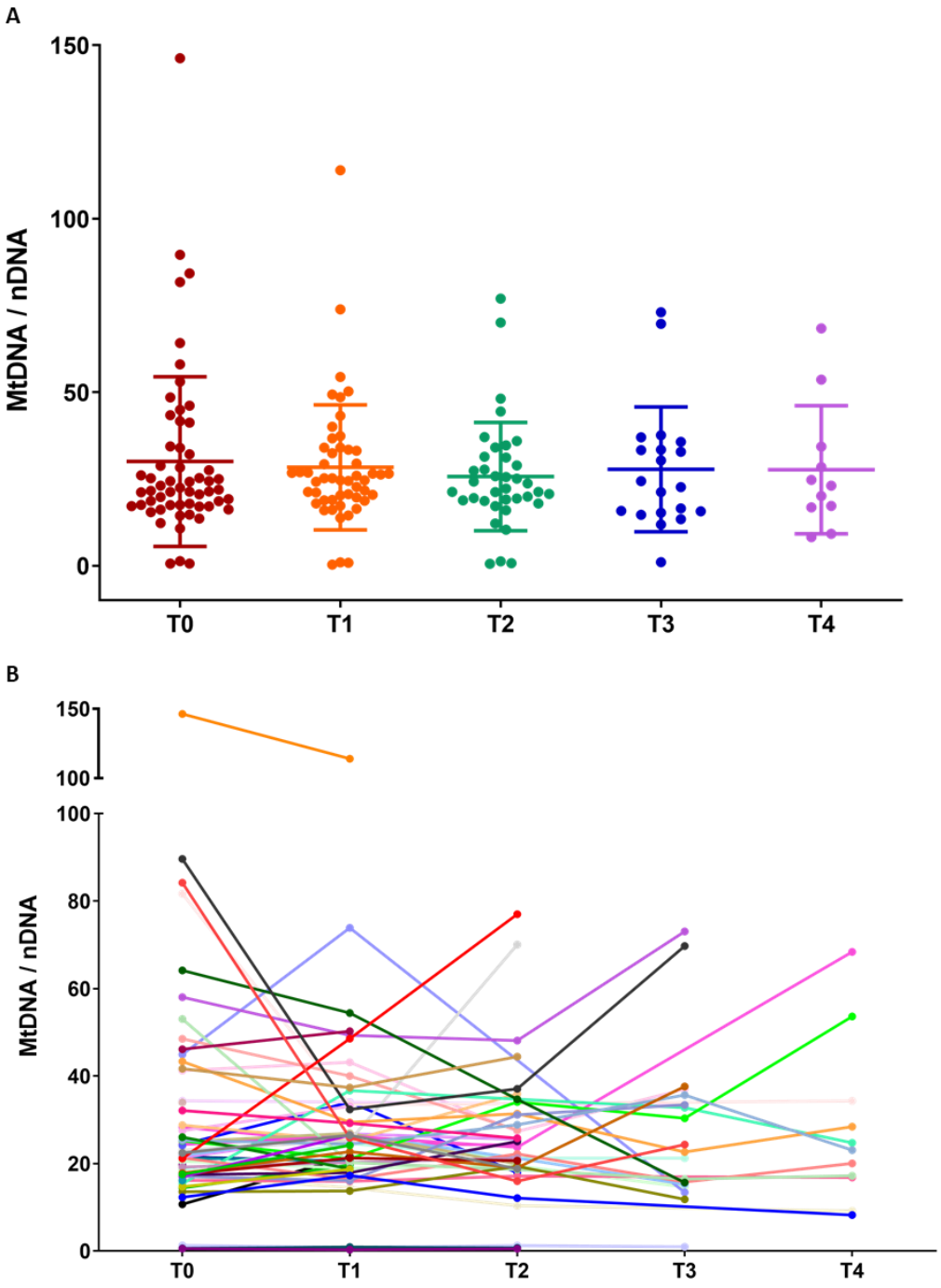

Figure 3-2 MtDNA levels in oxaliplatin-treated patients prior to, during and after the chemotherapy regimen

(A) MtDNA levels in patient blood at all time points investigated. Data are represented as mean ± SD. (B) MtDNA levels of individual patients over time. T0 n = 57; T1 n = 51; T2 n = 37; T3 n = 20; and T4 n = 11.

3.4 Discussion

MtDNA was investigated as a potential blood biomarker for OIPN in colorectal cancer patients. This study was based on our preclinical data showing increased MtDNA content in the whole blood of oxaliplatin-treated animals before the appearance of pain-like symptoms. MtDNA levels were successfully quantified in terms of MtDNA/nDNA ratio using qPCR. We observed a high degree of heterogeneity among patients at all time points investigated and, at times, throughout the course of the chemotherapy regimen. The variability observed here (e.g. MtDNA levels range at T0: 0 to 146, with an average (± SD) of 30 ± 25) was not unexpected and is indeed consistent with findings from other studies that used the same MtDNA quantification protocol described in this chapter (Czajka et al. 2015, Malik et al. 2015, Rosa et al. 2020). For instance, Rosa et al. investigated the MtDNA/nDNA ratio in the whole blood of 23 healthy controls and observed that MtDNA content ranged from 50 to 171, with a mean ratio of 84 ± 29 (Rosa et al. 2020). Additionally, the evaluation of 20 diabetic patients revealed similar results, with MtDNA/nDNA levels ranging from 35 to 138, with a mean ratio of 82 ± 25. However, it is worth mentioning that comparing our study with these results is not entirely appropriate, as MtDNA levels in the blood are heavily influenced by the pathological state, which differs between our study population and Rosa's. In addition, our investigation did not include healthy controls. Being able to compare our results with data from colorectal cancer patients would be the ideal scenario, as cancer itself is responsible for changes in MtDNA content. For instance, MtDNA levels in peripheral blood lymphocytes were significantly higher in chemotherapy-naïve colorectal cancer patients (range, 0.46 to 3.37, with a median of 1.03) compared with matched healthy controls (range, 0.48 to 3.06, with a median of 0.86) (Qu et al. 2011). Nevertheless, the use of different sample types, DNA isolation techniques, primers and analysis methods hinders the ability to draw any comparison between our investigation and the work by Qu and colleagues. Unfortunately, this issue applies to the whole range of studies evaluting MtDNA content, not only in cancer states, but in a wide variety of physiological and pathological conditions, and raises a bigger concern about the actual clinical utility of such studies in the absence of standardised protocols. As a result, standard levels of MtDNA in human blood have not yet been determined, despite the numerous studies conducted in the field (Rosa et al. 2020).

Patient recruitment for this study was completed in February 2020. All blood samples harvested from each patient were processed and data analysis was completed as well. After the first blood harvest at T0, it was not possible to collect blood samples at each time point for all patients. Firstly, patients recruited towards the end of the study had only just begun their chemotherapy regimen and further time points were not available. Secondly, other factors might have affected the collection of samples, including noncompliance with the therapy, withdrawal of consent to

participate to the study or death. Access to patient data, including neuropathy and pain scores from self-report questionnaires, chemotherapy regimen, compliance with therapy and withdrawal from study, could not be obtained because of COVID-19. Indeed, the pandemic took a heavy toll on the clinical team at the Royal Marsden Hospital and research work was postponed. Because of this, we cannot draw any conclusions from the results reported here. Access to the clinical database will be gained in the future and will inform us on the predictive role of MtDNA to identify patients susceptible to OIPN. MtDNA content at T0 will be compared between patients that developed OIPN over the course of the treatment to that of patients who did not develop the neuropathy. In addition, we will evaluate whether changes in MtDNA content after a single cycle of oxaliplatin (T1) correlated with neuropathy development. Later time points (T2-T4) will be useful to gain a better insight into the mechanisms leading to OIPN, specifically the mitochondrial involvement. If an association between MtDNA and neuropathy development is found, MtDNA content could represent an easy and feasible prediction tool to provide clinicians with more information on potential tolerability to oxaliplatin, thus improving patient quality of life. Although the small sample size of this study will prevent us from drawing any final conclusion, the results could help to design a larger case-controlled study in the future.

Malik et al. proposed that increased MtDNA levels are reflective of an upregulated mitochondrial biogenesis in the presence of a ROS-rich cellular environment (Malik and Czajka 2013). For instance, MtDNA levels in breast cancer patients' whole blood were inversely associated with antioxidant enzymes activity (Shen et al. 2010). ROS overproduction and poor antioxidant responses have been reported following oxaliplatin treatment (Di Cesare Mannelli et al. 2012, Janes et al. 2013, Toyama et al. 2014, Waseem et al. 2016, Areti et al. 2017a, Areti et al. 2017b, Areti et al. 2018). ROS are known potent mutagenic agents and MtDNA location in the mitochondrial matrix renders it extremely susceptible to oxidative damage. Additionally, oxaliplatin itself could also have a damaging effect on MtDNA. Oxaliplatin, like all members of the platinum compounds family, exerts its action by creating cross-links within the DNA, both nuclear and mitochondrial, and eventually leads to cell death. MtDNA is particularly susceptible to the formation of Pt-DNA adducts, as MtDNA repair mechanisms are not as efficient as those involved in nDNA damage. A direct damaging effect of platinum compounds on MtDNA has been in fact reported in the literature. For instance, cisplatin intercalated into the MtDNA in rat DRG neurons and inhibited its replication and transcription, which resulted in mitochondrial morphological abnormalities (Podratz et al. 2011). In human cancer cell lines, cisplatin induced MtDNA mutations, which impaired OXPHOS (Girolimetti et al. 2017). Oxaliplatin intrinsic mechanism of action might explain our preclinical observations, where oxaliplatin-treated rats displayed an early increase (64%) in MtDNA content compared with saline-treated controls 24

hours after the last oxaliplatin administration. Conversely, paclitaxel and bortezomib, whose mechanisms of action do not involve DNA cross-linking, did not alter MtDNA levels immediately after treatment cessation [under review (Trecarichi et al. 2020)]. The accumulation of ROS- and Pt-induced MtDNA lesions are likely to affect mitochondrial protein synthesis and functionality and to then aggravate mitochondrial dysfunction and ROS production. For instance, mutations in MtDNA have been associated with increased ROS production and the development of age-related diseases [reviewed in (Hahn and Zuryn 2019)]. In case of a persistently stressful environment, damaged MtDNA might lead to apoptosis and to the subsequent release of cell contents into the bloodstream (Malik 2018).

To our knowledge, MtDNA has never been investigated as biomarker for OIPN or CIPN in general. Altered MtDNA levels in peripheral blood and other bodily fluids were reported in many diseases and conditions [reviewed in (Malik and Czajka 2013, Castellani et al. 2020)]. MtDNA content was suggested as prognostic or diagnostic biomarker for HIV (Cossarizza et al. 2003, Chêne et al. 2007), diabetes (Xu et al. 2012), diabetic nephropathy and retinopathy (Malik et al. 2009, Malik et al. 2015), Parkinson's disease (Pyle et al. 2016), cardiac arrest (Arnalich et al. 2012), pulmonary embolism (Arnalich et al. 2013) and asthenospermia (Kao et al. 2004). Additionally, changes in MtDNA levels were observed following exposure to chemicals and toxins such as low-dose benzene (Carugno et al. 2012), cigarette smoke (Masayesva et al. 2006), herbicides (Lim et al. 2009) and pesticides (Budnik et al. 2013). Interestingly, cancer itself was associated with altered MtDNA content. Increased MtDNA levels were observed in the saliva of head and neck squamous cell carcinoma patients (Jiang et al. 2005), in the serum of testicular cancer patients (Ellinger et al. 2009) and in the cerebrospinal fluid cells of acute lymphoblastic leukaemia patients. Increased MtDNA levels in peripheral blood predisposed patients to higher risk of non-Hodgkin lymphoma (Lan et al. 2008), breast (Shen et al. 2010), pancreatic (Lynch et al. 2011), lung (Hosgood III et al. 2010) and colorectal cancer (Qu et al. 2011); increased MtDNA content in the plasma of advanced prostate cancer patients was associated with poor 2-year survival (Mehra et al. 2007); and increased MtDNA levels in the sputum were linked to higher risk of lung cancer (Bonner et al. 2009). Conversely, decreased MtDNA levels in peripheral blood were found in stage I breast cancer (Xia et al. 2009) and hepatocellular carcinoma patients (Zhao et al. 2011) and were associated with increased risk of renal cell carcinoma (Xing et al. 2008). The abundance of conflicting results on whether pathological states are associated with an increase rather than a decrease, or vice versa, in MtDNA levels could be partly explained by the technical differences in the methodology employed to isolate and quantify MtDNA [reviewed in (Malik and Czajka 2013)]. Particular attention must be paid to the design of primers for MtDNA to avoid co-amplification of nuclear genes. However, several studies amplified mitochondrial genes that are

also expressed in nuclear DNA. Similarly, amplification of nuclear DNA should avoid genes that are present in the nuclear genome as pseudogenes or are highly repetitive, as their amplification would not provide an accurate copy number quantification (Malik et al. 2011). To avoid these issues, we used primers that Malik and colleagues designed to amplify the mitochondrial sequence least similar to nuclear DNA and a unique nuclear region that was not repeated in the rest of the genome (Malik et al. 2011).

3.5 Conclusions

In conclusion, this clinical investigation showed that MtDNA levels can be quantified as MtDNA/nDNA ratio in the whole blood of colorectal cancer patients using specific primers that amplify unique regions of the nuclear and mitochondrial genomes. MtDNA content was highly variable among patients and over time. Upon obtaining access to patient data, it will be possible to understand whether altered MtDNA levels correlate with increased risk of developing OIPN. In case of a positive correlation, MtDNA content might provide a non-invasive prediction tool, which could be easily introduced in the clinic (i.e. blood is already harvested from patients before chemotherapy initiation) and help oncologists select a more adequate treatment approach for patients susceptible to OIPN development.

Chapter 4 Behavioural characterisation

4.1 Introduction

Over the years, many animal models of chemotherapy-induced peripheral neuropathy (CIPN) have been developed to investigate the causal mechanisms of the neuropathy and potential treatment strategies [reviewed in (Hopkins et al. 2016)]. A recent systematic review identified 183 models of CIPN based on species, strain, gender and chemotherapy, which have been repeatedly reported in the literature (Gadgil et al. 2019). In most cases, the development of CIPN is evaluated through behavioural tests that induce sensory pain-like symptoms to mechanical and thermal stimuli. In fewer cases, more complex behaviours are evaluated, including burrowing activity, conditioned place preference and thermal place preference, which allow to evaluate volunteer responses instead of a simple reflex. Additionally, a small number of models involve assessment of motor function, memory, reward and attention. The most common pain-like outcome is hypersensitivity to mechanical stimuli, particularly to von Frey filaments. The second most common outcome is cold-induced limb withdrawal, most frequently generated by exposure to cold-inducing compounds like acetone or menthol (Currie et al. 2019). The vast majority of studies on oxaliplatin-induced peripheral neuropathy (OIPN) are conducted in male rodents, without the presence of any tumour load. Clinically, OIPN appears in two distinct forms: acute OIPN develops early, during or after treatment, and is usually reversible. Patients often report paresthesias and dysesthesias in their hands and feet and in the perioral region, and difficulty in breathing and swallowing may occur. A typical symptom of acute OIPN is the development of acute cold allodynia within hours of oxaliplatin infusion. This side effect often lasts several days but resolves between infusion cycles. However, as the number of cycles increases, so does the duration of this cold hypersensitivity and cold-triggered symptoms take longer to disappear. On the other hand, chronic OIPN develops progressively with cumulative doses of oxaliplatin and may persist for months after treatment cessation (Pasetto et al. 2006, Argyriou et al. 2008). Based on the oxaliplatin treatment regimen (single or repeated administration), preclinical models reproduce both the acute and chronic OIPN syndromes, mostly measured in terms of mechanical and thermal hypersensitivity [reviewed in (Hopkins et al. 2016)].

A systemic administration of low-dose oxaliplatin at 2 mg/kg on four alternate days has proven to lead to the progressive development of mechanical hypersensitivity that persisted long after treatment completion (Boyette-Davis and Dougherty 2011). The intermittent administration of oxaliplatin mimics the clinical treatment schedule, where patients receive oxaliplatin cycles every 2/3 weeks. Another low-dose regimen (2 mg/kg on five consecutive days) resulted in the

concomitant development of mechanical hypersensitivity (Zheng et al. 2011, Xiao et al. 2012) and cold allodynia, which persisted for approximately ten weeks after oxaliplatin administration (Xiao et al. 2012). Additionally, these dosing schedules only impacted weight gain slightly and weight gain rates between oxaliplatin- and vehicle-treated animals were similar upon treatment completion (Boyette-Davis and Dougherty 2011, Xiao et al. 2012). Importantly, a 10 mg/kg cumulative dose did not lead to animal death (Xiao et al. 2012). Therefore, it proved that a low-dose regimen is sufficient to produce a chronic peripheral neuropathy comparable to the clinical syndrome, without developing the toxicities such as ascites, alopecia, abdominal bloating, peritoneal inflammation, reduced motor strength, weight loss/reduced weight gain and, in some cases, death, observed at higher doses (29.6-48.0 mg/kg) (Holmes et al. 1998, Cavaletti et al. 2001, Jamieson et al. 2005, Ling et al. 2007a, Sakurai et al. 2009).

Spontaneous or ongoing pain and numbness in hands/feet are the most common symptoms reported by CIPN patients. However, measuring such symptoms in preclinical models is a challenging task, as clinical evaluation of this side effects relies on verbal reports. Recently, an increasing number of preclinical studies are employing ethological behaviour assessments, including burrowing behaviour and spontaneous wheel running. However, we are not aware of studies that have investigated these behaviours in OIPN models. These tests rely on the evaluation of normal animal behaviour and assume that any deficit observed in natural behaviour can be an indicator of ongoing pain. Wheel running is observed not only in laboratory animals, but also in wild rodents when wheels are placed in their natural habitats (Meijer and Robbers 2014). The use of a wheel apparatus connected to a recording software allows to observe spontaneous running behaviour continuously, for instance overnight, when rats are most active and carry out most of their running activity (Eikelboom and Mills 1988). Additionally, the voluntary behaviour can be quantified objectively, as there is no need for the experimenter to be present, and in a stress-free environment, as wheels are placed in the animal home-cage or a similar environment. Using different paradigms of wheel access and activity recording, deficits in spontaneous wheel running have been reported in a variety of painful conditions, including neuropathic (Whitehead et al. 2017, Griffiths et al. 2018) and inflammatory pain (Cobos et al. 2012, Grace et al. 2014, Kandasamy et al. 2016), osteoarthritis (Stevenson et al. 2011) and migraine pain (Kandasamy et al. 2017).

Numbness is not typically assessed in preclinical models of pain, but one research group has reported sensory deficits in a mouse model of cisplatin-induced neuropathy (Mao-Ying et al. 2014, Krukowski et al. 2017, Maj et al. 2017). The test used to evaluate loss of sensation was the adhesive removal test, which was initially developed by Schallert and colleagues (1982) to evaluate somatosensory and motor function deficits following unilateral nigrostriatal damage.

Performance of the test is relatively easy: adhesive labels are applied to different body parts of the animals and the time required to notice the label and remove it is recorded. Ever since its development, the adhesive removal test has been successfully used in several models of brain injury or disorders and it would be useful to test its effectiveness in assessing sensory loss in peripheral neuropathies as well.

4.2 Aims

The aim of these studies was to develop the skills to investigate and characterise different behavioural responses of a rat model of OIPN that had been used in the lab in the past, although only the time course of mechanical hypersensitivity had been established then. Rats received intraperitoneal injections of oxaliplatin or saline and were assessed for the development of mechanical hypersensitivity through von Frey testing. Further characterisation of the model included the evaluation of cold allodynia (i.e. acetone test) and of ongoing pain, which was investigated through the quantification of spontaneous wheel running behaviour. Additionally, the adhesive removal test was tested for its potential use as a behavioural task indicative of numbness development following oxaliplatin treatment.

4.3 Results

4.3.1 Mechanical hypersensitivity

Animals received intraperitoneal (IP) administration of 2 mg/kg oxaliplatin or saline (see section 2.2.2) and the development of mechanical hypersensitivity to von Frey filaments was measured as described in section 2.2.4.1. Animals were divided into two groups of approximately equal average baseline von Frey responses, and the two groups were randomly allocated to saline or oxaliplatin treatment. Testing was performed under blind conditions for the entire duration of the study, until the peak pain time point was reached. Based on previous reports from the lab, oxaliplatin-treated animals reach the peak of their pain-like behaviour approximately 4/5 weeks after treatment initiation. Therefore, animals were tested weekly on days 7, 12-14, 19-20, 28 and 31-34 (animals from different cohorts were tested on different days, but always once a week). Mechanical hypersensitivity became evident around day 12-14 and developed progressively, until it reached its peak at day 28-34. Animals were allocated to further experiments (see Chapter 5 and Chapter 6) at day 7 or at the peak of their mechanical sensitivity (Figure 4-1). Hence, they were not tested beyond the peak pain time point.

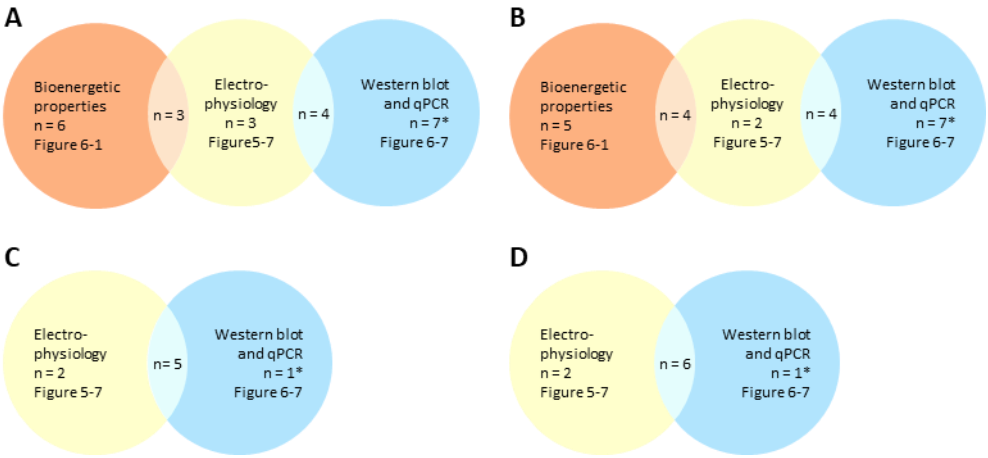

Figure 4-1 Allocation of saline- and oxaliplatin-treated animals to experiments

A total of 31 saline-treated animals and 31 oxaliplatin-treated animals were tested for mechanical hypersensitivity (as shown in Figure 4-3) and allocated to experiments investigating electrophysiological activity and mitochondrial properties, which are described in further chapters. (A) Saline-treated animals culled at day 7. (B) Oxaliplatin-treated animals culled at day 7. (C) Saline-treated animals culled at peak pain (day 28-34). (D) Oxaliplatin-treated animals culled at peak pain (day 28-34). (A-D) Figure 5-7 includes a total of 17 saline-treated animals (10 animals were culled at day 7 and 7 animals were culled at peak pain) and 18 oxaliplatin-treated animals (10 animals were culled at day 7 and 8 animals were culled at peak pain). Figure 6-1 includes a total of 9 saline-treated animals and 9 oxaliplatin-treated animals culled at day 7 (4 animals/group were used for the Seahorse assay and 5 animals/group were used for the quantification of Complex I-V expression). Figure 6-7 includes 17 saline-treated animals (11 animals were culled at day 7 and 6 animals were culled at peak pain) and 18 oxaliplatin-treated animals (11animals were culled at day 7 and 7 animals were culled at peak pain). *Additionally, Figure 6-7 comprises 21 animals/group from 5 additional cohorts previously tested in the lab by Dr N. Duggett (saline day 7 n = 10; oxaliplatin day 7 n = 10; saline peak pain n = 11; oxaliplatin peak pain n = 11), for a total of 38 saline-treated animals and 39 oxaliplatin-treated animals.

Animal weight gain and general health were monitored throughout the study. There was no significant difference in weight gain between saline- and oxaliplatin-treated animals (Figure 4-2, ns RM two-way ANOVA, saline n = 5, oxaliplatin n = 5), and animals administered with oxaliplatin did not show any sign of ill health, like weight loss, alopecia or dullness.

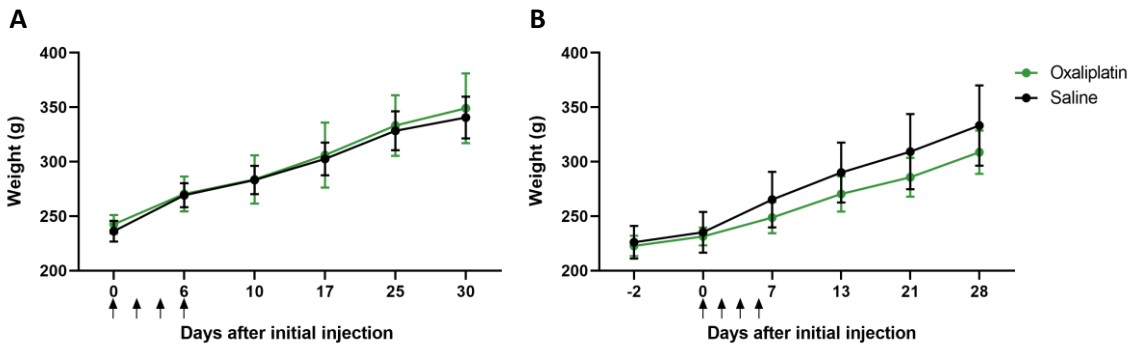

Figure 4-2 Weight gain in saline- and oxaliplatin-treated animals

Animals were weighed before treatment administration and regularly throughout the study. (A) and (B) represent the weight gain from two separate cohorts of animals run at different times. Data are expressed as mean ± SEM. Data were analysed with RM two-way ANOVA. Saline n = 5; oxaliplatin n = 5. Arrows indicate the administration of saline/oxaliplatin on four alternate days (0, 2, 4 and 6).

The use of increasing bending forces allows to discriminate between allodynic and hyperalgesic responses. Withdrawal responses to 4 g filaments are indicative of mechanical allodynia, as naïve rats rarely respond to this innocuous stimulus (< 5% of the times) (Figure 4-3 A). By contrast, approximately 30% of the times, normal rats respond to the 15 g stimulus. Therefore, withdrawal responses to 15 g filaments are indicative of mechanical hyperalgesia (Figure 4-3 C). Lastly, the 8 g force is an intermediate stimulus, as rats respond to it approximately 15% of the times (Figure 4-3 B). Figure 4-3 illustrates changes in mechanical hypersensitivity for all the animals tested by A. Trecarichi that were included in further studies discussed in this thesis (see Figure 4-1). Upon application of the 4 g filament, there was no difference in paw withdrawal responses between saline- and oxaliplatin-treated animals at day 7, 24 hours after the last oxaliplatin administration (Figure 4-3 A, ns two-tailed multiple-comparison unpaired t-tests with Holm-Sidak correction, saline n = 31, oxaliplatin n = 31). At peak pain (day 28-34), the oxaliplatin-treated group displayed a mean 5.3-fold increase in withdrawal frequency compared with the saline-treated controls. However, this finding did not reach statistical significance (Figure 4-3 A, ns two-tailed multiple-comparison unpaired t-tests, saline n = 8, oxaliplatin n = 9). Upon application of the 8 g filament, oxaliplatin-treated animals showed a mean 1.5-fold increase in paw withdrawal responses compared with saline-treated animals at day 7 (Figure 4-3 B, ns two-tailed multiple-comparison unpaired t-tests with Holm-Sidak correction, saline n = 31, oxaliplatin n = 31). At the peak pain time point (day 28-34), oxaliplatin-treated animals exhibited a significant 2.3-fold increase in paw withdrawal responses compared with saline-treated controls (Figure 4-3 B, $*p < 0.05$ two-tailed multiple-comparison unpaired t-tests with Holm-Sidak correction, saline n = 8, oxaliplatin n = 9). Similarly, paw withdrawal responses to 15 g filaments were slightly increased by 1.2-fold at day 7 following oxaliplatin administration, compared with

concurrent saline-treated control rats (Figure 4-3 C, ns two-tailed multiple-comparison unpaired t-tests, saline n = 31, oxaliplatin n = 31). At the peak pain time point (day 28-34), oxaliplatin treatment resulted in a significant 2.4-fold increase in paw withdrawal responses compared with the control group (Figure 4-3 C, *$p < 0.05$ two-tailed multiple-comparison unpaired t-tests with Holm-Sidak correction, saline n = 8, oxaliplatin n = 9).

As not all the animals had been tested after day 7, and therefore the number of repeated observations was not equal among animals, a RM two-way ANOVA could not be performed to analyse the entire cohort tested for mechanical hypersensitivity. However, a RM two-way ANOVA was conducted to analyse the time course of mechanical hypersensitivity between the saline- and oxaliplatin-treated animals that got tested until they reached the peak pain time point. The analysis failed to identify a significant difference between treatment groups over time in response to 4 g filaments (ns, RM two-way ANOVA, saline n = 8, oxaliplatin n = 9). A significant 'time x treatment' interaction was revealed at 8 g ($F_{(2,30)} = 4.652$, $p = 0.0174$, RM two-way ANOVA, saline n = 8, oxaliplatin n = 9), whilst time and treatment main effects were not significant. A simple effect analysis with Sidak *post hoc* to adjust for multiple comparisons identified a significant difference ($p = 0.012$) between saline- and oxaliplatin-treated animals at the peak pain time point (day 28-34). Lastly, a significant 'time x treatment' interaction was observed at 15 g as well ($F_{(2,30)} = 7.708$, $p = 0.0020$, RM two-way ANOVA, saline n = 8, oxaliplatin n = 9), and a simple effect analysis with Sidak *post hoc* confirmed a significant ($p < 0.01$) difference between treatment groups at peak pain (day 28-34). Treatment alone had no significant effect. The main effect of time resulted statistically significant ($F_{(2,30)} = 6.058$, $p = 0.0062$, RM two-way ANOVA, saline = 8, oxaliplatin n = 9). Nevertheless, this main effect was not considered meaningful, given that a significant interaction of time and treatment was observed (i.e. the oxaliplatin-treated group displayed increased mechanical hypersensitivity over time, whilst saline-treatment animals did not).

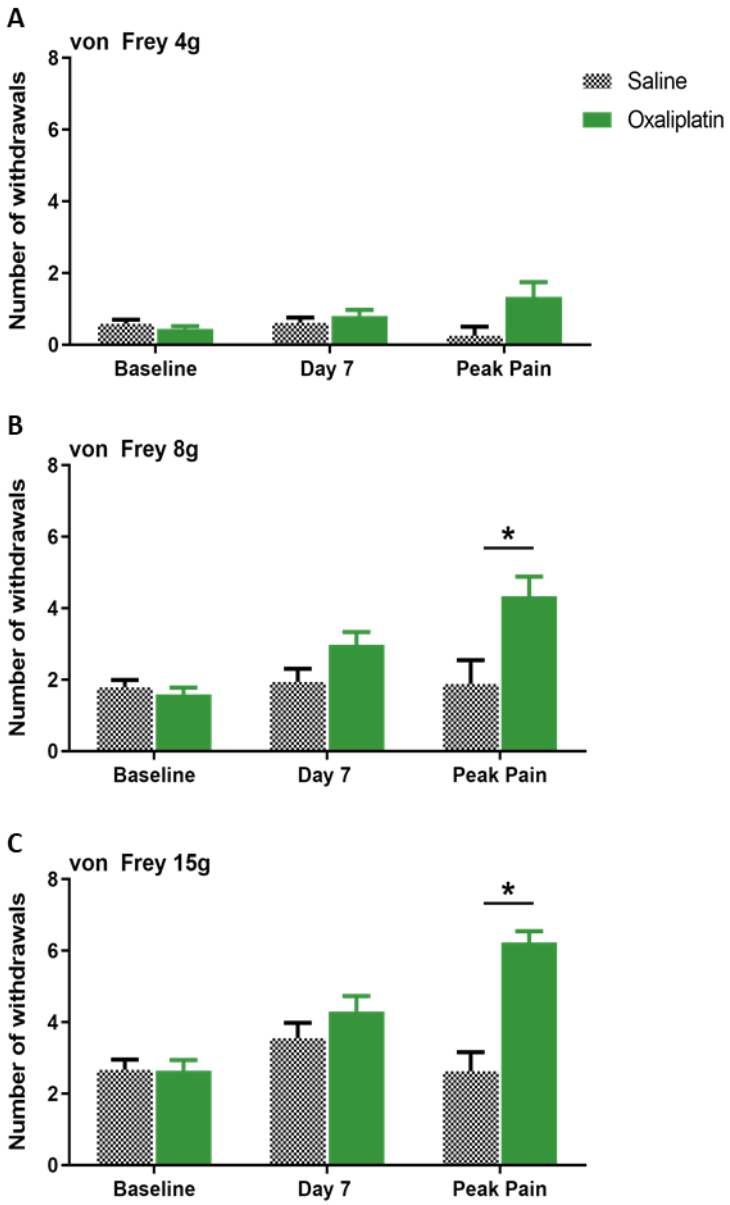

Figure 4-3 Mechanical hypersensitivity to von Frey filaments in saline- and oxaliplatin-treated animals

Mechanical hypersensitivity to 4 g (A), 8 g (B) and 15 g (C) von Frey filaments, expressed as number of withdrawals to 10 stimuli in total. Baseline and day 7: saline n = 31, oxaliplatin n = 31; peak pain (day 28-34): saline n = 8, oxaliplatin n = 9. Data are expressed as mean ± SEM. *p < 0.05, two-tailed multiple-comparison unpaired t-tests with Holm-Sidak correction.

4.3.2 Cold allodynia

The development of cold allodynia following the intermittent IP administration of 2 mg/kg oxaliplatin was investigated. A cold sensation was generated by the application of acetone to the hind paws, as described in section 2.2.4.2. Cold allodynia was assessed in three separate cohorts of animals, which have been pooled together in Figure 4-4. Animals in the first cohort were divided into two groups of almost equal average baseline cold scores, which were then randomly allocated to saline or oxaliplatin treatment. Animals from the remaining two cohorts were also tested for spontaneous running activity: animals had access to a running wheel overnight and were split into two groups that ran almost equally on the wheels during their baseline testing (see section 2.2.4.3). The two groups were randomly assigned to oxaliplatin or saline treatment administration. Animals were tested for cold allodynia weekly, under blind conditions, until the peak pain endpoint was reached. Based on previous findings on OIPN rat models, cold hypersensitivity development follows a similar time course to mechanical hypersensitivity. There was no difference in cold scores between oxaliplatin-treated animals and saline-treated controls (Figure 4-4, ns Friedman test, saline n = 17, oxaliplatin n = 17). As the analysis is nonparametric, the error bars appear larger than what is usually expected from a parametric analysis.

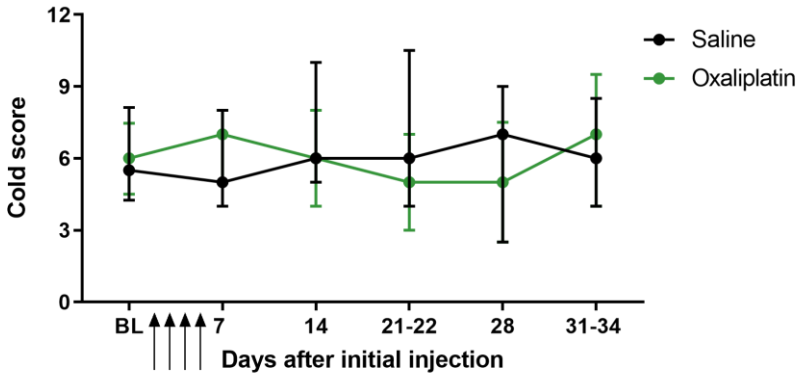

Figure 4-4 Cold allodynia in saline- and oxaliplatin-treated animals

Time course of cold allodynia in response to acetone application, expressed using a cold score (0 = no response, 18 = maximal response). Data are expressed as median ± interquartile range. Data were analysed with the Friedman test. Saline n = 17; oxaliplatin n = 17. BL = baseline. Arrows indicate the administration of saline/oxaliplatin on four alternate days (0, 2, 4 and 6).

The experimenter had no previous experience in performing the acetone test. It is then possible that the animals' responses were scored differently within and among cohorts. For instance, cold scores at the beginning of the testing may have been assigned differently compared with further time points, as more experience was gained in discerning cold-induced responses from normal behaviour (e.g. moving around the cage or grooming). To remove any potential baseline-scoring variability from the analysis, a difference score was generated by subtracting the baseline response from its respective cold score at any other time point. Difference scores > 0 represent an increase in cold-induced responses compared to baseline, whereas scores < 0 reflect a decrease relatively to baseline. Animals from the two treatment groups displayed opposite trends in their average difference scores: saline-treated animals exhibited higher cold scores throughout the study, while oxaliplatin-treated animals were characterised by a reduction in cold-induced responses at day 21 and 28 (Figure 4-5). Nevertheless, there was a high level of interindividual variability at all time points and differences in cold scores compared to baseline were not significant in either treatment group (Figure 4-5, ns Friedman test, saline n = 17, oxaliplatin n = 17).

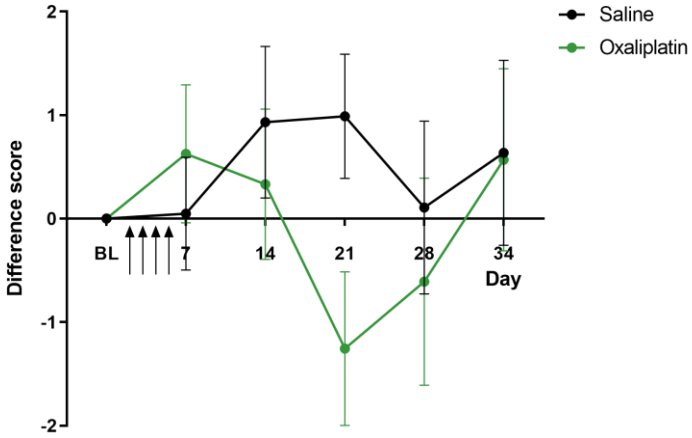

Figure 4-5 Difference score for cold allodynia in saline- and oxaliplatin-treated animals

Time course of cold allodynia in response to acetone application, expressed using a difference score (cold score at any time point – baseline cold score). Data are expressed as mean ± SEM. Data were analysed with the Friedman test. Saline n = 17; oxaliplatin n = 17. BL = baseline. Arrows indicate the administration of saline/oxaliplatin on four alternate days (0, 2, 4 and 6).

To better evaluate the interindividual variability of cold scores and to understand whether animals could be categorised as high and low 'responders', individual responses for each animal included in the investigation have been displayed in Figure 4-6. Cold-induced responses were characterised by a wide spread of data and animals did not cluster into clearly distinct low- and high-score subpopulations. Given the high variability and the lack of significant differences between the saline and oxaliplatin groups, results from this investigation on cold allodynia were considered inconclusive.

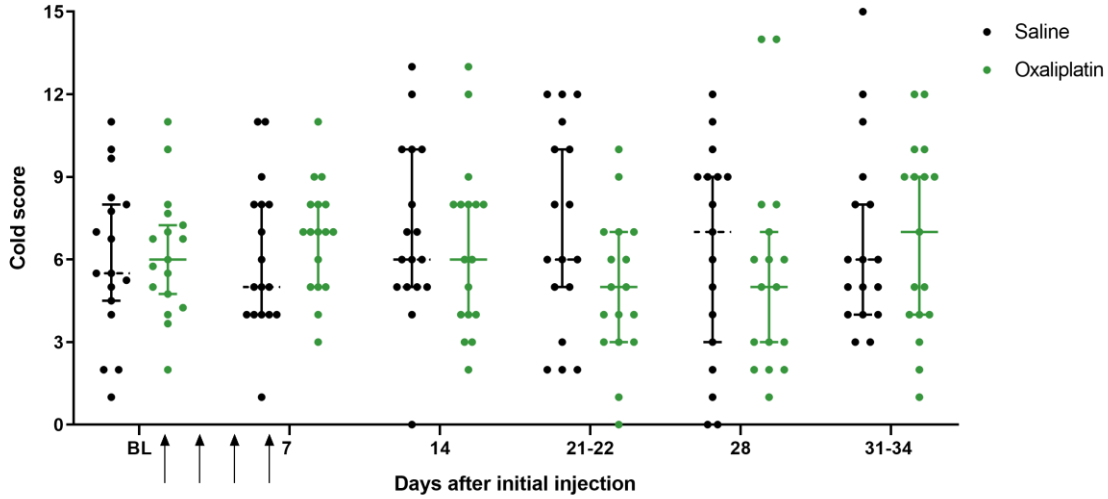

Figure 4-6 Individual cold allodynia responses in saline- and oxaliplatin-treated animals

Time course of cold allodynia in response to acetone application, expressed using a cold score (0 = no response, 18 = maximal response). Dots represent individual cold-induced responses, while lines represent the median ± interquartile range. Saline n = 17; oxaliplatin n = 17. BL = baseline. Arrows indicate the administration of saline/oxaliplatin on four alternate days (0, 2, 4 and 6).

4.3.3 Spontaneous running behaviour

To investigate whether oxaliplatin has any effect on spontaneous behaviour, animals were placed in activity wheel cages, as described in section 2.2.4.3. Their running activity was measured overnight, when animals are most active. Animals were divided into two groups that ran around the same average distance at baseline, and the two groups were randomly allocated to saline or oxaliplatin treatment. The random allocation of animals to their treatment group based on the average distance run at baseline ensured a similar distribution across groups and saline- and oxaliplatin-treated animals displayed similar baseline values for all parameters assessed (Table 4-1).

Table 4-1 Baseline measurements of parameters assessed for spontaneous wheel running behaviour

	Saline (mean ± SEM) n = 11	**Oxaliplatin (mean ± SEM) n = 11**
Total distance (m)	458.0 ± 56.3	418.3 ± 61.4
Mean speed (m/min)	17.1 ± 2.0	14.3 ± 0.9
Maximus speed (m/min)	36.3 ± 2.0	33.9 ± 2.9
Maximum acceleration (m/(min*s))	7.4 ± 0.6	6.9 ± 0.6
Access count	432.4 ± 47.3	452.3 ± 68.7
Active time (s)	1 726.4 ± 187.6	1 559.2 ± 200.9

Animals were tested weekly under blind conditions, until the peak pain endpoint was reached at day 28-34. Results were pooled from two cohorts of animals tested at different times. The same animals were tested for cold allodynia, as described in section 4.3.2. No confirmation of mechanical hypersensitivity development was carried out to avoid testing the animals with too many test modalities at the same time; indeed, excessive testing may cause unnecessary stress for the animals and affect their behaviour. The running parameters assessed were total distance run (Figure 4-7 A), mean speed (Figure 4-7 B), maximum speed (Figure 4-7 C), maximum acceleration (Figure 4-7 D), wheel access count (i.e. number of times the animal accessed the wheel; Figure 4-7 E) and total active time (i.e. time spent on the wheel; Figure 4-7 F). At any time point, there was no significant difference in any of the parameters investigated between oxaliplatin- and saline-treated animals (Figure 4-7, ns RM two-way ANOVA, saline n = 11, oxaliplatin n = 11).

Previous evidence from the lab (Duggett and Flatters 2017, Griffiths et al. 2018) suggested that baseline values are variable among animals and would then affect further time points recordings. For this reason, previous data were analysed using a RM ANCOVA analysis, where baseline measurements were defined as covariates in the experiment and accounted for as such. Nevertheless, ANCOVA analysis was not deemed the appropriate test for the data generated for this OIPN model. First of all, the data here failed to meet the homogeneity of regression slopes assumption that is essential for an ANCOVA analysis. This suggested that the relationship between the covariate (baseline measurement) and the dependent variable (each of the running parameters assessed) was not the same between treatments. Therefore, results from an ANCOVA analysis would be incorrect or misleading. Secondly, average baseline values and their variability were similar between treatment groups (Table 4-1), and therefore it was not deemed necessary to treat baseline recordings as covariates in this study.

At day 7, animals spent more time on the wheels compared with their respective baselines. Oxaliplatin-treated animals accessed the wheels approximately 100 times more than baseline and ran a significantly longer distance of 714 ± 110 m compared with the 418 ± 61 m ran at baseline (mean ± SEM) (Figure 4-7 A, *p < 0.05 RM two-way ANOVA with Dunnett's *post hoc* compared to baseline, saline n = 11, oxaliplatin n = 11). Maximum speed was also increased at day 7, and mean speed and maximum acceleration were significantly higher than baseline (Figure 4-7 B, D, *p < 0.05 RM two-way ANOVA with Dunnett's *post hoc* compared to baseline, saline n = 11, oxaliplatin n = 11). At day 14, the total distance ran by oxaliplatin-treated animals was still significantly longer than baseline (Figure 4-7 A, *p < 0.05 RM two-way ANOVA with Dunnett's *post hoc* compared to baseline, saline n = 11, oxaliplatin n = 11). Additionally, speed and acceleration parameters were significantly increased from baseline (Figure 4-7 B-D, *p < 0.05 RM two-way ANOVA with Dunnett's *post hoc* compared to baseline, saline n = 11, oxaliplatin n = 11). However, engagement on the wheels in terms of time spent on them started to progressively decrease, and by day 28 all parameters investigated returned to similar values to their respective baselines. The last recording on day 34 showed that all parameters were once again higher than baseline, with speed and acceleration parameters significantly so (Figure 4-7 B-D, *p < 0.05 RM two-way ANOVA with Dunnett's *post hoc* compared to baseline, saline n = 11, oxaliplatin n = 11). The running behaviour of saline-treated animals followed a similar time course. At day 7 and 14, all parameters were increased compared with baseline, although only maximum speed and maximum acceleration were characterised by statistical significance (Figure 4-7 C, D, *p < 0.05 RM two-way ANOVA with Dunnett's *post hoc* compared to baseline, saline n = 11, oxaliplatin n = 11). A small decrease in all parameters was observed at day 28. Lastly, at day 34, total distance run, maximum speed and maximum acceleration were significantly higher than baseline (Figure 4-7 A, C-D, *p < 0.05 RM two-way ANOVA with Dunnett's *post hoc* compared to baseline, saline n = 11, oxaliplatin n = 11). Despite similar baseline values between treatment groups, at further time points it was observed that the individual variability for most parameters was higher among saline-treated animals compared with the oxaliplatin group.

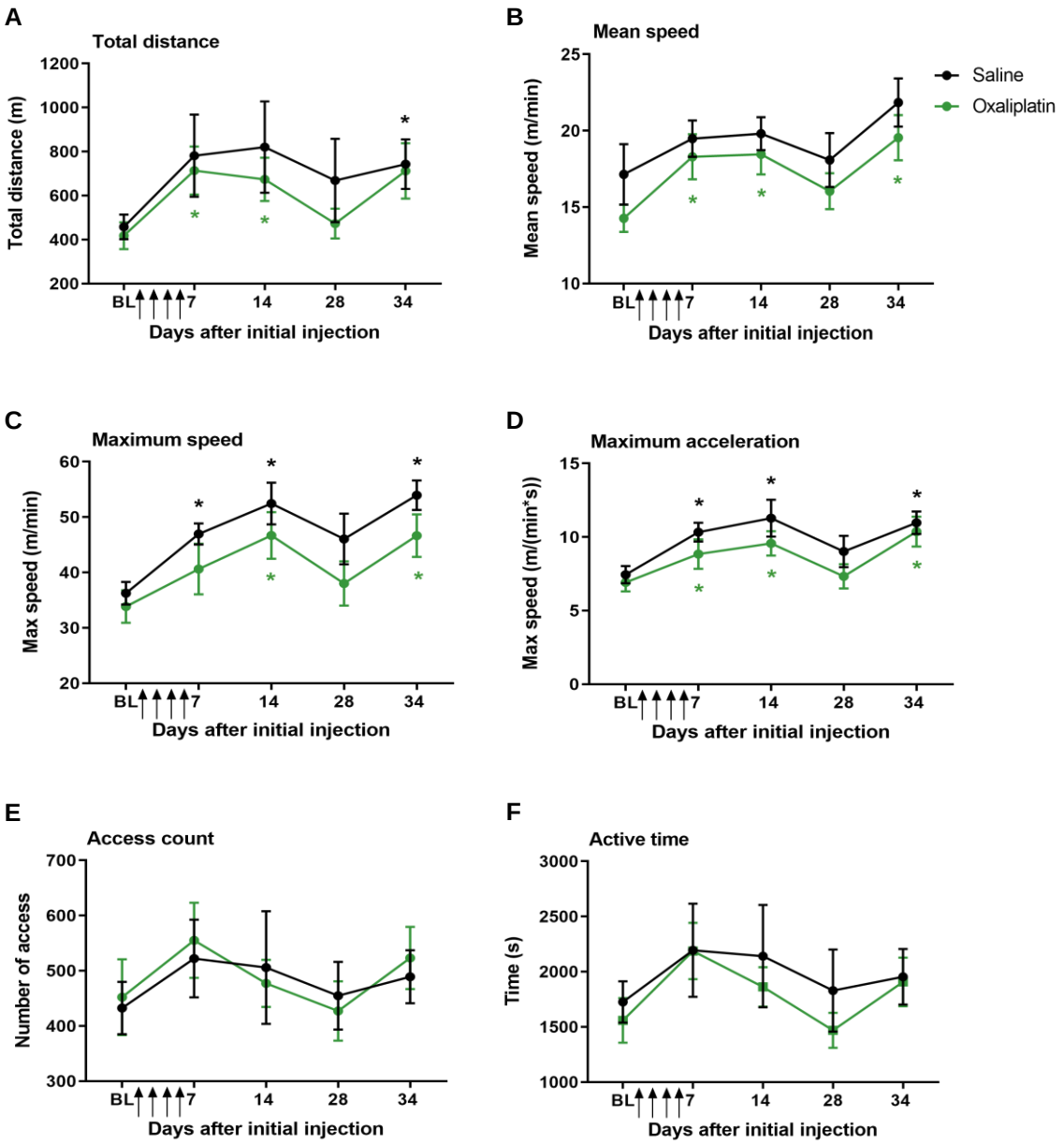

Figure 4-7 Spontaneous running activity in saline- and oxaliplatin-treated animals

Animals were placed in wheel activity cages overnight and running parameters were recorded. (A) Total distance run. (B) Mean speed. (C) Maximum speed. (D) Maximum acceleration. (E) Access count to the wheel. (F) Active time on the wheel. Data are expressed as mean ± SEM. *$p < 0.05$, RM two-way ANOVA (with Dunnett's *post hoc* compared to baseline). Saline n = 11; oxaliplatin n = 11. BL = baseline. Arrows indicate the administration of saline/oxaliplatin on four alternate days (0, 2, 4 and 6).

4.3.4 Adhesive removal behaviour

The adhesive removal test allows to assess both sensory and motor function in animal models (Schallert et al. 1982). Here, it was performed as described in section 2.2.4.4.1, in order to evaluate its ability to assess somatosensory impairment (i.e. numbness) in oxaliplatin-treated animals. Animals included in this study belonged to the first cohort of animals tested for cold allodynia (see section 4.3.2). They were split into two groups of roughly the same baseline cold scores, and the two groups were randomly allocated to receive either saline or oxaliplatin. Animals were trained for three days before one baseline measurement was recorded. Further testing was performed weekly, until day 28-31. Oxaliplatin- and saline-treated animals did not display any difference in time required to sense the presence of the label (Figure 4-8 A, ns RM two-way ANOVA, saline n = 6, oxaliplatin n = 6). Similarly, there was no significant difference in time to remove the label between the two treatment groups (Figure 4-8 B, ns mixed effects model, saline n = 6, oxaliplatin n = 6). One saline-treated animal failed to remove the label in the 5 minutes allocated to the test on two different occasions (day 14 and 28), therefore a RM two-way ANOVA could not be performed. Individual variability within groups was not consistent across groups and time points. Despite the initial training sessions and the care taken to minimise the stress for the animals, the hold required to apply the label remained a source of major stress for the rats. Initial responses to the pad application varied between complete lack of movement and cage exploring, stress- and fear-induced diarrhoea and urination, piloerection or immediate interaction with the sticky pad. Unfortunately, there was no consistency in this initial behaviour across days, nor during the same day when comparing response on the left and right paws. A modified version of the adhesive removal test (Sughrue et al. 2006, Komotar et al. 2007) was developed to overcome the limitations of Schallert's method, in particular the need to train rats for several days before being able to perform the test. Therefore, a new cohort of rats was tested using the modified protocol, as described in section 2.2.4.4.2. Animals included in this study were also tested for spontaneous wheel running (see section 4.3.3). They were split into two groups of approximately equal baseline distance run, and the two were randomly allocated to saline or oxaliplatin treatment. A baseline recording was taken after a single training session and testing was then performed under blind conditions at day 7, 21 and 29. As recommended by Sughrue and Komotar (Sughrue et al. 2006, Komotar et al. 2007), animals were trained only once before the experiment began. Here, such a short training period was not enough to habituate animals to the experimental conditions. In particular, the application of the tape around the forepaw was particularly stress-inducing and required the presence of a second experimenter to completely restrain the animal. Stress-induced responses similar to the ones described for the first protocol were observed upon tape application. The test failed to identify

any difference between oxaliplatin- and saline-treated animals (Figure 4-8 C, ns RM two-way ANOVA, saline n = 5, oxaliplatin n = 5). By the end of the study on day 29, animals from both groups spent less time trying to remove the tape compared with baseline, suggesting that they may have gotten used to the presence of the tape.

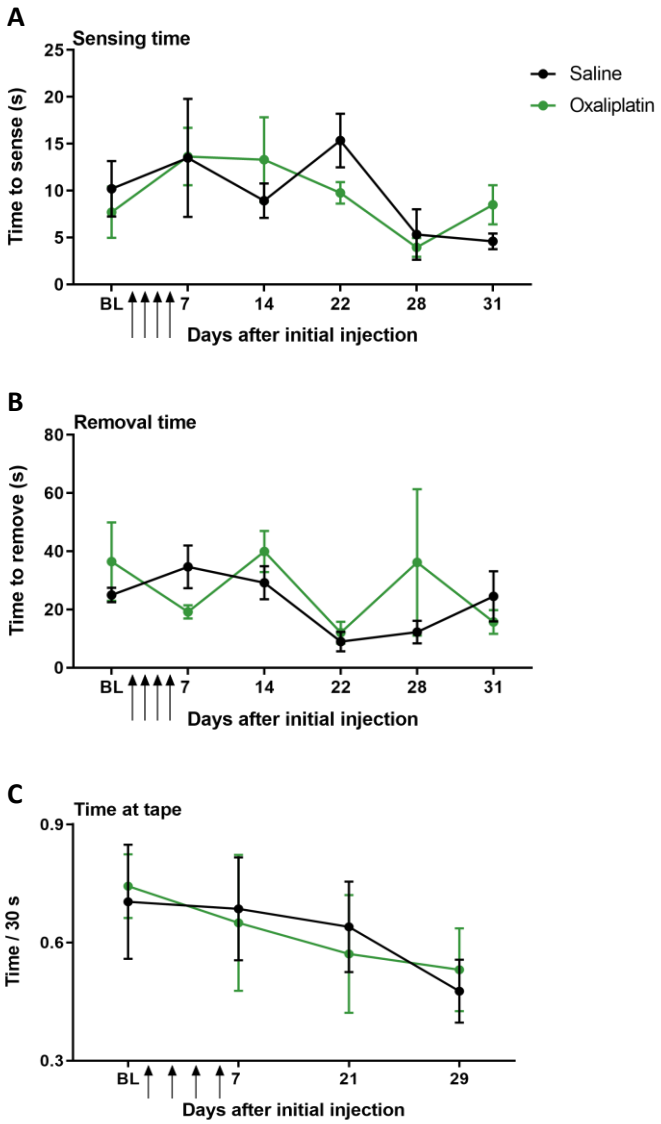

Figure 4-8 Adhesive removal test in saline- and oxaliplatin-treated animals

(A-B) A round adhesive pad was applied to the dorsal surface of the forepaw and animals were allowed 5 minutes to recognise the presence of the pad and remove it. (A) Average time to sense the presence of the pad. Data are expressed as mean ± SEM. RM two-way ANOVA. Saline n = 6; oxaliplatin n = 6. (B) Average time to remove the pad. Data are expressed as mean ± SEM. Mixed effects model. Saline n = 6; oxaliplatin n = 6. (C) A rectangular piece of tape was wrapped around the forepaw and animals were observed for 30 seconds. The graph shows the ratio of time the animals spent attending to the pad over 30 s. Data are expressed as mean ± SEM. RM two-way ANOVA. Saline n = 5; oxaliplatin n = 5. BL = baseline. Arrows represent administration of saline/oxaliplatin on four alternate days (0, 2, 4 and 6).

4.4 Discussion

Systemic (IP) administration of 2 mg/kg oxaliplatin on four alternate days resulted in the development of mechanical hypersensitivity, expressed both as mechano-allodynia and hyperalgesia, which is consistent with a previous report using the same OIPN rat model (Boyette-Davis and Dougherty 2011). Oxaliplatin-treated animals were healthy for the whole duration of the study, gain weight remained normal and they did not display any sign of ill health or distress (e.g. weight loss, alopecia or dullness). The day after treatment cessation, oxaliplatin-treated animals did not display mechanical hypersensitivity compared with saline-treated controls, thus suggesting a lack of oxaliplatin-induced acute syndrome. The chronic neuropathy was evident at day 28-34, when withdrawal responses to 4 g, 8 g and 15 g von Frey filaments were increased by ≥ 2.3-fold compared with their respective controls. Our OIPN model is partially reproducing clinical observations: almost all patients display transient symptoms during or immediately after oxaliplatin administration (Griffith et al. 2017), but we were not able to observe this acute syndrome. Conversely, up to 80% of patients go on to develop a chronic syndrome upon cumulative doses of chemotherapy (Griffith et al. 2017), as observed here in oxaliplatin-treated animals.

The translational value of this OIPN model is enhanced by the use of clinically formulated oxaliplatin. Clinically, the dilution vehicle for oxaliplatin infusion is 5% glucose and many preclinical models use glucose as vehicle. Extensive work was conducted in our lab in the past to select the most appropriate vehicle for oxaliplatin. The use of 5% glucose limited the development of mechanical hypersensitivity when compared with saline as diluent. Therefore, it was decided that 0.9% saline would be the most suitable vehicle for the OIPN model in our lab. Early on in this project, an attempt was made to use 5% glucose as vehicle for oxaliplatin dilution in a cohort of animals. However, no difference in mechanical hypersensitivity was observed between oxaliplatin- and vehicle-treated animals and results were deemed inconclusive, partly due to the inexperience of the experimenter with behavioural testing. No other attempt was carried out with 5% glucose, as the OIPN model using saline as vehicle was already established in the lab. Furthermore, it was considered beyond the scope of this project and would have overlooked the need to minimise the number of animals used in research, as defined by the 3Rs principles (Replacement, Refinement and Reduction).

Increased sensitivity to cold temperatures is a typical early side effect of oxaliplatin treatment. In rat models, a single administration of oxaliplatin (dose range 2-12 mg/kg) resulted in the appearance of acute cold allodynia within hours of oxaliplatin administration (Ling et al. 2007b, Ling et al. 2008, Joseph and Levine 2009, Nassini et al. 2011, Balayssac et al. 2014, Yamamoto et

al. 2015, Yamamoto et al. 2016a, Yamamoto et al. 2016b, Chukyo et al. 2018, Xu et al. 2018, Choi et al. 2019). Repeated administration of both low-dose and high-dose oxaliplatin (cumulative dose: 6-32 mg/kg) (Ling et al. 2007a, Sakurai et al. 2009, Kawashiri et al. 2011, Meyer et al. 2011, Kawashiri et al. 2012, Xiao et al. 2012, Abd-Elsayed et al. 2015, Yamamoto et al. 2018) also led to the development of cold allodynia during or immediately after oxaliplatin administration. In some cases, sensitivity to cold temperature persisted for weeks, if not months, and resolved up to 15 weeks after treatment cessation (Ling et al. 2007a, Meyer et al. 2011, Xiao et al. 2012, Abd-Elsayed et al. 2015).

The acetone test and scoring system as described by Flatters and Bennet (Flatters and Bennett 2004) has been successfully used in our lab and identified the development of cold allodynia following paclitaxel and bortezomib administration (Duggett and Flatters 2017, Griffiths et al. 2018). Unfortunately, the OIPN model investigated here failed to show the development of cold allodynia to acetone application over time. Many variables may have affected the outcome of this study. Testing was occasionally performed when construction works took place in the same building. The noise had a negative impact on the animals' stress levels and may have influenced their performance on the day. As any other behavioural test, the acetone test presents some limitations. In particular, the test is inherently biased by the subjectivity of the scoring system and the experimenter's inexperience with the test may be partially responsible for the negative results observed here. Despite the care taken to assign consistent cold scores to similar behavioural patterns (i.e. amount of flicking and licking), it is likely that withdrawal responses were over- or underestimated. A potential solution to the inconsistent scoring would be the evaluation of cold allodynia in terms of number or duration of withdrawals. Another caveat to consider is that the evaporation rate of acetone, and therefore the duration of the cold sensation, is dependent on the room temperature, which may vary from day to day. Moreover, despite being considered an innocuous stimulus, acetone application itself may offer a simultaneous mechanical and chemical stimulation (Vissers and Meert 2005). Therefore, it could be more accurate to consider the acetone test as a multimodal stimulus, rather than a simple cold one. It is also worth mentioning that acetone possesses a distinctive smell and animals may react to the olfactory stimulus, thus reducing the sensitivity of the test (Colburn et al. 2007). As cold allodynia is a hallmark of OIPN, more work is required to develop an optimal technique to reproduce it in this OIPN model. In this respect, it would be useful to also try other testing methodologies, like the cold plate or the thermal preference test, to assess cold-induced responses to specific innocuous and noxious temperatures.

In recent years, spontaneous running behaviour has been evaluated as measurement of ongoing pain in preclinical models. Based on previous published data from the lab that showed significant changes in running behaviour in a bortezomib- and a paclitaxel-induced neuropathy model (Duggett and Flatters 2017, Griffiths et al. 2018), voluntary wheel running was monitored in this OIPN model. However, no difference was observed between oxaliplatin-treated animals and saline-treated controls. The lack of a deficit in spontaneous running activity suggests that animals are in good health, despite oxaliplatin administration, and present no motor deficit. It should be mentioned that past experiments on paclitaxel and bortezomib models were conducted on a Sprague-Dawley colony imported from the Netherlands, whilst rats employed here derived from a colony supplied from the UK, which may be genetically distinct from the Dutch one. It has been shown that voluntary running behaviour in mice is dependent upon several factors, including gender, age, wheel design, diet, environmental conditions and genetic background [reviewed in (Sherwin 1998, Manzanares et al. 2018)]. The same variables are likely affecting the running performance of rats. While elements like gender, age and wheel design were consistent across studies, genetic background may have affected results in this OIPN model. An important factor that must be taken into account when interpreting spontaneous running behaviour data is the potential effect of experience and learning. Animals usually start running within minutes of being able to access a wheel and progressively increase their running activity in the first days of exposure, to then reach a stable plateau and occasionally decline after that [reviewed in (Sherwin 1998, Manzanares et al. 2018)]. Here, animals followed a similar pattern, even though exposure to the wheels was not continuous but limited to a small number of occasions. By the second recording of wheel activity (day 7), control animals ran more than baseline and their activity remained quite stable throughout the study, with the exception of a small deflection on day 28. Oxaliplatin-treated animals quickly reached their peak of activity at day 7 and then showed a progressive decline at day 14 and 28, before their running behaviour increased again at day 34. The decrease observed at day 28 was unlikely due to a direct effect of oxaliplatin on running behaviour, as saline-treated controls displayed a similar decline. Furthermore, none of the parameters assessed showed the presence of an oxaliplatin-induced deficit compared with baseline recordings. Another factor that may affect spontaneous running behaviour is the novelty of the wheel apparatus. As animals are removed from their home cages and placed into a new environment, they may simply be attracted to the wheels and get active on them. However, this was not considered a caveat in this OIPN model. Animals were always acclimatised to the wheel cages for an hour in the morning prior to overnight recordings, so the novelty of the wheel would have faded by the time the experiment was started in the evening.

Additionally, the first hours of running behaviour during the light cycle (before 7 pm), when animals had just got access to the wheels, were not included in the final analysis.

A substantial limitation of the spontaneous wheel running assessment is the high degree of interindividual variability. Here, interindividual variability was especially evident in the saline-treated group. The intrinsic variability of the spontaneous running behaviour makes it hard to interpret results and reports in the literature are often in contrast with each other. The most common interpretation is that spontaneous wheel running is depressed by pain conditions. Decreased wheel running activity was reported in rodent models of paclitaxel-induced neuropathy (Griffiths et al. 2018), chronic sciatic neuropathy (Whitehead et al. 2017), hind paw inflammatory pain (Cobos et al. 2012, Grace et al. 2014, Kandasamy et al. 2016), osteoarthritis (Stevenson et al. 2011) and migraine pain (Kandasamy et al. 2017), which were simultaneously characterised by persistent mechanical allodynia, with the exception of the migraine pain model. By contrast, several studies suggest that regular exercise (i.e. swimming and forced or voluntary wheel running) has an analgesic effect in several pain-associated syndromes (Pitcher 2018). Spontaneous wheel running both prevented and reversed the development of mechanical and cold allodynia in paclitaxel-induced neuropathy (Slivicki et al. 2019) and after sciatic nerve injury (Grace et al. 2016). Likewise, voluntary wheel running was able to prevent the development of thermal hypersensitivity in hind paw inflammatory pain (Pitcher et al. 2017) and of mechanical allodynia in chronic musculoskeletal pain (Leung et al. 2016, Sabharwal et al. 2016). It also alleviated mechanical and thermal hypersensitivity in mice models of pre-diabetes (Groover et al. 2013), chronic musculoskeletal pain (Sluka et al. 2013), experimental autoimmune encephalomyelitis (Benson et al. 2015) and antiretroviral therapy-induced neuropathy (Ye et al. 2018). Lastly, some groups have reported a lack of deficit in voluntary wheel running activity between experimental groups, similarly to our results in the OIPN model. No running deficits were observed in rodent models of neuropathy following paclitaxel administration (Slivicki et al. 2019) and chronic constriction injury of the sciatic nerve (Grace et al. 2016). Given the abundance of clashing reports, it is currently difficult to understand whether spontaneous running behaviour can be used as a reliable measurement of ongoing pain in OIPN.

Numbness is a typical side effect reported by oxaliplatin-treated patients. Nevertheless, it is difficult to evaluate it in preclinical settings. Hence, reports of oxaliplatin-induced numbness in rodent models are missing in the literature. The adhesive removal test is an appropriate task to investigate, as it allows to evaluate both sensory and motor impairments (Schallert et al. 1982). Two different protocols were attempted to evaluate the feasibility of the task in the OIPN rat model. In both cases, no difference between oxaliplatin-treated and control rats could be detected. A constant issue observed in both cases was the substantial degree of interindividual

and day-to-day variability when performing the task. A potential source of variability was the occasional noise from construction works, as already discussed for the cold allodynia results. However, the major source of variability could be attributed to the handling procedures. The first protocol consisted in the application of a round label to the dorsal surface of the forepaws. Each animal behaved differently in response to being held and to the pad application and the stress-induced behaviour was not consistent across days nor between trials performed on the same day on different paws. Consequently, the time to sense and remove the pad was not just a direct and reliable measurement of the sensory and motor functions but was dependent on the initial stress-induced response. Because of this limitation, no real conclusion could be drawn from the results of the first adhesive removal protocol. The second protocol involved the wrapping of a piece of tape around the forepaw but was characterized by similar problems to the first trial. This protocol was found to be extremely distressing to the animals, who had to be restrained completely by one experimenter while another applied the tape. Moreover, removal of the tape upon task completion was particularly challenging and harmful on occasions, and some fur loss was inevitable. The task was recommended to be repeated 3-5 times per paw, including only the two best performances in the final analysis (Sughrue et al. 2006, Komotar et al. 2007). However, this paradigm was considered excessively upsetting for the animals and potentially unethical. Therefore, the test was limited to one trial per paw. Limiting the task to a single trial and not including the best performances may be partially responsible for the high degree of individual variability observed in this OIPN model.

The mechanism leading to chemotherapy-induced numbness is not entirely known, but it has been hypothesised that loss of intraepidermal nerve fibres (IENFs) may play a key role in it (Boyette-Davis and Dougherty 2011). Significant IENFs loss has been observed in oxaliplatin-treated patients (Burakgazi et al. 2011) and in preclinical models. In particular, a rat model of OIPN generated using the same treatment schedule and vehicle described in this thesis displayed significant IENFs loss after two and four weeks from treatment administration (Boyette-Davis and Dougherty 2011). The authors also observed significantly increased mechanical hypersensitivity compared with vehicle-treated controls, which led them to hypothesise that IENFs loss is involved in the maintenance of the neuropathy (Boyette-Davis and Dougherty 2011). Similarly, cisplatin led to a loss of IENFs in mice that displayed both mechanical allodynia and numbness compared with vehicle-treated animals (Mao-Ying et al. 2014, Krukowski et al. 2017, Maj et al. 2017). While fibre loss could explain the numbness often reported by patients early after chemotherapy treatment, central sensitisation mechanisms (e.g. increased neuronal excitability, enhanced spontaneous nerve activity, loss of descending inhibitory mechanisms etcetera) may mediate enhanced pain sensitivity as the neuropathy

progresses and fibre loss increases (Boyette-Davis and Dougherty 2011). As the OIPN model used here was the same as the one described by Boyette-Davis and Dougherty (Boyette-Davis and Dougherty 2011), it is likely that oxaliplatin-treated rats included in this work also had less IENFs than saline-treated controls, and could therefore present decreased pain sensitivity. As numbness usually precedes the appearance of allodynic and hyperalgesic symptoms in the clinic, employing the adhesive removal test more frequently in the acute setting (e.g. between treatment administrations and before the onset of pain-like behaviour) would have been appropriate to evaluate numbness development in this model. Nevertheless, both adhesive removal protocols attempted here were thought to be too unreliable to be able to assess numbness in animal models of CIPN.

It should be noted that the adhesive removal test is commonly used to evaluate functional deficits following damage to the central nervous system, including unilateral nigrostriatal damage (Schallert et al. 1982), stroke (Schallert et al. 2000, Schaar et al. 2010), spinal cord injury (Schallert et al. 2000, Bradbury et al. 2002) and Parkinson's disease (Schallert et al. 2000). In these conditions, sensorimotor impairments are particularly severe and frequently affect only one limb function, which may be completely lost. Hence, differences between the affected limb and the unaffected one can be easily detected by the adhesive removal test. By comparison, chemotherapy-induced deficits are not as marked, and the adhesive removal test may not be sensitive enough to recognise them. At present, the adhesive removal test has only been employed in a mouse model of cisplatin-induced neuropathy, where cisplatin-treated animals displayed significantly increased latency to notice the presence of the pad compared with saline-treated controls (Mao-Ying et al. 2014, Krukowski et al. 2017, Maj et al. 2017). No other CIPN preclinical model has investigated chemotherapy-induced numbness. In future, it could be useful to attempt to optimise the test protocol in this OIPN model, so to reduce interindividual variability and stress-induced responses and be able to evaluate only chemotherapy-induced deficits.

Lastly, a limitation of this model was the use of male animals only. Although colorectal cancer is more common and has a higher mortality rate in males compared with females (White et al. 2018), further studies should include female rodents as well. Historically, female animals have been excluded from research, as they were believed to introduce a high degree of variability and complexity due to the oestrous cycle. However, recent meta-analyses have shown that females are no more variable than males (Prendergast et al. 2014, Itoh and Arnold 2015, Becker et al. 2016). Indeed, researchers are encouraged to use both male and female animals to avoid creating a male bias, thus expanding the generalisability of their results. Furthermore, the inclusion of both sexes is particularly important in studies on CIPN and chronic pain in general,

as growing evidence suggests that pain processing is different between males and females (Pieretti et al. 2016). It is therefore imperative that preclinical studies address this sexual dimorphism in order to identify cellular and molecular mechanisms of pain and develop new analgesic compounds.

4.5 Conclusions

In conclusion, this investigation showed that repeated oxaliplatin administration results in the development of significant hypersensitivity to mechanical stimuli. There was no general toxicity associated with oxaliplatin intraperitoneal administration, as animals gained weight normally and showed no signs of ill health or distress. The typical cold hypersensitivity reported by patients was not reproduced in this OIPN model, suggesting that more efforts are needed to develop an optimal experimental protocol to assess this important feature of OIPN. Spontaneous wheel running behaviour showed no difference in running activity between oxaliplatin-treated animals and controls. However, the ability of the test to accurately quantify ongoing pain in rodents was brought into question. Experiments on oxaliplatin-induced numbness were inconclusive and future attempts should focus on optimising the protocol to eliminate the high degree of stress-induced individual variability. Given the need to establish optimal assays to investigate cold-allodynia, ongoing pain and numbness, the presence of OIPN in oxaliplatin-treated animals allocated to further experiments in this thesis was assessed in terms of mechanical hypersensitivity.

Chapter 5 Electrophysiological investigation

5.1 Introduction

Nerve conduction properties can be assessed following electrical stimulation, which generates a compound action potential (CAP). CAPs were first characterised in the early 1920s in isolated nerves electrically stimulated with increasing currents (Erlanger and Gasser 1924). The authors of the study observed that the CAP shape varied, and additional peak appeared as the current intensity increased, thus suggesting that different fibre populations within the nerve were activated by different current amplitudes. CAPs represent the summation of all action potentials generated by the simultaneous and synchronous recruitment of many individual fibres within the nerve (Parker et al. 2018). Unlike the all-or-none action potential of an individual fibre, CAPs are described as graded responses: large myelinated fibres and those closest to the stimulating electrode are recruited early by low intensity stimulations; as the current intensity gradually increases, more fibres, including small myelinated and unmyelinated ones, are activated, thus generating a CAP with longer duration.

Chemotherapy-induced peripheral neuropathy (CIPN) assessment through clinical oncology grading scales and patients' self-reports remains a highly subjective diagnostic tool and lacks a standardised approach. A more objective diagnostic tool can be used to evaluate neurophysiological deficits. Nerve conduction studies (NCS) are the gold standard for the objective evaluation of large myelinated fibre damage in CIPN, but they cannot provide information about nociceptive Aδ- or C-fibres. Peripheral nerves are stimulated with small electrical impulses through electrodes placed on the skin and the amplitude and conduction velocity of both sensory and motor CAPs can be measured [reviewed in (Park et al. 2013)]. Acute and chronic oxaliplatin-induced peripheral neuropathy (OIPN) are defined by distinctive electrophysiological profiles. The acute syndrome, characterised by cold-induced paresthesias of the hands and throat, peri-oral numbness, jaw tightness and muscle cramps [reviewed in (Argyriou et al. 2008)], appears at the same time as abnormal motor conduction. NCS performed shortly after oxaliplatin infusion revealed the presence of small, repetitive compound muscle action potential after the initial one elicited by electrical stimulation (Wilson et al. 2002, Lehky et al. 2004, Heide et al. 2018). Oxaliplatin-treated patients also displayed spontaneous muscle fibre discharges in needle electromyography examination, while sensory nerve properties were not affected (Wilson et al. 2002, Lehky et al. 2004). The authors of these studies suggested that repetitive firing and spontaneous discharges are likely to affect both sensory and motor nerves after oxaliplatin administration, but NCS methods may not be sensitive enough to detect sensory hyperexcitability (Wilson et al. 2002, Lehky et al. 2004). The chronic syndrome is characterised

by distal sensory deficits and abnormal proprioception, which are representative of a distal, axonal neuropathy without motor components [reviewed in (Argyriou et al. 2008). Electrophysiological investigations in oxaliplatin-treated patients revealed that chronic OIPN is characterised by decreased sensory CAP amplitude and, among the sensory nerves evaluated, the sural nerve is the most affected; sensory conduction velocity remains relatively preserved in most studies but some groups observed a significant reduction after oxaliplatin administration (Cascinu et al. 2002, Lehky et al. 2004, Krishnan et al. 2005, Pietrangeli et al. 2006, Argyriou et al. 2007, Park et al. 2009a, Park et al. 2009b, Kokotis et al. 2016, Kim et al. 2018, Krøigård et al. 2020). Progression of CIPN from grade 1 to grade 2 and 3 in patients administered with different chemotherapeutic compounds, including oxaliplatin, was associated with a significant and progressive reduction in sural nerve CAP amplitude, whilst conduction velocity was not as markedly affected (Matsuoka et al. 2016). No motor involvement has been identified in chronic OIPN (Lehky et al. 2004, Krishnan et al. 2005, Argyriou et al. 2007, Park et al. 2009a, Kim et al. 2018). Although most NCS revealed that abnormal sensory nerve CAPs appear late in the oxaliplatin treatment regimen after several cumulative doses, a few studies identified 'early' sensory CAP abnormalities. Patients still undergoing treatment with oxaliplatin (between 5 and 10 cycles) displayed an ~ 40% deficit in the sural nerve sensory action potential compared with healthy controls (McHugh et al. 2012). Reduced amplitude of sensory nerve action potential of the radial, dorsal sural, sural and median nerves at mid-treatment were also associated with increased risk of severe OIPN (Velasco et al. 2014, Alberti et al. 2018, Kim et al. 2018). These results suggest that these electrophysiological deficits might be predictive biomarkers of high-grade OIPN.

In vitro exposure of rodent and human nerves to high concentrations of oxaliplatin has been useful to understand some of the molecular mechanisms of acute OIPN. Rat sural and vagal nerves exposed *in vitro* to 250 µM oxaliplatin displayed increased amplitude and duration of A-fibres CAP (A-CAP), which was attributed to an oxaliplatin-induced delay in voltage-gated Na^+ (Na_v) channels inactivation (Adelsberger et al. 2000). Interestingly, there was no change in the CAP of C-fibres (C-CAP), thus suggesting that oxaliplatin modulation of Na_v channels is limited to specific channel isoforms expressed only on a subtype of sensory fibres (Adelsberger et al. 2000). Rat and human sural nerves exposed to 30 µM oxaliplatin displayed increased duration of the A-CAP and repetitive firing that lasted up to 10 ms after electrical stimulation (Sittl et al. 2010). In mouse and human sural nerves, exposure to 100 µM oxaliplatin in combination with cool temperatures slowed the inactivation of $Na_v1.6$ channels and induced bursts of after-potentials in A- but not C-fibres (Sittl et al. 2012). The role of $Na_v1.6$ in OIPN was supported by the observation that knockout mice that did not express a functional $Na_v1.6$ channel did not display

repetitive after-potentials after exposure to oxaliplatin and cooling (Sittl et al. 2012). *In vitro* exposure to oxaliplatin induced bursts of repetitive firing in the rat sciatic nerve as well (Kagiava et al. 2008), where an inhibitory role of oxaliplatin on voltage-gated K^+ (K_v) channels was suggested. Exposure of rat sciatic nerves to high concentration oxaliplatin (100 and 500 µM) had no effect on Na_v channel functionality, as the CAP peak amplitude and rise-time were not affected. By contrast, a progressive time- and concentration-dependent increase in the duration of the repolarisation phase, when fast K^+ channels are activated, and an intense hyperpolarisation phase, when slow K^+ channels are activated, were observed following oxaliplatin administration (Kagiava et al. 2008). Similar results were also obtained in the mouse sciatic nerve exposed to 25 µM oxaliplatin (Kagiava et al. 2015). The same research group used intra-axonal recordings of the rat sciatic nerve to show that the oxaliplatin-induced changes in the CAP are directly linked to changes in the action potentials of individual nerve fibres: the depolarisation phase remained unchanged while the repolarisation phase was significantly broadened (Kagiava et al. 2013). More *in vitro* studies on non-mammalian tissues supported the hypothesis that changes in Na_v and K_v channels are involved in OIPN. Electrical stimulation of nodes of Ranvier of single myelinated fibres isolated from the frog sciatic nerve exposed to 10 and 100 µmol/l oxaliplatin resulted in a dose-dependent decrease in Na^+ and K^+ current amplitudes (Benoit et al. 2006). Whole patch-clamp recordings of the cockroach dorsal unpaired median neurons exposed to 40–500 mM oxaliplatin, or 500 mM of its metabolite oxalate, displayed decreased inward Na^+ current amplitude (Grolleau et al. 2001). Despite the evidence for ion channels involvement in the development of OIPN, several channel modulators (e.g. carbamazepine, gabapentin, pregabalin, Ca/Mg infusions) failed to show any efficacy in clinical trials for the prevention or treatment of OIPN [reviewed in (Hershman et al. 2014, Hu et al. 2019)], thus suggesting that further investigations are required to better understand the role of ion channels in OIPN.

Oxaliplatin effect on electrophysiological properties has been widely investigated in rodent preclinical models of OIPN. The majority of studies have employed the sciatic nerve (McKeage et al. 2001, Jamieson et al. 2005, Meyer et al. 2011, Kanbara et al. 2014), as it represents the largest nerve in the body and is a mixed-function nerve, containing both motor and sensory fibres (Schmalbruch 1986). Additionally, the sciatic nerve, and in particular its sural and tibial branches, innervates the lateral and central area of the hind paw (Cobianchi et al. 2014), which are usually mechanically and/or thermally stimulated for the evaluation of nociceptive behaviour. Experiments on tail and digital nerves have been reported as well (Cavaletti et al. 2001, Renn et al. 2011). A single injection of oxaliplatin (10 mg/kg) was enough to cause a significant reduction in the sciatic nerve conduction velocity two weeks after treatment and

lasting up to four months, compared with vehicle-treated control rats (McKeage et al. 2001). Nerve conduction studies performed upon completion of chronic oxaliplatin regimens showed reduction in the sensory conduction velocity and amplitude compared with vehicle-treated rats (Cavaletti et al. 2001, Jamieson et al. 2005) and mice (Renn et al. 2011), whilst the motor function was not affected (Jamieson et al. 2005). Similar results were obtained during *ex vivo* recordings of the rat sciatic nerve in a set-up similar to the one described in this thesis: animals administered with repeated injections of oxaliplatin (cumulative dose: 6 and 16 mg/kg) displayed decreased CAP amplitude and conduction velocity compared with vehicle-treated controls (Meyer et al. 2011, Kanbara et al. 2014). Given that chronic OIPN is characterised by purely sensory deficits, our investigation focused on the saphenous nerve, which comprises entirely sensory fibres. The nerve is the termination branch of the femoral nerve and originates from the dorsal roots L3/L4 in the spinal cord (Rea 2015). It innervates the medial portion of the hind paw (Cobianchi et al. 2014), which is partly affected by the stimulations in behavioural investigations. To date, no study has investigated the electrophysiological properties of the saphenous nerve following oxaliplatin exposure, either *in vitro* or *in vivo*.

5.2 Aims

The studies described below had two aims. First of all, to optimise the experimental settings to record A- and C-CAPs *ex vivo* from the rat saphenous nerve. The effects of substrate supplementation and nerve crushing were evaluated. Second of all, to characterise A- and C-CAP waveforms in oxaliplatin- and saline-treated animals. Rats received oxaliplatin or saline through an intraperitoneal (IP) injection and pain-like behaviour was assessed through mechanical hypersensitivity to von Frey filaments. CAPs were recorded in the saphenous nerves at day 7 (24 hours after the last treatment administration) and at the peak of pain-like behaviour (day 28-33).

5.3 Results

Nerve conduction properties were investigated in terms of several characterising parameters of the A- and C-CAPs. A- and C-CAPs were assessed separately by different protocols. In both cases, nerves were stimulated with a threshold protocol, consisting of stimulations of increasing intensity in small increments, in order to identify the threshold current required to initiate the CAP (A-CAP: 0-0.3 mA in 0.01 mA increments, 50 µs square pulse width, 0.2 Hz; C-CAP: 0 to 4 mA in 0.1 mA increments, 1 ms square pulse width, 0.2 Hz). A characterisation protocol was then applied to the nerves to evaluate other CAP parameters (A-CAP: 0-0.5 mA in 0.02 mA increments, 50 µs square pulse width, 0.2 Hz; C-CAP: 0 to 10 mA in 0. 5 mA increments, 1 ms square pulse width, 0.2 Hz). Figure 5-1 and Figure 5-2 show representative traces for A- and C-

CAP and how the different parameters were measured. A-CAP parameters assessed with the characterisation protocols include peak to peak amplitude, area under the curve (AUC, expressed in arbitrary units, AU), duration, latency to onset of the waveform and conduction velocity at the onset of the waveform, when only the fastest fibres are recruited following electrical stimulation (Figure 5-1).

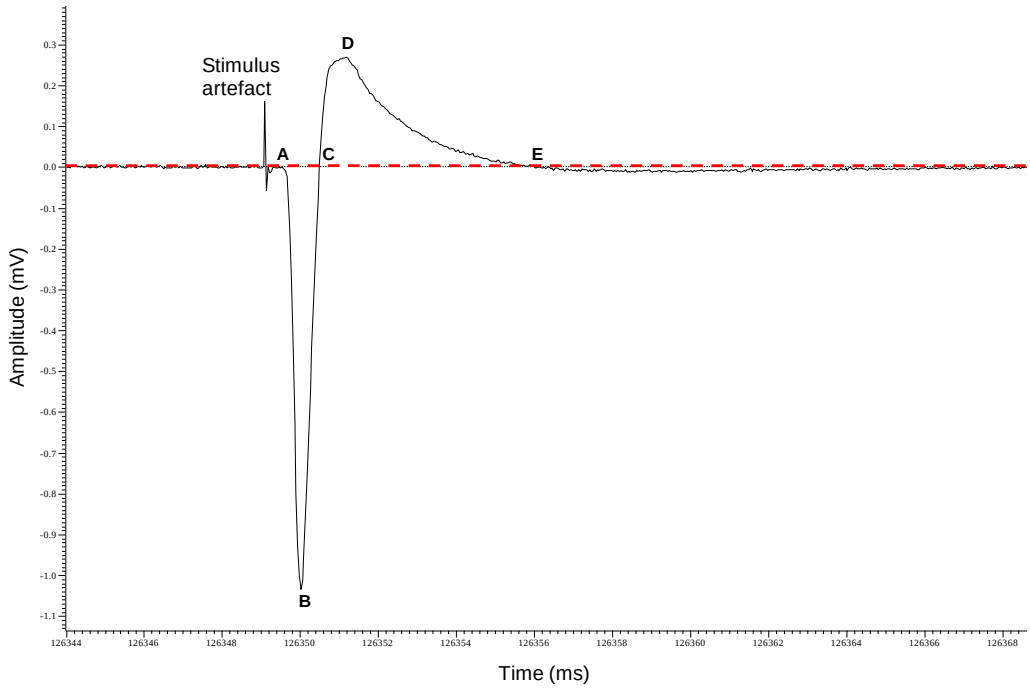

Figure 5-1 Representative trace of the A-CAP waveform

Typical A-CAP waveform generated by electrical stimulation and visualised in the Spike2 software. The stimulus artefact can be distinguished before the start of the negative deflection of the waveform. The red dotted line represents the 0-mV baseline. A: onset of the A-CAP; B: trough; C: end of the negative deflection and start of the positive deflection; D: peak; E: end of the A-CAP. Peak to peak amplitude was measured from B to D. The A-CAP area under the curve (AUC) was a summation of both the negative (A to C) and the positive (C to E) AUC. A-CAP duration was measured from A to E. Latency and conduction velocity were measured at A.

For C-CAP, similar parameters were investigated: peak amplitude, area under the curve (in AU), duration, latency to peak of the waveform and conduction velocity at peak (Figure 5-2). C-CAPs are often triphasic (negative deflection - positive deflection - negative deflection) and their amplitude is significantly smaller compared with A-CAPs. Assessing C-CAP features was challenging at times, due to the presence of background electrical noise that can obscure the C-fibres response. Therefore, obtaining robust C-CAP recordings proved to be significantly harder than A-CAPs. To facilitate and standardise C-CAP analysis, only the positive deflection was taken in consideration. Similarly, identifying the start of the C-fibres waveform was not always

possible. To avoid this issue, conduction velocity of the C-fibres was calculated at the peak of the waveform, thus providing an indication of the average conduction velocity, rather than of the fastest fibres in the nerve.

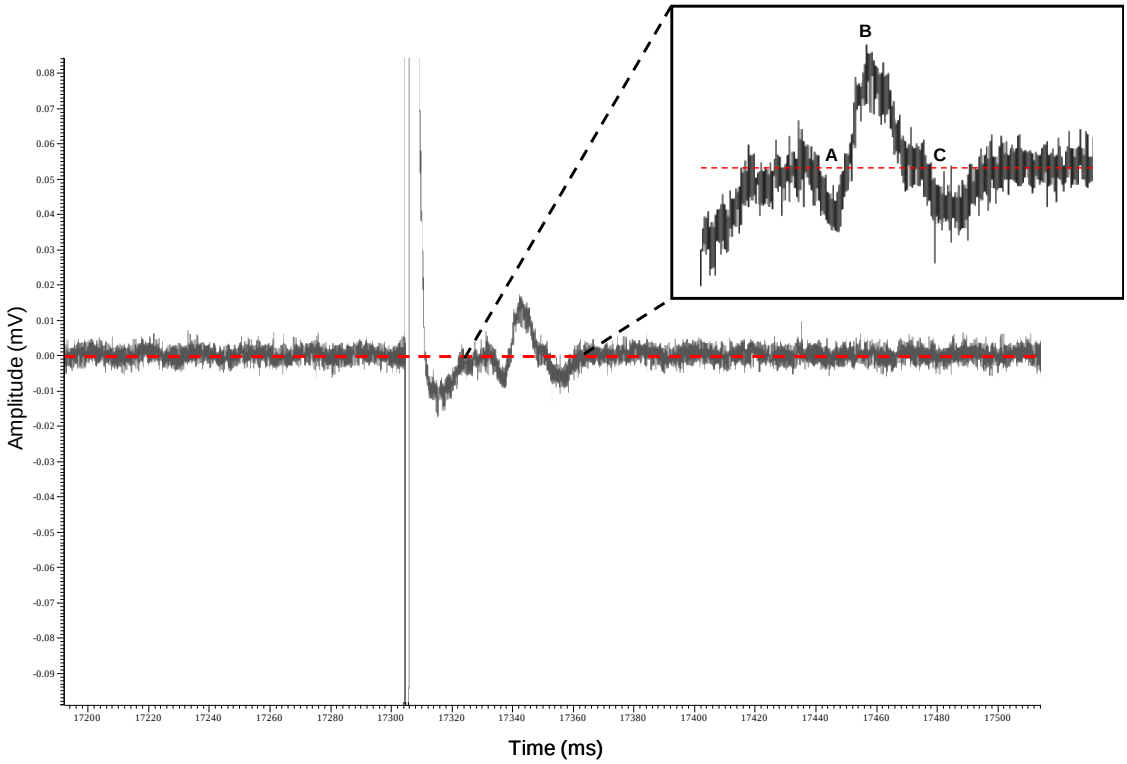

Figure 5-2 Representative trace of the C-CAP waveform

Typical C-CAP waveform generated by electrical stimulation and visualised in the Spike2 software. The C-CAP appears after the fast A-fibres and is smaller in amplitude. The red dotted line represents the 0-mV baseline. A: start of the C-CAP; B: peak; C: end of the C-CAP. The C-CAP is often triphasic (negative deflection, positive deflection, negative deflection). To simplify the analysis, only the positive deflection was considered (A to C). Peak amplitude was measured at B. The C-CAP area under the curve (AUC) and duration were measured from A to C. Latency and conduction velocity were measured at B.

5.3.1 Optimisation of experimental protocols

Extensive work was conducted in order to optimise experimental variables including temperature, nerve length, distance between electrodes and nerve desheathing, and to set up the electronic and hydraulic components of the electrophysiology rig to record CAPs from the saphenous nerve. Temperature changes have a significant effect on CAP duration and amplitude. Clinically, CAPs recorded at warmer cutaneous temperatures had reduced amplitudes and shorter durations, while cool temperatures produced bigger and broader CAPs (Bolton et al. 1981). With the exception of recordings performed early on during the optimisation attempts, a constant bath temperature of 34-35°C was maintained during recordings throughout the study. Another experimental factor that may have a profound effect

on CAP is the distance between recording electrodes (Li et al. 2014), where the shorter the distance, the harder it is to visualise the CAP. After initial attempts when recording electrodes were kept close together, the distance between electrode pairs was increased and was never less than 5 mm, which has been reported as optimal in the rat median nerve (Li et al. 2014). Lastly, stretching of the nerve may also affect the CAP (Ochs et al. 2000). Care was taken when dissecting the nerves to obtain nerve sections long enough to avoid stretching them across the electrodes. Additionally, the epineural sheath was not removed from the nerves before recording, thus allowing to maintain nerve integrity and prevent additional stretching.

5.3.1.1 Comparison of glucose and fructose as substrates for CAP recordings

Previous unpublished data from the lab were generated using glucose as substrate in the bicarbonate recording solution. A recent study on mouse sciatic nerves suggested that fructose may be an equally good substrate, as it maintained both A- and C-fibre excitability (Rich and Brown 2018). A small pilot study was carried out to compare the effects of 20 mM fructose and 10 mM glucose on the rat saphenous nerves and assess potential advantages of using fructose with the protocols we had in place already. Nerves were harvested from naïve animals and were electrically stimulated (for both A- and C-CAP) in 10 mM glucose-supplemented bicarbonate solution. After a washout period to eliminate all the glucose from the recording chamber, nerves were exposed to 20 mM fructose-supplemented bicarbonate solution, and A- and C-CAP protocols were recorded again. No difference could be detected in A-CAP amplitudes between 10 mM glucose and 20 mM fructose preparations and traces recorded with the two different substrates overlapped almost completely (Figure 5-3 A, ns RM two-way ANOVA, n = 4 nerves). Consequently, the AUC analysis showed extremely similar results between groups, with mean values of 1.191 ± 0.07 AU and 1.199 ± 0.13 AU (mean ± SEM) for glucose and fructose recordings, respectively (Figure 5-3 A insert, ns paired two-tailed t-test, n = 4 nerves). No significant difference was observed in the AUC of the A-CAP waveform (Figure 5-3 B, ns RM two-way ANOVA - Figure 5-3 B insert, ns paired two-tailed t-test, n = 4 nerves) nor in its duration (Figure 5-3 C, ns RM two-way ANOVA - Figure 5-3 C insert, ns paired two-tailed t-test, n = 4 nerves) between glucose- and fructose-supplemented recordings. No significant difference was detected in latency to the onset of the A-CAP (Figure 5-3 D, ns paired two-tailed t-test, n = 4 nerves). A-CAPs recorded in the presence of 20 mM fructose displayed slower conduction velocities at the onset of the A-CAP (60.05 ± 5.7 m/s) compared with A-CAPs recorded in 10 mM glucose (73.4 ± 8.3 m/s), however this difference was not statistically significant (Figure 5-3 E, ns paired two-tailed t-test, n = 4 nerves). Fructose slightly increased the A-fibre activation threshold to 0.04 ± 0.009 mA compared with 0.03 ± 0.003 mA able to activate A-fibres in glucose.

Nevertheless, the difference was not statistically significant (Figure 5-3 F, ns paired two-tailed t-test, n = 4 nerves).

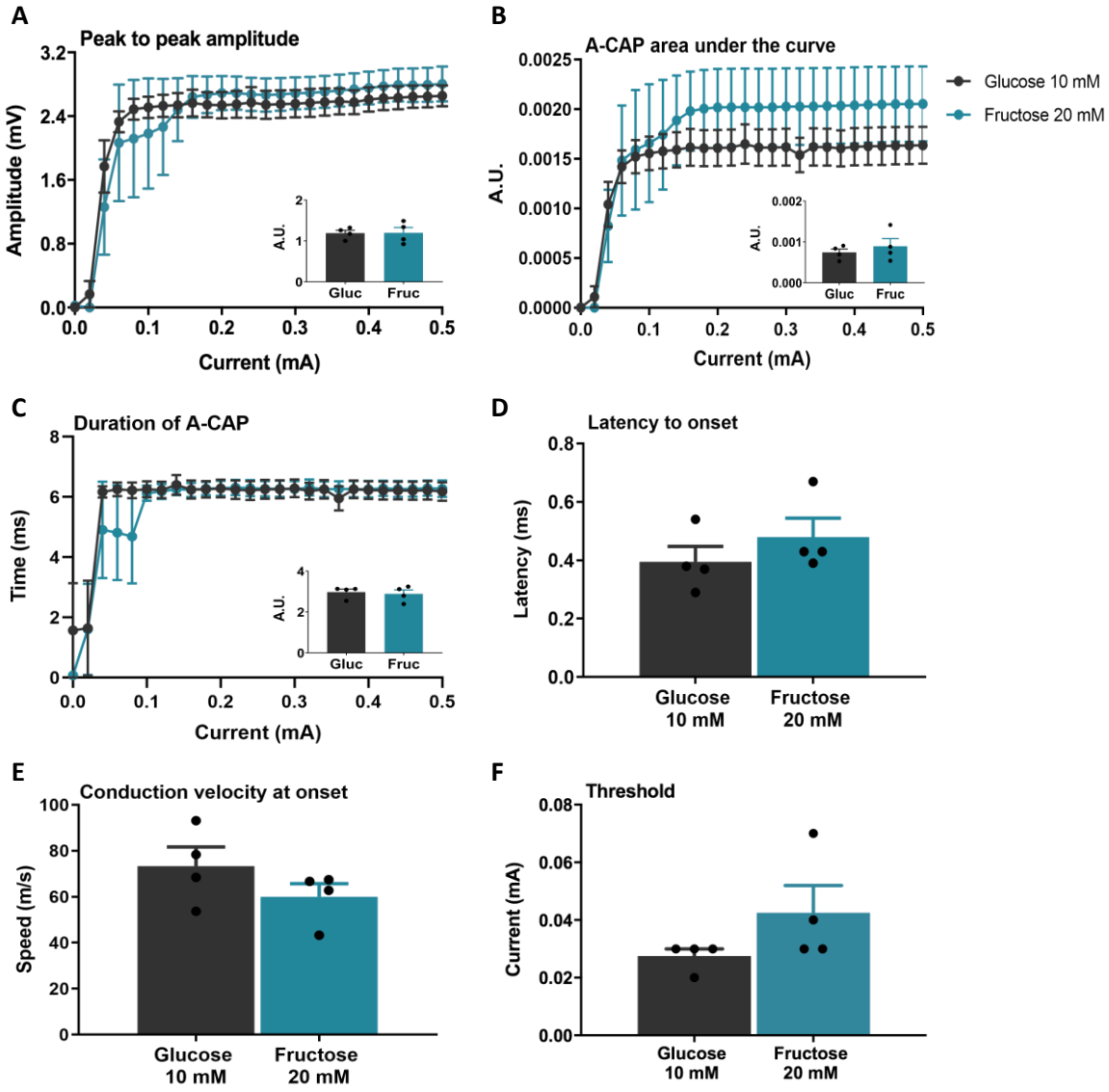

Figure 5-3 Effect of 10 mM glucose and 20 mM fructose on the A-CAP in naïve animals

Saphenous nerves were harvested from naïve animals and superfused with bicarbonate solution supplemented with 10 mM glucose for electrical stimulation. After a washout period of 30-60 minutes, nerves were superfused with bicarbonate solution supplemented with 20 mM fructose for electrical stimulation. Nerves were electrically stimulated with increasing current intensities from 0 to 0.5 mA in 0.02 mA increments (50 µs square pulse width, 0.2 Hz). A-CAP parameters investigated were peak to peak amplitude (A); area under the curve (AUC) of the A-CAP waveform (B); duration (C); latency to onset of the A-CAP waveform (D); and conduction velocity at the onset of the A-CAP waveform (E). For threshold assessment (F), nerves were electrically stimulated with increasing current intensities from 0 to 0.3 mA in 0.01 mA increments (50 µs square pulse width, 0.2 Hz). Inserts (A-C) represent the AUC analysis of traces in (A-C). A.U. is arbitrary units. Data are expressed as mean ± SEM. (A-C) RM two-way ANOVA; (D-F and inserts A-C) paired two-tailed t-test. 10 mM glucose and 20 mM fructose n = 4 nerves.

Before the glucose solution was washed out, nerves were stimulated with the C-CAP protocol as well. Because of a mistake when setting up the protocol, no recording was made at 0 mA. Upon completion of data analysis for all the C-CAPs included in this work, it was clear that a maximal C-CAP response was obtained with the very first stimulation intensities and any stimulus beyond that was supramaximal (Figure 5-4 A, Figure 5-6 A, Figure 5-9 A, and Figure 5-11 A). Therefore, it was decided to exclude the high intensity stimulations from analysis and focus only on the first current applications, where the nerve response was maximal. As nerves from different experimental groups reached their maximal amplitude at different currents, C-CAPs at 0.5, 1.0 and 1.5 mA were included in the analysis, to confirm that stimulus intensity was sufficient to reach the maximal response. Due to the susceptible nature of C-fibres, C-CAPs for the investigation of substrate supplementation were obtained only from two recordings out of four. Results for C-CAP analysis are shown in Figure 5-4, although no conclusion can be drawn from it due the insufficient sample size (n = 2 nerves). Despite the small sample size of this study, it was concluded that no advantage was obtained by the use of fructose rather than glucose in our experimental settings. Therefore, all further experiments were conducted in 10 mM glucose.

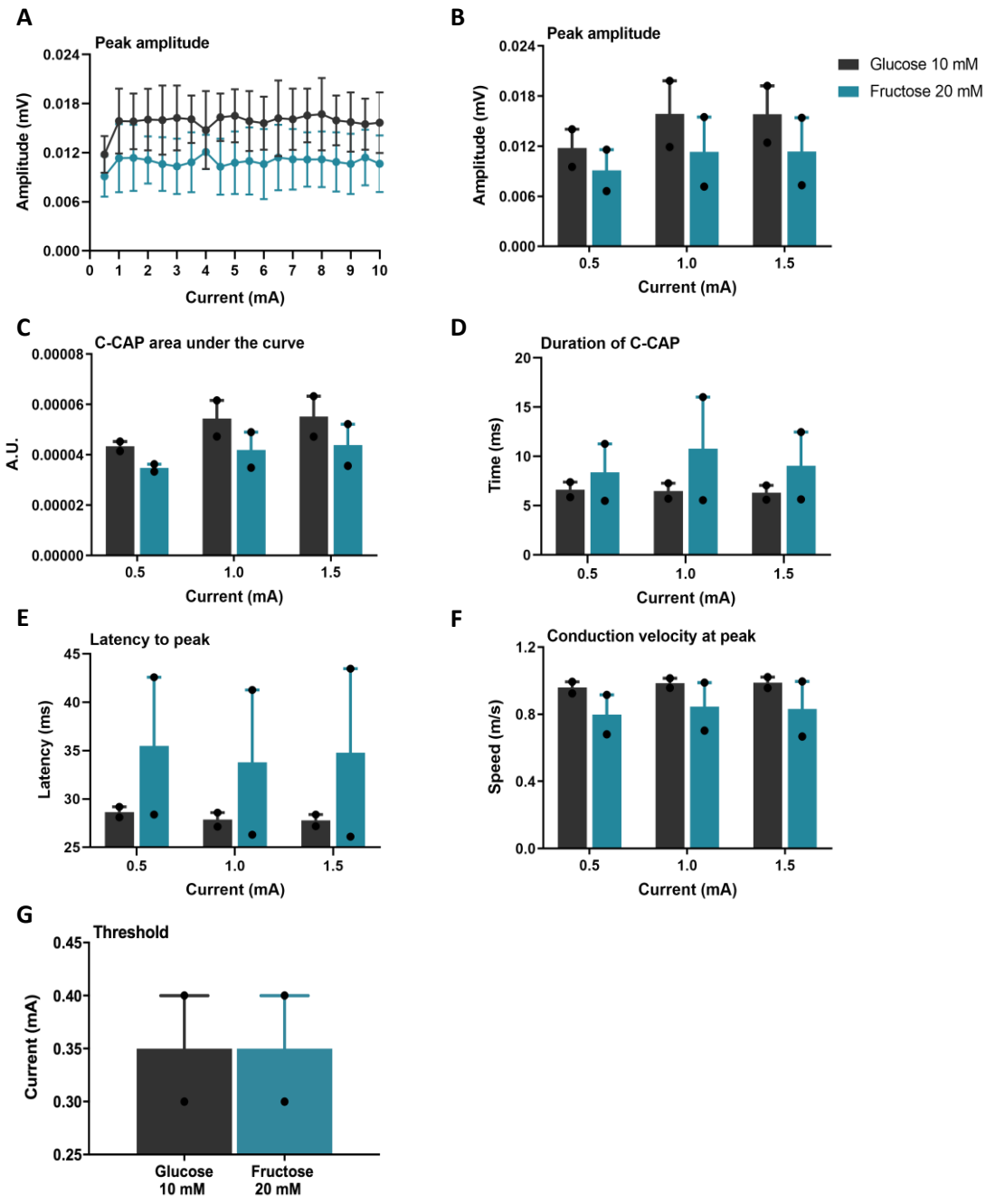

Figure 5-4 Effect of 10 mM glucose and 20 mM fructose on the C-CAP in naïve animals

Saphenous nerves were harvested from naïve animals and superfused with bicarbonate solution supplemented with 10 mM glucose for electrical stimulation. After a washout period of 30-60 minutes, nerves were superfused with bicarbonate solution supplemented with 20 mM fructose for electrical stimulation. Nerves were electrically stimulated with increasing current intensities from 0.5 to 10 mA in 0.5 mA increments (1 ms square pulse width, 0.2 Hz). (A) shows peak amplitude at all current intensities. (B-F) show C-CAP parameters only at 0.5, 1.0 and 1.5 mA. C-CAP parameters investigated were peak amplitude (B); area under the curve of the C-CAP waveform (C); duration (D); latency to the peak of the C-CAP waveform (E); and conduction velocity at the peak of the C-CAP waveform (F). For threshold assessment (G), nerves were electrically stimulated with increasing current intensities from 0 to 4 mA in

0.1 mA increments (1 ms square pulse width, 0.2 Hz). A.U. is arbitrary units. Data are expressed as mean ± SEM. No statistical analysis was performed. 10 mM glucose and 20 mM fructose n = 2 nerves.

5.3.1.2 Effect of nerve crushing on CAP recordings

Further optimisation attempts involved comparing the effect of crushing the nerves or simply placing their cut ends on the second recording electrode (distal electrode) in order to obtain monophasic recordings. Only saline-treated animals were included in this analysis. Nerves from oxaliplatin-treated animals were excluded, as oxaliplatin would represent another variable that might affect the nerve conductive properties. For both the crushed and uncrushed group, results of nerves harvested at day 7 and day 28-37 from saline-treated animals were collated, as no saline-induced effect would be expected at any time point. Crushing the nerve on the recording electrode appeared to slightly damage the nerve conductive properties. At the last stimulation, nerve crushing led to a 35% decrease in peak to peak amplitude compared with the uncrushed group (crushed [mean, *95% CI*]: 1.10 mV, *0.69-1.51*; uncrushed: 1.70 mV, *0.98-2.42*) (Figure 5-5 A, ns RM two-way ANOVA, crushed n = 22 nerves, uncrushed n = 10 nerves), which was confirmed by AUC analysis (Figure 5-5 A insert, ns unpaired two-tailed t-test, crushed n = 22 nerves, uncrushed n = 10 nerves). However, this change was not statistically significant. Nerve crushing had also a slight negative effect on the mean AUC of the A-fibres waveform (mean, *95% CI*: 0.0009 AU, *0.0006-0.0013*), that decreased by 25% compared with uncrushed nerves (mean, *95% CI*: 0.0012 AU, *0.0007-0.0017*) at the end of the protocol. Nevertheless, this decrease was not statistically significant (Figure 5-5 B, ns RM two-way ANOVA - Figure 5-5 B insert, ns unpaired two-tailed t-test, crushed n = 22 nerves, uncrushed n = 10 nerves). There was no difference in the duration of the A-CAP between groups (Figure 5-5 C, ns RM two-way ANOVA - Figure 5-5 C insert, ns unpaired two-tailed t-test, crushed n = 22 nerves, uncrushed n = 10 nerves). Conduction velocity was not significantly affected: A-fibres in the crushed nerves conducted at 48.10 ± 3.6 m/s, while uncrushed fibres at 53.59 ± 5.5 m/s (mean ± SEM) (Figure 5-5 E, ns unpaired two-tailed t-test, crushed n = 22 nerves, uncrushed n = 10 nerves). The average stimulus intensity required to stimulate an A-CAP following nerve crushing was 0.03 ± 0.004 mA, whilst uncrushed nerves could be activated slightly earlier, at a lower threshold of 0.02 ± 0.005 mA (Figure 5-5 F, ns unpaired two-tailed t-test, crushed n = 22 nerves, uncrushed n = 10 nerves). However, this difference was not statistically significant.

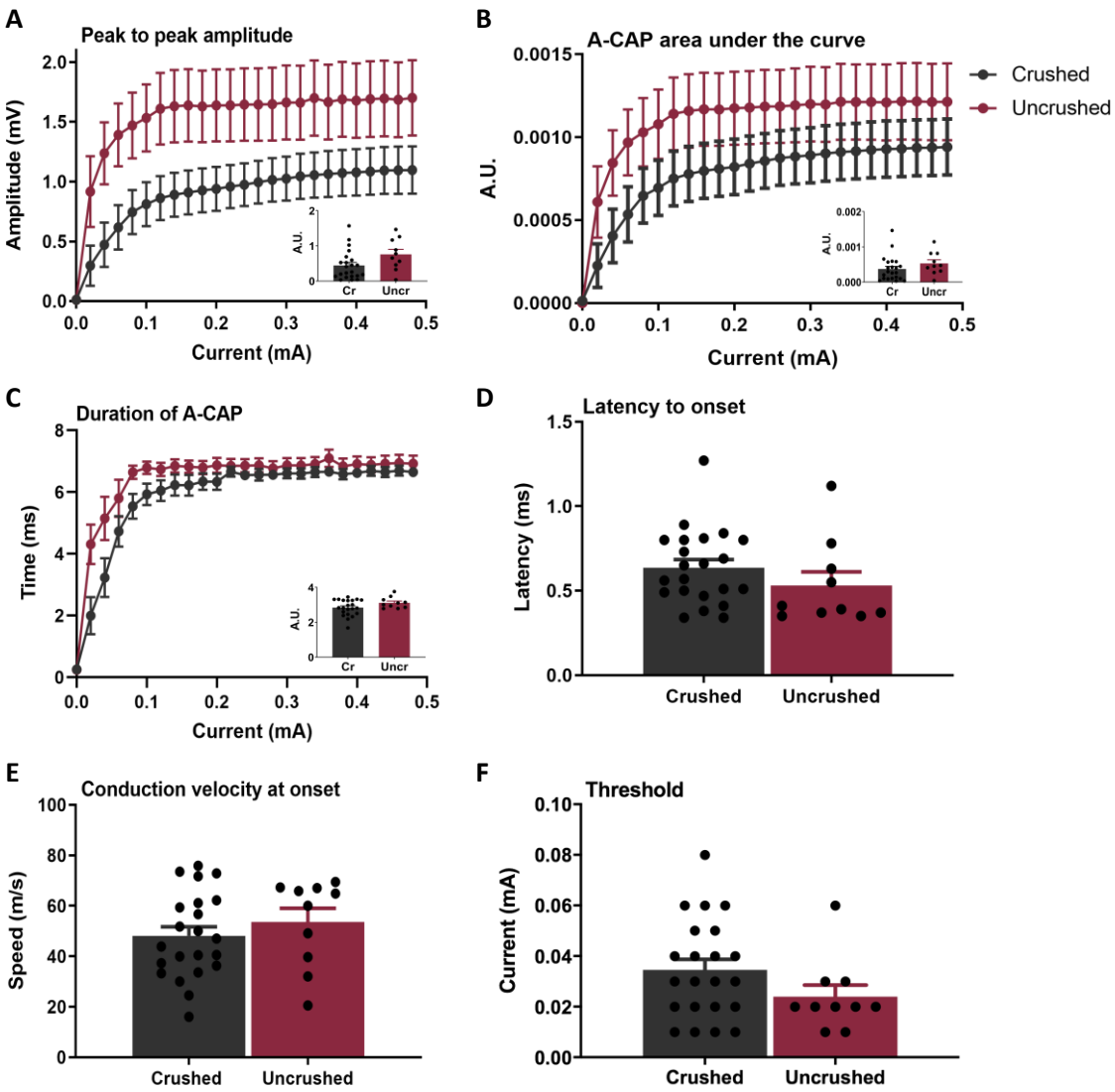

Figure 5-5 Effect of nerve crushing on the A-CAP in naïve animals

Saphenous nerves were harvested from saline-treated animals at day 7 and day 28-37 and placed in the recording chamber for electrical stimulation. Nerves in the uncrushed group were simply laid across the electrodes. Nerves in the crushed group were gently crushed on the second recording electrode with a pair of forceps. Nerves were electrically stimulated with increasing current intensities from 0 to 0.5 mA in 0.02 mA increments (50 µs square pulse width, 0.2 Hz). A-CAP parameters investigated were peak to peak amplitude (A); area under the curve (AUC) of the A-CAP waveform (B); duration (C); latency to onset of the A-CAP waveform (D); and conduction velocity at the onset of the A-CAP waveform (E). For threshold assessment (F), nerves were electrically stimulated with increasing current intensities from 0 to 0.3 mA in 0.01 mA increments (50 µs square pulse width, 0.2 Hz). Inserts (A-C) represent the AUC analysis of traces in (A-C). A.U. is arbitrary units. Data are expressed as mean ± SEM. (A-C) RM two-way ANOVA; (B-F and inserts A-C) unpaired two-tailed t-test. Crushed n = 22 nerves; uncrushed n = 10 nerves.

More marked differences between the two experimental groups were observed for C-CAP recordings. Due to a mistake when setting up the protocol for early recordings with uncrushed nerves, no recording was made at 0 mA. Figure 5-6 A shows reduced C-CAP peak amplitudes in crushed nerves compared with the uncrushed group. RM two-way ANOVA analysis displayed an overall significant decreasing effect of nerve crushing on peak amplitude (Figure 5-6 A, $F_{(1,26)}$ = 4.571, p = 0.0421 RM two-way ANOVA, crushed n = 19 nerves, uncrushed n = 9 nerves), yet Holm-Sidak *post hoc* comparisons failed to identify statistically significant differences at any specific current intensity. At 0.5, 1.0 and 1.5 mA, nerve crushing (mean*, 95% CI*: 0.013 mV, *0.009-0.016*; 0.014 mV*, 0.010-0.017*; and 0.012 mV*, 0.009-0.015*) determined a reduction in the mean peak amplitude by 54%, 39%, and 48%, respectively, compared with uncrushed nerves (mean, *95% CI*: 0.028 mV, *0.012-0.044;* 0.023 mV*, 0.008-0.037*; and 0.023 mV*, 0.008-0.038*) (Figure 5-6 B, ns unpaired two-tailed t-test with Welch's correction for unequal variances, crushed n = 19 nerves, uncrushed n = 9 nerves). Performing multiple t-test with Holm-Sidak correction was not considered necessary for these data, because the relationship between different currents was not a factor of interest. Like peak amplitudes, the AUC of C-CAP waveforms was higher in the uncrushed group, but the difference between crushed and uncrushed nerves was not statistically significant (Figure 5-6 C, ns unpaired two-tailed t-test with Welch's correction for unequal variances, crushed n = 19 nerves, uncrushed n = 9 nerves). The crushing-induced decrease in peak amplitude and AUC was associated with significantly broader C-CAP waveforms, which lasted 4-5 ms longer than C-CAPs generated in uncrushed nerves (Figure 5-6 D, *p < 0.05 unpaired two-tailed t-test with Welch's correction for unequal variances, crushed n = 19 nerves, uncrushed n = 9 nerves). Latency to peak was significantly increased by 35% in the crushed group (mean, *95% CI*: 47.0 ms, *42.1-51.9* at 0.5 mA; 46.4 ms, *42.0-50.7* at 1.0 mA; and 45.8 ms, *41.4-50.3* at 1.5 mA) compared with the uncrushed one (mean, *95% CI*: 30.7 ms, *24.0-37.4* at 0.5 mA; 29.9 ms, *22.2-37.7* at 1.0 mA; and 29.7 ms, *23.1-36.4* at 1.5 mA) (Figure 5-6 E, *p < 0.05 unpaired two-tailed t-test, crushed n = 19 nerves, uncrushed n = 9 nerves). Consequently, uncrushed nerves were able to generate significantly faster C-CAPs (mean, *95% CI*: 0.79 m/s, *0.66-0.92* at 0.5 mA; 0.81 m/s, *0.66-0.95* at 1.0 mA; and 0.82 m/s, *0.69-0.94* at 1.5 mA) than crushed nerves, whose conduction velocity was approximately 20% slower (mean, *95% CI*: 0.64 m/s, *0.59-0.69* at 0.5 mA; 0.64 m/s, *0.60-0.69* at 1.0 mA; and 0.65 m/s, *0.61-0.70* at 1.5 mA) (Figure 5-6 F, *p < 0.05 unpaired two-tailed t-test, crushed n = 19 nerves, uncrushed n = 9 nerves). Lastly, nerve crushing also increased the threshold to initiate the C-CAP, with an average threshold value of 0.25 ± 0.026 mA compared with a significantly lower 0.13 ± 0.017 mA (mean ± SEM) required to activate C-fibres in the uncrushed group (Figure 5-6 G, *p < 0.05 unpaired two-tailed t-test, crushed n = 15 nerves, uncrushed n = 9 nerves). Four nerves from the crushed

group could not be included in the threshold analysis because the C-CAP was either not easily distinguishable from the background noise (n = 2 nerves) or not present after the nerve was left to rest in the bath (n = 2 nerves). Despite the slight damaging effect that crushing had on the nerve conductive properties, it provided the advantage of obtaining monophasic recordings at all times. By contrast, A-CAPs recorded from uncrushed nerves were occasionally biphasic (and therefore could not be included in the analysis). Ensuring that only the cut end of the nerve was always placed on the distal electrode was challenging, especially when the recording chamber was immersed in mineral oil. Consequently, the nerve-electrode contact was not always optimal. For these reasons, all recordings for the OIPN model were conducted on crushed nerves.

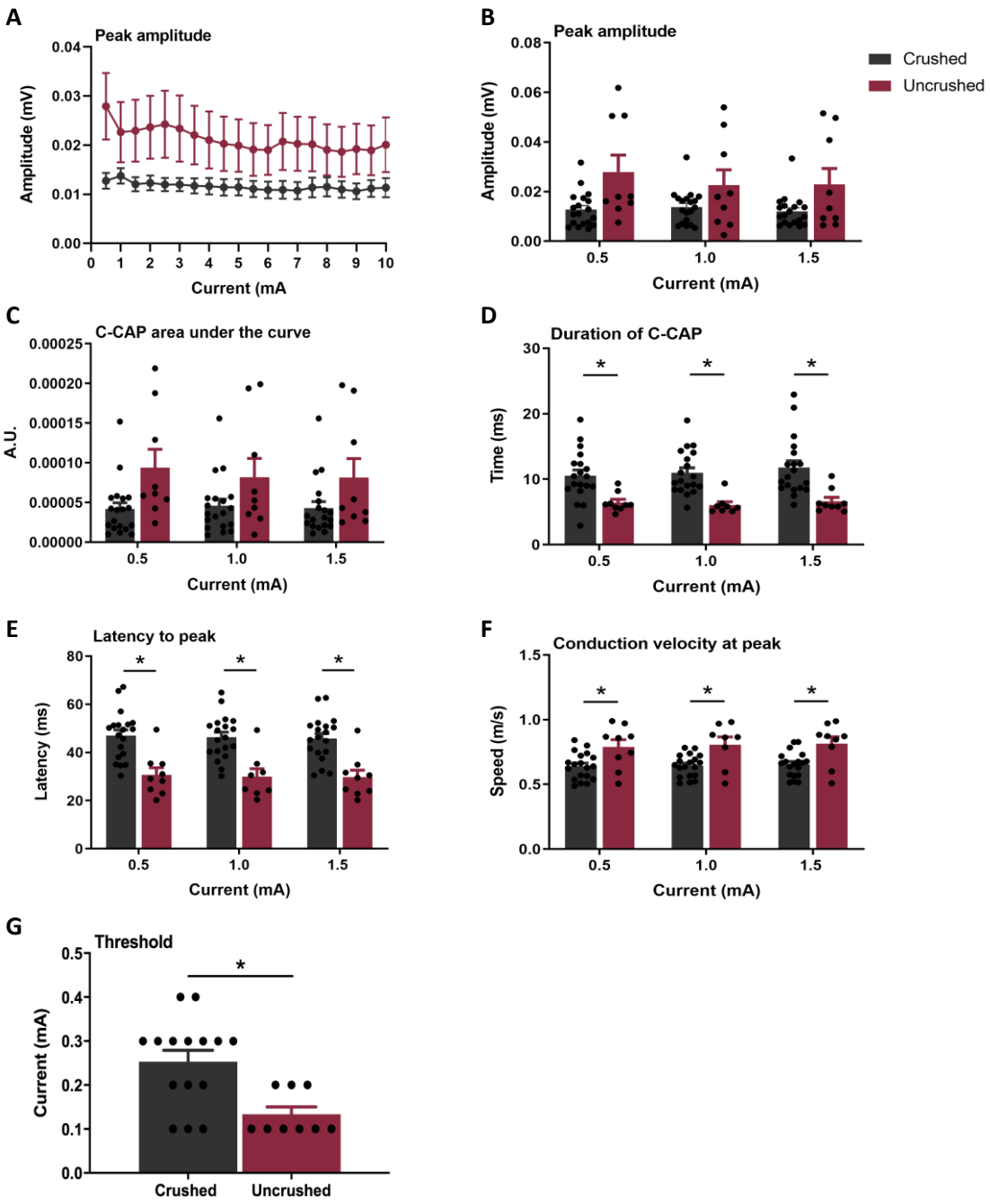

Figure 5-6 Effect of nerve crushing on the C-CAP in naïve animals

Saphenous nerves were harvested from saline-treated animals at day 7 and day 28-37 and placed in the recording chamber for electrical stimulation. Nerves in the uncrushed group were simply laid across the electrodes. Nerves in the crushed group were gently crushed on the second recording electrode with a pair of forceps. Nerves were electrically stimulated with increasing current intensities from 0.5 to 10 mA in 0.5 mA increments (1 ms square pulse width, 0.2 Hz). (A) shows peak amplitude at all current intensities. (B-F) show C-CAP parameters only at 0.5, 1.0 and 1.5 mA. C-CAP parameters investigated were peak amplitude (B); area under the curve of the C-CAP waveform (C); duration (D); latency to the peak of the C-CAP waveform (E); and conduction velocity at the peak of the C-CAP waveform (F). A.U. is arbitrary units. Data are expressed as mean ± SEM. *$p < 0.05$, (A) RM two-way ANOVA; (B-D) unpaired two-tailed t-test with Welch's correction for unequal variances; (E-F) unpaired two-tailed t-test. Crushed n = 19

nerves; uncrushed n = 9 nerves. For threshold assessment (G), nerves were electrically stimulated with increasing current intensities from 0 to 4 mA in 0.1 mA increments (1 ms square pulse width, 0.2 Hz). Data are expressed as mean ± SEM. *p < 0.05, unpaired two-tailed t-test. Crushed n = 15 nerves; uncrushed n = 9 nerves.

5.3.2 A- and C-CAP properties in saline- and oxaliplatin-treated animals

Animals received systemic (IP) injections of 2 mg/kg oxaliplatin or saline on four alternate days and the development of pain-like behaviour was assessed through von Frey testing. Animals were divided into two groups of approximately equal average baseline scores and randomly allocated to the saline or oxaliplatin group. At day 7, oxaliplatin-treated animals did not display mechanical hypersensitivity compared with saline-treated controls (Figure 5-7 A-C, ns two-tailed multiple-comparison unpaired t-tests with Holm-Sidak correction, saline n = 17, oxaliplatin n = 18). At the peak pain time point (day 28 to 33), oxaliplatin-treated animals exhibited increased mechanical hypersensitivity to 4 g, 8 g and 15 g binding forces, but only responses to 15 g filaments were statistically significant in comparison to saline-treated controls (Figure 5-7 A-C, *p < 0.05 two-tailed multiple-comparison unpaired t-tests with Holm-Sidak correction, saline n = 7, oxaliplatin n = 8). Animals were sacrificed at day 7 or during the peak pain period and the saphenous nerves were harvested for electrical stimulation.

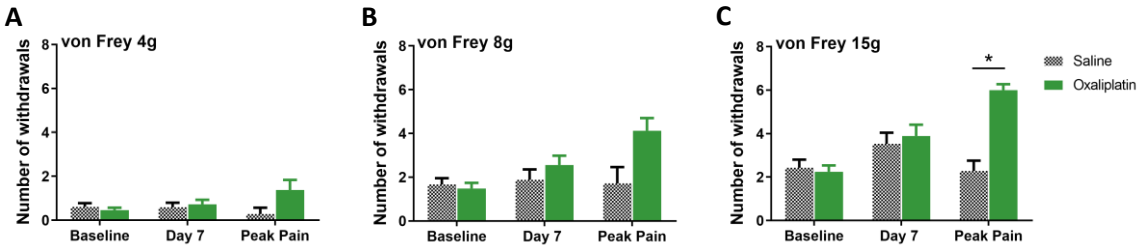

Figure 5-7 Mechanical hypersensitivity to von Frey filaments following oxaliplatin administration

Mechanical hypersensitivity to 4 g (A), 8 g (B) and 15 g (C) von Frey filaments, expressed as number of withdrawals to 10 stimuli in total. Baseline and day 7: saline n = 17, oxaliplatin n = 18; peak pain (day 28-33): saline n = 7, oxaliplatin n = 8. Data are expressed as mean ± SEM. *p < 0.05, two-tailed multiple-comparison unpaired t-tests with Holm-Sidak correction.

5.3.2.1 CAP recordings prior to oxaliplatin-induced mechanical hypersensitivity

At day 7, a significant overall effect was observed between the two treatment groups, with oxaliplatin-treated animals displaying increased A-CAP peak to peak amplitude compared with saline controls (Figure 5-8 A, $F_{(1,19)} = 6.771$, $p = 0.0175$ RM two-way ANOVA, saline n = 13 nerves, oxaliplatin n = 8 nerves). Nevertheless, Holm-Sidak *post hoc* comparisons failed to identify statistically significant differences at any specific current intensity. The maximal amplitude response was reached at 0.48 mA in both saline- and oxaliplatin-treated groups, yet at this stimulus intensity the average peak to peak amplitude of nerves from oxaliplatin-treated animals (mean, *95% CI*: 1.80 mV, *0.96-2.65*) was increased by 137% compared with the nerves from saline-treated animals (mean*, 95% CI*: 0.76 mV, *0.33-1.20*). AUC analysis confirmed the presence of a significant global effect (143% increment) of oxaliplatin treatment (mean, *95% CI*: 0.73 AU, *0.33-1.13*) on A-CAP amplitudes compared with the saline-treated group (mean, *95% CI*: 0.30 AU, *0.12-0.47*) (Figure 5-8 A insert, **p* < 0.05 unpaired two-tailed t-test, saline n = 13 nerves, oxaliplatin n = 8 nerves). The AUC of the A-CAP waveform was also significantly increased by the oxaliplatin treatment (Figure 5-8 B, $F_{(1,19)} = 7.952$, $p = 0.0109$ RM two-way ANOVA, saline n = 13 nerves, oxaliplatin n = 8 nerves), but again Holm-Sidak *post hoc* comparisons did not identify statistically significant differences at any specific current intensity. The presence of an overall significant effect was confirmed by AUC analysis that showed a significant 161% AUC increase following oxaliplatin treatment (mean, *95% CI* oxaliplatin: 0.00073 AU*, 0.00035-0.0011*; saline: 0.00028 AU*, 0.00010-0.00045*) (Figure 5-8 B insert, **p* < 0.05 unpaired two-tailed t-test, saline n = 13 nerves, oxaliplatin n = 8 nerves). Oxaliplatin administration had a significant overall effect on the duration of the A-CAP and nerves from oxaliplatin-treated animals displayed broader A-CAPs than nerves from the saline group (Figure 5-8 C, $F_{(1,19)} = 8.286$, $p = 0.0096$ RM two-way ANOVA, saline n = 13 nerves, oxaliplatin n = 8 nerves). However, Holm-Sidak *post hoc* comparisons did not identify statistically significant differences at any specific current intensity. AUC analysis confirmed the longer duration of the A-CAP in the oxaliplatin group compared with saline-treated animals (Figure 5-8 C insert, **p* < 0.05 unpaired two-tailed t-test, saline n = 13 nerves, oxaliplatin n = 8 nerves). The latency to onset of the A-CAP waveform was significantly reduced to 0.51 ± 0.06 ms in the oxaliplatin group compared with 0.73 ± 0.06 ms (mean ± SEM) in the saline group (Figure 5-8 D, **p* < 0.05 unpaired two-tailed t-test, saline n = 13 nerves, oxaliplatin n = 8 nerves). As a result, there was a significant increase in conduction velocity of the fastest A-fibres in oxaliplatin-treated animals compared with saline-treated controls (Figure 5-8 E, **p* < 0.05 unpaired two-tailed t-test, saline n = 13 nerves, oxaliplatin n = 8 nerves). The oxaliplatin-treated group displayed an overall 53% increase in conduction velocity (mean, *95% CI*: 58.93 m/s*, 42.28-75.58*) compared with the saline-treated group (mean, *95% CI*: 38.48 m/s,

31.39-45.58). Lastly, there was no significant difference in the activation threshold of nerves from oxaliplatin-treated animals (0.02 ± 0.006 mA) compared with their respective saline-treated controls (0.04 ± 0.006 mA) (Figure 5-8 F, ns unpaired two-tailed t-test, saline n = 13 nerves, oxaliplatin n = 8 nerves). Sample size was unequal between saline and oxaliplatin groups because recording was not always possible for all the nerves harvested from the animals.

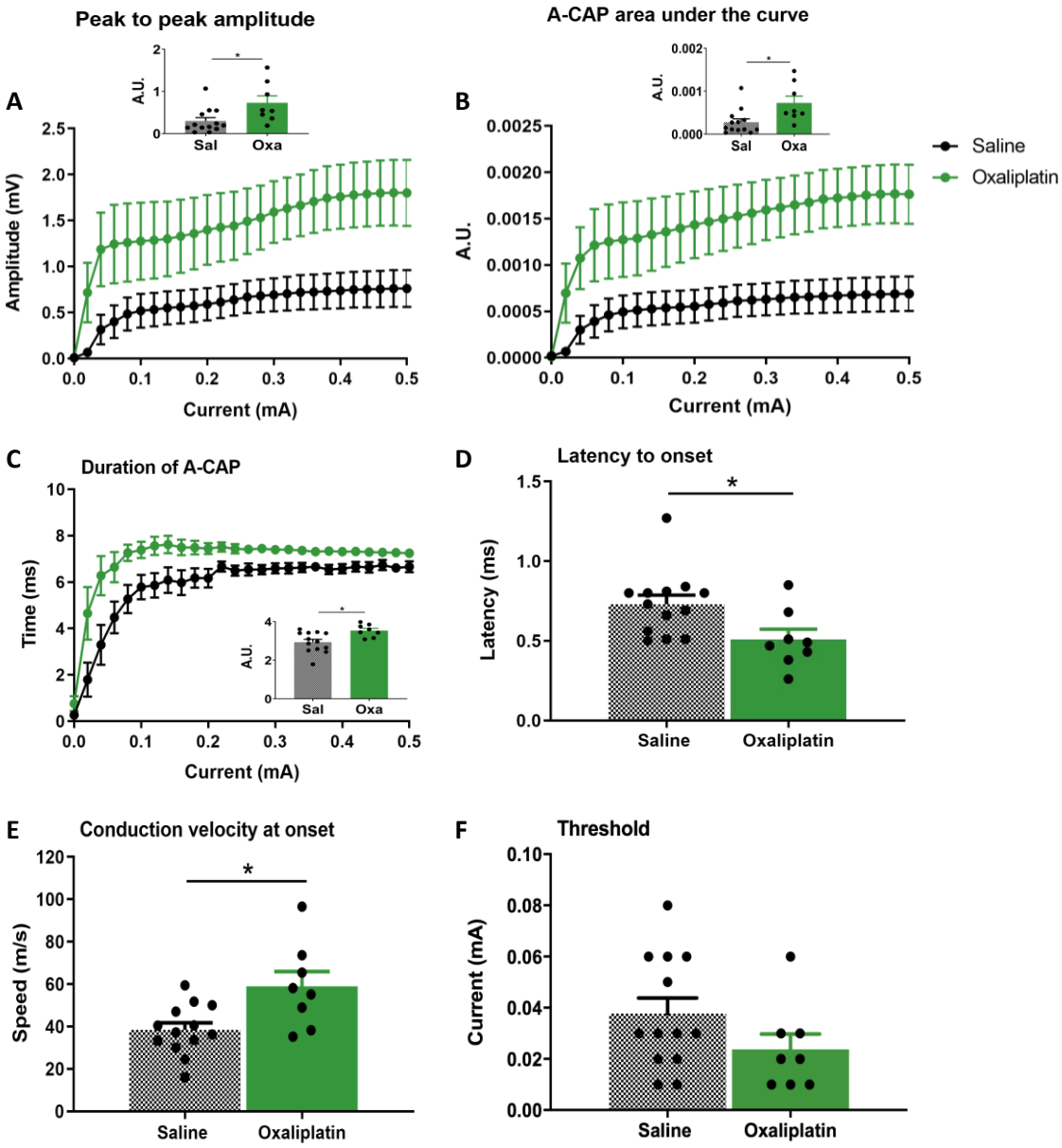

Figure 5-8 A-CAP parameters at day 7 in oxaliplatin- and saline-treated animals

Saphenous nerves were harvested from saline- and oxaliplatin-treated animals and electrically stimulated with increasing current intensities from 0 to 0.5 mA in 0.02 mA increments (50 µs square pulse width, 0.2 Hz). A-CAP parameters investigated were peak to peak amplitude (A); area under the curve (AUC) of the A-CAP waveform (B); duration (C); latency to onset of the A-CAP waveform (D); and conduction velocity at the onset of the A-CAP waveform (E). For threshold assessment (F), nerves were electrically stimulated with increasing current intensities from 0 to 0.3 mA in 0.01 mA increments (50 µs square pulse width, 0.2

Hz). Inserts (A-C) represent the AUC analysis of traces in (A-C). A.U. is arbitrary units. Data are expressed as mean ± SEM. *p < 0.05, (A-C) RM two-way ANOVA; (B-F and inserts A-C) unpaired two-tailed t-test. Saline n = 13 nerves; oxaliplatin n = 8 nerves.

At day 7, there was no overall difference in the C-CAP peak amplitude between oxaliplatin- and saline-treated groups and both groups reached their maximal amplitude response early in the recording protocol (Figure 5-9 A, ns RM two-way ANOVA, saline n = 10 nerves, oxaliplatin n = 11 nerves). Nerves from oxaliplatin-treated animals reached the highest peak amplitude of 0.016 ± 0.003 mV (mean ± SEM) after the first stimulus (0.5 mA). After 0.5 mA, the amplitude dropped slightly and immediately reached a plateau that remained constant until the end of the protocol. Nerves from saline-treated animals displayed the same highest peak amplitude of 0.016 ± 0.001 mV after the second stimulus (1.0 mA), but then the amplitude progressively decreased till it reached an average value of 0.009 mV ± 0.002 mV at the last stimulus. This was reflective of the difficulty in obtaining robust C-fibre recordings from beginning to end of the protocol. Indeed, in some cases, the C-fibre response peaked at low current intensities to then progressively decrease and even disappear at higher intensities that were deemed to be too damaging for nerve integrity. Unpaired two-tailed t-tests confirmed the lack of difference in peak amplitude at 0.5, 1.0 and 1.5 mA between saline and oxaliplatin groups (Figure 5-9 B, ns unpaired two-tailed t-test with Welch's correction for unequal variances, saline n = 10 nerves, oxaliplatin n = 11 nerves). There was no difference in the AUC of the C-CAP waveform (Figure 5-9 C, ns unpaired two-tailed t-test, saline n = 10 nerves, oxaliplatin n = 11 nerves), in its duration (Figure 5-9 D, ns unpaired two-tailed t-test, saline n = 10 nerves, oxaliplatin n = 11 nerves), in the latency to the peak of the waveform (Figure 5-9 E, ns unpaired two-tailed t-test, saline n = 10 nerves, oxaliplatin n = 11 nerves), nor in the conduction velocity measured at peak (Figure 5-9 F, ns unpaired two-tailed t-test, saline n = 10 nerves, oxaliplatin n = 11 nerves). However, nerves from oxaliplatin-treated animals required a significantly lower stimulus intensity (0.2 ± 0.03 mA) to initiate a C-CAP compared with the saline-treated controls (0.3 ± 0.03 mA) (Figure 5-9 G, *p < 0.05 unpaired two-tailed t-test, saline n = 9 nerves, oxaliplatin n = 10 nerves). Activating threshold could not be measured for 1 nerve/group. In case of the saline group, the C-CAP amplitude was not big enough to be discernible from the background noise. In the oxaliplatin group, the C-CAP was not present after the nerve was left to rest in the bath.

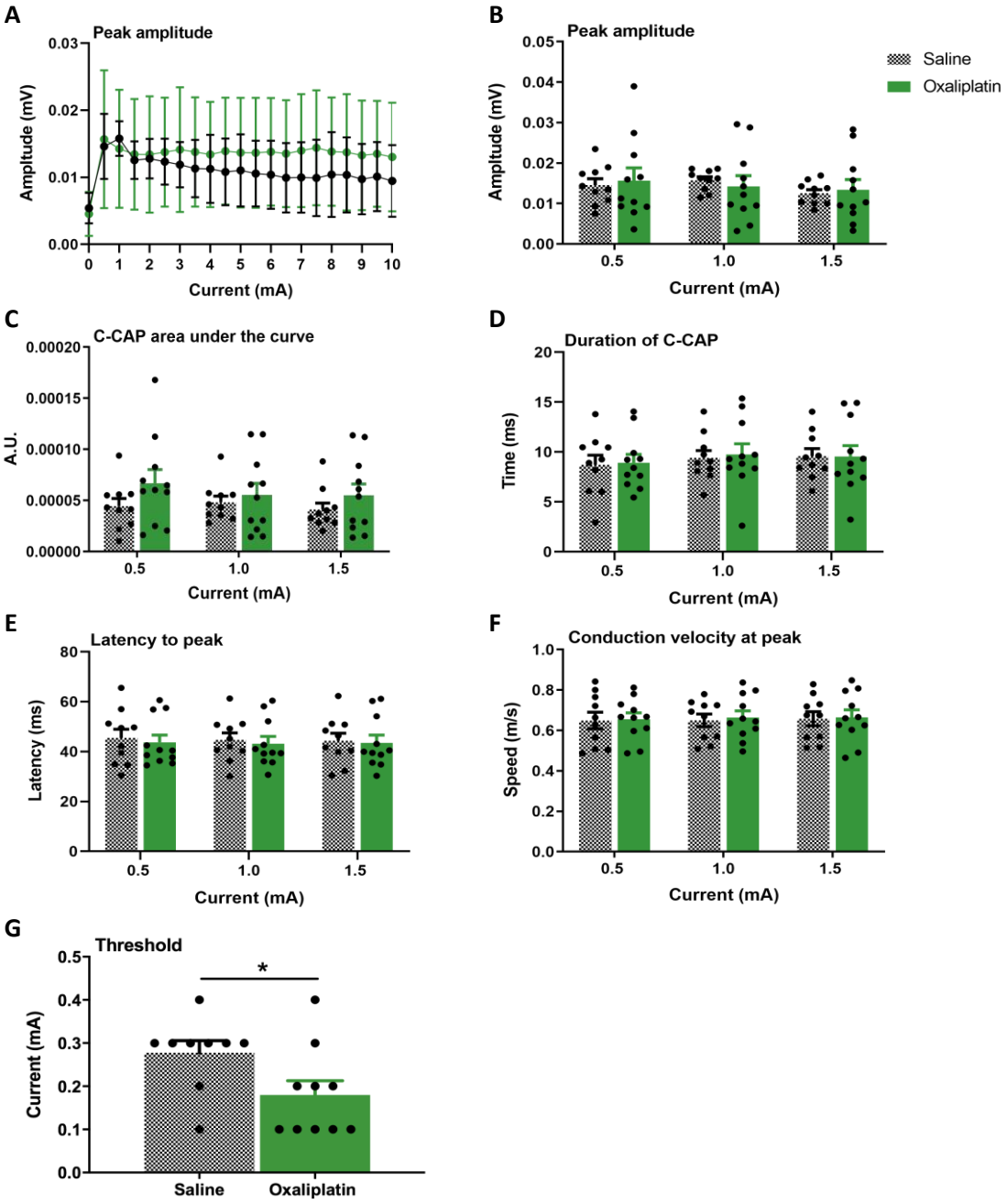

Figure 5-9 C-CAP parameters at day 7 in oxaliplatin- and saline-treated animals

Saphenous nerves were harvested from saline- and oxaliplatin-treated animals and electrically stimulated with increasing current intensities from 0 to 10 mA in 0.5 mA increments (1 ms square pulse width, 0.2 Hz). (A) shows peak amplitude at all current intensities. (B-F) show C-CAP parameters only at 0.5, 1.0 and 1.5 mA. C-CAP parameters investigated were peak amplitude (B); area under the curve of the C-CAP waveform (C); duration (D); latency to the peak of the C-CAP waveform (E); and conduction velocity at the peak of the C-CAP waveform (F). A.U. is arbitrary units. Data are expressed as mean ± SEM. (A) RM two-way ANOVA; (B) unpaired two-tailed t-test with Welch's correction for unequal variances; (C-F) unpaired two-tailed t-test. Saline n = 10 nerves; oxaliplatin n = 11 nerves. For threshold assessment (G), nerves were electrically stimulated with increasing current intensities from 0 to 4 mA in 0.1 mA increments

(1 ms square pulse width, 0.2 Hz). Data are expressed as mean ± SEM. *$p < 0.05$, unpaired two-tailed t-test. Saline n = 9 nerves; oxaliplatin n = 10 nerves.

5.3.2.2 CAP recordings at the peak of oxaliplatin-induced mechanical hypersensitivity

At peak pain (day 28-33), there was no significant difference in the A-CAP peak to peak amplitude between the two treatment groups (Figure 5-10 A, ns RM two-way ANOVA, saline n = 9 nerves, oxaliplatin n = 11 nerves). AUC analysis confirmed that there was no difference between treatments (Figure 5-10 A insert, ns unpaired two-tailed t-test, saline n = 9 nerves, oxaliplatin n = 11 nerves). There was no significant difference in the AUC of the A-CAP waveform (Figure 5-10 B, ns RM two-way ANOVA – Figure 5-10 B insert, ns unpaired two-tailed t-test, saline n = 9 nerves, oxaliplatin n = 11 nerves). The A-CAP duration was not different between treatment groups (Figure 5-10 C, ns RM two-way ANOVA – Figure 5-10 C insert, ns unpaired two-tailed t-test, saline n = 9 nerves, oxaliplatin n = 11 nerves). No difference was detected in the latency to the onset of the A-CAP (Figure 5-10 D, ns unpaired two-tailed t-test, saline n = 9 nerves, oxaliplatin n = 11 nerves), nor in the conduction velocity of the fastest fibres between the two treatment groups (Figure 5-10 E, ns unpaired two-tailed t-test, saline n = 9 nerves, oxaliplatin n = 11 nerves). Lastly, an average current of 0.03 mA was sufficient to initiate the A-CAP in both the oxaliplatin and saline group (Figure 5-10 F, ns unpaired two-tailed t-test, saline n = 9 nerves, oxaliplatin n = 11 nerves).

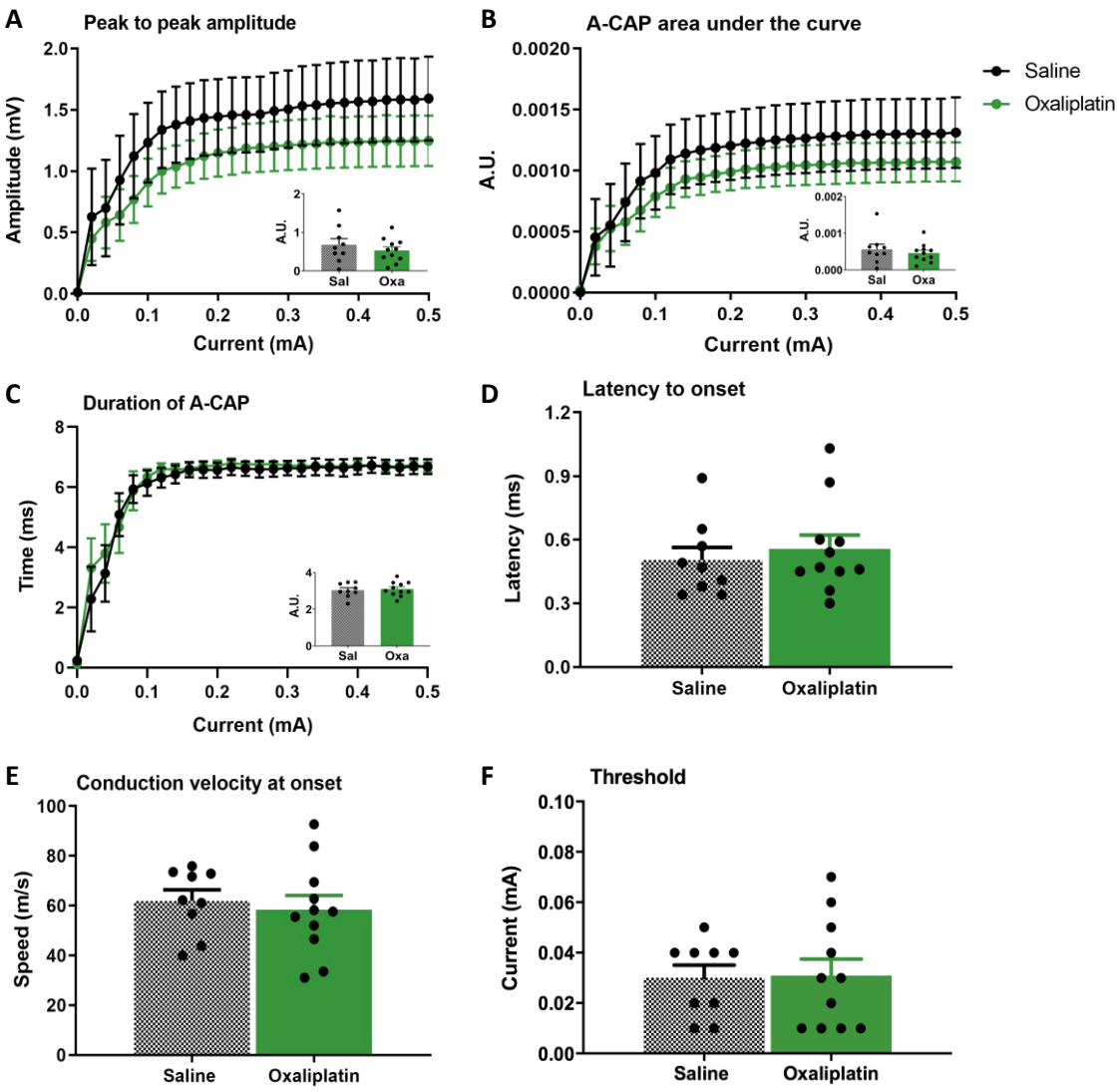

Figure 5-10 A-CAP parameters at peak pain in oxaliplatin- and saline-treated animals

Saphenous nerves were harvested from saline- and oxaliplatin-treated animals and electrically stimulated with increasing current intensities from 0 to 0.5 mA in 0.02 mA increments (50 µs square pulse width, 0.2 Hz). A-CAP parameters investigated were peak to peak amplitude (A); area under the curve (AUC) of the A-CAP waveform (B); duration (C); latency to onset of the A-CAP waveform (D); and conduction velocity at the onset of the A-CAP waveform (E). For threshold assessment (F), nerves were electrically stimulated with increasing current intensities from 0 to 0.3 mA in 0.01 mA increments (50 µs square pulse width, 0.2 Hz). Inserts (A-C) represent the AUC analysis of traces in (A-C). A.U. is arbitrary units. Data are expressed as mean ± SEM. (A-C) RM two-way ANOVA; (B-F and inserts A-C) unpaired two-tailed t-test. Saline n = 9 nerves; oxaliplatin n = 11 nerves.

At peak pain, there was no overall difference in the C-CAP peak amplitude between oxaliplatin- and saline-treated groups (Figure 5-11 A, RM two-way ANOVA, saline n = 9 nerves, oxaliplatin n = 12 nerves). At 0.5, 1.0 and 1.5 mA, nerves from saline and oxaliplatin groups displayed no difference in any of the C-CAP parameters assessed (Figure 5-11 B-F, ns unpaired two-tailed t-test, saline n = 9 nerves, oxaliplatin n = 12 nerves). There was no difference in activating threshold between groups and C-fibres from both treatment groups were activated at an average current intensity of 0.2 ± 0.05 mA (mean ± SEM) (Figure 5-11 G, ns unpaired two-tailed t-test, saline n = 6 nerves, oxaliplatin n = 8 nerves). Threshold could not be measured for all nerves included in the characterisation analysis. Three nerves from saline-treated animals could not be included in the threshold investigation because the C-CAP was not easily identifiable in between the background noise (n = 1 nerve) and because the C-CAP was not present in the post-resting recording (n = 2 nerves). Four nerves from oxaliplatin-treated animals were excluded for the same reasons (noisy recording: n = 2 nerves; no C-CAP after rest: n = 2 nerves).

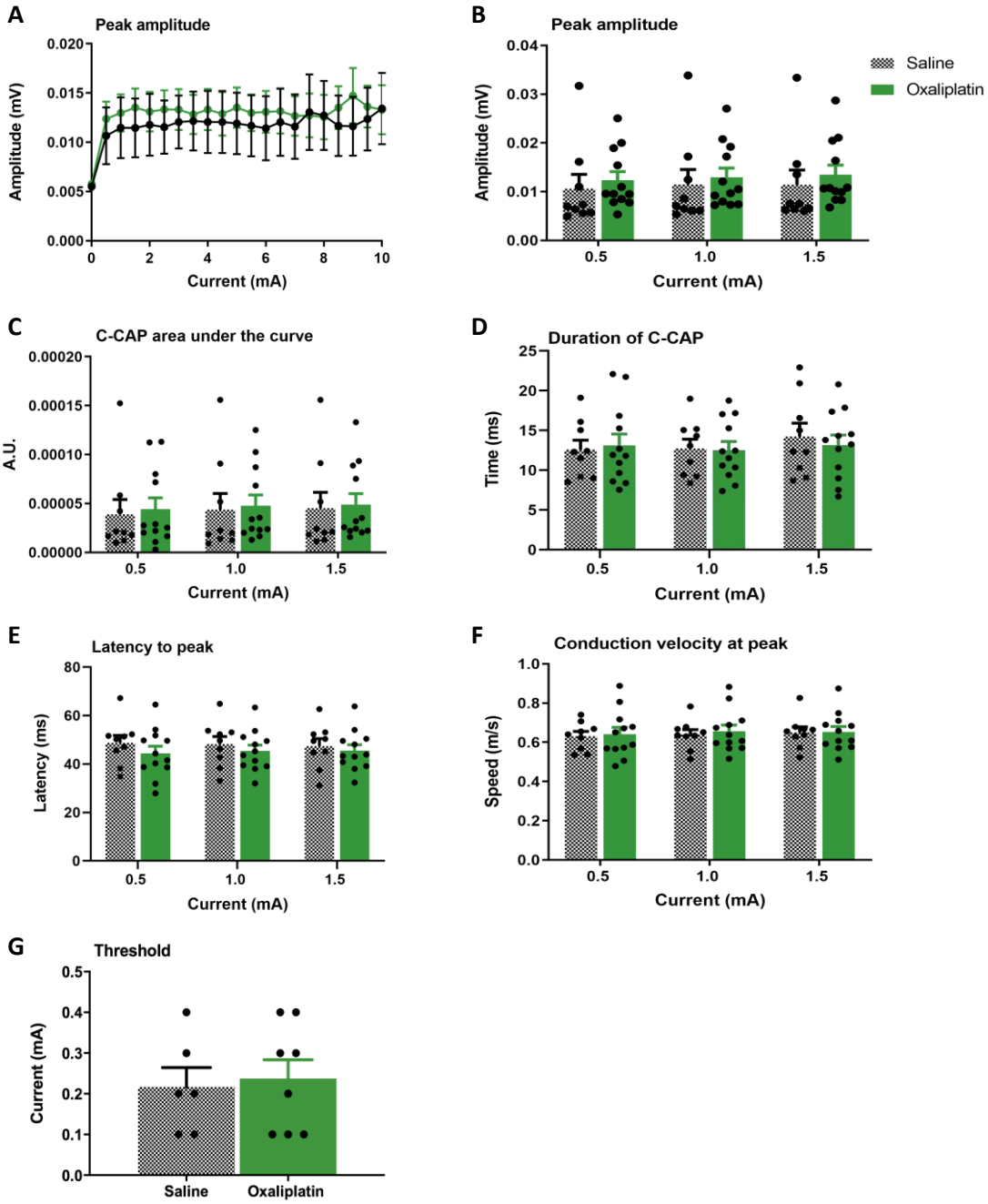

Figure 5-11 C-CAP parameters at peak pain in oxaliplatin- and saline-treated animals

Saphenous nerves were harvested from saline- and oxaliplatin-treated animals and electrically stimulated with increasing current intensities from 0 to 10 mA in 0.5 mA increments (1 ms square pulse width, 0.2 Hz). (A) shows peak amplitude at all current intensities. (B-F) show C-CAP parameters only at 0.5, 1.0 and 1.5 mA. C-CAP parameters investigated were peak amplitude (B); area under the curve of the C-CAP waveform (C); duration (D); latency to the peak of the C-CAP waveform (E); and conduction velocity at the peak of the C-CAP waveform (F). A.U. is arbitrary units. Data are expressed as mean ± SEM. (A) RM two-way ANOVA; (B-F) unpaired two-tailed t-test. Saline n = 9 nerves; oxaliplatin n = 12 nerves. For threshold assessment (G), nerves were electrically stimulated with increasing current intensities from 0 to 4 mA in 0.1 mA increments (1 ms square pulse width, 0.2 Hz). Data are expressed as mean ± SEM. Unpaired two-tailed t-test. Saline n = 6 nerves; oxaliplatin n = 8 nerves.

5.4 Discussion

Conduction properties of A- and C-fibres were assessed via CAP recordings in *ex vivo* preparations of the saphenous nerve. A-CAP recordings were efficiently obtained from the nerves. Conversely, obtaining robust recordings for C-CAPs was challenging at times and C-CAP analysis was standardised by including results obtained at supramaximal stimulations between 0.5 and 1.5 mA. To the best of our knowledge, this was the first CAP investigation in a chronic OIPN model (and CIPN in general) that used the saphenous nerve, which is purely involved in sensory processing. As chronic OIPN is associated with sensory symptoms, without any motor involvement, the saphenous nerve represents an optimal model to investigate potential oxaliplatin-induced electrophysiological changes.

Ex vivo nerve recordings are usually performed in bicarbonate solution supplemented with glucose to sustain the peripheral nerves' metabolism. A recent investigation on non-glucose substrates reported that both 10 mM glucose and 20 mM fructose were able to maintain A- and C-CAPs in the mouse sciatic nerve for up to 8 hours (Rich and Brown 2018). As the experimental set-up and the nerve under investigation in our study were different from those described by (Rich and Brown 2018), evaluating the effect of fructose on the saphenous nerve conductive properties was deemed of interest. Here, the use of 20 mM fructose did not introduce any advantage over 10 mM glucose. There was no difference in amplitude, AUC and duration of the A-CAP between recordings made in glucose and those in fructose, although a slight worsening in conduction velocity and activation threshold was observed following fructose supplementation. Nevertheless, the sample size of this investigation was too low to draw any proper conclusion. In particular, C-CAP recordings were obtained only for two nerves, therefore no statistical analysis could be performed. Despite the very small sample size, the use of fructose did not show any remarkable difference in A-CAP properties that justified carrying out a more extensive investigation. Additionally, all optimisation attempts performed prior to this small study were conducted with glucose supplementation, which allowed to successfully record both A- and C-CAPs. Moreover, preliminary results from our lab on sciatic nerves were conducted in glucose. Therefore, all further experiments were conducted in 10 mM glucose.

Nerve crushing on the distal recording electrode had a negative impact on CAP properties. The most notable effect on the A-CAP was a small, non-significant decrease in peak to peak amplitude. The C-CAP was more affected by the physical crushing, as demonstrated by significant increases in its duration, latency to peak and activation threshold, together with slower conduction velocity compared with uncrushed nerves. Placing the cut end of the nerve on the distal recording electrode may be considered a monophasic recording in practice, as the

second electrode would be in contact with a dead region of the nerve. However, due to the difficulties in ensuring that only the dead end would be on the distal electrode, there is a risk that both recording electrodes may be in contact with active sections of the nerve. Consequently, the recording would be biphasic rather than monophasic. Despite the damage on nerve conduction properties, nerve crushing was considered preferable to uncrushed nerve preparations, as it always ensured monophasic recordings. When the distance between stimulating and recording electrodes is long enough, monophasic recordings allow to distinguish between different nerve fibres that conduct at different velocities (McAllister and Calder 1995). Here, the relatively small distance between electrodes impaired the visualisation of distinct A-fibre types, but A- and C-fibres could be easily distinguished.

The conduction properties of the saphenous nerves after chronic administration of oxaliplatin have not been investigated before. Here, oxaliplatin-treated animals did not display any sign of pain-like behaviour at day 7, 24 hours after the last oxaliplatin injection, but mechanical hypersensitivity was evident at the peak pain time point (day 28-33). At day 7, oxaliplatin-treated animals displayed increased A-CAP peak to peak amplitude, area under the curve, duration and conduction velocity compared with saline-treated controls. Changes in CAP properties in *ex vivo* recordings may be ascribable to many experimental and physiological factors. Experimental variables were not considered a caveat of this investigation: the temperature was kept constant throughout the study, distance between recording electrodes was never < 5 mm, and nerve integrity was maintained by careful dissections and lack of desheathing. Given that experimental variables were controlled for, a more likely hypothesis is that oxaliplatin administration has an acute direct effect on electrophysiological parameters. Nerves from oxaliplatin-treated animals displayed a small reduction in the activation threshold of A-fibres compared with control animals, thus suggesting that oxaliplatin might sensitise the A-fibres. Indeed, the threshold for Aβ-fibres activation was lowered in a rat model of acute OIPN (Yamamoto et al. 2016b). Moreover, A-fibres may become hyperexcitable after exposure to oxaliplatin. This hypothesis is supported by several *in vitro* studies that associated acute OIPN with altered Na_v (Adelsberger et al. 2000, Grolleau et al. 2001, Benoit et al. 2006, Wu et al. 2009, Sittl et al. 2012) and K_v (Benoit et al. 2006, Kagiava et al. 2008, Kagiava et al. 2013) channels activity. Nevertheless, the translational relevance of these *in vitro* models is limited, as they don't reflect the oxaliplatin levels that nerves are exposed to in oxaliplatin-treated patients. The role of voltage-gated channels in OIPN has been extensively investigated in clinical settings as well. Nerve excitability studies on sensory and motor axons in oxaliplatin-treated patients confirmed the role of Na_v channels dysfunction in acute OIPN (Krishnan et al. 2005, Krishnan et al. 2006, Park et al. 2009a, Park et al. 2009b, Heide et al. 2018). Interestingly, patients who

developed chronic neuropathy at the end of the treatment were characterised by bigger alterations between pre- and post-infusion excitability studies, while smaller and reversible changes were observed in patients that did not develop chronic neuropathy (Krishnan et al. 2006, Park et al. 2009a, Park et al. 2009b). A prospective multicentre genotyping study on single nucleotide polymorphisms (SNPs) potentially associated with OIPN identified two SNPs in genes encoding for Na_v channels that were predictive for both incidence and severity of acute OIPN (Argyriou et al. 2013a). OIPN acute syndrome is associated with repetitive motor CAP and spontaneous muscle fibre discharges (Wilson et al. 2002, Lehky et al. 2004). Similar symptoms are typically observed in neuromyotonia, a condition that manifests with muscle stiffness and delayed muscle relaxation due to nerve hyperexcitability (A. Vincent 2000). The nerve hyperexcitability characteristic of neuromyotonia has been attributed to dysfunction in Na_v and K_v channels (Vincent 2000, Wilson et al. 2002), which could result in a prolonged depolarisation phase and subsequently in increased release of neurotransmitters and repetitive firing (Lehky et al. 2004). Therefore, it is possible that an association between K_v channels dysfunction and nerve hyperexcitability exists in acute OIPN as well.

Conduction velocity is directly related to the diameter of the nerve fibre, where large myelinated fibres conduct action potentials faster than the small myelinated and unmyelinated ones (Hursh 1939). There is no consensus on the myelination status of peripheral nerves after oxaliplatin treatment. Xiao et al. reported a slowing in sensory conduction velocity in rat peripheral nerves that was not associated with demyelination or axonal degeneration (Xiao et al. 2012). By contrast, other groups reported oxaliplatin-induced demyelination and nerve degeneration (Kawashiri et al. 2011, Al Moundhri et al. 2013, Guillaumot et al. 2019), although it is worth mentioning that higher cumulative doses of oxaliplatin were employed (32-36 mg/kg) (Kawashiri et al. 2011, Al Moundhri et al. 2013). Nevertheless, oxaliplatin-induced alterations of conduction velocity typically manifest as a reduction in the conduction velocity of sensory nerves. The increase in A-CAP velocity reported here at day 7 in oxaliplatin-treated animals is unlikely associated with an increase in the myelination status of the A-fibres. Action potential generation and propagation relies on clusters of Na_v channels at the initial segment of the axon and at nodes of Ranvier, while fast K_v channels cluster at juxtaparanodal regions (Rasband and Trimmer 2001, Kress and Mennerick 2009, Leterrier et al. 2011). Whole-cell patch clamp and single-axon recordings of unmyelinated hippocampal neurons showed that the presence of nodal Na_v clusters increased conduction velocity when compared with neurons lacking these clusters (Freeman et al. 2015). It is possible that oxaliplatin induces an increase in Na_v channels expression, which eventually might affect conduction velocity. For instance, $Na_v1.8$ mRNA expression was increased in the DRG of oxaliplatin-treated rats (Descoeur et al. 2011). However,

we are not aware of reports of increased mRNA or protein expression of Na_v channels in the peripheral nerves of oxaliplatin-treated animals. Further investigations are necessary to fully understand the mechanisms underlying changes in conduction velocity that are not associated with demyelination or axonal degeneration.

No difference between oxaliplatin and saline group was recorded at day 7 for C-CAP amplitude, AUC, duration, latency and conduction velocity. Lack of C-CAP alterations in acute OIPN has already been reported in human and rodent peripheral nerves exposed *in vitro* to oxaliplatin (Adelsberger et al. 2000, Sittl et al. 2010, Sittl et al. 2012). The only oxaliplatin-induced change observed here was a reduction in the activation threshold of C-fibres. This observation suggested that oxaliplatin sensitises the unmyelinated fibres. This hypothesis is supported by the evidence that the paw withdrawal threshold to a 5 Hz sine-wave stimulation, which specifically activates C-fibres, was significantly reduced after systemic administration of 6 mg/kg oxaliplatin (Yamamoto et al. 2016b). Furthermore, the threshold reduction was associated with the development of cold allodynia, which is typical of acute OIPN (Yamamoto et al. 2016b).

Here, no significant difference in A- or C-CAP parameters of the saphenous nerve was detected between oxaliplatin and saline group at peak pain. A potential explanation as to why nerve conduction properties are altered acutely at day 7 but not at peak pain involves oxaliplatin accumulation within the nerves. In rat models of OIPN, platinum accumulation within nerves has been reported in the sciatic (Screnci et al. 2000, Cavaletti et al. 2001, Ip et al. 2013, Nishida et al. 2018) and sural (Screnci et al. 2000) nerve soon after treatment completion. The saphenous nerve has not been examined, but oxaliplatin is likely to accumulate there as well. After treatment cessation, and as time goes by, Pt levels in the nerve decrease and the effect on nerve conductivity may decrease as well (Cavaletti et al. 2001), thus potentially explaining the lack of deficits observed here at the peak pain time point. However, it remains unclear why oxaliplatin-treated animals display significant mechanical hypersensitivity when no sensory electrophysiological changes can be observed. Moreover, our results are conflicting with evidence in the literature showing that oxaliplatin induces deficits in the amplitude and conduction velocity of both human (Cascinu et al. 2002, Lehky et al. 2004, Krishnan et al. 2005, Pietrangeli et al. 2006, Argyriou et al. 2007, Park et al. 2009a, Park et al. 2009b, Kokotis et al. 2016, Matsuoka et al. 2016, Kim et al. 2018, Krøigård et al. 2020) and rodent sensory nerves (Cavaletti et al. 2001, McKeage et al. 2001, Jamieson et al. 2005, Meyer et al. 2011, Renn et al. 2011, Kanbara et al. 2014) after treatment completion. Unlike our treatment paradigm (2 mg/kg on four alternate days), the majority of preclinical OIPN models were generated by systemic administration of intermediate or high cumulative doses of oxaliplatin (16 to 48 mg/kg) in longer treatment schedules (intermittent administration for 3 up to 8 weeks). The low-dose of

oxaliplatin used here may explain the lack of deficits in A- and C-CAP parameters at peak pain. However, this hypothesis seems unlikely, as chronic low-dose oxaliplatin administration (1 mg/kg twice weekly for three weeks) was enough to decrease the CAP amplitude and conduction velocity in the sciatic nerve (Meyer et al. 2011). Furthermore, even a single injection of 10 mg/kg oxaliplatin resulted in a progressive deficit in the conduction velocity of the sciatic nerve that only resolved three months after oxaliplatin administration (McKeage et al. 2001).

In general, the great variety of electrophysiological techniques and of animal models employed by different research groups may be partially responsible for the high variability in results among studies. The development of more standardised electrophysiological methodologies could help obtain more consistent results and get a better understanding of the mechanisms underlying OIPN.

5.5 Conclusions

In conclusion, our data show that A- and C-CAPs can be successfully recorded from saphenous nerves and that nerves are efficiently responding to electrical stimulation, even without removal of the epineural sheath. Substitution of glucose in the bicarbonate solution superfusing the nerves with fructose did not provide any benefit in A-CAP recordings. Crushing the nerve on the distal electrode had a slight damaging effect on its conduction properties. Yet, it ensured a stable nerve-electrode contact and monophasic recordings. At day 7, oxaliplatin-treated animals did not display symptoms of pain-like behaviour. However, oxaliplatin evoked an increase in A-CAP amplitude, AUC, duration and conduction velocity, which might be ascribable to altered Na_v and K_v channel functionality. By contrast, C-CAP properties were not affected by oxaliplatin, with the exception of a lowered activating threshold, which suggests an oxaliplatin-induced sensitisation of the unmyelinated fibres. At peak pain, no significant change was observed in A- and C-CAP parameters between oxaliplatin- and saline-treated animals, even though oxaliplatin-induced mechanical hypersensitivity had developed by the time of the recordings. Results at peak pain were discordant with preclinical and clinical studies reporting sensory deficits following cumulative doses of oxaliplatin. In future, more efforts could be made to standardise both *in vitro* and *in vivo* electrophysiological investigations to obtain more consistent results across studies.

Chapter 6 Mitochondrial properties and functionality

6.1 Introduction

Mitochondrial dysfunction plays a major role in the pathophysiology of chemotherapy-induced peripheral neuropathy (CIPN) [reviewed in (Trecarichi and Flatters 2019)]. Among the different manifestations of mitochondrial dysfunction, altered mitochondrial respiratory functionality has often been identified in CIPN models. A significant reduction in Complex I- and Complex-II-mediated activity and ATP production was observed in *ex vivo* preparations of teased sciatic nerves from oxaliplatin- treated rats (cumulative dose: 10 mg/kg) compared with control animals, both prior to and at the peak of pain-like behaviour (Zheng et al. 2011). A significant deficit in Complex I- and Complex II-mediated ATP production was also observed in the saphenous nerves of oxaliplatin- treated animals (cumulative dose: 10 mg/kg) at the peak of mechanical hypersensitivity (Janes et al. 2013).

Mitochondrial functionality can also be assessed *in vitro* using two major approaches: isolated mitochondria and intact cells [reviewed in(Brand and Nicholls 2011)]. The former provides a pure and easy system, where substrates and reagents to assess mitochondrial function can be added directly onto mitochondria. However, the isolation techniques may damage the organelles. The latter provides a more physiologically relevant environment, without the risk of damaging the mitochondria. However, not all substrates/reagents can permeate the cell and the cellular complexity may lead to difficulties in interpreting results [reviewed in (Brand and Nicholls 2011)]. Areti and colleagues isolated mitochondria from the sciatic nerves of oxaliplatin-treated rats (cumulative dose: 36 mg/kg). Their results showed a significant decrease in Complex I and II and, to a lesser extent, of Complex III and IV activity, coupled with significantly reduced ATP production compared with the control group (Areti et al. 2017a, Areti et al. 2017b, Areti et al. 2018). Changes in respiratory activity were also associated with significant deficits in Complex I, II and V protein expression following oxaliplatin administration (Areti et al. 2017a). Additionally, oxaliplatin induced a significant reduction in $\Delta\psi_m$ (Areti et al. 2017a, Areti et al. 2017b, Areti et al. 2018). Similarly, 16 mg/kg oxaliplatin significantly reduced the activity of Complex I, II, III and V in isolated brain mitochondria compared with control animals (Waseem et al. 2016). The Seahorse extracellular flux (XF) Analyzer allows to use intact cells and to simultaneously measure mitochondrial respiration and glycolytic function. Whilst the effect of *in vivo* exposure to oxaliplatin has not been investigated in intact cells using the Seahorse XF Analyzer, reports on mitochondrial functionality following systemic administration of cisplatin are present in the literature. In particular, isolated DRG neurons and tibial nerves from cisplatin-

treated mice (cumulative dose: 23 mg/kg) displayed a significant deficit in several bioenergetic parameters (Krukowski et al. 2017, Maj et al. 2017).

Another fundamental role of mitochondria within the cell is the maintenance of Ca^{2+} homeostasis, which is finely regulated by channel proteins in the outer and inner mitochondrial membranes, including the voltage-dependent anion-selective channel proteins (VDACs), the mitochondrial calcium uniporter (MCU) and the $Na^{+}/Ca^{2+}/Li^{+}$ exchanger (NCLX) [reviewed in (Giorgi et al. 2018)]. Among its many functions as second messenger, Ca^{2+} is involved in the regulation of mitochondrial functionality, including oxidative phosphorylation (OXPHOS). For instance, Ca^{2+} accumulation within mitochondria stimulates ATP production, whereas Ca^{2+} depletion is associated with reduced levels of ATP (Jouaville et al. 1999). Therefore, any dysregulation of the intracellular Ca^{2+} concentration ($[Ca^{2+}]_i$) may impact mitochondrial bioenergetics as well, and contribute to the pathophysiology of oxaliplatin-induced peripheral neuropathy (OIPN). This hypothesis is supported by the efficacy of pharmacological compounds that modulate Ca^{2+} influx and efflux in affecting pain-like behaviour in animal models. Kaempferol, a natural flavonoid, activates MCU and stimulates mitochondrial Ca^{2+} uptake (Montero et al. 2004). In diabetic rats, kaempferol reduced both thermal and mechanical hyperalgesia (Kishore et al. 2018). Conversely, Ru360 acts as a specific MCU inhibitor but was also able to inhibit the development of NMDA (N-methyl-D-aspartate)-induced hyperalgesia in mice (Kim et al. 2011). The role of mitochondrial channels in OIPN has not been investigated. Most studies focused on the effect of microtubule stabilising and/or destabilising agents (i.e. taxanes and vinca alkaloids) on VDAC activity. Electron microscopy studies have identified tubulin within the mitochondrial membrane, where it is associated with VDAC (Carré et al. 2002) and alters its permeability to ADP/ATP and metabolic substrates [reviewed in (Puurand et al. 2019)]. Consequently, taxanes and vinca alkaloids binding to the tubulin dimers, and the conformational changes derived by it, may affect the interaction between tubulin and VDAC, and VDAC functionality itself [reviewed in (Rovini 2019)]. The effects of platinum compounds on VDAC activity, and subsequent cytotoxicity, have been evaluated following cisplatin administration. *In vitro*, exposure of human cervical, ovarian and lung carcinoma cell lines to increasing concentrations of cisplatin induced an overexpression of VDAC1 and an increase in intracellular Ca^{2+} levels (Weisthal et al. 2014). Moreover, cisplatin was also found predominantly associated with VDAC in head and neck squamous cell carcinoma cells following 1-hour exposure to the compound (Yang et al. 2006). Systemic administration of 23 mg/kg cisplatin in mice resulted in a decreased VDAC expression in the tibial nerves compared with control animals, which was associated with a functional deficit in mitochondrial respiration (Krukowski et al. 2017). Given their analogous mechanisms of action, oxaliplatin may affect VDAC expression

and/or activity in a similar way to cisplatin. However, we are not aware of studies that have tested this hypothesis. Likewise, no work has been carried out to investigate the effects of oxaliplatin on MCU and NCLX expression and activity.

6.2 Aims

The aim of the following studies was to evaluate the effect of oxaliplatin on different aspects of mitochondrial functionality. Mitochondrial respiration, glycolytic function and expression of OXPHOS complexes were assessed in dissociated DRG neurons from oxaliplatin- and saline-treated animals 24 hours after treatment cessation (day 7). DRG neurons from naïve animals were exposed *in vitro* to increasing concentrations of oxaliplatin to investigate its direct effect on bioenergetic properties. Additionally, mRNA and protein expression of fundamental mitochondrial channels involved in Ca^{2+} influx/efflux (MCU, VDAC and NCLX) were investigated in the DRG, sciatic and saphenous nerves of oxaliplatin- and saline-treated animals prior to (day 7) and at the peak (day 28 to 34) of pain-like behaviour.

6.3 Results

6.3.1 Bioenergetic properties after *in vivo* exposure to oxaliplatin

In order to assess whether systemic (intraperitoneal, IP) oxaliplatin administration (cumulative dose: 8 mg/kg) affects the metabolic properties of peripheral tissues, bioenergetic profiles were evaluated in isolated DRG neurons. Bioenergetic profiles were measured in terms of oxygen consumption rate (OCR) and extracellular acidification rate (ECAR). The OCR is a direct measurement of mitochondrial respiration, which can be evaluated through different parameters following the injection of mitochondrial inhibitors in the cell medium: oligomycin inhibits Complex V, thus decreasing the flow of electrons through the mitochondrial electron transport chain (ETC); carbonyl cyanide-4 (trifluoromethoxy) phenylhydrazone (FCCP) uncouples ATP synthesis from electron transport chain function, thus collapsing the proton gradient and disrupting the $\Delta\psi_m$; lastly, antimycin A and rotenone inhibit Complex III and Complex I, respectively, thus blocking mitochondrial respiration altogether. OCR measurements after injection of these inhibitors in the medium allow to identify six parameters of respiratory function: basal respiration; ATP turnover-linked respiration; proton leak; maximal respiration; spare reserve capacity (i.e. the ability of cells to respond to stressful conditions); and non-mitochondrial respiration. At the same time, the glycolytic process leads to the acidification of the medium by excretion of protons and conversion of pyruvate to lactate, the end product of glycolysis. Therefore, ECAR measurements provide an indirect measurement of basal glycolysis and glycolytic capacity (i.e. the ability of cells to switch from OXPHOS to glycolysis).

The output of the metabolic XF assay are raw OCR and ECAR measurements generated by cells located only in the middle the well, within an area limited by three molded stops at the bottom of the plate. Therefore, cells at the edge of the well do not contribute to bioenergetic profiles. When normalising OCR and ECAR data, one should bear that in mind. Due to COVID-19, normalisation to cell content through imaging techniques was not possible and was performed based on total protein content instead. Normalisation to protein content is associated with some caveats. Firstly, proteins were extracted from all cells in the well, thus including cells that did not contribute to the OCR and ECAR profiles. Secondly, some cells might have been lost when moving them from the well into microcentrifuge tubes for protein extraction. Nonetheless, the use of total protein content as normalisation parameter was deemed sufficiently valid as an alternative method to imaging.

The same animal model described previously was used for these experiments. Two separate cohorts of animals tested at different times during the project were used in the following investigations. The day after the last oxaliplatin/saline IP injection (day 7), oxaliplatin-treated animals did not display mechanical hypersensitivity compared with saline-treated controls (Figure 6-1, ns two-tailed multiple-comparison unpaired t-tests with Holm-Sidak correction, saline n = 9, oxaliplatin n = 9). Animals were sacrificed at day 7 (n = 4) and DRG were harvested and processed to isolate neurons. Cells were incubated overnight before measurement of bioenergetic profiles.

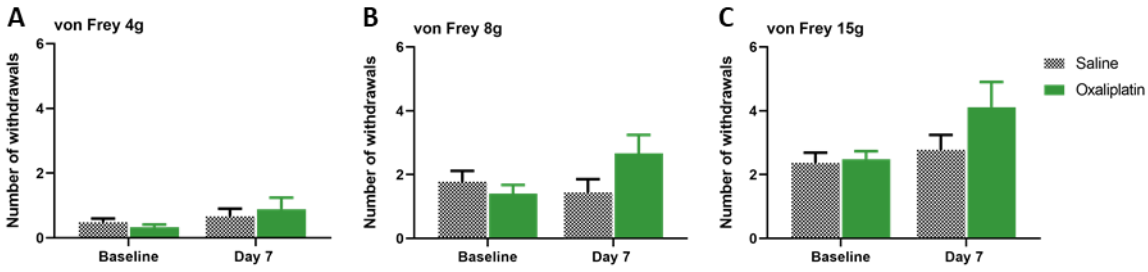

Figure 6-1 Mechanical hypersensitivity to von Frey filaments following oxaliplatin administration

Mechanical hypersensitivity to 4 g (A), 8 g (B) and 15 g (C) von Frey filaments, expressed as number of withdrawals to 10 stimuli in total. Saline n = 9; oxaliplatin n = 9. Data are expressed as mean ± SEM. Two-tailed multiple-comparison unpaired t-tests with Holm-Sidak correction.

Figure 6-2 A and Figure 6-3 A show typical raw bioenergetic profiles of isolated DRG neurons and illustrate which parameters of mitochondrial respiration and glycolytic function were measured. At day 7, there was no difference in OCR or ECAR profiles between oxaliplatin- and saline-treated animals (Figure 6-2 A and Figure 6-3 A, ns RM two-way ANOVA, saline n = 4 animals, oxaliplatin n = 4 animals). Quantification of mitochondrial respiration parameters showed that there was no difference in basal respiration, ATP turnover, maximal respiration,

spare reserve capacity and proton leak between treatment groups (Figure 6-2 B, ns paired two-tailed t-test, saline n = 4 animals, oxaliplatin n = 4 animals). Likewise, basal glycolysis and glycolytic capacity did not differ between saline- and oxaliplatin-treated animals (Figure 6-3 B, ns paired two-tailed t-test, saline n = 4 animals, oxaliplatin n = 4 animals).

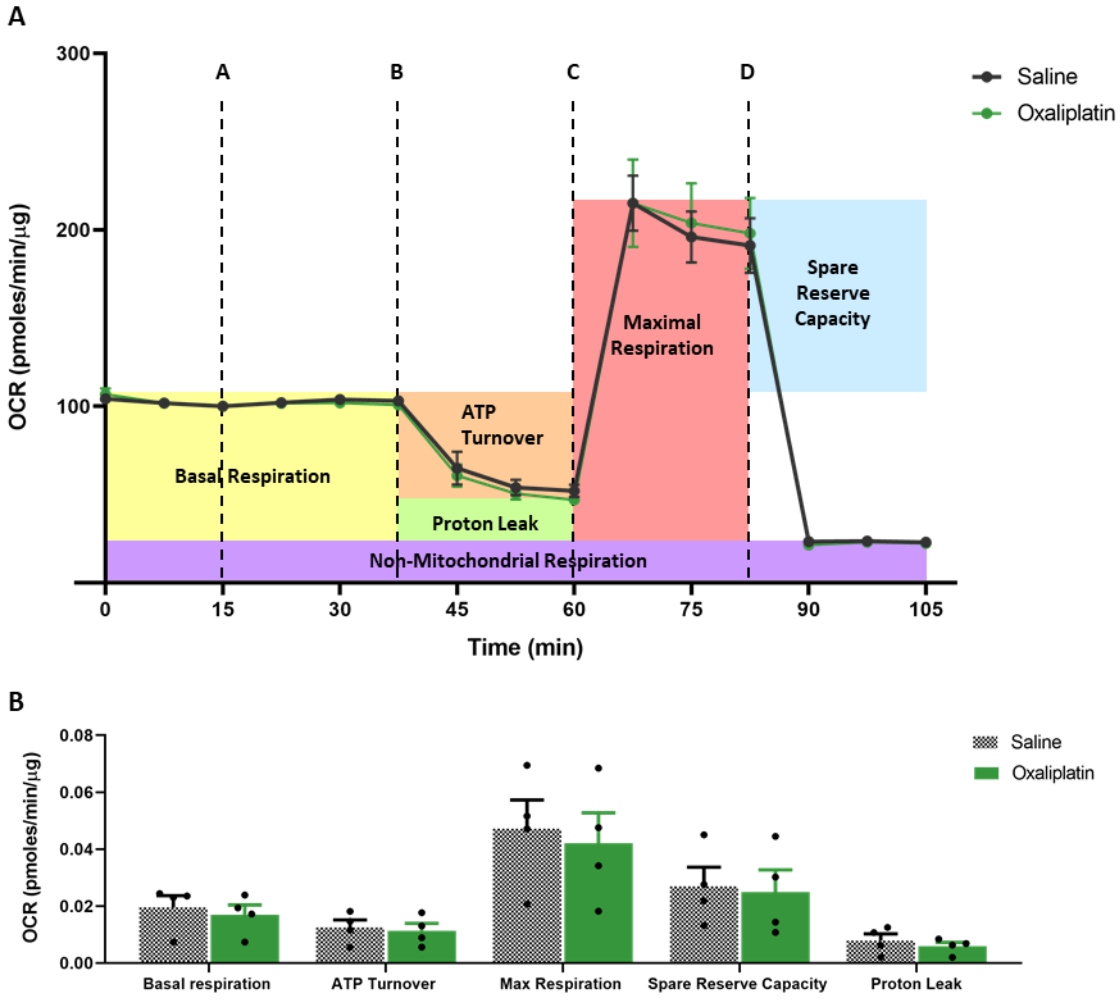

Figure 6-2 Mitochondrial bioenergetics in isolated DRG neurons from oxaliplatin- and saline-treated animals at day 7

(A) Typical raw OCR profiles (before normalisation to protein content) of DRG neurons visualised with the XF24 Seahorse Analyzer following injection of mitochondrial inhibitors (represented as dashed lines): A = DMSO (vehicle); B = oligomycin; C = FCCP; D = rotenone and antimycin A. Data are expressed as percentage of the baseline (i.e. last measurement taken before the injection of DMSO). (B) Quantification of mitochondrial respiration parameters: basal respiration (before DMSO injection); ATP turnover and proton leak (after oligomycin injection); maximal respiration and spare reserve capacity (after FCCP injection); and non-mitochondrial respiration (after rotenone and antimycin A injection). Data are normalised to the total protein content (in µg) in each well. (A) RM two-way ANOVA; (B) paired two-tailed t-test. (A-B) Data are expressed as mean ± SEM. Saline n = 4 animals; oxaliplatin n = 4 animals. 6-10 wells were analysed per animal. ATP is adenosine triphosphate; OCR is oxygen consumption rate.

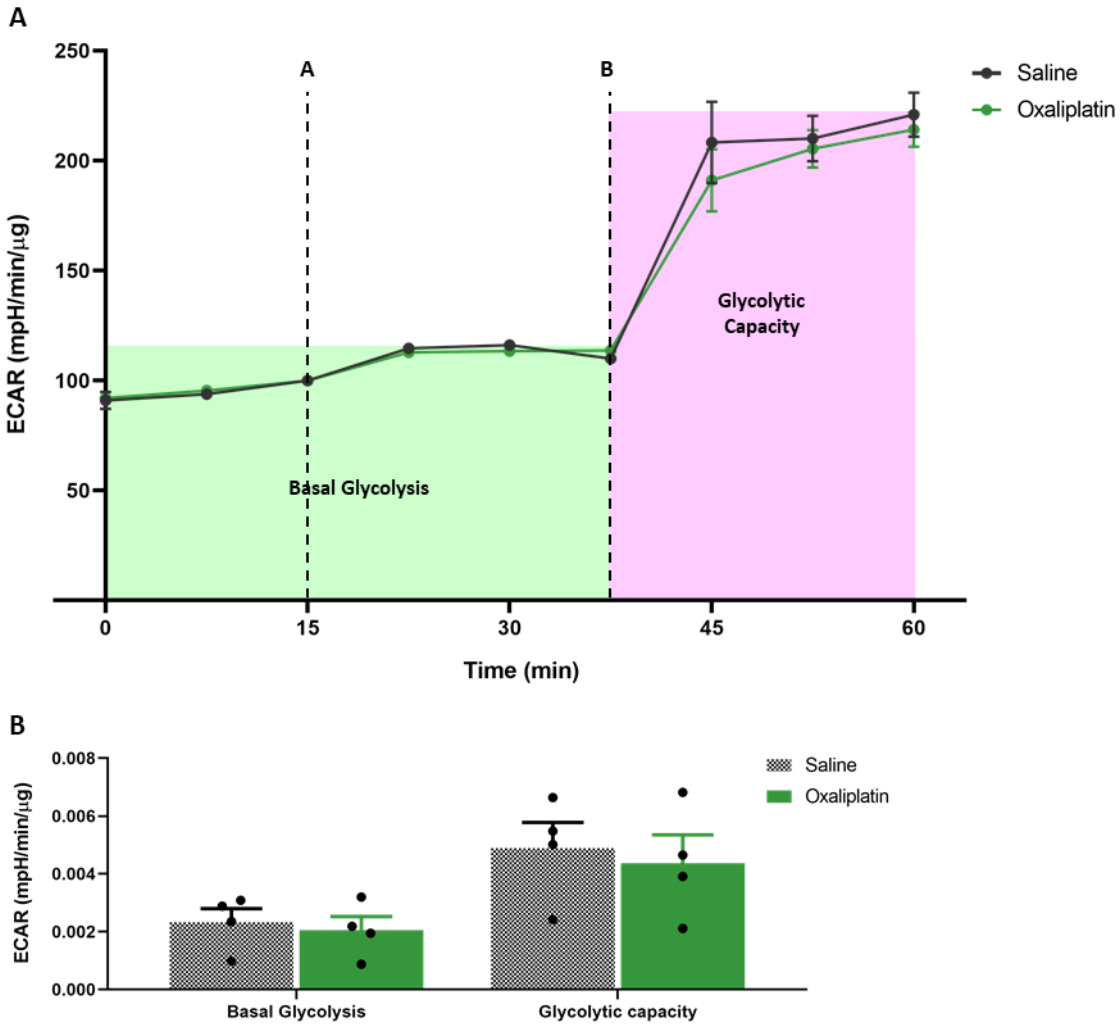

Figure 6-3 Glycolytic function in isolated DRG neurons from oxaliplatin- and saline-treated animals at day 7

(A) Typical raw ECAR profiles (before normalisation to protein content) of DRG neurons visualised with the XF24 Seahorse Analyzer following injection of mitochondrial inhibitors (represented as dashed lines): A = DMSO (vehicle); B = oligomycin. Data are expressed as percentage of the baseline (i.e. last measurement taken before the injection of DMSO). (B) Quantification of the parameters of glycolytic functionality: basal glycolysis (before DMSO injection) and glycolytic capacity (after oligomycin injection). Data are normalised to the total protein content (in µg) in each well. (A) RM two-way ANOVA; (B) paired two-tailed t-test. (A-B) Data are expressed as mean ± SEM. Saline n = 4 animals; oxaliplatin n = 4 animals. 6-10 wells were analysed per animal. ECAR is extracellular acidification rate.

6.3.2 Protein expression of OXPHOS complexes after *in vivo* exposure to oxaliplatin

Oligomycin, rotenone and antimycin A affect the bioenergetic functionality of cells by acting on the OXPHOS complexes, specifically Complex V, I and III, respectively. Despite its lack of effect on mitochondrial respiration, oxaliplatin might affect the protein expression of these complexes. Therefore, the protein levels of Complex I to V were quantified in the DRG of saline-and oxaliplatin-treated animals at day 7. Experiments were conducted on a different cohort of animals (n = 5 animals) from the Seahorse assays, so that enough DRG were collected for both experiments. Following behavioural testing (Figure 6-1), DRG were harvested and proteins were extracted for quantification through western blot. All five complexes could be identified in DRG samples in both treatment groups (Figure 6-4 A) but no difference was detected in protein expression between oxaliplatin- and saline-treated animals (Figure 6-4 B, ns two-tailed unpaired t-tests, saline n = 5 animals, oxaliplatin n = 5 animals).

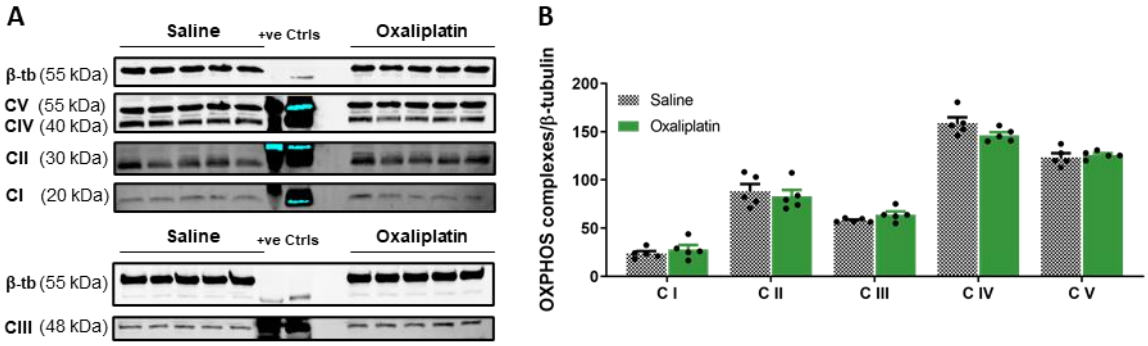

Figure 6-4 Protein expression of mitochondrial complexes in DRG from oxaliplatin- and saline-treated animals at day 7

(A) Western blot images of Complex I (CI), Complex II (CII), Complex III (CIII), Complex IV (CIV) and Complex V (CV) in the DRG. n = 5. β-tubulin (β-tb) was used as loading control. Total liver lysate and rat heart mitochondria were run in the gel as positive controls (+ve Ctrls) alongside DRG samples. Light blue bands indicate high intensity bands. (B) Corresponding densitometric semiquantitative analysis of Complex I-V protein expression. Data are normalised to β-tubulin expression. Saline n = 5 animals; oxaliplatin n = 5 animals. Data are expressed as mean ± SEM. Unpaired two-tailed t-test. OXPHOS is oxidative phosphorylation.

6.3.3 Bioenergetic properties after *in vitro* exposure to oxaliplatin

As platinum accumulates within the DRG and is present there at day 7 (see section 1.3.4), naïve DRG neurons were exposed *in vitro* to oxaliplatin, in order to investigate its direct effect on mitochondrial and glycolytic functionality. Oxaliplatin was introduced in the culture wells directly in the XF24 Analyzer, so that its effect on basal respiration and basal glycolysis could be assessed before injection of mitochondrial modulator compounds (Figure 6-5 A and Figure 6-6 A, ns RM two-way ANOVA, n = 2-3 animals). When used in adjuvant therapy (e.g. FOLFOX: oxaliplatin with 5-fluorouracil and leucovorin; FOLFOXIRI: oxaliplatin with irinotecan, 5-fluorouracil and leucovorin), the recommended dose for oxaliplatin in adults is 85 mg/m^2 every two weeks ("Colon Cancer Treatment Regimens"). Alternatively, oxaliplatin can be administered in combination with capecitabine at a recommended dose of 130 mg/m^2 every three weeks ("Colon Cancer Treatment Regimens"). Pharmacokinetics studies have revealed that the peak plasma concentration (C_{max}) of oxaliplatin after a two-hour infusion was 1.92 ± 0.338 µg/ml (determined at cycle 3; mean ± SD) and 3.61 ± 0.43 µg/ml (determined at cycle 5; mean ± SD) for the 85 mg/m^2 and 130 mg/m^2 regimens, respectively (Graham et al. 2000). The concentrations of oxaliplatin for *in vitro* exposure were determined according to the patient plasma C_{max}. The plasma C_{max} of 1.92 µg/ml corresponds to 4.83 µM oxaliplatin, which was rounded off to 5 µM, whilst 3.61 µg/ml correspond to 9.09 µM, which was rounded off to 10 µM. 50 nM and 100 µM were chosen as additional 100-fold lower and higher concentrations, respectively.

None of these concentrations had any effect on basal respiration, ATP turnover, maximal respiration, spare reserve capacity and proton leak compared with naïve DRG exposed to Seahorse (SH) medium alone (Figure 6-5 B-G, ns one way ANOVA, n = 2-3 animals). DRG neurons were exposed to 50 nM and 50 µM oxaliplatin on three separate occasions (n = 3 animals). Nevertheless, results from one animal per concentration were excluded from the final analysis because of technical issues with the plating of the cells in the XF24 cell culture microplate. Due to the lack of effect of 50 nM-100 µM oxaliplatin, naïve DRG neurons were additionally exposed to 250 µM and 500 µM oxaliplatin. Nevertheless, even these two high concentrations had no effect on mitochondrial respiration parameters (Figure 6-5 B-G, ns one-way ANOVA, n = 3 animals).

Similarly, one-hour *in vitro* exposure to 50 nM-500 µM oxaliplatin had no effect on basal glycolysis nor on the glycolytic capacity of naïve DRG neurons compared with cells exposed to SH medium alone (Figure 6-6 B-D, ns one way ANOVA, n = 2-3 animals).

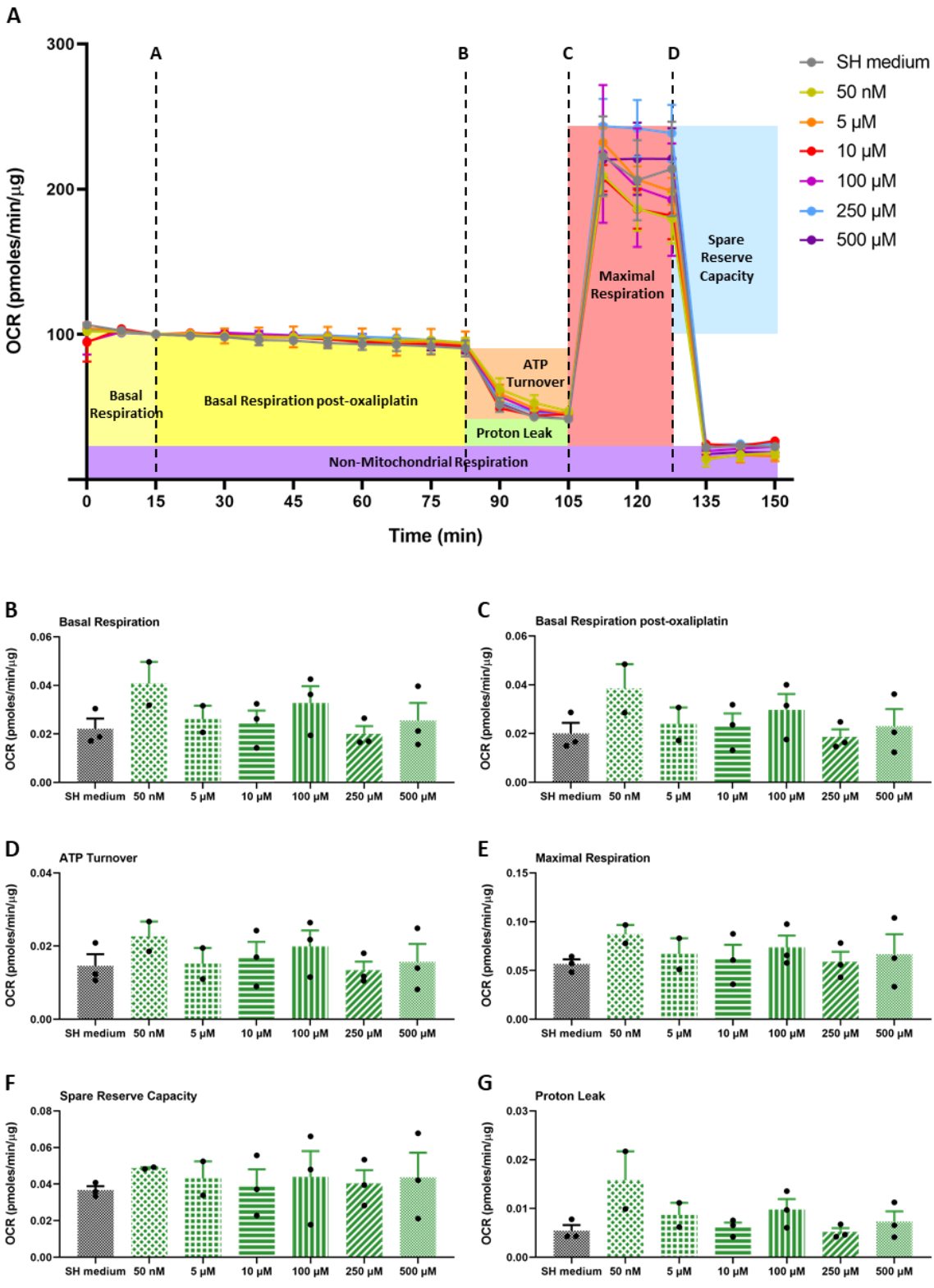

Figure 6-5 Mitochondrial bioenergetics in isolated naïve DRG neurons after *in vitro* exposure to increasing concentrations of oxaliplatin

(A) Typical raw OCR profiles (before normalisation to protein content) of naïve DRG neurons visualised with the XF24 Seahorse Analyzer following exposure to oxaliplatin for 1 hour and injection of mitochondrial inhibitors (represented as dashed lines): A = Seahorse (SH) medium or oxaliplatin; B = oligomycin; C = FCCP; D = rotenone and antimycin. Data are expressed as percentage of the baseline

(i.e. last measurement taken before the injection of SH medium/oxaliplatin). Quantification of mitochondrial respiration parameters: basal respiration (B); basal respiration following oxaliplatin injection (C); ATP turnover (D); maximal respiration (E); spare reserve capacity (F); and proton leak (G). Data are normalised to the total protein content (in µg) in each well. (A) RM two-way ANOVA; (B-G) one-way ANOVA with Dunnett's *post hoc* compared to SH medium. (A-G) Data are expressed as mean ± SEM. SH medium, 10 µM, 100 µM, 250 µM and 500 µM: n = 3 animals. 50 nM and 5 µM: n = 2 animals. 6-10 wells were analysed per animal. ATP is adenosine triphosphate; OCR is oxygen consumption rate.

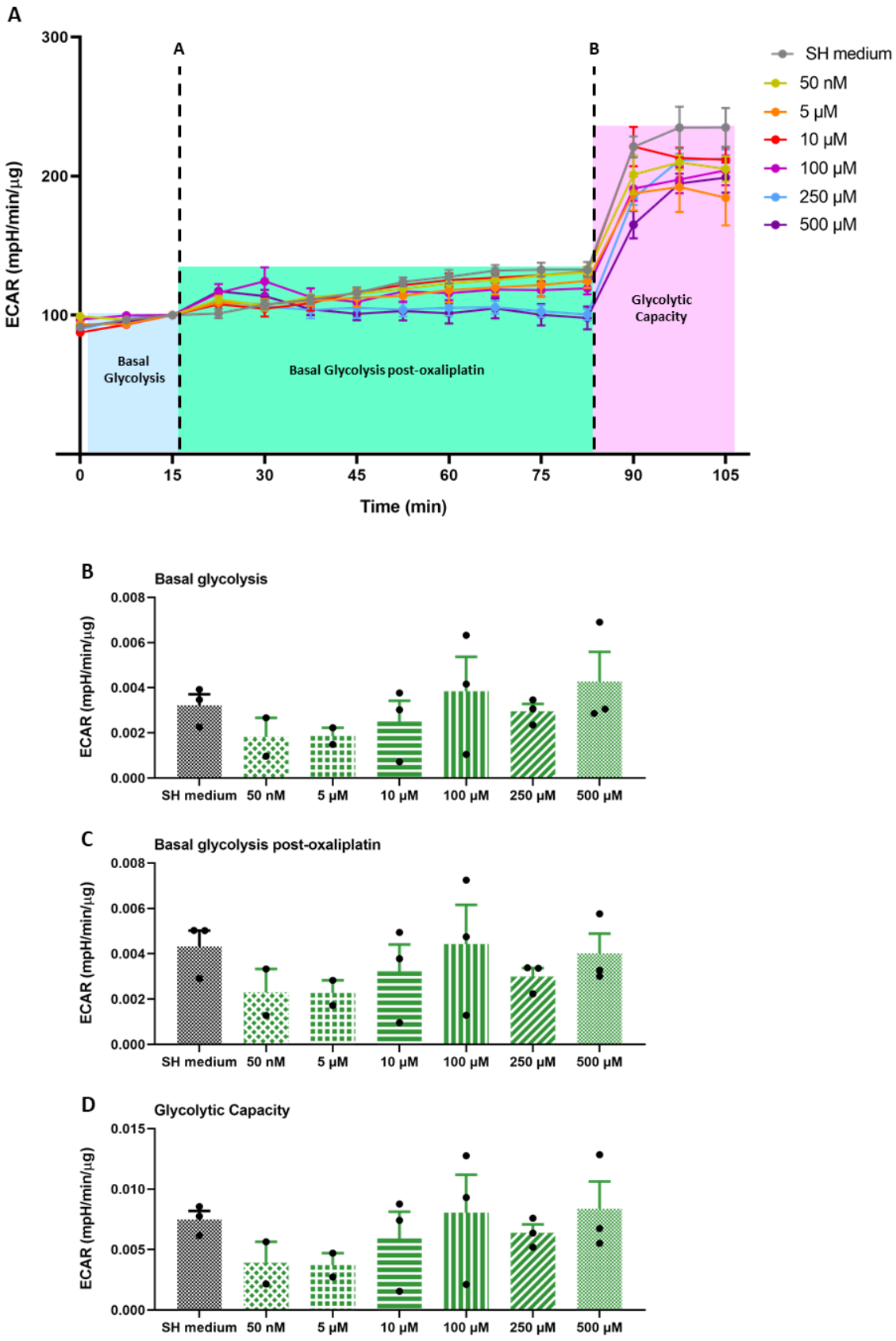

Figure 6-6 Glycolytic function in isolated naïve DRG neurons after *in vitro* exposure to increasing concentrations of oxaliplatin

(A) Typical raw ECAR profiles (before normalisation to protein content) of naïve DRG neurons visualised with the XF24 Seahorse Analyzer following exposure to oxaliplatin for 1 hour and injection of

mitochondrial inhibitors (represented as dashed lines): A = Seahorse (SH) medium or oxaliplatin; B = oligomycin. Data are expressed as percentage of the baseline (i.e. last measurement taken before the injection of SH medium/oxaliplatin). Quantification of glycolytic function parameters: basal glycolysis (B); basal glycolysis following oxaliplatin injection (C); and glycolytic capacity (D). Data are normalised to the total protein content (in µg) in each well. (A) RM two-way ANOVA; (B-D) one-way ANOVA. (A-D) Data are expressed as mean ± SEM. SH medium, 10 µM, 100 µM, 250 µM and 500 µM: n = 3 animals. 50 nM and 5 µM: n = 2 animals. 6-10 wells were analysed per animal. ECAR is extracellular acidification rate.

6.3.4 Expression of mitochondrial Ca^{2+} channels

To assess the effects of oxaliplatin on mitochondrial Ca^{2+} handling, expression of MCU, VDAC and NCLX was evaluated. Mitochondrial content following oxaliplatin treatment was also assessed in terms of citrate synthase (CS) expression. The expression of these essential mitochondrial channels and CS was investigated, both at mRNA and protein level, in different peripheral nervous tissues. Figure 6-7 illustrates changes in mechanical hypersensitivity for all the animals included in gene and protein expression analyses. Experiments were conducted on samples from several animal cohorts, based on the availability of tissues at the time points of interest. In particular, tissues were collected from 5 animal cohorts generated during this PhD project by A.Trecarichi and from 5 cohorts generated previously by another member of the lab (Dr N. Duggett) for other projects. Tissue samples collected by N. Duggett were kept at -80 °C as part of a tissue bank used in our lab to minimise the number of animals used in experiments. At day 7, oxaliplatin-treated animals did not display mechanical hypersensitivity compared with saline-treated controls (Figure 6-7 A-C, ns two-tailed multiple-comparison unpaired t-tests with Holm-Sidak correction, saline n = 38, oxaliplatin n = 39). At the peak pain time point (day 28 to 34), oxaliplatin-treated animals exhibited a significant 3.28-, 2.09- and 2.00-fold increase in mechanical hypersensitivity to 4 g, 8 g and 15 g binding forces, respectively, compared with saline-treated controls (Figure 6-7 A-C, $*p < 0.05$ two-tailed multiple-comparison unpaired t-tests with Holm-Sidak correction, saline n = 17, oxaliplatin n = 18). Animals were sacrificed at day 7 or during the peak pain period and DRG, sciatic and saphenous nerves were collected. RNA and proteins were isolated for real-time quantitative PCR (qPCR) and western blot assays, respectively.

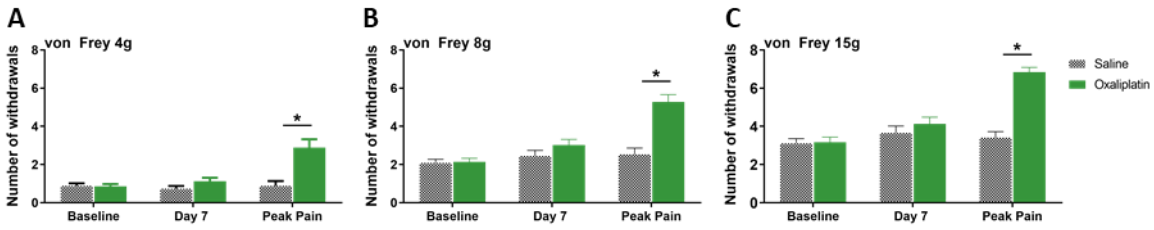

Figure 6-7 Mechanical hypersensitivity to von Frey filaments following oxaliplatin administration

Mechanical hypersensitivity to 4 g (A), 8 g (B) and 15 g (C) von Frey filaments, expressed as number of withdrawals to 10 stimuli in total. Baseline and day 7: saline n = 38, oxaliplatin n = 39; peak pain (day 28 to 34): saline n = 17, oxaliplatin n = 18. Data are collated from several cohorts tested at different time points in the lab, and include animals tested by either A. Trecarichi or N. Duggett. Data are expressed as mean ± SEM. $*p < 0.05$, two-tailed multiple-comparison unpaired t-tests with Holm-Sidak correction.

At day 7, there was no significant difference in gene expression of *Mcu*, *Vdac*, *Nclx* or *Cs* in the DRG (Figure 6-8 A, ns unpaired two-tailed t-test, saline n = 5 animals, oxaliplatin n = 5 animals), sciatic (Figure 6-8 C, ns unpaired two-tailed t-test, saline n = 5 animals, oxaliplatin n = 5 animals) and saphenous nerves (Figure 6-8 E, ns unpaired two-tailed t-test, saline n = 3-4 animals, oxaliplatin n = 4 animals). Likewise, no difference in *Vdac*, *Nclx* and *Cs* gene expression was observed in the DRG (Figure 6-8 B, ns unpaired two-tailed t-test, saline n = 6 animals, oxaliplatin n = 6 animals), sciatic (Figure 6-8 D, ns unpaired two-tailed t-test, saline n = 6 animals, oxaliplatin n = 6 animals) and saphenous (Figure 6-8 F, ns unpaired two-tailed t-test, saline n = 6 animals, oxaliplatin n = 6 animals) nerves at the peak of pain-like behaviour. Only expression of *Mcu* resulted decreased in the sciatic nerves of oxaliplatin-treated animals compared with saline-treated controls at the peak pain time point (Figure 6-8 D, $*p < 0.05$ unpaired two-tailed t-test, saline n = 6 animals, oxaliplatin n = 6 animals). However, no difference was observed in *Mcu* gene expression between treatment groups in the DRG (Figure 6-8 B, ns unpaired two-tailed t-test, saline n = 6 animals, oxaliplatin n = 6 animals) and saphenous nerves (Figure 6-8 F, ns unpaired two-tailed t-test, saline n = 6 animals, oxaliplatin n = 6 animals).

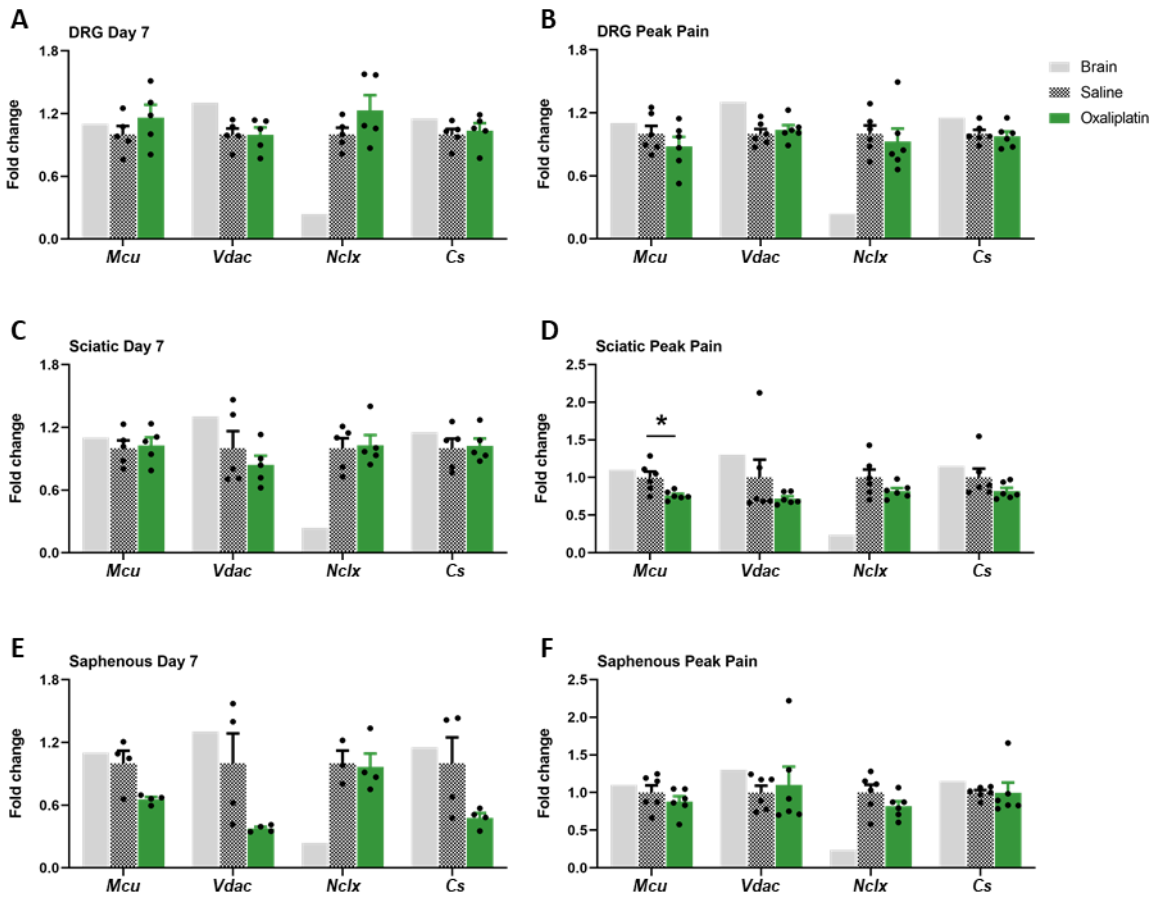

Figure 6-8 mRNA expression of mitochondrial Ca^{2+} channels and citrate synthase in peripheral nervous tissues from oxaliplatin- and saline-treated animals at day 7 and peak pain

The mRNA expression of mitochondrial calcium uniporter *(Mcu),* voltage-dependent anion-selective channel protein 1 *(Vdac),* $Na^{+}/Ca^{2+}/Li^{+}$ exchanger *(Nclx)* and citrate synthase *(Cs)* was quantified through real-time qPCR in the DRG, sciatic and saphenous nerves. A brain from a naïve animal was used as positive control and is included in the graphs (light grey) as reference for the expression of genes of interest in the central nervous tissue. (A) mRNA expression in the DRG at day 7. Saline n = 5 animals; oxaliplatin n = 5 animals. (B) mRNA expression in the DRG at peak pain. Saline n = 6 animals; oxaliplatin n = 6. (C) mRNA expression in the sciatic nerves at day 7. Saline n = 5 animals; oxaliplatin n = 5 animals. (D) mRNA expression in the sciatic nerves at peak pain. Saline n = 6 animals; oxaliplatin n = 6 animals. (E) mRNA expression in the saphenous nerves at day 7. Saline n = 4 animals (except for *Nclx*: n = 3 animals); oxaliplatin n = 4 animals. (F) mRNA expression in the saphenous nerves at peak pain. Saline n = 6 animals; oxaliplatin n = 6 animals. Data are expressed as mean ± SEM. *$p < 0.05$, unpaired two-tailed t-test compared to saline-treated samples.

The blots shown in Figure 6-9 to Figure 6-12 represent results obtained after several homogenisation and western blot attempts performed with different lysing buffers, homogenisation times and denaturation temperatures.

Protein expression of MCU in the DRG did not differ between saline- and oxaliplatin treated animals at day 7 (Figure 6-9 B, ns unpaired two-tailed t-test, saline n = 6 animals, oxaliplatin n = 6 animals) nor at the peak of mechanical hypersensitivity (Figure 6-9 C, ns unpaired two-tailed t-test, saline n = 6 animals, oxaliplatin n = 7 animals). MCU expression in the sciatic nerve was significantly increased in oxaliplatin-treated animals compared with saline-treated controls at day 7 (Figure 6-9 E, $*p < 0.05$ unpaired two-tailed t-test, saline n = 6 animals, oxaliplatin n = 6 animals). However, the MCU bands detected in the sciatic nerves collected at the peak of mechanical hypersensitivity were faint and/or not clearly identifiable Figure 6-9 D, right). Therefore, bands were not analysable, which was probably due to technical issues. Indeed, homogenisation of the sciatic nerves for protein extraction was often difficult and lysates were clumpy and viscous. As a result, it is likely that proteins were loaded onto the gel inconsistently, even though care was taken to add the same volume of lysates in every well. For instance, β-actin bands, which should act as a loading control, are not uniform across the gel. The same issues also affected the protein bands in the saphenous nerves, and it was not possible to perform a densitometry analysis on these samples (Figure 6-9 F).

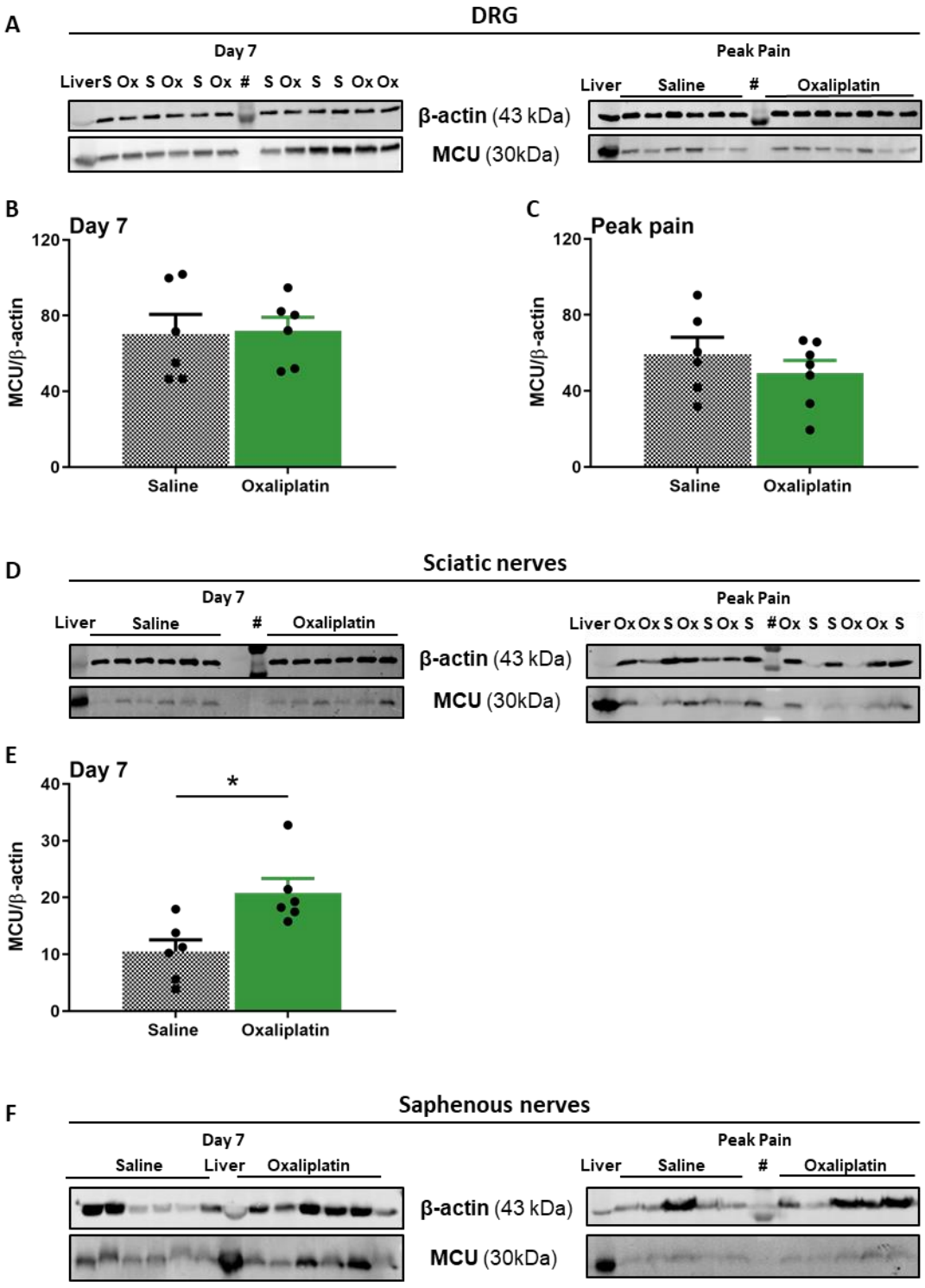

Figure 6-9 MCU protein expression in peripheral nervous tissues from oxaliplatin- and saline-treated animals at day 7 and peak pain

(A) Western blot images of mitochondrial calcium uniporter *(*MCU) in the DRG of saline- and oxaliplatin-treated animals at day 7 (left) and peak pain (right). S = saline; Ox = oxaliplatin. (B-C) Corresponding densitometric semiquantitative analysis of MCU protein expression at day 7 (B) and peak pain (C). Data are normalised to β-actin expression. Day 7: saline n = 6 animals; oxaliplatin n = 6 animals. Peak pain: saline n = 6 animals; oxaliplatin n = 7 animals. Data are expressed as mean ± SEM. Unpaired two-tailed t-

test. (D) Western blot images of MCU in the sciatic nerves of saline- and oxaliplatin-treated animals at day 7 (left) and peak pain (right). S = Saline; Ox = oxaliplatin. (E) Corresponding densitometric semiquantitative analysis of MCU protein expression at day 7. Data are normalised to β-actin expression. Saline n = 6 animals; oxaliplatin n = 6 animals. Data are expressed as mean ± SEM. *$p < 0.05$, unpaired two-tailed t-test. (F) Western blot images of MCU in the saphenous nerves of saline- and oxaliplatin-treated animals at day 7 (left) and peak pain (right). (A, D and F) β-actin was used as loading control. Total liver lysate was run in the gel as positive control alongside DRG/nerve samples. # = protein ladder.

There was no change in VDAC expression in the DRG between saline- and oxaliplatin-treated animals at day 7 (Figure 6-10 B, ns unpaired two-tailed t-test, saline n = 6 animals, oxaliplatin n = 6 animals) and at the peak pain time point (Figure 6-10 C, ns unpaired two-tailed t-test, saline n = 5 animals, oxaliplatin n = 7 animals). Additionally, two unspecific bands could be detected at higher molecular weights (approximately 50 and 100 kDa) than the expected band for VDAC (31 kDa) (Figure 6-10 A). The technical issues regarding the use of the sciatic nerves also affected the experiments on VDAC expression and no densitometry analysis could be performed (Figure 6-10 D). Furthermore, sciatic nerve samples at both time points of interest showed a very intense unspecific protein band at 50 kDa, whereas bands at the expected molecular weight (31 kDa) were very faint. Western blot was not performed on saphenous nerve samples because of time constraints.

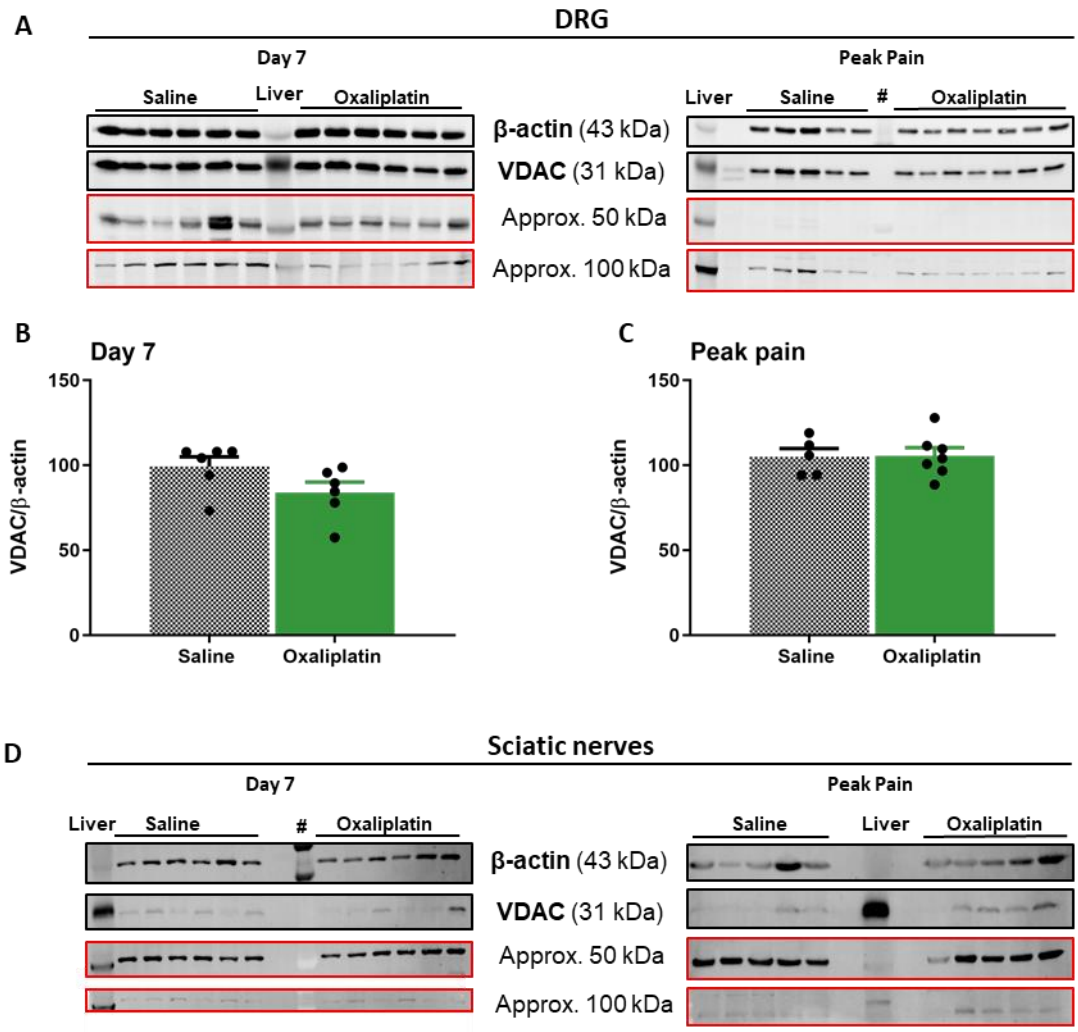

Figure 6-10 VDAC protein expression in peripheral nervous tissues from oxaliplatin- and saline-treated animals at day 7 and peak pain

(A) Western blot images of voltage-dependent anion-selective channel protein (VDAC) in the DRG of saline- and oxaliplatin-treated animals at day 7 (left) and peak pain (right). The primary antibody used here was specific for isoform 1. (B-C) Corresponding densitometric semiquantitative analysis of VDAC protein expression at day 7 (B) and peak pain (C). Data are normalised to β-actin expression. Day 7: saline n = 6 animals; oxaliplatin n = 6 animals. Peak pain: saline n = 5 animals; oxaliplatin n = 7 animals. Data are expressed as mean ± SEM. Unpaired two-tailed t-test. (D) Western blot images of VDAC in the sciatic nerves of saline- and oxaliplatin-treated animals at day 7 (left) and peak pain (right). (A and D) β-actin was used as loading control. Total liver lysate was run in the gel as positive control alongside DRG/nerve samples. # = protein ladder. Red borders indicate unspecific bands at different molecular weights compared with the expected molecular weight for VDAC.

NCLX expression in the DRG was significantly decreased by oxaliplatin at day 7 (Figure 6-11 B, *$p < 0.05$ unpaired two-tailed t-test, saline n = 6 animals, oxaliplatin n = 6 animals). Conversely, oxaliplatin-treated animals showed a significantly higher NCLX expression at the peak of mechanical hypersensitivity compared with saline-treated controls (Figure 6-11 C, *$p < 0.05$ unpaired two-tailed t-test, saline n = 6 animals, oxaliplatin n = 7 animals). NCLX was expressed in the saphenous nerves of both saline- and oxaliplatin-treated animals at day 7 (Figure 6-11 D, left), but could not be detected at the peak pain time point (Figure 6-11 D, right). Densitometry analysis was not performed on day 7 samples due to the uneven loading of proteins, as observable across the β-actin bands (Figure 6-11 D, left), which would lead to inaccurate results. Western blot was not performed on sciatic nerve samples because of time constraints.

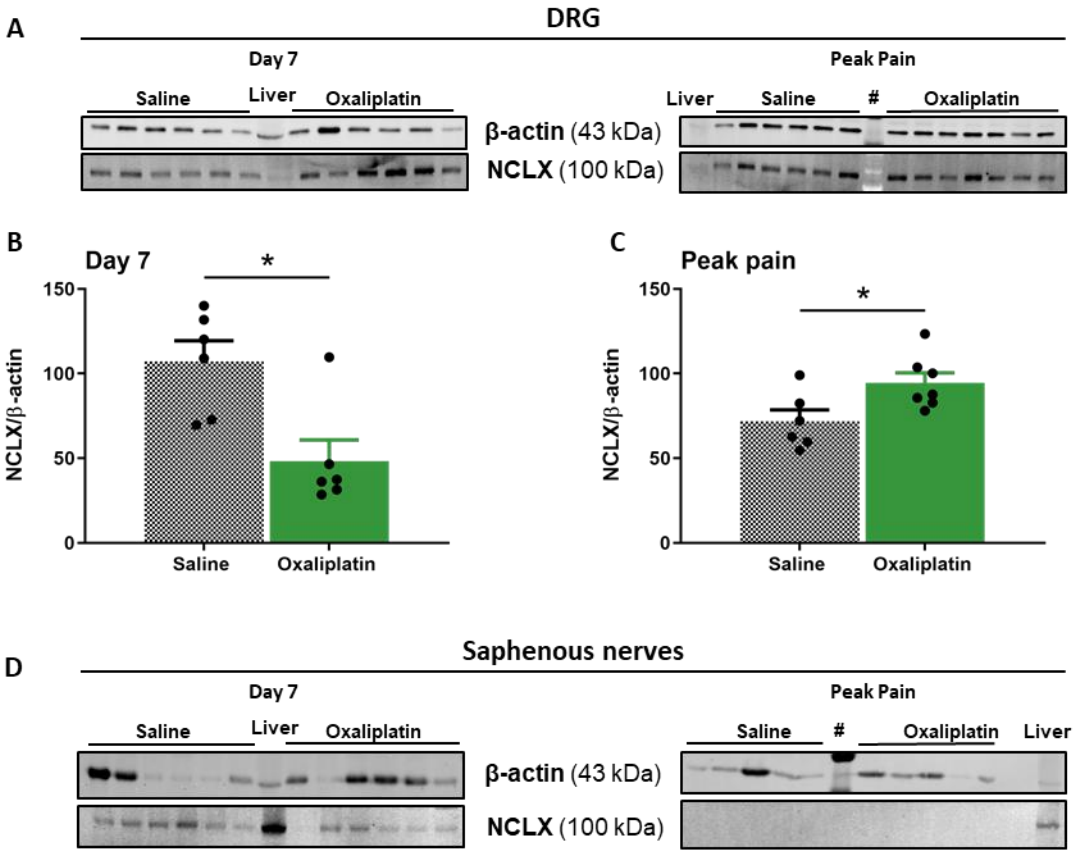

Figure 6-11 NCLX protein expression in peripheral nervous tissues from oxaliplatin- and saline-treated animals at day 7 and peak pain

(A) Western blot images of $Na^+/Ca^{2+}/Li^+$ exchanger (NCLX) in the DRG of saline- and oxaliplatin-treated animals at day 7 (left) and peak pain (right). (B-C) Corresponding densitometric semiquantitative analysis of NCLX protein expression at day 7 (B) and peak pain (C). Data are normalised to β-actin expression. Day 7: n = 6. Peak pain: saline n = 6 animals; oxaliplatin n = 7 animals. Data are expressed as mean ± SEM. *$p < 0.05$, unpaired two-tailed t-test. (D) Western blot images of NCLX in the saphenous nerves of saline- and oxaliplatin-treated animals at day 7 (left) and peak pain (right). (A and D) β-actin was used as loading control. Total liver lysate was run in the gel as positive control alongside DRG/nerve samples. # = protein ladder.

CS was detected in the DRG at both day 7 and peak pain (Figure 6-12 A). At day 7, there was no significant difference in its expression between treatment groups (Figure 6-12 B, ns unpaired two-tailed t-test, saline n = 6 animals, oxaliplatin n = 6 animals). In comparison, at the peak of mechanical hypersensitivity, CS expression was significantly increased in the DRG of oxaliplatin-treated animals compared with saline-treated controls (Figure 6-12 C, $*p < 0.05$ unpaired two-tailed t-test, saline n = 6 animals, oxaliplatin n = 7 animals). Western blot was not performed on sciatic nerves at day 7 because of time constraints. CS was detected in sciatic nerves at the peak pain time point (Figure 6-12 D), although it appeared as an unexpected double band. Lastly, CS was detected in the saphenous nerves at both day 7 (Figure 6-12 E, left) and peak pain (as a double band; Figure 6-12 E, right). Given the inaccuracy of loading and/or the unexpected double band detected on the gels, densitometry analysis was not performed on nerve samples.

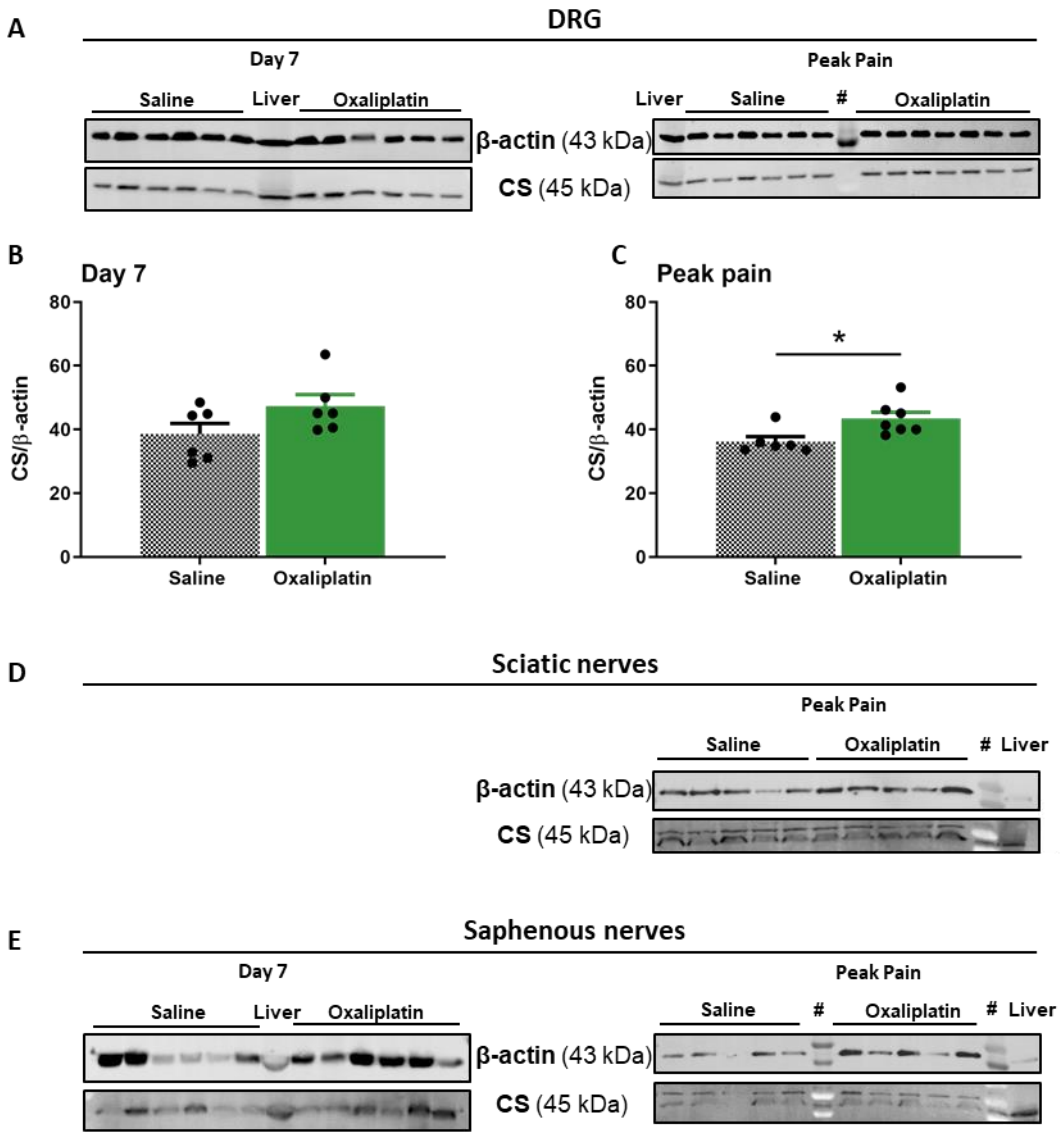

Figure 6-12 Citrate synthase protein expression in peripheral nervous tissues from oxaliplatin- and saline-treated animals at day 7 and peak pain

(A) Western blot images of citrate synthase (CS) in the DRG of saline- and oxaliplatin-treated animals at day 7 (left) and peak pain (right). (B-C) Corresponding densitometric semiquantitative analysis of CS protein expression at day 7 (B) and peak pain (C). Data are normalised to β-actin expression. Day 7: n = 6. Peak pain: saline n = 6 animals; oxaliplatin n = 7 animals. Data are expressed as mean ± SEM. *$p < 0.05$, unpaired two-tailed t-test. (D) Western blot image of CS in the sciatic nerves of saline- and oxaliplatin-treated animals at peak pain. (E) Western blot images of CS in the saphenous nerves of saline- and oxaliplatin-treated animals at day 7 (left) and peak pain (right) (A, D and E) β-actin was used as loading control. Total liver lysate was run in the gel as positive control alongside DRG/nerve samples. # = protein ladder.

6.4 Discussion

Mitochondrial metabolic functionality was assessed in isolated DRG neurons following the IP administration of low-dose oxaliplatin and before animals displayed symptoms of pain-like behaviour (day 7). At this time point, oxaliplatin-treated animals displayed no deficit in mitochondrial respiration nor in glycolysis functionality compared with saline-treated controls. This result is in contrast with previous reports of decreased Complex I- and II-mediated activity and ATP production in the sciatic nerve of oxaliplatin-treated rats (cumulative dose: 10 mg/kg) prior to the development of mechanical hypersensitivity (Zheng et al. 2011). Altered axonal transport, the movement of organelles, proteins and other molecules to and from the cell body and the nerve endings, might help to explain why respiratory deficits affect the sciatic nerve but not the DRG. Oxaliplatin impaired retrograde neuronal transport (i.e. from the nerve endings to the cell body) in mice compared with control animals (Schellingerhout et al. 2012). Impairment of retrograde transport might then hinder mitochondrial functionality. For instance, primary motor neurons displaying deficits in retrograde mitochondrial transport also displayed significantly decreased $\Delta\psi_m$ and Complex I activity and increased oxidative stress in their neuronal processes (Kalmar et al. 2017). The respiratory deficits reported by Zheng et al. in the sciatic nerves may also be a direct consequence of an oxaliplatin-induced increase in swollen, vacuolated and dysfunctional mitochondria in the peripheral nerves. Abnormal mitochondria have been observed in the saphenous nerves of oxaliplatin-treated animals when rats reached the peak of mechanical and cold hypersensitivity (Xiao et al. 2012), but their incidence at day 7 has not been reported yet. It is also worth mentioning that the metabolic assay used by Zheng and colleagues differs from the system used here, thus potentially contributing to differences between results from our groups. Additionally, evaluation of Complex-II mediated respiration was not possible with the Seahorse XF Analyzer, as the cell membrane is not permeable to succinate, the substrate metabolised by Complex II.

Reduced Complex I-IV activity and ATP levels were recorded in isolated mitochondria from sciatic nerves of oxaliplatin-treated rats (Areti et al. 2017a, Areti et al. 2017b, Areti et al. 2018). However, the use of intact DRG was preferred here over isolated mitochondria, as the isolation protocol would be too harsh on atypical, swollen mitochondria present in both saline- and oxaliplatin-treated animals. Indeed, swollen organelles are unlikely to survive the isolation techniques, thus leaving a mitochondrial population biased towards normal mitochondria, which would not be reflective of the *in vivo* state. To the best of our knowledge, this was the first investigation on the effects of a systemic exposure to oxaliplatin on bioenergetics using the Seahorse XF Analyzer.

Any change, or lack thereof, in OXPHOS complexes activity might be associated with changes in protein expression in one or more complexes. Expression of all five OXPHOS complexes was unaltered between oxaliplatin- and saline-treated animals, thus confirming that oxaliplatin did not affect mitochondrial respiration functionality at day 7.

The bioenergetic status of DRG neurons was not evaluated when animals reached the peak of pain-like behaviour, due to COVID-19-induced time-constraints. Baseline recordings of mechanical hypersensitivity were taken for an additional cohort of animals, but lockdown restrictions were put in place soon after that. Therefore, administration of chemotherapy and subsequent behavioural assessments were not feasible. The sample size of the day 7 cohort was limited to n = 4 because of the same COVID-19 restrictions, which impaired the addition of 2 more animals per group in the dataset.

Platinum accumulates within the DRG following systemic administration of oxaliplatin in rodent models (Holmes et al. 1998, Cavaletti et al. 2001, Ip et al. 2013, Park et al. 2015, Nishida et al. 2018, Fujita et al. 2019), even when administered at a relatively low dose (i.e. 16 mg/kg over the course of two weeks) (Nishida et al. 2018). Hence, it is likely that oxaliplatin is present within the DRG after treatment cessation (day 7) in the rat model used here as well. *In vitro* exposure to clinically relevant concentrations of oxaliplatin was performed to gain a better understanding of the direct effect of oxaliplatin on the mitochondrial (and glycolytic) functionality of DRG neurons, which, to the best our knowledge, had not been described in the literature at the time of the studies conducted here. However, none of the parameters of respiratory and glycolytic function were affected compared with exposure to vehicle alone. This result suggests that a prolonged exposure to oxaliplatin may be required to observe platinum accumulation and potential mitochondrial functional deficits. Indeed, the short exposure time of DRG neurons to oxaliplatin is a limitation that we are aware of. A recently published paper from Leo and colleagues described the bioenergetic status of cultured DRG neurons that had been exposed to 10 µM oxaliplatin for 24 hours (Leo et al. 2020). Using the same mitochondrial stress assay employed in our investigation, they observed a significant oxaliplatin-induced reduction in every parameter obtained from the OCR profile (basal respiration, maximal respiration, spare reserve capacity, proton leak, ATP turnover and non-mitochondrial respiration) compared with control neurons (Leo et al. 2020). Longer exposures would have been attempted here as well, but COVID-19 restrictions put a halt to all bioenergetic investigations. In addition, maintaining these DRG neurons cultures for extended periods (e.g. days) is challenging, and oxaliplatin cytotoxic effect would have to be taken into consideration to ensure cell viability. For these reasons, performing a dose escalation with a short exposure time was considered a first, practical solution. Moreover, there is evidence for oxaliplatin accumulation and toxic action in DRG

neurons after short exposure times. Platinum accumulation in DRG neurons has been observed after exposure to 30, 100 and 300 µM oxaliplatin for as little as five minutes and up to two hours (Jong et al. 2011, Liu et al. 2013). Also, oxaliplatin neurotoxicity was observed after *in vitro* exposure of DRG to 50-350 µM for just 30 minutes, which resulted in a significant dose-dependent inhibition of neurite outgrowth (Luo et al. 1999).

The gene expression of mitochondrial channels involved in Ca^{2+} influx and efflux were investigated in peripheral tissues following the IP administration of oxaliplatin, prior to (day 7) and at the peak (day 28 to 34) of mechanical hypersensitivity. At both time points, there was no significant difference in *Mcu*, *Vdac* and *Nclx* expression in the DRG, sciatic and saphenous nerves of oxaliplatin- and saline-treated animals. The only exception was a significantly reduced expression of *Mcu* in the sciatic nerves of oxaliplatin-treated animals at the peak pain time point. This deficit in the sciatic nerve, but not in the DRG, could be indicative of reduced axonal transport following oxaliplatin administration. Indeed, a progressive and irreversible deficit in retrograde transport has been reported using *in vivo* molecular imaging in mice administered with oxaliplatin (cumulative dose: 30 mg/kg) compared with control animals (Schellingerhout et al. 2012). Additionally, using a computer-assisted system, Goshima and colleagues revealed that both anterograde and retrograde transport in cultured chick DRG neurons were impaired after exposure to 100 µM oxaliplatin (Goshima et al. 2010).

Gene expression does not always correlate with protein expression, because of several mechanisms of post-transcriptional and post-translational regulation. For this reason, protein expression of MCU, VDAC and NCLX was also assessed. Proteins were successfully quantified for DRG samples. There was no change in MCU or VDAC expression between saline- and oxaliplatin-treated animals at both time points. NCLX expression was significantly reduced at day 7. This could lead to a deficit in Ca^{2+} efflux, which might not be counterbalanced by decreased Ca^{2+} influx within the mitochondria (i.e. reduced MCU expression). Changes in mitochondrial calcium concentration $[Ca^{2+}]_m$ might then alter mitochondrial functionality and channel expression. This hypothesis was tested in a study investigating the loss of frataxin (Purroy et al. 2018), a critical mitochondrial protein involved in the assembly of iron-sulfur clusters and whose deficiency leads to Friedreich's ataxia (Koeppen 2011). NCLX expression was reduced in frataxin-depleted DRG neurons, whilst MCU expression remained unchanged compared with control neurons (Purroy et al. 2018). Reduced NCLX expression can be induced by the excess of Ca^{2+} within the mitochondria itself: for instance, the endoplasmic reticulum expresses the Na^{+}/Ca^{2+} exchanger (NCX), which was cleaved by Ca^{2+}-activated proteases (Samanta et al. 2010); a similar proteolytic cleavage could affect NCLX in case of mitochondrial Ca^{2+} overload. Indeed, treatment of frataxin-deficient DRG neurons with BAPTA, a highly selective cell-permeant Ca^{2+} chelator, partly

restored NCLX levels compared with untreated cells, but had no effect on MCU expression levels (Purroy et al. 2018). Nevertheless, mitochondria seemed to be able to cope with a NCLX deficit, as we did not observe any deficit in mitochondrial respiration in oxaliplatin-treated animals at day 7, nor in dissociated DRG neurons exposed to oxaliplatin *in vitro*. When animals reached the peak pain time point, the expression of NCLX was significantly increased. Once more, MCU expression was not altered to maintain the $[Ca^{2+}]_m$ equilibrium. This switch in NCLX expression compared with day 7 might be the mitochondrial response to the early Ca^{2+} overload.

Alterations to NCLX expression and activity have downstream effects on the activity of the mitochondrial permeability transition pore (mPTP), in which VDAC might play a regulatory role. Specifically, increased $[Ca^{2+}]_m$ can activate the opening of mPTP and lead to mitochondrial swelling (see section 1.4.5.1). Indeed, frataxin knockout cardiomyocytes showed abnormal, swollen mitochondria and increased distance between cristae compared with control cells (Purroy et al. 2018). Inhibition of mPTP opening with cyclosporin A can reduce mitochondrial swelling, as reported in isolated brain mitochondria exposed to high concentrations of calcium (Hansson et al. 2004) and in frataxin-deficient cardiomyocytes (Purroy et al. 2018). *In vivo*, cyclosporin A had a neuroprotective effect in rats following partial sciatic nerve injury, and they did not develop mechanical hypersensitivity compared with rats administered with saline only (Kim et al. 2012). Despite this positive result, the use of cyclosporin A in CIPN would not be beneficial, as it has been long associated with neurotoxicity as well (Gijtenbeek et al. 1999). Nevertheless, the development of other pharmacological modulators targeting mPTP might be a promising strategy to prevent mitochondrial dysfunction in CIPN. It would also be interesting to test the efficacy of NCLX modulators. CGP-37157 is the most selective and effective NCLX inhibitor [reviewed in (Palty et al. 2012)]. It prevented cortical neurons from NMDA receptor-mediated excitotoxicity (Ruiz et al. 2014), but its effects have not been tested using *in vivo* pain models yet.

Protein expression analysis was not feasible in saphenous and sciatic nerves because of various technical issues. Further optimisation of the protein extraction and western blot protocols would be necessary to obtain homogenous protein lysates and quantifiable immunostained bands. However, an extensive optimisation was not possible here, due partly to limited access to laboratory facilities because of COVID-19, and partly to the unavailability of more nerve samples (e.g. most saphenous nerves collected during this PhD project had been used for electrophysiology experiments). The only quantifiable blot showed a significant increase in MCU expression in the sciatic nerves of oxaliplatin-treated animals at day 7. It would be interesting to compare MCU expression to that of NCLX, in order to understand whether expression of these two channels in the sciatic nerve is kept balanced, as opposed to the DRG. Analysis of MCU

expression in the sciatic nerve at peak pain would also be useful to find out whether the oxaliplatin-induced reduction in gene expression was accompanied by a reduction in protein levels as well. It should also be noted that evaluation of protein expression is not informative of protein activity, or in this case, of channel opening. To this end, combining expression analyses with calcium imaging could provide a deeper understanding of the Ca^{2+} distribution within the cell and the contribution of membrane channels to it.

Citrate synthase (CS), located in the mitochondrial matrix, is a fundamental enzyme in the citric acid cycle [reviewed in (Wiegand and Remington 1986)] and CS activity is commonly used as a quantitative marker for intact mitochondria (mitochondrial content). CS mRNA expression was not altered by oxaliplatin at both time points. Protein expression was not significantly different in the DRG between treatment groups at day 7. In comparison, CS expression was significantly increased in the DRG of oxaliplatin-treated animals compared with controls at the peak of mechanical hypersensitivity. Increased CS expression might suggest an increase in mitochondrial content within the DRG, which could compensate for an oxaliplatin-induced mitochondrial dysfunction and could also explain why NCLX protein levels were increased at the peak pain time point. Nonetheless, this hypothesis would have to be confirmed by evaluating more accurate biomarkers of mitochondrial content, such as CS activity assays, rather than CS expression, or by investigating the mitochondrial network in real-time in live cells. It also cannot be excluded that mitochondrial content remains unchanged and only protein expression is maximised instead. The result observed here is in disagreement with a previous study showing that oxaliplatin did not affect the mitochondrial number in rat sciatic nerves prior to and at the peak of pain-like behaviour compared with control animals (Zheng et al. 2011). However, it is important to notice that Zheng et al. evaluated CS activity and not expression. This methodological difference, together with the evaluation of two different peripheral nervous tissues, may contribute to the discrepancy between our results.

6.5 Conclusions

In conclusion, this investigation showed that exposure to oxaliplatin *in vitro* and *in vivo* did not impair the metabolic functionality of DRG neurons acutely. Mitochondrial respiration and glycolytic function were unaltered between oxaliplatin- and saline-treated animals before they displayed symptoms of pain-like behaviour (day 7). *In vitro* exposure of DRG neurons to increasing concentrations of oxaliplatin also did not affect metabolic profiles, thus suggesting that longer exposure to the compound might be necessary to impact on mitochondrial functionality. Expression of the main mitochondrial channels for Ca^{2+} influx/efflux (MCU, VDAC and NCLX) was unchanged at gene level between oxaliplatin- and saline-treated animals in most peripheral tissues (DRG, sciatic and saphenous nerves). In the DRG, oxaliplatin significantly reduced NCLX expression at day 7. This deficit could result in a Ca^{2+} overload within the mitochondria, thus activating the opening of mPTP and in turn causing the typical mitochondrial swelling observed in OIPN models. Conversely, NCLX expression was enhanced in the DRG of oxaliplatin-treated animals at the peak of mechanical hypersensitivity, which might be a consequence of increased mitochondrial content, measured here in terms of increased CS expression.

Chapter 7 General discussion

The work presented in this thesis has investigated the hypothesis that oxaliplatin alters mitochondrial functionality and nerve electrical activity, thus leading to the development and the maintenance of oxaliplatin-induced peripheral neuropathy (OIPN). Studies have been conducted on a chronic rat model of OIPN, generated by the intraperitoneal (IP) administration of oxaliplatin on four alternate days, for a total cumulative dose of 8 mg/kg. The intermittent treatment schedule mimicked the clinical treatment regimen, where patients receive cycles of oxaliplatin, alone or in adjuvant therapy, every 2-3 weeks. Our model partially reproduced OIPN symptoms, in terms of mechanical allodynia and hyperalgesia, whose severity peaked after 4-5 weeks from treatment initiation. However, the cold-induced syndrome typical of oxaliplatin could not be replicated. Similarly, assessment of ongoing pain and numbness, which are typically reported by OIPN patients, proved to be technically challenging and measurement of these symptoms was unreliable. These results confirmed once again how limiting animal models are for a comprehensive assessment of OIPN symptoms and for the study of pain in general, and that many improvements are still needed in this field.

In order to investigate the acute effects of oxaliplatin exposure, studies were conducted 24 hours after the last administration of chemotherapy (day 7). At this time point, animals did not display signs of mechanical hypersensitivity. Despite the lack of pain-like behavioural symptoms following oxaliplatin administration, *ex vivo* electrophysiological studies on the saphenous nerve revealed significant acute changes in conduction parameters of both A- and C-fibres, measured as compound action potentials (CAPs). Increased peak to peak amplitude, area under the curve, duration and conduction velocity were coupled with a shorter latency to onset in A-fibres, suggesting their hyperexcitability following exposure to oxaliplatin. The only significant change in C-CAP conduction parameters was a reduction in the activation threshold, which might suggest an oxaliplatin-induced sensitisation of unmyelinated fibres. These acute changes might be explained by the accumulation of platinum (Pt) within peripheral nerves after treatment, as observed in other OIPN rat models (Cavaletti et al. 2001, Ip et al. 2013, Nishida et al. 2018).

In particular, Nishida and colleagues showed that Pt accumulated dose-dependently within the mitochondrial fraction of the sciatic nerve in oxaliplatin-treated rats (Nishida et al. 2018). Pt accumulation within the mitochondria is likely to be responsible for and/or to exacerbate their dysfunction, in terms of damaged mitochondrial DNA (MtDNA), altered morphology and/or functionality. Changes in mitochondrial functionality could in turn lead to altered nerve conduction properties. For instance, Ru360-mediated inhibition of the mitochondrial calcium uniporter (MCU) activity (i.e. reduced mitochondrial Ca^{2+} uptake) resulted in reduced

spontaneous electrical activity in the rat brain (Sanganahalli et al. 2013). Conversely, increased MCU activity by kaempferol treatment enhanced neuronal activity (Sanganahalli et al. 2013). A potential explanation as to why MCU regulates neuronal electrical properties is that mitochondrial Ca^{2+} accumulation leads to an increase in ATP production (Jouaville et al. 1999); ATP itself is fundamental for the generation of action potentials, as it sustains the Na^{+}/K^{+} ATPase, thus maintaining the ionic imbalance across the plasma membrane. Trevisiol and colleagues recently demonstrated the relationship between ATP levels and CAPs generation in *ex vivo* preparations of the optic nerve using real-time imaging and electrical stimulation (Trevisiol et al. 2017). They observed that ATP levels decreased as the stimulation frequency increased, whereas blockage of mitochondrial respiration, and therefore of ATP production, resulted in a quick decline in CAPs (Trevisiol et al. 2017).

In keeping with this hypothesis, western blot analysis showed increased expression of MCU in the sciatic nerve of oxaliplatin-treated animals at day 7. However, it is worth noting that MCU expression in the saphenous nerve could not be measured. As MCU works in synergy with other proteins and complexes, including the $Na^{+}/Ca^{2+}/Li^{+}$ exchanger (NCLX) and the voltage-dependent anion-selective channel proteins (VDACs), investigating their expression in peripheral nerves is necessary to obtain a more comprehensive picture of oxaliplatin effect on cellular Ca^{2+} homeostasis and on its potential role in nerve activity. However, despite many efforts to optimise experimental protocols for protein quantification in sciatic and saphenous nerves, NCLX and VDAC expression has not been quantifiable over the course of this project.

At day 7, NCLX expression was significantly decreased in the DRG of oxaliplatin-treated animals compared with controls. A deficit in NCLX expression might trigger ATP synthesis in a similar way to increased MCU expression; indeed, reduced NCLX expression could lead to a deficit in Ca^{2+} efflux and to Ca^{2+} accumulation within the mitochondria. Despite the change in NCLX expression, the bioenergetic status of DRG neurons at day 7 was not affected: none of the parameters of mitochondrial respiration or glycolytic function showed a difference between treatment groups. Additionally, protein expression of all five complexes involved in oxidative phosphorylation (OXPHOS) was unaltered at this time point. These results suggest that the deficit in NCLX expression was not enough to effectively alter mitochondrial respiration.

Alternatively, it is possible that the oxaliplatin-induced damage to the organelles triggered mitochondrial biogenesis. Mitochondrial biogenesis is a way for cells to increase their mitochondrial content in stressful conditions. Citrate synthase (CS) activity is commonly used as marker of intact, functional mitochondria. Here, systemic (IP) administration of oxaliplatin did not lead to significant changes in CS expression in the DRG compared with control animals at

day 7, thus suggesting that mitochondrial content was not affected. Nonetheless, it is also possible that CS expression did not differ between treatment groups because new mitochondria were produced, whilst dysfunctional ones were destroyed, thus maintaining a balance in overall mitochondrial content. A higher incidence of swollen, vacuolated mitochondria has been reported in both A- and C-fibres in the saphenous nerve of oxaliplatin-treated rats (Xiao et al. 2012). These studies were conducted at the peak severity of pain-like behaviour (day 35) and we are not aware of similar studies performed before the appearance of pain-like symptoms. However, it is likely that oxaliplatin also leads to early mitochondrial morphological changes, when its levels in nerves are maximal. Likewise, dysfunctional mitochondria might be present in the DRG as well, where Pt accumulates at the highest concentrations among all other nervous tissues. Moreover, the reduction in NCLX expression observed in the DRG of oxaliplatin-treated animals at day 7 has the potential consequence of an excessive mitochondrial Ca^{2+} accumulation, which in turn might trigger the opening of the mitochondrial permeability transition pore (mPTP) and lead to mitochondrial swelling. In future, it would be interesting to investigate whether mitochondrial biogenesis is indeed enhanced within neuronal tissues at day 7 to counterbalance a mitochondrial degeneration. However, more refined techniques, like real-time cell imaging exploiting mitochondria-targeted probes, would be required to effectively visualise and quantify the mitochondrial dynamics in live, intact cells.

Mitochondrial and glycolytic functionality was also maintained in DRG exposed to physiologically relevant concentrations of oxaliplatin for one hour *in vitro*, thus suggesting that longer exposure to oxaliplatin would be required to observe changes in bioenergetics. It is worth mentioning that the mitochondrial bioenergetic status in the DRG might not necessarily reflect the axonal one, as changes in axonal trafficking could affect transport of mRNA, proteins and organelles between cell bodies and axons. Zheng and colleagues have shown deficits in parameters of mitochondrial respiration and ATP production in the sciatic nerve of oxaliplatin-treated rats before the appearance of pain-like behaviour (Zheng et al. 2011). It might be useful to test if our OIPN model also displayed altered mitochondrial respiration in peripheral nerves and to investigate whether inhibiting MCU function (as its expression was increased in the sciatic nerve) could lead to a deficit in ATP production and nerve conduction properties.

To investigate the mechanisms involved in chronic OIPN, animals were tested regularly until they reached the peak severity of pain-like behaviour, which occurred at day 28 to 34 (peak pain). At peak pain, oxaliplatin-treated animals displayed a significant increase in withdrawal responses to von Frey filaments compared with saline-treated controls. Surprisingly, A- and C-CAP parameters of the saphenous nerve were not different between treatment groups at this time point. Cavaletti and colleagues showed that Pt levels in the sciatic nerve were higher

immediately after treatment cessation than after a follow-up period, thus indicating that Pt levels decrease over time (Cavaletti et al. 2001). It is possible that Pt levels in the saphenous nerve in our OIPN model were low enough to not elicit electrophysiological deficits at day 28-34. Nevertheless, in contrast to our result, another study reported that a single administration of 10 mg/kg oxaliplatin progressively impaired conduction velocity in the sciatic nerve, which then resolved after approximately three months from treatment (McKeage et al. 2001). To our knowledge, Pt accumulation in the saphenous nerve and/or following the treatment schedule used here has not been investigated. Therefore, it would be interesting to measure Pt levels following the treatment regimen administered here, in order to understand whether the difference in nerve activity between day 7 and peak pain could be effectively ascribed to changes in Pt accumulation within the nerves. Evaluation of the bioenergetic status of DRG neurons would also provide a further understanding of the mitochondrial involvement and of the ATP status at the peak pain time point.

Gene expression analysis through qPCR showed that expression of Ca^{2+} channels was not different between oxaliplatin- and saline-treated animals in the DRG, sciatic and saphenous nerves at day 7 and once they reached the peak pain time point. The only exception was a reduction in *Mcu* levels in the sciatic nerve of oxaliplatin-treated rats, which might be due to alterations in axonal transport. Still, no real conclusion can be reached regarding the expression of these channels in the nerves and their potential involvement in nerve conduction, as protein quantification proved to be technically challenging. Western blot analysis showed that NCLX expression in the DRG was significantly increased in oxaliplatin-treated animals at the peak of pain-like behaviour. It could be hypothesised that this increased expression is an attempt to cope with the mitochondrial Ca^{2+} overload at day 7, when NCLX expression was decreased. Expression of citrate synthase in the DRG was also significantly increased in oxaliplatin-treated animals, which might reflect an increase in overall mitochondrial content through mitochondrial biogenesis.

In the past, our lab has hypothesised that the oxaliplatin-induced mitochondrial dysfunction triggers mitochondrial biogenesis and/or MtDNA replication to compensate for the lack of functional organelles [under review (Trecarichi et al. 2020); see section 6.1]. We showed a significant increase in MtDNA content in the peripheral blood of oxaliplatin-treated rats at day 7, compared with saline-treated controls. Conversely, no difference was evident at peak pain [under review (Trecarichi et al. 2020)]. These results led us to conduct a small clinical study to evaluate MtDNA as predictive biomarker for OIPN in colorectal cancer patients, which was another aim of this PhD project. MtDNA was quantified relatively to nuclear DNA using qPCR. Analysis was conducted on whole blood collected prior to, during and after the chemotherapy

regimen and revealed a high degree of heterogeneity in MtDNA content among patients and time points. Upon access to patient data, we will be able to understand whether MtDNA content can predict the susceptibility to OIPN development.

7.1 Conclusions

In conclusion, this thesis encompassed preclinical investigations on behavioural characteristics, electrophysiological properties and mitochondrial functionality in a rat model of OIPN. Additionally, it comprised a clinical study investigating a biomarker for OIPN. The conduction properties of the saphenous nerve were investigated for the first time *ex vivo* in a chronic OIPN model and showed that nerve fibres respond to electrical stimulation in different ways at the two time points of interest, before the appearance of pain-like behaviour and at the peak of nociceptive severity. Oxaliplatin did not elicit acute changes in the bioenergetics of DRG neurons, as mitochondrial respiration parameters and glycolytic functionality remained unaltered compared with controls. Mitochondrial Ca^{2+} handling seemed to be affected at both time points, as expression of Ca^{2+} channels was altered by oxaliplatin administration. Alterations to the Ca^{2+} homeostasis might then impact on the electrical activity of the nerves. This thesis provided a further insight into the causal mechanisms of OIPN, yet more work is needed to better appreciate how all the different aspects of mitochondrial and nerve functionality converge to induce the neuropathy. In the meantime, the identification of a biomarker to predict the susceptibility to OIPN development would help clinicians to select more tolerable treatment options and improve the overall quality of life of patients. To this scope, MtDNA content was efficiently amplified and quantified in the peripheral blood of cancer patients undergoing an oxaliplatin treatment. It now remains to understand whether it effectively correlates with increased risk of OIPN development.

References

Abd-Elsayed AA, Ikeda R, Jia Z, Ling J, Zuo X, Li M and Gu JG (2015). KCNQ channels in nociceptive cold-sensing trigeminal ganglion neurons as therapeutic targets for treating orofacial cold hyperalgesia. *Mol Pain.* 11: 45.

Adelsberger H, Quasthoff S, Grosskreutz J, Lepier A, Eckel F and Lersch C (2000). The chemotherapeutic oxaliplatin alters voltage-gated Na(+) channel kinetics on rat sensory neurons. *Eur J Pharmacol.* 406(1): 25-32.

Ajaz S, Czajka A and Malik A (2015). Accurate Measurement of Circulating Mitochondrial DNA Content from Human Blood Samples Using Real-Time Quantitative PCR. *Methods Mol Biol*. 1264:117-131.

Al-Chalabi M, Reddy V and Alsalman I (2021). Neuroanatomy, Posterior Column (Dorsal Column). *StatPearls*. Treasure Island (FL), StatPearls Publishing. Copyright © 2021, StatPearls Publishing LLC.

Al Moundhri MS, Al-Salam S, Al Mahrouqee A, Beegam S and Ali BH (2013). The effect of curcumin on oxaliplatin and cisplatin neurotoxicity in rats: some behavioral, biochemical, and histopathological studies. *J Med Toxicol.* 9(1): 25-33.

Alberti P, Rossi E, Argyriou AA, Kalofonos HP, Briani C, Cacciavillani M, Campagnolo M, Bruna J, Velasco R, Cazzaniga ME, Cortinovis D, Valsecchi MG and Cavaletti G (2018). Risk stratification of oxaliplatin induced peripheral neurotoxicity applying electrophysiological testing of dorsal sural nerve. *Support Care Cancer.* 26(9): 3143-3151.

Alcindor T and Beauger N (2011). Oxaliplatin: a review in the era of molecularly targeted therapy. *Curr Oncol.* 18(1): 18-25.

Alejandro LM, Behrendt CE, Chen K, Openshaw H and Shibata S (2013). Predicting acute and persistent neuropathy associated with oxaliplatin. *Am J Clin Oncol.* 36(4): 331-337.

Allchorne AJ, Broom DC and Woolf CJ (2005). Detection of cold pain, cold allodynia and cold hyperalgesia in freely behaving rats. *Mol Pain.* 1: 36.

Altmann R (1890). Die Elementarorganismen und ihre beziehungen zu den zellen. Veit, Leipzig, Germany.

Arany Z, Wagner BK, Ma Y, Chinsomboon J, Laznik D and Spiegelman BM (2008). Gene expression-based screening identifies microtubule inhibitors as inducers of PGC-1α and oxidative phosphorylation. *Proc Natl Acad Sci U S A.* 105(12): 4721-4726.

Areti A, Komirishetty P, Akuthota M, Malik RA and Kumar A (2017a). Melatonin prevents mitochondrial dysfunction and promotes neuroprotection by inducing autophagy during oxaliplatin-evoked peripheral neuropathy. *J Pineal Res.* 62(3): e12393.

Areti A, Komirishetty P, Kalvala AK, Nellaiappan K and Kumar A (2018). Rosmarinic Acid Mitigates Mitochondrial Dysfunction and Spinal Glial Activation in Oxaliplatin-induced Peripheral Neuropathy. *Mol Neurobiol.* 55(9): 7463-7475.

Areti A, Komirishetty P and Kumar A (2017b). Carvedilol prevents functional deficits in peripheral nerve mitochondria of rats with oxaliplatin-evoked painful peripheral neuropathy. *Toxicol Appl Pharmacol.* 322: 97-103.

Argyriou AA, Cavaletti G, Antonacopoulou A, Genazzani AA, Briani C, Bruna J, Terrazzino S, Velasco R, Alberti P, Campagnolo M, Lonardi S, Cortinovis D, Cazzaniga M, Santos C, Psaromyalou A, Angelopoulou A and Kalofonos HP (2013a). Voltage-gated sodium channel polymorphisms play a pivotal role in the development of oxaliplatin-induced peripheral neurotoxicity: results from a prospective multicenter study. *Cancer.* 119(19): 3570-3577.

Argyriou AA, Cavaletti G, Briani C, Velasco R, Bruna J, Campagnolo M, Alberti P, Bergamo F, Cortinovis D, Cazzaniga M, Santos C, Papadimitriou K and Kalofonos HP (2013b). Clinical pattern and associations of oxaliplatin acute neurotoxicity: a prospective study in 170 patients with colorectal cancer. *Cancer.* 119(2): 438-444.

Argyriou AA, Park SB, Islam B, Tamburin S, Velasco R, Alberti P, Bruna J, Psimaras D, Cavaletti G and Cornblath DR (2019). Neurophysiological, nerve imaging and other techniques to assess chemotherapy-induced peripheral neurotoxicity in the clinical and research settings. *J Neurol Neurosurg Psychiatry.* 90(12): 1361-1369.

Argyriou AA, Polychronopoulos P, Iconomou G, Chroni E and Kalofonos HP (2008). A review on oxaliplatin-induced peripheral nerve damage. *Cancer Treat Rev.* 34(4): 368-377.

Argyriou AA, Polychronopoulos P, Iconomou G, Koutras A, Makatsoris T, Gerolymos MK, Gourzis P, Assimakopoulos K, Kalofonos HP and Chroni E (2007). Incidence and characteristics of peripheral neuropathy during oxaliplatin-based chemotherapy for metastatic colon cancer. *Acta Oncol.* 46(8): 1131-1137.

Argyriou AA, Velasco R, Briani C, Cavaletti G, Bruna J, Alberti P, Cacciavillani M, Lonardi S, Santos C, Cortinovis D, Cazzaniga M and Kalofonos HP (2012). Peripheral neurotoxicity of oxaliplatin in combination with 5-fluorouracil (FOLFOX) or capecitabine (XELOX): a prospective evaluation of 150 colorectal cancer patients. *Ann Oncol.* 23(12): 3116-3122.

Arnalich F, Codoceo R, López-Collazo E and Montiel C (2012). Circulating cell-free mitochondrial DNA: a better early prognostic marker in patients with out-of-hospital cardiac arrest. *Resuscitation.* 83(7): e162-163.

Arnalich F, Maldifassi MC, Ciria E, Codoceo R, Renart J, Fernández-Capitán C, Herruzo R, Garcia-Rio F, López-Collazo E and Montiel C (2013). Plasma levels of mitochondrial and nuclear DNA in patients with massive pulmonary embolism in the emergency department: a prospective cohort study. *Crit Care.* 17(3): R90.

Aromolaran KA and Goldstein PA (2017). Ion channels and neuronal hyperexcitability in chemotherapy-induced peripheral neuropathy; cause and effect? *Mol Pain.* 13: 1744806917714693.

Attal N, Bouhassira D, Gautron M, Vaillant JN, Mitry E, Lepère C, Rougier P and Guirimand F (2009). Thermal hyperalgesia as a marker of oxaliplatin neurotoxicity: a prospective quantified sensory assessment study. *Pain.* 144(3): 245-252.

Bakitas MA (2007). Background noise: the experience of chemotherapy-induced peripheral neuropathy. *Nurs Res.* 56(5): 323-331.

Balayssac D, Ling B, Ferrier J, Pereira B, Eschalier A and Authier N (2014). Assessment of thermal sensitivity in rats using the thermal place preference test: description and application in the study of oxaliplatin-induced acute thermal hypersensitivity and inflammatory pain models. *Behav Pharmacol.* 25(2): 99-111.

Baraniuk JN (2012). Rise of the sensors: nociception and pruritus. *Curr Allergy Asthma Rep.* 12(2): 104-114.

Barrière DA, Rieusset J, Chanteranne D, Busserolles J, Chauvin MA, Chapuis L, Salles J, Dubray C and Morio B (2012). Paclitaxel therapy potentiates cold hyperalgesia in streptozotocin-induced diabetic rats through enhanced mitochondrial reactive oxygen species production and TRPA1 sensitization. *Pain.* 153(3): 553-561.

Basbaum A, Bushnell CM and Devor M (2008). Pain: basic mechanisms. *Pain 2008 – An Updated Review: Refresher Course Syllabus* IASP Press S.

Basbaum AI, Bautista DM, Scherrer G and Julius D (2009). Cellular and molecular mechanisms of pain. *Cell.* 139(2): 267-284.

Bean BP (2007). The action potential in mammalian central neurons. *Nat Rev Neurosci.* 8(6): 451-465.

Becker JB, Prendergast BJ and Liang JW (2016). Female rats are not more variable than male rats: a meta-analysis of neuroscience studies. *Biol Sex Differ.* 7(1): 34.

Benarroch EE (2015). Ion channels in nociceptors: recent developments. *Neurology.* 84(11): 1153-1164.

Benda C (1898). Ueber die spermatogenese der vertebraten und höherer evertebraten, II. Theil: Die histiogenese der spermien. *Arch Anat Physiol* 73: 393–398.

Bennett DL, Clark AJ, Huang J, Waxman SG and Dib-Hajj SD (2019a). The Role of Voltage-Gated Sodium Channels in Pain Signaling. *Physiol Rev.* 99(2): 1079-1151.

Bennett MI, Kaasa S, Barke A, Korwisi B, Rief W and Treede R-D (2019b). The IASP classification of chronic pain for ICD-11: chronic cancer-related pain. *Pain.* 160(1): 38-44.

Benoit E, Brienza S and Dubois JM (2006). Oxaliplatin, an anticancer agent that affects both Na+ and K+ channels in frog peripheral myelinated axons. *Gen Physiol Biophys.* 25(3): 263-276.

Benson C, Paylor JW, Tenorio G, Winship I, Baker G and Kerr BJ (2015). Voluntary wheel running delays disease onset and reduces pain hypersensitivity in early experimental autoimmune encephalomyelitis (EAE). *Exp Neurol.* 271: 279-290.

Bhatnagar B, Gilmore S, Goloubeva O, Pelser C, Medeiros M, Chumsri S, Tkaczuk K, Edelman M and Bao T (2014). Chemotherapy dose reduction due to chemotherapy induced peripheral neuropathy in breast cancer patients receiving chemotherapy in the neoadjuvant or adjuvant settings: a single-center experience. *Springerplus.* 3: 366.

Boadas-Vaello P, Castany S, Homs J, Álvarez-Pérez B, Deulofeu M and Verdú E (2016). Neuroplasticity of ascending and descending pathways after somatosensory system injury: reviewing knowledge to identify neuropathic pain therapeutic targets. *Spinal Cord.* 54(5): 330-340.

Bobylev I, Joshi AR, Barham M, Ritter C, Neiss WF, Höke A and Lehmann HC (2015). Paclitaxel inhibits mRNA transport in axons. *Neurobiol Dis.* 82: 321-331.

Bogenhagen DF (2012). Mitochondrial DNA nucleoid structure. *Biochim Biophys Acta.* 1819(9): 914-920.

Bolton CF, Sawa GM and Carter K (1981). The effects of temperature on human compound action potentials. *J Neurol Neurosurg Psychiatry.* 44(5): 407-413.

Bonen L, Cunningham RS, Gray MW and Doolittle WF (1977). Wheat embryo mitochondrial 18S ribosomal RNA: evidence for its prokaryotic nature. *Nucleic Acids Res.* 4(3): 663-671.

Bonner MR, Shen M, Liu C-S, Divita M, He X and Lan Q (2009). Mitochondrial DNA content and lung cancer risk in Xuan Wei, China. *Lung Cancer.* 63(3): 331-334.

Bordet T, Buisson B, Michaud M, Abitbol J-L, Marchand F, Grist J, Andriambeloson E, Malcangio M and Pruss RM (2008). Specific Antinociceptive Activity of Cholest-4-en-3-one, Oxime (TRO19622) in Experimental Models of Painful Diabetic and Chemotherapy-Induced Neuropathy. *J Pharmacol Exp Ther.* 326(2): 623-632.

Bouhassira D, Lantéri-Minet M, Attal N, Laurent B and Touboul C (2008). Prevalence of chronic pain with neuropathic characteristics in the general population. *Pain.* 136(3): 380-387.

"Bowel cancer incidence statistics." (Cancer Research UK 2020). from https://www.cancerresearchuk.org/health-professional/cancer-statistics/statistics-by-cancer-type/bowel-cancer/incidence.

Boyette-Davis J and Dougherty PM (2011). Protection against oxaliplatin-induced mechanical hyperalgesia and intraepidermal nerve fiber loss by minocycline. *Exp Neurol.* 229(2): 353-357.

Boyette-Davis JA, Eng C, Wang XS, Cleeland CS, Wendelschafer-Crabb G, Kennedy WR, Simone DA, Zhang H and Dougherty PM (2012). Subclinical peripheral neuropathy is a common finding in colorectal cancer patients prior to chemotherapy. *Clin Cancer Res.* 18(11): 3180-3187.

Bradbury EJ, Moon LDF, Popat RJ, King VR, Bennett GS, Patel PN, Fawcett JW and McMahon SB (2002). Chondroitinase ABC promotes functional recovery after spinal cord injury. *Nature.* 416(6881): 636-640.

Brand MD and Nicholls DG (2011). Assessing mitochondrial dysfunction in cells. *Biochem J.* 435(2): 297-312.

Bray F, Ferlay J, Soerjomataram I, Siegel RL, Torre LA and Jemal A (2018). Global cancer statistics 2018: GLOBOCAN estimates of incidence and mortality worldwide for 36 cancers in 185 countries. *CA Cancer J Clin.* 68(6): 394-424.

Briani C, Argyriou AA, Izquierdo C, Velasco R, Campagnolo M, Alberti P, Frigeni B, Cacciavillani M, Bergamo F, Cortinovis D, Cazzaniga M, Bruna J, Cavaletti G and Kalofonos HP (2014). Long-term course of oxaliplatin-induced polyneuropathy: a prospective 2-year follow-up study. *J Peripher Nerv Syst.* 19(4): 299-306.

Brown AG, Fyffe RE, Rose PK and Snow PJ (1981). Spinal cord collaterals from axons of type II slowly adapting units in the cat. *J Physiol.* 316: 469-480.

Bruna J, Videla S, Argyriou AA, Velasco R, Villoria J, Santos C, Nadal C, Cavaletti G, Alberti P, Briani C, Kalofonos HP, Cortinovis D, Sust M, Vaqué A, Klein T and Plata-Salamán C (2018). Efficacy of a Novel Sigma-1 Receptor Antagonist for Oxaliplatin-Induced Neuropathy: A Randomized, Double-Blind, Placebo-Controlled Phase IIa Clinical Trial. *Neurotherapeutics.* 15(1): 178-189.

Budnik LT, Kloth S, Baur X, Preisser AM and Schwarzenbach H (2013). Circulating mitochondrial DNA as biomarker linking environmental chemical exposure to early preclinical lesions elevation of mtDNA in human serum after exposure to carcinogenic halo-alkane-based pesticides. *PLoS One.* 8(5): e64413.

Burakgazi AZ, Messersmith W, Vaidya D, Hauer P, Hoke A and Polydefkis M (2011). Longitudinal assessment of oxaliplatin-induced neuropathy. *Neurology.* 77(10): 980-986.

Burma NE, Leduc-Pessah H, Fan CY and Trang T (2017). Animal models of chronic pain: Advances and challenges for clinical translation. *J Neurosci Res.* 95(6): 1242-1256.

Bushnell MC, Ceko M and Low LA (2013). Cognitive and emotional control of pain and its disruption in chronic pain. *Nat Rev Neurosci.* 14(7): 502-511.

Calcutt NA, Smith DR, Frizzi K, Sabbir MG, Chowdhury SKR, Mixcoatl-Zecuatl T, Saleh A, Muttalib N, Van der Ploeg R, Ochoa J, Gopaul A, Tessler L, Wess J, Jolivalt CG and Fernyhough P (2017). Selective antagonism of muscarinic receptors is neuroprotective in peripheral neuropathy. *J Clin Invest.* 127(2): 608-622.

Caldwell JH, Schaller KL, Lasher RS, Peles E and Levinson SR (2000). Sodium channel Na(v)1.6 is localized at nodes of Ranvier, dendrites, and synapses. *Proc Natl Acad Sci U S A.* 97(10): 5616-5620.

Calhoun EA, Welshman EE, Chang CH, Lurain JR, Fishman DA, Hunt TL and Cella D (2003). Psychometric evaluation of the Functional Assessment of Cancer Therapy/Gynecologic Oncology Group-Neurotoxicity (Fact/GOG-Ntx) questionnaire for patients receiving systemic chemotherapy. *Int J Gynecol Cancer.* 13(6): 741-748.

Calvert AH, Harland SJ, Newell DR, Siddik ZH, Jones AC, McElwain TJ, Raju S, Wiltshaw E, Smith IE, Baker JM, Peckham MJ and Harrap KR (1982). Early clinical studies with cis-diammine-1,1-cyclobutane dicarboxylate platinum II. *Cancer Chemother Pharmacol.* 9(3): 140-147.

Carré M, André N, Carles G, Borghi H, Brichese L, Briand C and Braguer D (2002). Tubulin is an inherent component of mitochondrial membranes that interacts with the voltage-dependent anion channel. *J Biol Chem.* 277(37): 33664-33669.

Carugno M, Pesatori AC, Dioni L, Hoxha M, Bollati V, Albetti B, Byun H-M, Bonzini M, Fustinoni S, Cocco P, Satta G, Zucca M, Merlo DF, Cipolla M, Bertazzi PA and Baccarelli A (2012). Increased mitochondrial DNA copy number in occupations associated with low-dose benzene exposure. *Environ Health Perspect.* 120(2): 210-215.

Cascinu S, Catalano V, Cordella L, Labianca R, Giordani P, Baldelli AM, Beretta GD, Ubiali E and Catalano G (2002). Neuroprotective effect of reduced glutathione on oxaliplatin-based chemotherapy in advanced colorectal cancer: a randomized, double-blind, placebo-controlled trial. *J Clin Oncol.* 20(16): 3478-3483.

Castellani CA, Longchamps RJ, Sun J, Guallar E and Arking DE (2020). Thinking outside the nucleus: Mitochondrial DNA copy number in health and disease. *Mitochondrion.* 53: 214-223.

Cavaletti G, Tredici G, Petruccioli MG, Donde E, Tredici P, Marmiroli P, Minoia C, Ronchi A, Bayssas M and Etienne GG (2001). Effects of different schedules of oxaliplatin treatment on the peripheral nervous system of the rat. *Eur J Cancer.* 37(18): 2457-2463.

Chaplan SR, Bach FW, Pogrel JW, Chung JM and Yaksh TL (1994). Quantitative assessment of tactile allodynia in the rat paw. *J Neurosci Methods.* 53(1): 55-63.

Chappell AS, Desaiah D, Liu-Seifert H, Zhang S, Skljarevski V, Belenkov Y and Brown JP (2011). A double-blind, randomized, placebo-controlled study of the efficacy and safety of duloxetine for the treatment of chronic pain due to osteoarthritis of the knee. *Pain Pract.* 11(1): 33-41.

Chen L-H, Sun Y-T, Chen Y-F, Lee M-Y, Chang L-Y, Chang J-Y and Shen M-R (2015). Integrating Image-Based High-Content Screening with Mouse Models Identifies 5-Hydroxydecanoate as a Neuroprotective Drug for Paclitaxel-Induced Neuropathy. *Mol Cancer Ther.* 14(10): 2206-2214.

Chen X, Stubblefield MD, Custodio CM, Hudis CA, Seidman AD and DeAngelis LM (2013). Electrophysiological Features of Taxane-Induced Polyneuropathy in Patients With Breast Cancer. *J Clin Neurophysiol.* 30(2): 199-203.

Chen Y-F, Chen L-H, Yeh Y-M, Wu P-Y, Chen Y-F, Chang L-Y, Chang J-Y and Shen M-R (2017). Minoxidil is a potential neuroprotective drug for paclitaxel-induced peripheral neuropathy. *Sci Rep.* 7(1): 45366.

Chêne G, Amellal B, Pédrono G, Gourlain K, Rancinan C, Journot V, Cotte L, Palmer P, Castro ND, Calvez V and Molina JM (2007). Changes in the peripheral blood mtDNA levels in naive patients treated by different nucleoside reverse transcriptase inhibitor combinations and their association with subsequent lipodystrophy. *AIDS Res Hum Retroviruses.* 23(1): 54-61.

Chinnery PF and Hudson G (2013). Mitochondrial genetics. *Br Med Bull.* 106(1): 135-159.

Choi J, Kong K, Mozaffar T and Holcombe RF (2006). Delayed oxaliplatin-associated neurotoxicity following adjuvant chemotherapy for stage III colon cancer. *Anticancer Drugs.* 17(1): 103-105.

Choi S, Chae HK, Heo H, Hahm D-H, Kim W and Kim SK (2019). Analgesic Effect of Melittin on Oxaliplatin-Induced Peripheral Neuropathy in Rats. *Toxins (Basel).* 11(7): 396.

Chrysafides SM, Bordes S and Sharma S (2020). Physiology, Resting Potential. *StatPearls*. Treasure Island (FL), StatPearls Publishing

Chukyo A, Chiba T, Kambe T, Yamamoto K, Kawakami K, Taguchi K and Abe K (2018). Oxaliplatin-induced changes in expression of transient receptor potential channels in the dorsal root ganglion as a neuropathic mechanism for cold hypersensitivity. *Neuropeptides.* 67: 95-101.

Cleeland CS and Ryan KM (1994). Pain assessment: global use of the Brief Pain Inventory. *Ann Acad Med Singap.* 23(2): 129-138.

Cliff J, Jorgensen AL, Lord R, Azam F, Cossar L, Carr DF and Pirmohamed M (2017). The molecular genetics of chemotherapy–induced peripheral neuropathy: A systematic review and meta-analysis. *Crit Rev Oncol Hematol.* 120: 127-140.

Cobianchi S, de Cruz J and Navarro X (2014). Assessment of sensory thresholds and nociceptive fiber growth after sciatic nerve injury reveals the differential contribution of collateral reinnervation and nerve regeneration to neuropathic pain. *Exp Neurol.* 255: 1-11.

Cobos EJ, Ghasemlou N, Araldi D, Segal D, Duong K and Woolf CJ (2012). Inflammation-induced decrease in voluntary wheel running in mice: a nonreflexive test for evaluating inflammatory pain and analgesia. *Pain.* 153(4): 876-884.

Colburn RW, Lubin ML, Stone DJ, Jr., Wang Y, Lawrence D, D'Andrea Michael R, Brandt MR, Liu Y, Flores CM and Qin N (2007). Attenuated Cold Sensitivity in TRPM8 Null Mice. *Neuron.* 54(3): 379-386.

Colloca L, Ludman T, Bouhassira D, Baron R, Dickenson AH, Yarnitsky D, Freeman R, Truini A, Attal N, Finnerup NB, Eccleston C, Kalso E, Bennett DL, Dworkin RH and Raja SN (2017). Neuropathic pain. *Nat Rev Dis Primers.* 3: 17002.

"Colon Cancer Treatment Regimens." from https://www.cancertherapyadvisor.com/home/cancer-topics/gastrointestinal-cancers/gastrointestinal-cancers-treatment-regimens/colon-cancer-treatment-regimens/.

Cornblath DR, Chaudhry V, Carter K, Lee D, Seysedadr M, Miernicki M and Joh T (1999). Total neuropathy score: validation and reliability study. *Neurology.* 53(8): 1660-1664.

Cossarizza A, Riva A, Pinti M, Ammannato S, Fedeli P, Mussini C, Esposito R and Galli M (2003). Increased mitochondrial DNA content in peripheral blood lymphocytes from HIV-infected patients with lipodystrophy. *Antiviral therapy.* 8(4): 315-321.

Currie GL, Angel-Scott HN, Colvin L, Cramond F, Hair K, Khandoker L, Liao J, Macleod M, McCann SK, Morland R, Sherratt N, Stewart R, Tanriver-Ayder E, Thomas J, Wang Q, Wodarski R, Xiong R, Rice ASC and Sena ES (2019). Animal models of chemotherapy-induced peripheral neuropathy: A machine-assisted systematic review and meta-analysis. *PLoS Biol.* 17(5): e3000243.

Czajka A, Ajaz S, Gnudi L, Parsade CK, Jones P, Reid F and Malik AN (2015). Altered Mitochondrial Function, Mitochondrial DNA and Reduced Metabolic Flexibility in Patients With Diabetic Nephropathy. *EBioMedicine.* 2(6): 499-512.

D'amour FE and Smith Dl (1941). A method for determining loss of pain sensation. *J Pharmacol Exp Ther.* 72(1): 74-79.

de Carvalho Barbosa M, Kosturakis AK, Eng C, Wendelschafer-Crabb G, Kennedy WR, Simone DA, Wang XS, Cleeland CS and Dougherty PM (2014). A quantitative sensory analysis of peripheral neuropathy in colorectal cancer and its exacerbation by oxaliplatin chemotherapy. *Cancer Res.* 74(21): 5955-5962.

de Moraes Vieira ÉB, Garcia JBS, da Silva AAM, Mualem Araújo RLT and Jansen RCS (2012). Prevalence, Characteristics, and Factors Associated With Chronic Pain With and Without Neuropathic Characteristics in São Luís, Brazil. *J Pain Symptom Manage.* 44(2): 239-251.

De Stefani D, Bononi A, Romagnoli A, Messina A, De Pinto V, Pinton P and Rizzuto R (2012). VDAC1 selectively transfers apoptotic Ca2+ signals to mitochondria. *Cell Death Differ.* 19(2): 267-273.

De Stefani D, Raffaello A, Teardo E, Szabò I and Rizzuto R (2011). A forty-kilodalton protein of the inner membrane is the mitochondrial calcium uniporter. *Nature.* 476(7360): 336-340.

Deacon RM (2006). Burrowing in rodents: a sensitive method for detecting behavioral dysfunction. *Nat Protoc.* 1(1): 118-121.

Descoeur J, Pereira V, Pizzoccaro A, Francois A, Ling B, Maffre V, Couette B, Busserolles J, Courteix C, Noel J, Lazdunski M, Eschalier A, Authier N and Bourinet E (2011). Oxaliplatin-induced cold hypersensitivity is due to remodelling of ion channel expression in nociceptors. *EMBO Mol Med.* 3(5): 266-278.

Di Cesare Mannelli L, Zanardelli M, Failli P and Ghelardini C (2012). Oxaliplatin-induced neuropathy: oxidative stress as pathological mechanism. Protective effect of silibinin. *J Pain.* 13(3): 276-284.

Di Francesco AM, Ruggiero A and Riccardi R (2002). Cellular and molecular aspects of drugs of the future: oxaliplatin. *Cell Mol Life Sci.* 59(11): 1914-1927.

Díaz-Rubio E, Sastre J, Zaniboni A, Labianca R, Cortés-Funes H, de Braud F, Boni C, Benavides M, Dallavalle G and Homerin M (1998). Oxaliplatin as single agent in previously untreated colorectal carcinoma patients: a phase II multicentric study. *Ann Oncol.* 9(1): 105-108.

Dominy JE and Puigserver P (2013). Mitochondrial biogenesis through activation of nuclear signaling proteins. *Cold Spring Harb Perspect Biol.* 5(7): a015008.

Dougherty PM, Cata JP, Burton AW, Vu K and Weng H-R (2007). Dysfunction in Multiple Primary Afferent Fiber Subtypes Revealed By Quantitative Sensory Testing in Patients with Chronic Vincristine-Induced Pain. *J Pain Symptom Manage.* 33(2): 166-179.

Dougherty PM, Cata JP, Cordella JV, Burton A and Weng H-R (2004). Taxol-induced sensory disturbance is characterized by preferential impairment of myelinated fiber function in cancer patients. *Pain.* 109(1): 132-142.

Doyle T, Chen Z, Muscoli C, Bryant L, Esposito E, Cuzzocrea S, Dagostino C, Ryerse J, Rausaria S, Kamadulski A, Neumann WL and Salvemini D (2012). Targeting the Overproduction of Peroxynitrite for the Prevention and Reversal of Paclitaxel-Induced Neuropathic Pain. *J Neurosci.* 32(18): 6149-6160.

Duggett NA and Flatters SJL (2017). Characterization of a rat model of bortezomib-induced painful neuropathy. *Br J Pharmacol.* 174(24): 4812-4825.

Duggett NA, Griffiths LA and Flatters SJL (2017). Paclitaxel-induced painful neuropathy is associated with changes in mitochondrial bioenergetics, glycolysis, and an energy deficit in dorsal root ganglia neurons. *Pain.* 158(8): 1499-1508.

Duggett NA, Griffiths LA, McKenna OE, de Santis V, Yongsanguanchai N, Mokori EB and Flatters SJL (2016). Oxidative stress in the development, maintenance and resolution of paclitaxel-induced painful neuropathy. *Neuroscience.* 333: 13-26.

Eastman A (1983). Characterization of the adducts produced in DNA by cis-diamminedichloroplatinum(II) and cis-dichloro(ethylenediamine)platinum(II). *Biochemistry.* 22(16): 3927-3933.

Ebenezer GJ, Carlson K, Donovan D, Cobham M, Chuang E, Moore A, Cigler T, Ward M, Lane ME, Ramnarain A, Vahdat LT and Polydefkis M (2014). Ixabepilone-induced mitochondria and sensory axon loss in breast cancer patients. *Ann Clin Transl Neurol.* 1(9): 639-649.

Eikelboom R and Mills R (1988). A microanalysis of wheel running in male and female rats. *Physiol Behav.* 43(5): 625-630.

Ellinger J, Albers P, Müller SC, von Ruecker A and Bastian PJ (2009). Circulating mitochondrial DNA in the serum of patients with testicular germ cell cancer as a novel noninvasive diagnostic biomarker. *BJU Int.* 104(1): 48-52.

Elrod JW, Wong R, Mishra S, Vagnozzi RJ, Sakthievel B, Goonasekera SA, Karch J, Gabel S, Farber J, Force T, Brown JH, Murphy E and Molkentin JD (2010). Cyclophilin D controls mitochondrial pore-dependent Ca(2+) exchange, metabolic flexibility, and propensity for heart failure in mice. *J Clin Invest.* 120(10): 3680-3687.

Erlanger J and Gasser HS (1924). The compound nature of the action current of nerve as disclosed by the cathode ray oscillograph. *Am J Physiol.* 70(3): 624-666.

Etienne-Grimaldi MC, Boyer JC, Beroud C, Mbatchi L, van Kuilenburg A, Bobin-Dubigeon C, Thomas F, Chatelut E, Merlin JL, Pinguet F, Ferrand C, Meijer J, Evrard A, Llorca L, Romieu G, Follana P, Bachelot T, Chaigneau L, Pivot X, Dieras V, Largillier R, Mousseau M, Goncalves A, Roche H, Bonneterre J, Servent V, Dohollou N, Chateau Y, Chamorey E, Desvignes JP, Salgado D, Ferrero JM and Milano G (2017). New advances in DPYD genotype and risk of severe toxicity under capecitabine. *PloS one.* 12(5): e0175998.

Farquhar-Smith P (2011). Chemotherapy-induced neuropathic pain. *Curr Opin Support Palliat Care.* 5(1): 1-7.

Fazio R, Quattrini A, Bolognesi A, Bordogna G, Villa E, Previtali S, Canal N and Nemni R (1999). Docetaxel neuropathy: A distal axonopathy. *Acta Neuropathol.* 98(6): 651-653.

Ferrari LF, Chum A, Bogen O, Reichling DB and Levine JD (2011). Role of Drp1, a Key Mitochondrial Fission Protein, in Neuropathic Pain. *J Neurosci.* 31(31): 11404-11410.

Fichtinger-Schepman AM, van der Veer JL, den Hartog JH, Lohman PH and Reedijk J (1985). Adducts of the antitumor drug cis-diamminedichloroplatinum(II) with DNA: formation, identification, and quantitation. *Biochemistry.* 24(3): 707-713.

Fidanboylu M, Griffiths LA and Flatters SJ (2011). Global inhibition of reactive oxygen species (ROS) inhibits paclitaxel-induced painful peripheral neuropathy. *PLoS One.* 6(9): e25212.

Flatters SJ and Bennett GJ (2004). Ethosuximide reverses paclitaxel- and vincristine-induced painful peripheral neuropathy. *Pain.* 109(1-2): 150-161.

Flatters SJ and Bennett GJ (2006). Studies of peripheral sensory nerves in paclitaxel-induced painful peripheral neuropathy: evidence for mitochondrial dysfunction. *Pain.* 122(3): 245-257.

Flatters SJL, Dougherty PM and Colvin LA (2017). Clinical and preclinical perspectives on Chemotherapy-Induced Peripheral Neuropathy (CIPN): a narrative review. *Br J Anaesth.* 119(4): 737-749.

Flatters SJL, Xiao W-H and Bennett GJ (2006). Acetyl-l-carnitine prevents and reduces paclitaxel-induced painful peripheral neuropathy. *Neurosci Lett.* 397(3): 219-223.

Freeman SA, Desmazières A, Simonnet J, Gatta M, Pfeiffer F, Aigrot MS, Rappeneau Q, Guerreiro S, Michel PP, Yanagawa Y, Barbin G, Brophy PJ, Fricker D, Lubetzki C and Sol-Foulon N (2015). Acceleration of conduction velocity linked to clustering of nodal components precedes myelination. *Proc Natl Acad Sci U S A.* 112(3): E321-E328.

Fu X, Wan S, Lyu YL, Liu LF and Qi H (2008). Etoposide induces ATM-dependent mitochondrial biogenesis through AMPK activation. *PloS one.* 3(4): e2009.

Fujita S, Hirota T, Sakiyama R, Baba M and Ieiri I (2019). Identification of drug transporters contributing to oxaliplatin-induced peripheral neuropathy. *J Neurochem.* 148(3): 373-385.

Gabriel CM, Howard R, Kinsella N, Lucas S, McColl I, Saldanha G, Hall SM and Hughes RAC (2000). Prospective study of the usefulness of sural nerve biopsy. *J Neurol Neurosurg Psychiatry.* 69(4): 442-446.

Gadgil S, Ergun M, van den Heuvel SA, van der Wal SE, Scheffer GJ and Hooijmans CR (2019). A systematic summary and comparison of animal models for chemotherapy induced (peripheral) neuropathy (CIPN). *PLoS One.* 14(8): e0221787.

Galley HF, McCormick B, Wilson KL, Lowes DA, Colvin L and Torsney C (2017). Melatonin limits paclitaxel-induced mitochondrial dysfunction in vitro and protects against paclitaxel-induced neuropathic pain in the rat. *J Pineal Res.* 63(4): e12444.

Garcia JM, Cata JP, Dougherty PM and Smith RG (2008). Ghrelin Prevents Cisplatin-Induced Mechanical Hyperalgesia and Cachexia. *Endocrinology.* 149(2): 455-460.

Geng J, Zhao Q, Zhang T and Xiao B (2017). Chapter Six - In Touch With the Mechanosensitive Piezo Channels: Structure, Ion Permeation, and Mechanotransduction. *Current Topics in Membranes*, Academic Press. 79**:** 159-195.

Ghirardi O, Lo Giudice P, Pisano C, Vertechy M, Bellucci A, Vesci L, Cundari S, Miloso M, Rigamonti LM, Nicolini G, Zanna C and Carminati P (2005a). Acetyl-L-Carnitine prevents and reverts experimental chronic neurotoxicity induced by oxaliplatin, without altering its antitumor properties. *Anticancer Res.* 25(4): 2681-2687.

Ghirardi O, Vertechy M, Vesci L, Canta A, Nicolini G, Galbiati S, Ciogli C, Quattrini G, Pisano C, Cundari S and Rigamonti LM (2005b). Chemotherapy-induced allodinia: neuroprotective effect of acetyl-L-carnitine. *In Vivo.* 19(3): 631-637.

Gierthmühlen J and Baron R (2016). Neuropathic Pain. *Semin Neurol.* 36(5): 462-468.

Gijtenbeek JM, van den Bent MJ and Vecht CJ (1999). Cyclosporine neurotoxicity: a review. *J Neurol.* 246(5): 339-346.

Giles RE, Blanc H, Cann HM and Wallace DC (1980). Maternal inheritance of human mitochondrial DNA. *Proc Natl Acad Sci U S A.* 77(11): 6715-6719.

Giorgi C, Marchi S and Pinton P (2018). The machineries, regulation and cellular functions of mitochondrial calcium. *Nat Rev Mol Cell Biol.* 19(11): 713-730.

Girolimetti G, Guerra F, Iommarini L, Kurelac I, Vergara D, Maffia M, Vidone M, Amato LB, Leone G, Dusi S, Tiranti V, Perrone AM, Bucci C, Porcelli AM and Gasparre G (2017). Platinum-induced mitochondrial DNA mutations confer lower sensitivity to paclitaxel by impairing tubulin cytoskeletal organization. *Hum Mol Genet.* 26(15): 2961-2974.

Goldstein DJ, Lu Y, Detke MJ, Lee TC and Iyengar S (2005). Duloxetine vs. placebo in patients with painful diabetic neuropathy. *Pain.* 116(1-2): 109-118.

Gomis A (2015). TRP Channels and Mechanical Transduction. *TRP Channels in Sensory Transduction*, Springer International Publishing**:** 141-163.

Goodwin AW and Wheat HE (2020). Physiological Responses of Sensory Afferents in Glabrous and Hairy Skin of Humans and Monkeys. *The Senses: A Comprehensive Reference (Second Edition)*. Fritzsch B. Oxford, Elsevier**:** 110-124.

Gordon-Williams R and Farquhar-Smith P (2020). Recent advances in understanding chemotherapy-induced peripheral neuropathy. *F1000Res.* 9: F1000 Faculty Rev-1177.

Gorgun MF, Zhuo M and Englander EW (2017). Cisplatin Toxicity in Dorsal Root Ganglion Neurons Is Relieved by Meclizine via Diminution of Mitochondrial Compromise and Improved Clearance of DNA Damage. *Mol Neurobiol.* 54(10): 7883-7895.

Goshima Y, Usui H, Shiozawa T, Hida T, Kuraoka S, Takeshita S, Yamashita N, Ichikawa Y, Kamiya Y, Gotoh T and Gotoh T (2010). Computational analysis of the effects of antineoplastic agents on axonal transport. *J Pharmacol Sci.* 114(2): 168-179.

Grace PM, Fabisiak TJ, Green-Fulgham SM, Anderson ND, Strand KA, Kwilasz AJ, Galer EL, Walker FR, Greenwood BN, Maier SF, Fleshner M and Watkins LR (2016). Prior voluntary wheel running attenuates neuropathic pain. *Pain.* 157(9): 2012-2023.

Grace PM, Strand KA, Maier SF and Watkins LR (2014). Suppression of voluntary wheel running in rats is dependent on the site of inflammation: evidence for voluntary running as a measure of hind paw-evoked pain. *J Pain.* 15(2): 121-128.

Graham J, Mushin M and Kirkpatrick P (2004). Oxaliplatin. *Nat Rev Drug Discov.* 3(1): 11-12.

Graham MA, Lockwood GF, Greenslade D, Brienza S, Bayssas M and Gamelin E (2000). Clinical Pharmacokinetics of Oxaliplatin: A Critical Review. *Clin Cancer Res.* 6(4): 1205-1218.

Gregg RW, Molepo JM, Monpetit VJ, Mikael NZ, Redmond D, Gadia M and Stewart DJ (1992). Cisplatin neurotoxicity: the relationship between dosage, time, and platinum concentration in neurologic tissues, and morphologic evidence of toxicity. *J Clin Oncol.* 10(5): 795-803.

Griffith KA, Zhu S, Johantgen M, Kessler MD, Renn C, Beutler AS, Kanwar R, Ambulos N, Cavaletti G, Bruna J, Briani C, Argyriou AA, Kalofonos HP, Yerges-Armstrong LM and Dorsey SG (2017). Oxaliplatin-Induced Peripheral Neuropathy and Identification of Unique Severity Groups in Colorectal Cancer. *J Pain Symptom Manage.* 54(5): 701-706.e701.

Griffiths LA, Duggett NA, Pitcher AL and Flatters SJL (2018). Evoked and Ongoing Pain-Like Behaviours in a Rat Model of Paclitaxel-Induced Peripheral Neuropathy. *Pain Res Manag.* 2018: 8217613.

Griffiths LA and Flatters SJL (2015). Pharmacological Modulation of the Mitochondrial Electron Transport Chain in Paclitaxel-Induced Painful Peripheral Neuropathy. *J Pain.* 16(10): 981-994.

Grisold W, Cavaletti G and Windebank AJ (2012). Peripheral neuropathies from chemotherapeutics and targeted agents: diagnosis, treatment, and prevention. *Neuro Oncol.* 14 (Suppl 4): iv45-iv54.

Grolleau F, Gamelin L, Boisdron-Celle M, Lapied B, Pelhate M and Gamelin E (2001). A possible explanation for a neurotoxic effect of the anticancer agent oxaliplatin on neuronal voltage-gated sodium channels. *J Neurophysiol.* 85(5): 2293-2297.

Groover AL, Ryals JM, Guilford BL, Wilson NM, Christianson JA and Wright DE (2013). Exercise-mediated improvements in painful neuropathy associated with prediabetes in mice. *Pain.* 154(12): 2658-2667.

Guillaumot M-A, Cerles O, Bertrand HC, Benoit E, Nicco C, Chouzenoux S, Schmitt A, Batteux F, Policar C and Coriat R (2019). Oxaliplatin-induced neuropathy: the preventive effect of a new super-oxide dismutase modulator. *Oncotarget.* 10(60): 6418-6431.

Gupta KJ and Igamberdiev AU (2016). Reactive Nitrogen Species in Mitochondria and Their Implications in Plant Energy Status and Hypoxic Stress Tolerance. *Front Plant Sci.* 7(369).

Hahn A and Zuryn S (2019). Mitochondrial Genome (mtDNA) Mutations that Generate Reactive Oxygen Species. *Antioxidants (Basel).* 8(9): 392.

Hama A, Natsume T, Ogawa Sy, Higo N, Hayashi I and Takamatsu H (2018). Gaps in Understanding Mechanism and Lack of Treatments: Potential Use of a Nonhuman Primate Model of Oxaliplatin-Induced Neuropathic Pain. *Pain Res Manag.* 2018: 1630709.

Hamity MV, White SR, Walder RY, Schmidt MS, Brenner C and Hammond DL (2017). Nicotinamide riboside, a form of vitamin B3 and NAD+ precursor, relieves the nociceptive and aversive dimensions of paclitaxel-induced peripheral neuropathy in female rats. *Pain.* 158(5): 962-972.

Han Y and Smith MT (2013). Pathobiology of cancer chemotherapy-induced peripheral neuropathy (CIPN). *Front Pharmacol.* 4: 156.

Hansson MJ, Månsson R, Mattiasson G, Ohlsson J, Karlsson J, Keep MF and Elmér E (2004). Brain-derived respiring mitochondria exhibit homogeneous, complete and cyclosporin-sensitive permeability transition. *J Neurochem.* 89(3): 715-729.

Harder HC and Rosenberg B (1970). Inhibitory effects of anti-tumor platinum compounds on DNA, RNA and protein syntheses in mammalian cells in virtro. *Int J Cancer.* 6(2): 207-216.

Hayashi T and Su T-P (2007). Sigma-1 Receptor Chaperones at the ER- Mitochondrion Interface Regulate Ca(2+) Signaling and Cell Survival. *Cell.* 131(3): 596-610.

Heide R, Bostock H, Ventzel L, Grafe P, Bergmans J, Fuglsang-Frederiksen A, Finnerup NB and Tankisi H (2018). Axonal excitability changes and acute symptoms of oxaliplatin treatment: In vivo evidence for slowed sodium channel inactivation. *Clin Neurophysiol.* 129(3): 694-706.

Hershman DL, Lacchetti C, Dworkin RH, Smith EML, Bleeker J, Cavaletti G, Chauhan C, Gavin P, Lavino A, Lustberg MB, Paice J, Schneider B, Smith ML, Smith T, Terstriep S, Wagner-Johnston N, Bak K and Loprinzi CL (2014). Prevention and Management of Chemotherapy-Induced Peripheral Neuropathy in Survivors of Adult Cancers: American Society of Clinical Oncology Clinical Practice Guideline. *J Clin Oncol.* 32(18): 1941-1967.

Hershman DL, Unger JM, Crew KD, Minasian LM, Awad D, Moinpour CM, Hansen L, Lew DL, Greenlee H, Fehrenbacher L, Wade JL, 3rd, Wong SF, Hortobagyi GN, Meyskens FL and Albain KS (2013). Randomized double-blind placebo-controlled trial of acetyl-L-carnitine for the prevention of taxane-induced neuropathy in women undergoing adjuvant breast cancer therapy. *J Clin Oncol.* 31(20): 2627-2633.

Hock MB and Kralli A (2009). Transcriptional control of mitochondrial biogenesis and function. *Annu Rev Physiol.* 71: 177-203.

Hodgkin AL and Huxley AF (1939). Action Potentials Recorded from Inside a Nerve Fibre. *Nature.* 144(3651): 710-711.

Hodgkin AL and Huxley AF (1952). A quantitative description of membrane current and its application to conduction and excitation in nerve. *J Physiol.* 117(4): 500-544.

Holmes J, Stanko J, Varchenko M, Ding H, Madden VJ, Bagnell CR, Wyrick SD and Chaney SG (1998). Comparative neurotoxicity of oxaliplatin, cisplatin, and ormaplatin in a Wistar rat model. *Toxicol Sci.* 46(2): 342-351.

Hopkins HL, Duggett NA and Flatters SJL (2016). Chemotherapy-induced painful neuropathy: pain-like behaviours in rodent models and their response to commonly used analgesics. *Curr Opin Support Palliat Care.* 10(2): 119-128.

Hosgood III HD, Liu CS, Rothman N, Weinstein SJ, Bonner MR, Shen M, Lim U, Virtamo J, Cheng WL, Albanes D and Lan Q (2010). Mitochondrial DNA copy number and lung cancer risk in a prospective cohort study. *Carcinogenesis.* 31(5): 847-849.

Hosobuchi Y, Adams JE and Linchitz R (1977). Pain relief by electrical stimulation of the central gray matter in humans and its reversal by naloxone. *Science.* 197(4299): 183-186.

Hu LY, Mi W-L, Wu G-C, Wang Y-Q and Mao-Ying Q-L (2019). Prevention and Treatment for Chemotherapy-Induced Peripheral Neuropathy: Therapies Based on CIPN Mechanisms. *Curr Neuropharmacol.* 17(2): 184-196.

Hunt SP and Mantyh PW (2001). The molecular dynamics of pain control. *Nat Rev Neurosci.* 2(2): 83-91.

Hunt SP and Rossi J (1985). Peptide- and non-peptide-containing unmyelinated primary afferents: the parallel processing of nociceptive information. *Philos Trans R Soc Lond B Biol Sci.* 308(1136): 283-289.

Hursh JB (1939). Conduction velocity and diameter of nerve fibers. *Am J Physiol.* 127(1): 131-139.

Huxley AF and Stämpfli R (1949). Evidence for saltatory conduction in peripheral myelinated nerve fibres. *J Physiol.* 108(3): 315-339.

Huynh W and Kiernan MC (2015). Peripheral nerve axonal excitability studies: expanding the neurophysiologist's armamentarium. *Cerebellum Ataxias.* 2: 4.

"IASP Terminology." (2011). from https://www.iasp-pain.org/Education/Content.aspx?ItemNumber=1698&navItemNumber=576.

Ibrahim A, Hirschfeld S, Cohen MH, Griebel DJ, Williams GA and Pazdur R (2004). FDA drug approval summaries: oxaliplatin. *Oncologist.* 9(1): 8-12.

Iheanacho F and Vellipuram A (2020). Physiology, Mechanoreceptors. *StatPearls*. Treasure Island (FL): StatPearls Publishing; 2021

Ip V, Liu JJ and McKeage MJ (2013). Evaluation of effects of copper histidine on copper transporter 1-mediated accumulation of platinum and oxaliplatin-induced neurotoxicity in vitro and in vivo. *Clin Exp Pharmacol Physiol.* 40(6): 371-378.

Ishii N, Tsubouchi H, Miura A, Yanagi S, Ueno H, Shiomi K and Nakazato M (2018). Ghrelin alleviates paclitaxel-induced peripheral neuropathy by reducing oxidative stress and enhancing mitochondrial anti-oxidant functions in mice. *Eur J Pharmacol.* 819: 35-42.

Itoh Y and Arnold AP (2015). Are females more variable than males in gene expression? Meta-analysis of microarray datasets. *Biol Sex Differ.* 6(1): 18.

Jamieson SM, Liu J, Connor B and McKeage MJ (2005). Oxaliplatin causes selective atrophy of a subpopulation of dorsal root ganglion neurons without inducing cell loss. *Cancer Chemother Pharmacol.* 56(4): 391-399.

Janes K, Doyle T, Bryant L, Esposito E, Cuzzocrea S, Ryerse J, Bennett GJ and Salvemini D (2013). Bioenergetic deficits in peripheral nerve sensory axons during chemotherapy-induced neuropathic pain resulting from peroxynitrite-mediated post-translational nitration of mitochondrial superoxide dismutase. *Pain.* 154(11): 2432-2440.

Jensen TS, Baron R, Haanpää M, Kalso E, Loeser JD, Rice ASC and Treede R-D (2011). A new definition of neuropathic pain. *Pain.* 152(10): 2204-2205.

Jia M, Wu C, Gao F, Xiang H, Sun N, Peng P, Li J, Yuan X, Li H, Meng X, Tian B, Shi J and Li M (2017). Activation of NLRP3 inflammasome in peripheral nerve contributes to paclitaxel-induced neuropathic pain. *Mol Pain.* 13: 1744806917719804.

Jiang D, Zhao L and Clapham DE (2009). Genome-wide RNAi screen identifies Letm1 as a mitochondrial Ca2+/H+ antiporter. *Science* 326(5949): 144-147.

Jiang WW, Masayesva B, Zahurak M, Carvalho AL, Rosenbaum E, Mambo E, Zhou S, Minhas K, Benoit N, Westra WH, Alberg A, Sidransky D, Koch W and Califano J (2005). Increased Mitochondrial DNA Content in Saliva Associated with Head and Neck Cancer. *Clinical Cancer Research.* 11(7): 2486-2491.

Jin HW, Flatters SJL, Xiao WH, Mulhern HL and Bennett GJ (2008). Prevention of paclitaxel-evoked painful peripheral neuropathy by acetyl-l-carnitine: Effects on axonal mitochondria, sensory nerve fiber terminal arbors, and cutaneous Langerhans cells. *Exp Neurol.* 210(1): 229-237.

Jong NN, Nakanishi T, Liu JJ, Tamai I and McKeage MJ (2011). Oxaliplatin transport mediated by organic cation/carnitine transporters OCTN1 and OCTN2 in overexpressing human embryonic kidney 293 cells and rat dorsal root ganglion neurons. *J Pharmacol Exp Ther.* 338(2): 537-547.

Joseph EK and Levine JD (2006). Mitochondrial electron transport in models of neuropathic and inflammatory pain. *Pain.* 121(1): 105-114.

Joseph EK and Levine JD (2009). Comparison of oxaliplatin- and cisplatin-induced painful peripheral neuropathy in the rat. *J Pain.* 10(5): 534-541.

Jouaville LS, Pinton P, Bastianutto C, Rutter GA and Rizzuto R (1999). Regulation of mitochondrial ATP synthesis by calcium: evidence for a long-term metabolic priming. *Proc Natl Acad Sci U S A.* 96(24): 13807-13812.

Kagiava A, Kosmidis EK and Theophilidis G (2013). Oxaliplatin-induced hyperexcitation of rat sciatic nerve fibers: an intra-axonal study. *Anticancer Agents Med Chem.* 13(2): 373-379.

Kagiava A, Theophilidis G, Sargiannidou I, Kyriacou K and Kleopa KA (2015). Oxaliplatin-induced neurotoxicity is mediated through gap junction channels and hemichannels and can be prevented by octanol. *Neuropharmacology.* 97: 289-305.

Kagiava A, Tsingotjidou A, Emmanouilides C and Theophilidis G (2008). The effects of oxaliplatin, an anticancer drug, on potassium channels of the peripheral myelinated nerve fibres of the adult rat. *Neurotoxicology.* 29(6): 1100-1106.

Kalmar B, Innes A, Wanisch K, Kolaszynska AK, Pandraud A, Kelly G, Abramov AY, Reilly MM, Schiavo G and Greensmith L (2017). Mitochondrial deficits and abnormal mitochondrial retrograde axonal transport play a role in the pathogenesis of mutant Hsp27-induced Charcot Marie Tooth Disease. *Hum Mol Genet.* 26(17): 3313-3326.

Kanbara T, Nakamura A, Takasu K, Ogawa K, Shibasaki M, Mori T, Suzuki T, Hasegawa M, Sakaguchi G and Kanemasa T (2014). The contribution of Gi/o protein to opioid antinociception in an oxaliplatin-induced neuropathy rat model. *J Pharmacol Sci.* 126(3): 264-273.

Kandasamy R, Calsbeek JJ and Morgan MM (2016). Home cage wheel running is an objective and clinically relevant method to assess inflammatory pain in male and female rats. *J Neurosci Methods.* 263: 115-122.

Kandasamy R, Lee AT and Morgan MM (2017). Depression of home cage wheel running: a reliable and clinically relevant method to assess migraine pain in rats. *J Headache Pain.* 18(1): 5-5.

Kao SH, Chao HT, Liu HW, Liao TL and Wei YH (2004). Sperm mitochondrial DNA depletion in men with asthenospermia. *Fertil Steril.* 82(1): 66-73.

Kaplow R and Iyere K (2017). Grading chemotherapy-induced peripheral neuropathy in adults. *Nursing.* 47(2): 67-68.

Katz B and Miledi R (1967). Ionic requirements of synaptic transmitter release. *Nature.* 215(5101): 651.

Kawashiri T, Egashira N, Kurobe K, Tsutsumi K, Yamashita Y, Ushio S, Yano T and Oishi R (2012). L type Ca(2)+ channel blockers prevent oxaliplatin-induced cold hyperalgesia and TRPM8 overexpression in rats. *Mol Pain.* 8: 7.

Kawashiri T, Egashira N, Watanabe H, Ikegami Y, Hirakawa S, Mihara Y, Yano T, Ikesue H and Oishi R (2011). Prevention of oxaliplatin-induced mechanical allodynia and neurodegeneration by neurotropin in the rat model. *Eur J Pain.* 15(4): 344-350.

Kayalioglu G (2009). Chapter 10 - Projections from the Spinal Cord to the Brain. *The Spinal Cord*. Watson C, Paxinos G and Kayalioglu G. San Diego, Academic Press**:** 148-167.

Kennedy WR, Selim MM, Brink TS, Hodges JS, Wendelschafer-Crabb G, Foster SXYL, Nolano M, Provitera V and Simone DA (2011). A new device to quantify tactile sensation in neuropathy. *Neurology.* 76(19): 1642-1649.

Khasabova IA, Khasabov SG, Olson JK, Uhelski ML, Kim AH, Albino-Ramírez AM, Wagner CL, Seybold VS and Simone DA (2019). Pioglitazone, a PPARγ agonist, reduces cisplatin-evoked neuropathic pain by protecting against oxidative stress. *Pain.* 160(3): 688-701.

Kidani Y, Noji M and Tashiro T (1980). Antitumor activity of platinum(II) complexes of 1,2-diamino-cyclohexane isomers. *Gan.* 71(5): 637-643.

Kim HK, Hwang S-H and Abdi S (2017). Tempol Ameliorates and Prevents Mechanical Hyperalgesia in a Rat Model of Chemotherapy-Induced Neuropathic Pain. *Front Pharmacol.* 7: 532.

Kim HK, Zhang YP, Gwak YS and Abdi S (2010). Phenyl N-tert-butylnitrone, a Free Radical Scavenger, Reduces Mechanical Allodynia in Chemotherapy-induced Neuropathic Pain in Rats. *Anesthesiology.* 112(2): 432-439.

Kim HY, Lee KY, Lu Y, Wang J, Cui L, Kim SJ, Chung JM and Chung K (2011). Mitochondrial Ca2+ Uptake Is Essential for Synaptic Plasticity in Pain. *J Neurosci.* 31(36): 12982-12991.

Kim SH and Chung JM (1992). An experimental model for peripheral neuropathy produced by segmental spinal nerve ligation in the rat. *Pain.* 50(3): 355-363.

Kim SH, Kim W, Kim JH, Woo MK, Baek JY, Kim SY, Chung SH and Kim HJ (2018). A Prospective Study of Chronic Oxaliplatin-Induced Neuropathy in Patients with Colon Cancer: Long-Term Outcomes and Predictors of Severe Oxaliplatin-Induced Neuropathy. *J Clin Neurol.* 14(1): 81-89.

Kim WS, Park JY, Kim TK and Baik SW (2012). The changes of mitochondrial cytochrome c and GABAergic neuron in neuropathic pain model. *Korean J Anesthesiol.* 62(4): 365-370.

Kishore L, Kaur N and Singh R (2018). Effect of Kaempferol isolated from seeds of Eruca sativa on changes of pain sensitivity in Streptozotocin-induced diabetic neuropathy. *Inflammopharmacology.* 26(4): 993-1003.

Koeppen AH (2011). Friedreich's ataxia: Pathology, pathogenesis, and molecular genetics. *J Neurol Sci.* 303(1): 1-12.

Kokotis P, Schmelz M, Kostouros E, Karandreas N and Dimopoulos MA (2016). Oxaliplatin-Induced Neuropathy: A Long-Term Clinical and Neurophysiologic Follow-Up Study. *Clin Colorectal Cancer.* 15(3): e133-140.

Komotar RJ, Kim GH, Sughrue ME, Otten ML, Rynkowski MA, Kellner CP, Hahn DK, Merkow MB, Garrett MC, Starke RM and Connolly ES (2007). Neurologic assessment of somatosensory dysfunction following an experimental rodent model of cerebral ischemia. *Nat Protoc.* 2(10): 2345-2347.

Kosturakis AK, He Z, Li Y, Boyette-Davis JA, Shah N, Thomas SK, Zhang H, Vichaya EG, Wang XS, Wendelschafer-Crabb G, Kennedy WR, Simone DA, Cleeland CS and Dougherty PM (2014). Subclinical peripheral neuropathy in patients with multiple myeloma before chemotherapy is correlated with decreased fingertip innervation density. *J Clin Oncol.* 32(28): 3156-3162.

Kowaltowski AJ, de Souza-Pinto NC, Castilho RF and Vercesi AE (2009). Mitochondria and reactive oxygen species. *Free Radic Biol Med.* 47(4): 333-343.

Kraker AJ and Moore CW (1988). Accumulation of cis-diamminedichloroplatinum(II) and platinum analogues by platinum-resistant murine leukemia cells in vitro. *Cancer Res.* 48(1): 9-13.

Krarup-Hansen A, Helweg-Larsen S, Schmalbruch H, Rørth M and Krarup C (2007). Neuronal involvement in cisplatin neuropathy: prospective clinical and neurophysiological studies. *Brain.* 130(4): 1076-1088.

Kress GJ and Mennerick S (2009). Action potential initiation and propagation: Upstream influences on neurotransmission. *Neuroscience.* 158(1): 211-222.

Krishnan AV, Goldstein D, Friedlander M and Kiernan MC (2005). Oxaliplatin-induced neurotoxicity and the development of neuropathy. *Muscle Nerve.* 32(1): 51-60.

Krishnan AV, Goldstein D, Friedlander M and Kiernan MC (2006). Oxaliplatin and axonal Na+ channel function in vivo. *Clin Cancer Res.* 12(15): 4481-4484.

Krøigård T, Schrøder HD, Qvortrup C, Eckhoff L, Pfeiffer P, Gaist D and Sindrup SH (2014). Characterization and diagnostic evaluation of chronic polyneuropathies induced by oxaliplatin and docetaxel comparing skin biopsy to quantitative sensory testing and nerve conduction studies. *Eur J Neurol.* 21(4): 623-629.

Krøigård T, Svendsen TK, Wirenfeldt M, Schrøder HD, Qvortrup C, Pfeiffer P, Gaist D and Sindrup SH (2020). Early changes in tests of peripheral nerve function during oxaliplatin treatment and their correlation with chemotherapy-induced polyneuropathy symptoms and signs. *Eur J Neurol.* 27(1): 68-76.

Krukowski K, Ma J, Golonzhka O, Laumet GO, Gutti T, van Duzer JH, Mazitschek R, Jarpe MB, Heijnen CJ and Kavelaars A (2017). HDAC6 inhibition effectively reverses chemotherapy-induced peripheral neuropathy. *Pain.* 158(6): 1126-1137.

Krukowski K, Nijboer CH, Huo X, Kavelaars A and Heijnen CJ (2015). Prevention of chemotherapy-induced peripheral neuropathy by the small-molecule inhibitor pifithrin-μ. *Pain.* 156(11): 2184-2192.

Kühlbrandt W (2015). Structure and function of mitochondrial membrane protein complexes. *BMC Biology.* 13(1): 89.

Kupari J, Usoskin D, Parisien M, Lou D, Hu Y, Fatt M, Lönnerberg P, Spångberg M, Eriksson B, Barkas N, Kharchenko PV, Loré K, Khoury S, Diatchenko L and Ernfors P (2021). Single cell transcriptomics of primate sensory neurons identifies cell types associated with chronic pain. *Nat Commun.* 12(1): 1510.

Lan Q, Lim U, Liu C-S, Weinstein SJ, Chanock S, Bonner MR, Virtamo J, Albanes D and Rothman N (2008). A prospective study of mitochondrial DNA copy number and risk of non-Hodgkin lymphoma. *Blood.* 112(10): 4247-4249.

Land SR, Kopec JA, Cecchini RS, Ganz PA, Wieand HS, Colangelo LH, Murphy K, Kuebler JP, Seay TE, Needles BM, III JDB, Colman LK, Lanier KS, Jr ERP, Cella D, Smith RE, O'Connell MJ, Costantino JP and Wolmark N (2007). Neurotoxicity From Oxaliplatin Combined With Weekly Bolus Fluorouracil and Leucovorin As Surgical Adjuvant Chemotherapy for Stage II and III Colon Cancer: NSABP C-07. *J Clin Oncol.* 25(16): 2205-2211.

Lebovitz RM, Zhang H, Vogel H, Cartwright J, Jr., Dionne L, Lu N, Huang S and Matzuk MM (1996). Neurodegeneration, myocardial injury, and perinatal death in mitochondrial superoxide dismutase-deficient mice. *Proc Natl Acad Sci U S A.* 93(18): 9782-9787.

Lee HC, Yin PH, Lu CY, Chi CW and Wei YH (2000). Increase of mitochondria and mitochondrial DNA in response to oxidative stress in human cells. *Biochem J.* 348(Pt 2): 425-432.

Lehky TJ, Leonard GD, Wilson RH, Grem JL and Floeter MK (2004). Oxaliplatin-induced neurotoxicity: acute hyperexcitability and chronic neuropathy. *Muscle Nerve.* 29(3): 387-392.

Leo M, Schmitt LI, Küsterarent P, Kutritz A, Rassaf T, Kleinschnitz C, Hendgen-Cotta UB and Hagenacker T (2020). Platinum-Based Drugs Cause Mitochondrial Dysfunction in Cultured Dorsal Root Ganglion Neurons. *Int J Mol Sci.* 21(22): 8636.

Leterrier C, Brachet A, Dargent B and Vacher H (2011). Determinants of voltage-gated sodium channel clustering in neurons. *Semin Cell Dev Biol.* 22(2): 171-177.

Leung A, Gregory NS, Allen L-AH and Sluka KA (2016). Regular physical activity prevents chronic pain by altering resident muscle macrophage phenotype and increasing interleukin-10 in mice. *Pain.* 157(1): 70-79.

Levi F, Misset JL, Brienza S, Adam R, Metzger G, Itzakhi M, Caussanel JP, Kunstlinger F, Lecouturier S, Descorps-Declere A and et al. (1992). A chronopharmacologic phase II clinical trial with 5-fluorouracil, folinic acid, and oxaliplatin using an ambulatory multichannel programmable pump. High antitumor effectiveness against metastatic colorectal cancer. *Cancer.* 69(4): 893-900.

Li CL, Li KC, Wu D, Chen Y, Luo H, Zhao JR, Wang SS, Sun MM, Lu YJ, Zhong YQ, Hu XY, Hou R, Zhou BB, Bao L, Xiao HS and Zhang X (2016). Somatosensory neuron types identified by high-coverage single-cell RNA-sequencing and functional heterogeneity. *Cell Res.* 26(1): 83-102.

Li Y, Lao J, Zhao X, Tian D, Zhu Y and Wei X (2014). The optimal distance between two electrode tips during recording of compound nerve action potentials in the rat median nerve. *Neural Regen Res.* 9(2): 171-178.

Light AR and Perl ER (1979). Spinal termination of functionally identified primary afferent neurons with slowly conducting myelinated fibers. *J Comp Neurol.* 186(2): 133-150.

Lim S, Ahn SY, Song IC, Chung MH, Jang HC, Park KS, Lee K-U, Pak YK and Lee HK (2009). Chronic Exposure to the Herbicide, Atrazine, Causes Mitochondrial Dysfunction and Insulin Resistance. *PLOS ONE.* 4(4): e5186.

Ling B, Authier N, Balayssac D, Eschalier A and Coudore F (2007a). Behavioral and pharmacological description of oxaliplatin-induced painful neuropathy in rat. *Pain.* 128(3): 225-234.

Ling B, Coudoré-Civiale M-A, Balayssac D, Eschalier A, Coudoré F and Authier N (2007b). Behavioral and immunohistological assessment of painful neuropathy induced by a single oxaliplatin injection in the rat. *Toxicology.* 234(3): 176-184.

Ling B, Coudore F, Decalonne L, Eschalier A and Authier N (2008). Comparative antiallodynic activity of morphine, pregabalin and lidocaine in a rat model of neuropathic pain produced by one oxaliplatin injection. *Neuropharmacology.* 55(5): 724-728.

Liu JJ, Kim Y, Yan F, Ding Q, Ip V, Jong NN, Mercer JFB and McKeage MJ (2013). Contributions of rat Ctr1 to the uptake and toxicity of copper and platinum anticancer drugs in dorsal root ganglion neurons. *Biochem Pharmacol.* 85(2): 207-215.

LoCoco PM, Risinger AL, Smith HR, Chavera TS, Berg KA and Clarke WP (2017). Pharmacological augmentation of nicotinamide phosphoribosyltransferase (NAMPT) protects against paclitaxel-induced peripheral neuropathy. *eLife.* 6: e29626.

Lunenburg C, Henricks LM, Guchelaar HJ, Swen JJ, Deenen MJ, Schellens JHM and Gelderblom H (2016). Prospective DPYD genotyping to reduce the risk of fluoropyrimidine-induced severe toxicity: Ready for prime time. *European journal of cancer (Oxford, England : 1990).* 54: 40-48.

Luo FR, Wyrick SD and Chaney SG (1999). Comparative neurotoxicity of oxaliplatin, ormaplatin, and their biotransformation products utilizing a rat dorsal root ganglia in vitro explant culture model. *Cancer Chemother Pharmacol.* 44(1): 29-38.

Luongo TS, Lambert JP, Gross P, Nwokedi M, Lombardi AA, Shanmughapriya S, Carpenter AC, Kolmetzky D, Gao E, van Berlo JH, Tsai EJ, Molkentin JD, Chen X, Madesh M, Houser SR and Elrod JW (2017). The mitochondrial Na(+)/Ca(2+) exchanger is essential for Ca(2+) homeostasis and viability. *Nature.* 545(7652): 93-97.

Lynch SM, Weinstein SJ, Virtamo J, Lan Q, Liu CS, Cheng WL, Rothman N, Albanes D and Stolzenberg-Solomon RZ (2011). Mitochondrial DNA copy number and pancreatic cancer in the

alpha-tocopherol beta-carotene cancer prevention study. *Cancer Prev Res (Phila).* 4(11): 1912-1919.

Maj MA, Ma J, Krukowski KN, Kavelaars A and Heijnen CJ (2017). Inhibition of Mitochondrial p53 Accumulation by PFT-μ Prevents Cisplatin-Induced Peripheral Neuropathy. *Front Mol Neurosci.* 10(108).

Malik AN (2018). Mitochondrial DNA as a potential translational biomarker of mitochondrial dysfunction in drug induced toxicity studies. *Mitochondrial Dysfunction by Drug and Environmental Toxicants*. Wills Y and Dyken J, Wiley. 1.

Malik AN and Czajka A (2013). Is mitochondrial DNA content a potential biomarker of mitochondrial dysfunction? *Mitochondrion.* 13(5): 481-492.

Malik AN, Parsade CK, Ajaz S, Crosby-Nwaobi R, Gnudi L, Czajka A and Sivaprasad S (2015). Altered circulating mitochondrial DNA and increased inflammation in patients with diabetic retinopathy. *Diabetes Res Clin Pract.* 110(3): 257-265.

Malik AN, Shahni R and Iqbal MM (2009). Increased peripheral blood mitochondrial DNA in type 2 diabetic patients with nephropathy. *Diabetes research and clinical practice.* 86(2): e22-24.

Malik AN, Shahni R, Rodriguez-de-Ledesma A, Laftah A and Cunningham P (2011). Mitochondrial DNA as a non-invasive biomarker: Accurate quantification using real time quantitative PCR without co-amplification of pseudogenes and dilution bias. *Biochem Biophys Res Commun.* 412(1): 1-7.

Mangus LM, Rao DB and Ebenezer GJ (2020). Intraepidermal Nerve Fiber Analysis in Human Patients and Animal Models of Peripheral Neuropathy: A Comparative Review. *Toxicol Pathol.* 48(1): 59-70.

Manzanares G, Brito-da-Silva G and Gandra PG (2018). Voluntary wheel running: patterns and physiological effects in mice. *Braz J Med Biol Res.* 52(1): e7830-e7830.

Mao-Ying Q-L, Kavelaars A, Krukowski K, Huo X-J, Zhou W, Price TJ, Cleeland C and Heijnen CJ (2014). The anti-diabetic drug metformin protects against chemotherapy-induced peripheral neuropathy in a mouse model. *PloS one.* 9(6): e100701.

Martinez-Balibrea E, Martínez-Cardús A, Ginés A, Ruiz de Porras V, Moutinho C, Layos L, Manzano JL, Bugés C, Bystrup S, Esteller M and Abad A (2015). Tumor-Related Molecular Mechanisms of Oxaliplatin Resistance. *Mol Cancer Ther.* 14(8): 1767-1776.

Martinov T, Mack M, Sykes A and Chatterjea D (2013). Measuring changes in tactile sensitivity in the hind paw of mice using an electronic von Frey apparatus. *J Vis Exp.* (82): e51212.

Masayesva BG, Mambo E, Taylor RJ, Goloubeva OG, Zhou S, Cohen Y, Minhas K, Koch W, Sciubba J, Alberg AJ, Sidransky D and Califano J (2006). Mitochondrial DNA content increase in response to cigarette smoking. *Cancer Epidemiol Biomarkers Prev.* 15(1): 19-24.

Mathe G, Kidani Y, Noji M, Maral R, Bourut C and Chenu E (1985). Antitumor activity of l-OHP in mice. *Cancer Lett.* 27(2): 135-143.

Mathe G, Kidani Y, Segiguchi M, Eriguchi M, Fredj G, Peytavin G, Misset JL, Brienza S, de Vassals F, Chenu E and et al. (1989). Oxalato-platinum or 1-OHP, a third-generation platinum complex: an experimental and clinical appraisal and preliminary comparison with cis-platinum and carboplatinum. *Biomed Pharmacother.* 43(4): 237-250.

Mathe G, Kidani Y, Triana K, Brienza S, Ribaud P, Goldschmidt E, Ecstein E, Despax R, Musset M and Misset JL (1986). A phase I trial of trans-1-diaminocyclohexane oxalato-platinum (l-OHP). *Biomed Pharmacother.* 40(10): 372-376.

Matsuoka A, Mitsuma A, Maeda O, Kajiyama H, Kiyoi H, Kodera Y, Nagino M, Goto H and Ando Y (2016). Quantitative assessment of chemotherapy-induced peripheral neurotoxicity using a point-of-care nerve conduction device. *Cancer Sci.* 107(10): 1453-1457.

McAllister RM and Calder JS (1995). Paradoxical clinical consequences of peripheral nerve injury: conduction of nerve impulses does not occur across the site of injury immediately following nerve division and repair. *Br J Plast Surg.* 48(6): 371-383.

McCormick B, Lowes DA, Colvin L, Torsney C and Galley HF (2016). MitoVitE, a mitochondria-targeted antioxidant, limits paclitaxel-induced oxidative stress and mitochondrial damage in vitro, and paclitaxel-induced mechanical hypersensitivity in a rat pain model. *Br J Anaesth.* 117(5): 659-666.

McHugh JC, Tryfonopoulos D, Fennelly D, Crown J and Connolly S (2012). Electroclinical biomarkers of early peripheral neurotoxicity from oxaliplatin. *Eur J Cancer Care (Engl).* 21(6): 782-789.

McKeage MJ (1995). Comparative adverse effect profiles of platinum drugs. *Drug Saf.* 13(4): 228-244.

McKeage MJ, Hsu T, Screnci D, Haddad G and Baguley BC (2001). Nucleolar damage correlates with neurotoxicity induced by different platinum drugs. *Br J Cancer.* 85(8): 1219-1225.

Mehra N, Penning M, Maas J, van Daal N, Giles RH and Voest EE (2007). Circulating mitochondrial nucleic acids have prognostic value for survival in patients with advanced prostate cancer. *Clin Cancer Res.* 13(2 Pt 1): 421-426.

Meijer JH and Robbers Y (2014). Wheel running in the wild. *Proc Biol Sci.* 281(1786): 20140210.

Melzack R (1975). The McGill Pain Questionnaire: major properties and scoring methods. *Pain.* 1(3): 277-299.

Melzack R and Wall PD (1965). Pain mechanisms: a new theory. *Science.* 150(3699): 971-979.

Mendoza JE (2011). Spinoreticular Tract. *Encyclopedia of Clinical Neuropsychology*. Kreutzer JS, DeLuca J and Caplan B. New York, NY, Springer New York**:** 2358-2358.

Meyer L, Patte-Mensah C, Taleb O and Mensah-Nyagan AG (2011). Allopregnanolone prevents and suppresses oxaliplatin-evoked painful neuropathy: multi-parametric assessment and direct evidence. *Pain.* 152(1): 170-181.

Micetich KC, Barnes D and Erickson LC (1985). A Comparative Study of the Cytotoxicity and DNA-damaging Effects of cis-(Diammino)(1,1-cyclobutanedicarboxylato)-platinum(II) and cis-Diamminedichloroplatinum(II) on L1210 Cells. *Cancer Research.* 45(9): 4043-4047.

Mishra J, Jhun BS, Hurst S, O-Uchi J, Csordás G and Sheu S-S (2017). The Mitochondrial Ca(2+) Uniporter: Structure, Function, and Pharmacology. *Handb Exp Pharmacol.* 240: 129-156.

Mitchell P (1961). Coupling of phosphorylation to electron and hydrogen transfer by a chemi-osmotic type of mechanism. *Nature.* 191: 144-148.

Montero M, Lobatón CD, Hernández-Sanmiguel E, Santodomingo J, Vay L, Moreno A and Alvarez J (2004). Direct activation of the mitochondrial calcium uniporter by natural plant flavonoids. *Biochem J.* 384(Pt 1): 19-24.

Moqrich A, Hwang SW, Earley TJ, Petrus MJ, Murray AN, Spencer KS, Andahazy M, Story GM and Patapoutian A (2005). Impaired thermosensation in mice lacking TRPV3, a heat and camphor sensor in the skin. *Science.* 307(5714): 1468-1472.

Motta SC, Carobrez AP and Canteras NS (2017). The periaqueductal gray and primal emotional processing critical to influence complex defensive responses, fear learning and reward seeking. *Neurosci Biobehav Rev.* 76: 39-47.

Muller FL, Song W, Liu Y, Chaudhuri A, Pieke-Dahl S, Strong R, Huang T-T, Epstein CJ, Roberts LJ, Csete M, Faulkner JA and Van Remmen H (2006). Absence of CuZn superoxide dismutase leads to elevated oxidative stress and acceleration of age-dependent skeletal muscle atrophy. *Free Radic Biol Med.* 40(11): 1993-2004.

Murphy E, Pan X, Nguyen T, Liu J, Holmström KM and Finkel T (2014). Unresolved questions from the analysis of mice lacking MCU expression. *Biochem Biophys Res Commun.* 449(4): 384-385.

Nagasaka K, Yamanaka K, Ogawa S, Takamatsu H and Higo N (2017). Brain activity changes in a macaque model of oxaliplatin-induced neuropathic cold hypersensitivity. *Sci Rep.* 7(1): 4305.

Nassini R, Gees M, Harrison S, De Siena G, Materazzi S, Moretto N, Failli P, Preti D, Marchetti N, Cavazzini A, Mancini F, Pedretti P, Nilius B, Patacchini R and Geppetti P (2011). Oxaliplatin elicits mechanical and cold allodynia in rodents via TRPA1 receptor stimulation. *Pain.* 152(7): 1621-1631.

Nicholas M, Vlaeyen JWS, Rief W, Barke A, Aziz Q, Benoliel R, Cohen M, Evers S, Giamberardino MA, Goebel A, Korwisi B, Perrot S, Svensson P, Wang S-J and Treede R-D (2019). The IASP classification of chronic pain for ICD-11: chronic primary pain. *Pain.* 160(1): 28-37.

Nieto FR, Cendán CM, Cañizares FJ, Cubero MA, Vela JM, Fernández-Segura E and Baeyens JM (2014). Genetic inactivation and pharmacological blockade of sigma-1 receptors prevent paclitaxel-induced sensory-nerve mitochondrial abnormalities and neuropathic pain in mice. *Mol Pain.* 10: 11.

Nieto FR, Cendán CM, Sánchez-Fernández C, Cobos EJ, Entrena JM, Tejada MA, Zamanillo D, Vela JM and Baeyens JM (2012). Role of Sigma-1 Receptors in Paclitaxel-Induced Neuropathic Pain in Mice. *J Pain.* 13(11): 1107-1121.

Nishida K, Takeuchi K, Hosoda A, Sugano S, Morisaki E, Ohishi A and Nagasawa K (2018). Ergothioneine ameliorates oxaliplatin-induced peripheral neuropathy in rats. *Life Sci.* 207: 516-524.

Ochs S, Pourmand R, Si K and Friedman RN (2000). Stretch of mammalian nerve in vitro: effect on compound action potentials. *J Peripher Nerv Syst.* 5(4): 227-235.

Ogren SO and Berge OG (1984). Test-dependent variations in the antinociceptive effect of p-chloroamphetamine-induced release of 5-hydroxytryptamine. *Neuropharmacology.* 23(8): 915-924.

Oguri T, Mitsuma A, Inada-Inoue M, Morita S, Shibata T, Shimokata T, Sugishita M, Nakayama G, Uehara K, Hasegawa Y and Ando Y (2013). Genetic polymorphisms associated with oxaliplatin-induced peripheral neurotoxicity in Japanese patients with colorectal cancer. *Int J Clin Pharmacol Ther.* 51(6): 475-481.

Olausson H, Cole J, Rylander K, McGlone F, Lamarre Y, Wallin BG, Krämer H, Wessberg J, Elam M, Bushnell MC and Vallbo Å (2008). Functional role of unmyelinated tactile afferents in human hairy skin: sympathetic response and perceptual localization. *Exp Brain Res.* 184(1): 135-140.

Ossipov MH, Morimura K and Porreca F (2014). Descending pain modulation and chronification of pain. *Curr Opin Support Palliat Care.* 8(2): 143-151.

Pachman DR, Qin R, Seisler D, Smith EML, Kaggal S, Novotny P, Ruddy KJ, Lafky JM, Ta LE, Beutler AS, Wagner-Johnston ND, Staff NP, Grothey A, Dougherty PM, Cavaletti G and Loprinzi CL (2016). Comparison of oxaliplatin and paclitaxel-induced neuropathy (Alliance A151505). *Support Care Cancer.* 24(12): 5059-5068.

Pagliarini DJ and Rutter J (2013). Hallmarks of a new era in mitochondrial biochemistry. *Genes Dev.* 27(24): 2615-2627.

Palade GE (1953). An electron microscope study of the mitochondrial structure. *J Histochem Cytochem.* 1(4): 188-211.

Palty R, Hershfinkel M and Sekler I (2012). Molecular identity and functional properties of the mitochondrial Na+/Ca2+ exchanger. *J Biol Chem.* 287(38): 31650-31657.

Palty R, Ohana E, Hershfinkel M, Volokita M, Elgazar V, Beharier O, Silverman WF, Argaman M and Sekler I (2004). Lithium-calcium exchange is mediated by a distinct potassium-independent sodium-calcium exchanger. *J Biol Chem.* 279(24): 25234-25240.

Pan X, Liu J, Nguyen T, Liu C, Sun J, Teng Y, Fergusson MM, Rovira, II, Allen M, Springer DA, Aponte AM, Gucek M, Balaban RS, Murphy E and Finkel T (2013). The physiological role of mitochondrial calcium revealed by mice lacking the mitochondrial calcium uniporter. *Nat Cell Biol.* 15(12): 1464-1472.

Papa S, Martino PL, Capitanio G, Gaballo A, De Rasmo D, Signorile A and Petruzzella V (2012). The Oxidative Phosphorylation System in Mammalian Mitochondria. *Advances in Mitochondrial Medicine*. Scatena R, Bottoni P and Giardina B. Dordrecht, Springer Netherlands**:** 3-37.

Park J-H, Chae J, Roh K, Kil E-J, Lee M, Auh C-K, Lee M-A, Yeom C-H and Lee S (2015). Oxaliplatin-Induced Peripheral Neuropathy via TRPA1 Stimulation in Mice Dorsal Root Ganglion Is Correlated with Aluminum Accumulation. *PLOS ONE.* 10(4): e0124875.

Park SB, Goldstein D, Krishnan AV, Lin CS, Friedlander ML, Cassidy J, Koltzenburg M and Kiernan MC (2013). Chemotherapy-induced peripheral neurotoxicity: a critical analysis. *CA Cancer J Clin.* 63(6): 419-437.

Park SB, Goldstein D, Lin CS, Krishnan AV, Friedlander ML and Kiernan MC (2009a). Acute abnormalities of sensory nerve function associated with oxaliplatin-induced neurotoxicity. *J Clin Oncol.* 27(8): 1243-1249.

Park SB, Lin CS, Krishnan AV, Goldstein D, Friedlander ML and Kiernan MC (2009b). Oxaliplatin-induced neurotoxicity: changes in axonal excitability precede development of neuropathy. *Brain.* 132(Pt 10): 2712-2723.

Parker JL, Shariati NH and Karantonis DM (2018). Electrically evoked compound action potential recording in peripheral nerves. *Bioelectron Med.* 1(1): 71-83.

Pasetto LM, D'Andrea MR, Rossi E and Monfardini S (2006). Oxaliplatin-related neurotoxicity: How and why? *Crit Rev Oncol Hematol.* 59(2): 159-168.

Percie du Sert N and Rice ASC (2014). Improving the translation of analgesic drugs to the clinic: animal models of neuropathic pain. *Br J Pharmacol.* 171(12): 2951-2963.

Pieretti S, Di Giannuario A, Di Giovannandrea R, Marzoli F, Piccaro G, Minosi P and Aloisi AM (2016). Gender differences in pain and its relief. *Ann Ist Super Sanita.* 52(2): 184-189.

Pietrangeli A, Leandri M, Terzoli E, Jandolo B and Garufi C (2006). Persistence of high-dose oxaliplatin-induced neuropathy at long-term follow-up. *Eur Neurol.* 56(1): 13-16.

Pisano C, Pratesi G, Laccabue D, Zunino F, Lo Giudice P, Bellucci A, Pacifici L, Camerini B, Vesci L, Castorina M, Cicuzza S, Tredici G, Marmiroli P, Nicolini G, Galbiati S, Calvani M, Carminati P and

Cavaletti G (2003). Paclitaxel and Cisplatin-induced neurotoxicity: a protective role of acetyl-L-carnitine. *Clin Cancer Res.* 9(15): 5756-5767.

Pitcher MH (2018). The Impact of Exercise in Rodent Models of Chronic Pain. *Curr Osteoporos Rep.* 16(4): 344-359.

Pitcher MH, Tarum F, Rauf IZ, Low LA and Bushnell C (2017). Modest Amounts of Voluntary Exercise Reduce Pain- and Stress-Related Outcomes in a Rat Model of Persistent Hind Limb Inflammation. *J Pain.* 18(6): 687-701.

Pivovarov AS, Calahorro F and Walker RJ (2018). Na(+)/K(+)-pump and neurotransmitter membrane receptors. *Invert Neurosci.* 19(1): 1.

Podratz JL, Knight AM, Ta LE, Staff NP, Gass JM, Genelin K, Schlattau A, Lathroum L and Windebank AJ (2011). Cisplatin induced mitochondrial DNA damage in dorsal root ganglion neurons. *Neurobiol Dis.* 41(3): 661-668.

Postma TJ, Aaronson NK, Heimans JJ, Muller MJ, Hildebrand JG, Delattre JY, Hoang-Xuan K, Lantéri-Minet M, Grant R, Huddart R, Moynihan C, Maher J and Lucey R (2005). The development of an EORTC quality of life questionnaire to assess chemotherapy-induced peripheral neuropathy: The QLQ-CIPN20. *Eur J Cancer.* 41(8): 1135-1139.

Postma TJ, Heimans JJ, Muller MJ, Ossenkoppele GJ, Vermorken JB and Aaronson NK (1998). Pitfalls in grading severity of chemotherapy-induced peripheral neuropathy. *Ann Oncol.* 9(7): 739-744.

Prendergast BJ, Onishi KG and Zucker I (2014). Female mice liberated for inclusion in neuroscience and biomedical research. *Neurosci Biobehav Rev.* 40: 1-5.

Purroy R, Britti E, Delaspre F, Tamarit J and Ros J (2018). Mitochondrial pore opening and loss of Ca(2+) exchanger NCLX levels occur after frataxin depletion. *Biochim Biophys Acta Mol Basis Dis.* 1864(2): 618-631.

Puurand M, Tepp K, Timohhina N, Aid J, Shevchuk I, Chekulayev V and Kaambre T (2019). Tubulin βII and βIII Isoforms as the Regulators of VDAC Channel Permeability in Health and Disease. *Cells.* 8(3): 239.

Pyle A, Anugrha H, Kurzawa-Akanbi M, Yarnall A, Burn D and Hudson G (2016). Reduced mitochondrial DNA copy number is a biomarker of Parkinson's disease. *Neurobiol Aging.* 38: 216.e207-216.e210.

Pyle A, Hudson G, Wilson IJ, Coxhead J, Smertenko T, Herbert M, Santibanez-Koref M and Chinnery PF (2015). Extreme-Depth Re-sequencing of Mitochondrial DNA Finds No Evidence of Paternal Transmission in Humans. *PLoS Genet.* 11(5): e1005040.

Qu F, Liu X, Zhou F, Yang H, Bao G, He X and Xing J (2011). Association between mitochondrial DNA content in leukocytes and colorectal cancer risk: a case-control analysis. *Cancer.* 117(14): 3148-3155.

Radi R, Cassina A, Hodara R, Quijano C and Castro L (2002). Peroxynitrite reactions and formation in mitochondria. *Free Radic Biol Med.* 33(11): 1451-1464.

Raghavan M, Fee D and Barkhaus PE (2019). Generation and propagation of the action potential, Elsevier.

Raja SN, Carr DB, Cohen M, Finnerup NB, Flor H, Gibson S, Keefe FJ, Mogil JS, Ringkamp M, Sluka KA, Song XJ, Stevens B, Sullivan MD, Tutelman PR, Ushida T and Vader K (2020). The revised International Association for the Study of Pain definition of pain: concepts, challenges, and compromises. *Pain.* 161(9): 1976-1982.

Randall LO and Selitto JJ (1957). A method for measurement of analgesic activity on inflamed tissue. *Arch Int Pharmacodyn Ther.* 111(4): 409-419.

Ranjan R, Logette E, Marani M, Herzog M, Tâche V, Scantamburlo E, Buchillier V and Markram H (2019). A Kinetic Map of the Homomeric Voltage-Gated Potassium Channel (Kv) Family. *Front Cell Neurosci.* 13: 358.

Rasband MN and Trimmer JS (2001). Developmental Clustering of Ion Channels at and near the Node of Ranvier. *Dev Biol.* 236(1): 5-16.

Ray P, Torck A, Quigley L, Wangzhou A, Neiman M, Rao C, Lam T, Kim J-Y, Kim TH, Zhang MQ, Dussor G and Price TJ (2018). Comparative transcriptome profiling of the human and mouse dorsal root ganglia: an RNA-seq-based resource for pain and sensory neuroscience research. *Pain.* 159(7): 1325-1345.

Rea P (2015). Lower Limb Nerve Supply. *Essential Clinically Applied Anatomy of the Peripheral Nervous System in the Limbs*. Rea P, Academic Press**:** 101-177.

Reddy SM, Vergo MT, Paice JA, Kwon N, Helenowski IB, Benson AB, Mulcahy MF, Nimeiri HS and Harden RN (2016). Quantitative Sensory Testing at Baseline and During Cycle 1 Oxaliplatin Infusion Detects Subclinical Peripheral Neuropathy and Predicts Clinically Overt Chronic Neuropathy in Gastrointestinal Malignancies. *Clin Colorectal Cancer.* 15(1): 37-46.

Renn CL, Carozzi VA, Rhee P, Gallop D, Dorsey SG and Cavaletti G (2011). Multimodal assessment of painful peripheral neuropathy induced by chronic oxaliplatin-based chemotherapy in mice. *Mol Pain.* 7: 29.

Rexed B (1952). The cytoarchitectonic organization of the spinal cord in the cat. *J Comp Neurol.* 96(3): 414-495.

Reynolds DV (1969). Surgery in the rat during electrical analgesia induced by focal brain stimulation. *Science.* 164(3878): 444-445.

Rich LR and Brown AM (2018). Fibre sub-type specific conduction reveals metabolic function in mouse sciatic nerve. *J Physiol.* 596(10): 1795-1812.

Richardson DE and Akil H (1977). Pain reduction by electrical brain stimulation in man. Part 1: Acute administration in periaqueductal and periventricular sites. *J Neurosurg.* 47(2): 178-183.

Rigaud M, Gemes G, Barabas M-E, Chernoff DI, Abram SE, Stucky CL and Hogan QH (2008). Species and strain differences in rodent sciatic nerve anatomy: implications for studies of neuropathic pain. *Pain.* 136(1-2): 188-201.

Rixe O, Ortuzar W, Alvarez M, Parker R, Reed E, Paull K and Fojo T (1996). Oxaliplatin, tetraplatin, cisplatin, and carboplatin: spectrum of activity in drug-resistant cell lines and in the cell lines of the National Cancer Institute's Anticancer Drug Screen panel. *Biochem Pharmacol.* 52(12): 1855-1865.

Roldan CJ, Johnson C, Lee SO, Peng A, Dougherty PM and Huh B (2018). Subclinical Peripheral Neuropathy in Patients with Head and Neck Cancer: A Quantitative Sensory Testing (QST) Study. *Pain Physician.* 21(4): e419-e427.

Rosa HS, Ajaz S, Gnudi L and Malik AN (2020). A case for measuring both cellular and cell-free mitochondrial DNA as a disease biomarker in human blood. *The FASEB Journal.* 34(9): 12278-12288.

Rosenberg B (1985). Fundamental studies with cisplatin. *Cancer.* 55(10): 2303-2306.

Rosenberg B, Van Camp L, Grimley EB and Thomson AJ (1967). The inhibition of growth or cell division in Escherichia coli by different ionic species of platinum(IV) complexes. *J Biol Chem.* 242(6): 1347-1352.

Rosenberg B, Van Camp L and Krigas T (1965). Inhibition of Cell Division in Escherichia coli by Electrolysis Products from a Platinum Electrode. *Nature.* 205(4972): 698-699.

Rosenberg B and VanCamp L (1970). The successful regression of large solid sarcoma 180 tumors by platinum compounds. *Cancer Res.* 30(6): 1799-1802.

Rosenberg B, Vancamp L, Trosko JE and Mansour VH (1969). Platinum Compounds: a New Class of Potent Antitumour Agents. *Nature.* 222(5191): 385-386.

Rovini A (2019). Tubulin-VDAC Interaction: Molecular Basis for Mitochondrial Dysfunction in Chemotherapy-Induced Peripheral Neuropathy. *Front Physiol.* 10: 671.

Ruiz A, Alberdi E and Matute C (2014). CGP37157, an inhibitor of the mitochondrial Na+/Ca2+ exchanger, protects neurons from excitotoxicity by blocking voltage-gated Ca2+ channels. *Cell Death Dis.* 5(4): e1156.

Russell IJ, Mease PJ, Smith TR, Kajdasz DK, Wohlreich MM, Detke MJ, Walker DJ, Chappell AS and Arnold LM (2008). Efficacy and safety of duloxetine for treatment of fibromyalgia in patients

with or without major depressive disorder: Results from a 6-month, randomized, double-blind, placebo-controlled, fixed-dose trial. *Pain.* 136(3): 432-444.

Sabharwal R, Rasmussen L, Sluka KA and Chapleau MW (2016). Exercise prevents development of autonomic dysregulation and hyperalgesia in a mouse model of chronic muscle pain. *Pain.* 157(2): 387-398.

Sadick JS and Darling EM (2017). Processing fixed and stored adipose-derived stem cells for quantitative protein array assays. *BioTechniques.* 63(6): 275-280.

Sagan L (1967). On the origin of mitosing cells. *J Theor Biol.* 14(3): 255-274.

Sahenk Z, Barohn R, New P and Mendell JR (1994). Taxol Neuropathy: Electrodiagnostic and Sural Nerve Biopsy Findings. *Arch Neurol.* 51(7): 726-729.

Sakurai M, Egashira N, Kawashiri T, Yano T, Ikesue H and Oishi R (2009). Oxaliplatin-induced neuropathy in the rat: involvement of oxalate in cold hyperalgesia but not mechanical allodynia. *Pain.* 147(1-3): 165-174.

Samanta K, Kar P, Chakraborti T and Chakraborti S (2010). Calcium-dependent cleavage of the Na(+)/Ca(2+) exchanger by m-calpain in isolated endoplasmic reticulum. *J Biochem.* 147(2): 225-235.

Sanganahalli BG, Herman P, Hyder F and Kannurpatti SS (2013). Mitochondrial functional state impacts spontaneous neocortical activity and resting state FMRI. *PLoS One.* 8(5): e63317.

Saris CP, van de Vaart PJ, Rietbroek RC and Blommaert FA (1996). In vitro formation of DNA adducts by cisplatin, lobaplatin and oxaliplatin in calf thymus DNA in solution and in cultured human cells. *Carcinogenesis.* 17(12): 2763-2769.

Schaar KL, Brenneman MM and Savitz SI (2010). Functional assessments in the rodent stroke model. *Exp Transl Stroke Med.* 2(1): 13.

Schallert T, Fleming SM, Leasure JL, Tillerson JL and Bland ST (2000). CNS plasticity and assessment of forelimb sensorimotor outcome in unilateral rat models of stroke, cortical ablation, parkinsonism and spinal cord injury. *Neuropharmacology.* 39(5): 777-787.

Schallert T, Upchurch M, Lobaugh N, Farrar SB, Spirduso WW, Gilliam P, Vaughn D and Wilcox RE (1982). Tactile extinction: distinguishing between sensorimotor and motor asymmetries in rats with unilateral nigrostriatal damage. *Pharmacol Biochem Behav.* 16(3): 455-462.

Schellingerhout D, LeRoux LG, Hobbs BP and Bredow S (2012). Impairment of retrograde neuronal transport in oxaliplatin-induced neuropathy demonstrated by molecular imaging. *PloS one.* 7(9): e45776.

Schmalbruch H (1986). Fiber composition of the rat sciatic nerve. *The Anatomical Record.* 215(1): 71-81.

Scholz J, Finnerup NB, Attal N, Aziz Q, Baron R, Bennett MI, Benoliel R, Cohen M, Cruccu G, Davis KD, Evers S, First M, Giamberardino MA, Hansson P, Kaasa S, Korwisi B, Kosek E, Lavand'homme P, Nicholas M, Nurmikko T, Perrot S, Raja SN, Rice ASC, Rowbotham MC, Schug S, Simpson DM, Smith BH, Svensson P, Vlaeyen JWS, Wang S-J, Barke A, Rief W and Treede R-D (2019). The IASP classification of chronic pain for ICD-11: chronic neuropathic pain. *Pain.* 160(1): 53-59.

Schug SA, Lavand'homme P, Barke A, Korwisi B, Rief W and Treede R-D (2019). The IASP classification of chronic pain for ICD-11: chronic postsurgical or posttraumatic pain. *Pain.* 160(1): 45-52.

Screnci D, McKeage MJ, Galettis P, Hambley TW, Palmer BD and Baguley BC (2000). Relationships between hydrophobicity, reactivity, accumulation and peripheral nerve toxicity of a series of platinum drugs. *Br J Cancer.* 82(4): 966-972.

Sengul G and Watson C (2015). Ascending and Descending Pathways in the Spinal Cord. *The Rat Nervous System (Fourth Edition)*. Paxinos G. San Diego, Academic Press**:** 115-130.

Seretny M, Currie GL, Sena ES, Ramnarine S, Grant R, MacLeod MR, Colvin LA and Fallon M (2014). Incidence, prevalence, and predictors of chemotherapy-induced peripheral neuropathy: A systematic review and meta-analysis. *Pain.* 155(12): 2461-2470.

Shen J, Platek M, Mahasneh A, Ambrosone CB and Zhao H (2010). Mitochondrial copy number and risk of breast cancer: a pilot study. *Mitochondrion.* 10(1): 62-68.

Sherwin CM (1998). Voluntary wheel running: a review and novel interpretation. *Anim Behav.* 56(1): 11-27.

Shidahara Y, Ogawa S, Nakamura M, Nemoto S, Awaga Y, Takashima M, Hama A, Matsuda A and Takamatsu H (2016). Pharmacological comparison of a nonhuman primate and a rat model of oxaliplatin-induced neuropathic cold hypersensitivity. *Pharmacol Res Perspect.* 4(1): e00216.

Shimozuma K, Ohashi Y, Takeuchi A, Aranishi T, Morita S, Kuroi K, Ohsumi S, Makino H, Mukai H, Katsumata N, Sunada Y, Watanabe T and Hausheer FH (2009). Feasibility and validity of the Patient Neurotoxicity Questionnaire during taxane chemotherapy in a phase III randomized trial in patients with breast cancer: N-SAS BC 02. *Support Care Cancer.* 17(12): 1483-1491.

Shoshan-Barmatz V, De S and Meir A (2017). The Mitochondrial Voltage-Dependent Anion Channel 1, Ca(2+) Transport, Apoptosis, and Their Regulation. *Front Oncol.* 7: 60.

Siao P and Cros DP (2003). Quantitative sensory testing. *Phys Med Rehabil Clin N Am.* 14(2): 261-286.

Sittl R, Carr RW, Fleckenstein J and Grafe P (2010). Enhancement of axonal potassium conductance reduces nerve hyperexcitability in an in vitro model of oxaliplatin-induced acute neuropathy. *NeuroToxicology.* 31(6): 694-700.

Sittl R, Lampert A, Huth T, Schuy ET, Link AS, Fleckenstein J, Alzheimer C, Grafe P and Carr RW (2012). Anticancer drug oxaliplatin induces acute cooling-aggravated neuropathy via sodium channel subtype Na(V)1.6-resurgent and persistent current. *Proc Natl Acad Sci U S A.* 109(17): 6704-6709.

Sjostrand FS (1953). Electron microscopy of mitochondria and cytoplasmic double membranes. *Nature.* 171(4340): 30-32.

Slivicki RA, Mali SS and Hohmann AG (2019). Voluntary exercise reduces both chemotherapy-induced neuropathic nociception and deficits in hippocampal cellular proliferation in a mouse model of paclitaxel-induced peripheral neuropathy. *Neurobiol Pain.* 6: 100035.

Sluka KA, O'Donnell JM, Danielson J and Rasmussen LA (2013). Regular physical activity prevents development of chronic pain and activation of central neurons. *J Appl Physiol (1985).* 114(6): 725-733.

Smith EML, Beck SL and Cohen J (2008). The total neuropathy score: a tool for measuring chemotherapy-induced peripheral neuropathy. *Oncol Nurs Forum.* 35(1): 96-102.

Smith EML, Pang H, Cirrincione C, Fleishman S, Paskett ED, Ahles T, Bressler LR, Fadul CE, Knox C, Le-Lindqwister N, Gilman PB, Shapiro CL and Alliance for Clinical Trials in O (2013). Effect of duloxetine on pain, function, and quality of life among patients with chemotherapy-induced painful peripheral neuropathy: a randomized clinical trial. *JAMA.* 309(13): 1359-1367.

Soveri LM, Lamminmäki A, Hänninen UA, Karhunen M, Bono P and Osterlund P (2019). Long-term neuropathy and quality of life in colorectal cancer patients treated with oxaliplatin containing adjuvant chemotherapy. *Acta Oncol.* 58(4): 398-406.

Speck RM, DeMichele A, Farrar JT, Hennessy S, Mao JJ, Stineman MG and Barg FK (2012). Scope of symptoms and self-management strategies for chemotherapy-induced peripheral neuropathy in breast cancer patients. *Support Care Cancer.* 20(10): 2433-2439.

Staff NP, Grisold A, Grisold W and Windebank AJ (2017). Chemotherapy-induced peripheral neuropathy: A current review. *Ann Neurol.* 81(6): 772-781.

Stevenson GW, Mercer H, Cormier J, Dunbar C, Benoit L, Adams C, Jezierski J, Luginbuhl A and Bilsky EJ (2011). Monosodium iodoacetate-induced osteoarthritis produces pain-depressed wheel running in rats: implications for preclinical behavioral assessment of chronic pain. *Pharmacol Biochem Behav.* 98(1): 35-42.

Stewart KT, Rosenwasser AM and Adler NT (1985). Interactions between nocturnal feeding and wheel running patterns in the rat. *Physiol Behav.* 34(4): 601-608.

Storey DJ, Sakala M, McLean CM, Phillips HA, Dawson LK, Wall LR, Fallon MT and Clive S (2010). Capecitabine combined with oxaliplatin (CapOx) in clinical practice: how significant is peripheral neuropathy? *Ann Oncol.* 21(8): 1657-1661.

Sughrue ME, Mocco J, Komotar RJ, Mehra A, D'Ambrosio AL, Grobelny BT, Penn DL and Connolly ES (2006). An improved test of neurological dysfunction following transient focal cerebral ischemia in rats. *J Neurosci Methods.* 151(2): 83-89.

Sugiura Y, Lee CL and Perl ER (1986). Central projections of identified, unmyelinated (C) afferent fibers innervating mammalian skin. *Science.* 234(4774): 358-361.

Sutovsky P, Moreno RD, Ramalho-Santos J, Dominko T, Simerly C and Schatten G (1999). Ubiquitin tag for sperm mitochondria. *Nature.* 402(6760): 371-372.

Ta LE, Espeset L, Podratz J and Windebank AJ (2006). Neurotoxicity of oxaliplatin and cisplatin for dorsal root ganglion neurons correlates with platinum-DNA binding. *Neurotoxicology.* 27(6): 992-1002.

Tasaki I (1939). The electro-saltatory transmission of the nerve impulse and the effect of narcosis upon the nerve fiber. *Am J Physiol.* 127(2): 211-227.

Tashiro T, Kawada Y, Sakurai Y and Kidani Y (1989). Antitumor activity of a new platinum complex, oxalato (trans-l-1,2-diaminocyclohexane)platinum (II): new experimental data. *Biomed Pharmacother.* 43(4): 251-260.

Terrazzino S, Argyriou AA, Cargnin S, Antonacopoulou AG, Briani C, Bruna J, Velasco R, Alberti P, Campagnolo M, Lonardi S, Cortinovis D, Cazzaniga M, Santos C, Kalofonos HP, Canonico PL, Genazzani AA and Cavaletti G (2015). Genetic determinants of chronic oxaliplatin-induced peripheral neurotoxicity: a genome-wide study replication and meta-analysis. *J Peripher Nerv Syst.* 20(1): 15-23.

Thompson SW, Davis LE, Kornfeld M, Hilgers RD and Standefer JC (1984). Cisplatin neuropathy. Clinical, electrophysiologic, morphologic, and toxicologic studies. *Cancer.* 54(7): 1269-1275.

Torrance N, Smith BH, Bennett MI and Lee AJ (2006). The epidemiology of chronic pain of predominantly neuropathic origin. Results from a general population survey. *J Pain.* 7(4): 281-289.

Toyama S, Shimoyama N, Ishida Y, Koyasu T, Szeto HH and Shimoyama M (2014). Characterization of acute and chronic neuropathies induced by oxaliplatin in mice and differential effects of a novel mitochondria-targeted antioxidant on the neuropathies. *Anesthesiology.* 120(2): 459-473.

Toyama S, Shimoyama N, Szeto HH, Schiller PW and Shimoyama M (2018). Protective Effect of a Mitochondria-Targeted Peptide against the Development of Chemotherapy-Induced Peripheral Neuropathy in Mice. *ACS Chem Neurosci.* 9(7): 1566-1571.

Trecarichi A, Duggett NA, Granat L, Lo S, Malik AN, Zuliani-Álvarez L and Flatters SJL (2020). Preclinical evidence for mitochondrial DNA as a potential blood biomarker for chemotherapy-induced peripheral neuropathy. *Mitochondrion.*

Trecarichi A and Flatters SJL (2019). Mitochondrial dysfunction in the pathogenesis of chemotherapy-induced peripheral neuropathy. *Int Rev Neurobiol.* 145: 83-126.

Treede R-D, Rief W, Barke A, Aziz Q, Bennett MI, Benoliel R, Cohen M, Evers S, Finnerup NB, First MB, Giamberardino MA, Kaasa S, Korwisi B, Kosek E, Lavand'homme P, Nicholas M, Perrot S, Scholz J, Schug S, Smith BH, Svensson P, Vlaeyen JWS and Wang S-J (2019). Chronic pain as a symptom or a disease: the IASP Classification of Chronic Pain for the International Classification of Diseases (ICD-11). *Pain.* 160(1): 19-27.

Treede R-D, Rief W, Barke A, Aziz Q, Bennett MI, Benoliel R, Cohen M, Evers S, Finnerup NB, First MB, Giamberardino MA, Kaasa S, Kosek E, Lavand'homme P, Nicholas M, Perrot S, Scholz J, Schug S, Smith BH, Svensson P, Vlaeyen JWS and Wang S-J (2015). A classification of chronic pain for ICD-11. *Pain.* 156(6): 1003-1007.

Trevisiol A, Saab AS, Winkler U, Marx G, Imamura H, Möbius W, Kusch K, Nave KA and Hirrlinger J (2017). Monitoring ATP dynamics in electrically active white matter tracts. *eLife.* 6: e24241.

Tryon VL and Mizumori SJY (2018). A Novel Role for the Periaqueductal Gray in Consummatory Behavior. *Front Behav Neurosci.* 12: 178-178.

Tsou K and Jang CS (1964). Studies on the site of analgesic action of morphine by intracerebral micro-injection. *Sci Sin.* 13: 1099-1109.

Tsujimoto Y and Shimizu S (2007). Role of the mitochondrial membrane permeability transition in cell death. *Apoptosis.* 12(5): 835-840.

Usoskin D, Furlan A, Islam S, Abdo H, Lönnerberg P, Lou D, Hjerling-Leffler J, Haeggström J, Kharchenko O, Kharchenko PV, Linnarsson S and Ernfors P (2015). Unbiased classification of sensory neuron types by large-scale single-cell RNA sequencing. *Nat Neurosci.* 18(1): 145-153.

Vallbo AB, Olausson H and Wessberg J (1999). Unmyelinated afferents constitute a second system coding tactile stimuli of the human hairy skin. *J Neurophysiol.* 81(6): 2753-2763.

Van Helleputte L, Kater M, Cook DP, Eykens C, Rossaert E, Haeck W, Jaspers T, Geens N, Vanden Berghe P, Gysemans C, Mathieu C, Robberecht W, Van Damme P, Cavaletti G, Jarpe M and Van Den Bosch L (2018). Inhibition of histone deacetylase 6 (HDAC6) protects against vincristine-induced peripheral neuropathies and inhibits tumor growth. *Neurobiol Dis.* 111: 59-69.

Velasco R, Bruna J, Briani C, Argyriou AA, Cavaletti G, Alberti P, Frigeni B, Cacciavillani M, Lonardi S, Cortinovis D, Cazzaniga M, Santos C and Kalofonos HP (2014). Early predictors of oxaliplatin-induced cumulative neuropathy in colorectal cancer patients. *J Neurol Neurosurg Psychiatry.* 85(4): 392-398.

Velasco R, Petit J, Clapés V, Verdú E, Navarro X and Bruna J (2010). Neurological monitoring reduces the incidence of bortezomib-induced peripheral neuropathy in multiple myeloma patients. *J Peripher Nerv Syst.* 15(1): 17-25.

Vichaya EG, Wang XS, Boyette-Davis JA, Mendoza TR, He Z, Thomas SK, Shah N, Williams LA, Cleeland CS and Dougherty PM (2013). Subclinical pretreatment sensory deficits appear to predict the development of pain and numbness in patients with multiple myeloma undergoing chemotherapy. *Cancer Chemother Pharmacol.* 71(6): 1531-1540.

Vincent A (2000). Understanding neuromyotonia. *Muscle Nerve.* 23(5): 655-657.

Vissers K and Meert T (2005). A Behavioral and Pharmacological Validation of the Acetone Spray Test in Gerbils with a Chronic Constriction Injury. *Anesth Analg.* 101(2): 457-464.

Wagner BK, Kitami T, Gilbert TJ, Peck D, Ramanathan A, Schreiber SL, Golub TR and Mootha VK (2008). Large-scale chemical dissection of mitochondrial function. *Nat Biotechnol.* 26(3): 343-351.

Waldeck-Weiermair M, Jean-Quartier C, Rost R, Khan MJ, Vishnu N, Bondarenko AI, Imamura H, Malli R and Graier WF (2011). Leucine zipper EF hand-containing transmembrane protein 1 (Letm1) and uncoupling proteins 2 and 3 (UCP2/3) contribute to two distinct mitochondrial Ca2+ uptake pathways. *J Biol Chem.* 286(32): 28444-28455.

Wallace DC (2013). A mitochondrial bioenergetic etiology of disease. *J Clin Invest.* 123(4): 1405-1412.

Wang XS, Shi Q, Dougherty PM, Eng C, Mendoza TR, Williams LA, Fogelman DR and Cleeland CS (2016). Prechemotherapy Touch Sensation Deficits Predict Oxaliplatin-Induced Neuropathy in Patients with Colorectal Cancer. *Oncology.* 90(3): 127-135.

Waseem M and Parvez S (2016). Neuroprotective activities of curcumin and quercetin with potential relevance to mitochondrial dysfunction induced by oxaliplatin. *Protoplasma.* 253(2): 417-430.

Waseem M, Tabassum H and Parvez S (2016). Neuroprotective effects of melatonin as evidenced by abrogation of oxaliplatin induced behavioral alterations, mitochondrial dysfunction and neurotoxicity in rat brain. *Mitochondrion.* 30: 168-176.

Weisthal S, Keinan N, Ben-Hail D, Arif T and Shoshan-Barmatz V (2014). Ca2+-mediated regulation of VDAC1 expression levels is associated with cell death induction. *Biochim Biophys Acta.* 1843(10): 2270-2281.

Westlund K (2008). Pain Pathways: Peripheral, Spinal, Ascending, and Descending Pathways. *Raj's Practical Management of Pain***:** 119-134.

White A, Ironmonger L, Steele RJC, Ormiston-Smith N, Crawford C and Seims A (2018). A review of sex-related differences in colorectal cancer incidence, screening uptake, routes to diagnosis, cancer stage and survival in the UK. *BMC cancer.* 18(1): 906-906.

Whitehead RA, Lam NL, Sun MS, Sanchez J, Noor S, Vanderwall AG, Petersen TR, Martin HB and Milligan ED (2017). Chronic Sciatic Neuropathy in Rat Reduces Voluntary Wheel-Running Activity With Concurrent Chronic Mechanical Allodynia. *Anesth Analg.* 124(1): 346-355.

Wiegand G and Remington SJ (1986). Citrate synthase: structure, control, and mechanism. *Annu Rev Biophys Biophys Chem.* 15(1): 97-117.

Wilson RH, Lehky T, Thomas RR, Quinn MG, Floeter MK and Grem JL (2002). Acute oxaliplatin-induced peripheral nerve hyperexcitability. *J Clin Oncol.* 20(7): 1767-1774.

Wolf SG, Mutsafi Y, Dadosh T, Ilani T, Lansky Z, Horowitz B, Rubin S, Elbaum M and Fass D (2017). 3D visualization of mitochondrial solid-phase calcium stores in whole cells. *eLife.* 6: e29929.

Won HH, Lee J, Park JO, Park YS, Lim HY, Kang WK, Kim JW, Lee SY and Park SH (2012). Polymorphic markers associated with severe oxaliplatin-induced, chronic peripheral neuropathy in colon cancer patients. *Cancer.* 118(11): 2828-2836.

Woolf CJ and Fitzgerald M (1986). Somatotopic organization of cutaneous afferent terminals and dorsal horn neuronal receptive fields in the superficial and deep laminae of the rat lumbar spinal cord. *J Comp Neurol.* 251(4): 517-531.

Woolfe G and Macdonald AD (1944). The evaluation of the analgesic action of pethidine hydrochloride (demerol). *J Pharmacol Exp Ther.* 80(3): 300-307.

Woynarowski JM, Chapman WG, Napier C, Herzig MC and Juniewicz P (1998). Sequence- and region-specificity of oxaliplatin adducts in naked and cellular DNA. *Mol Pharmacol.* 54(5): 770-777.

Woynarowski JM, Faivre S, Herzig MCS, Arnett B, Chapman WG, Trevino AV, Raymond E, Chaney SG, Vaisman A, Varchenko M and Juniewicz PE (2000). Oxaliplatin-Induced Damage of Cellular DNA. *Mol Pharmacol.* 58(5): 920-927.

Wu P and Chen Y (2019). Evodiamine ameliorates paclitaxel-induced neuropathic pain by inhibiting inflammation and maintaining mitochondrial anti-oxidant functions. *Hum Cell.* 32(3): 251-259.

Wu S-N, Chen B-S, Wu Y-H, Peng H and Chen L-T (2009). The mechanism of the actions of oxaliplatin on ion currents and action potentials in differentiated NG108-15 neuronal cells. *Neurotoxicology.* 30(4): 677-685.

Wu Y, Li J, Zhou J and Feng Y (2014). Dynamic long-term microstructural and ultrastructural alterations in sensory nerves of rats of paclitaxel-induced neuropathic pain. *Chin Med J (Engl).* 127(16): 2945-2952.

Xia P, An H-X, Dang C-X, Radpour R, Kohler C, Fokas E, Engenhart-Cabillic R, Holzgreve W and Zhong XY (2009). Decreased mitochondrial DNA content in blood samples of patients with stage I breast cancer. *BMC Cancer.* 9(1): 454.

Xiao WH and Bennett GJ (2012). Effects of mitochondrial poisons on the neuropathic pain produced by the chemotherapeutic agents, paclitaxel and oxaliplatin. *Pain.* 153(3): 704-709.

Xiao WH, Zheng FY, Bennett GJ, Bordet T and Pruss RM (2009). Olesoxime (cholest-4-en-3-one, oxime): analgesic and neuroprotective effects in a rat model of painful peripheral neuropathy produced by the chemotherapeutic agent, paclitaxel. *Pain.* 147(1-3): 202-209.

Xiao WH, Zheng H and Bennett GJ (2012). Characterization of oxaliplatin-induced chronic painful peripheral neuropathy in the rat and comparison with the neuropathy induced by paclitaxel. *Neuroscience.* 203: 194-206.

Xiao WH, Zheng H, Zheng FY, Nuydens R, Meert TF and Bennett GJ (2011). Mitochondrial abnormality in sensory, but not motor, axons in paclitaxel-evoked painful peripheral neuropathy in the rat. *Neuroscience.* 199: 461-469.

Xing J, Chen M, Wood CG, Lin J, Spitz MR, Ma J, Amos CI, Shields PG, Benowitz NL, Gu J, de Andrade M, Swan GE and Wu X (2008). Mitochondrial DNA content: its genetic heritability and association with renal cell carcinoma. *J Natl Cancer Inst.* 100(15): 1104-1112.

Xu D, Zhao H, Gao H, Zhao H, Liu D and Li J (2018). Participation of pro-inflammatory cytokines in neuropathic pain evoked by chemotherapeutic oxaliplatin via central GABAergic pathway. *Mol Pain.* 14: 1744806918783535.

Xu FX, Zhou X, Shen F, Pang R and Liu SM (2012). Decreased peripheral blood mitochondrial DNA content is related to HbA1c, fasting plasma glucose level and age of onset in type 2 diabetes mellitus. *Diabet Med.* 29(7): e47-54.

Xu J, Wang W, Zhong X-X, Feng Y, Wei X and Liu X-G (2016). EXPRESS: Methylcobalamin ameliorates neuropathic pain induced by vincristine in rats: Effect on loss of peripheral nerve fibers and imbalance of cytokines in the spinal dorsal horn. *Mol Pain.* 12: 1744806916657089.

Yamamoto K, Chiba N, Chiba T, Kambe T, Abe K, Kawakami K, Utsunomiya I and Taguchi K (2015). Transient receptor potential ankyrin 1 that is induced in dorsal root ganglion neurons contributes to acute cold hypersensitivity after oxaliplatin administration. *Mol Pain.* 11: 69.

Yamamoto K, Tsuboi M, Kambe T, Abe K, Nakatani Y, Kawakami K, Utsunomiya I and Taguchi K (2016a). Oxaliplatin administration increases expression of the voltage-dependent calcium channel α2δ-1 subunit in the rat spinal cord. *J Pharmacol Sci.* 130(2): 117-122.

Yamamoto S, Egashira N, Tsuda M and Masuda S (2018). Riluzole prevents oxaliplatin-induced cold allodynia via inhibition of overexpression of transient receptor potential melastatin 8 in rats. *J Pharmacol Sci.* 138(3): 214-217.

Yamamoto S, Ono H, Kume K and Ohsawa M (2016b). Oxaliplatin treatment changes the function of sensory nerves in rats. *J Pharmacol Sci.* 130(4): 189-193.

Yang D, Oyaizu Y, Oyaizu H, Olsen GJ and Woese CR (1985). Mitochondrial origins. *Proc Natl Acad Sci U S A.* 82(13): 4443-4447.

Yang Z, Schumaker LM, Egorin MJ, Zuhowski EG, Guo Z and Cullen KJ (2006). Cisplatin Preferentially Binds Mitochondrial DNA and Voltage-Dependent Anion Channel Protein in the Mitochondrial Membrane of Head and Neck Squamous Cell Carcinoma: Possible Role in Apoptosis. *Clin Cancer Res.* 12(19): 5817-5825.

Yawn BP, Wollan PC, Weingarten TN, Watson JC, Hooten WM and Melton LJ, III (2009). The Prevalence of Neuropathic Pain: Clinical Evaluation Compared with Screening Tools in a Community Population. *Pain Med.* 10(3): 586-593.

Ye H, Du X and Hua Q (2018). Effects of voluntary exercise on antiretroviral therapy-induced neuropathic pain in mice. *J Physiol Sci.* 68(4): 521-530.

Yezierski RP (2013). Spinomesencephalic Tract. *Encyclopedia of Pain*. Gebhart GF and Schmidt RF. Berlin, Heidelberg, Springer Berlin Heidelberg**:** 3612-3618.

Yoon C, Young Wook Y, Heung Sik N, Sun Ho K and Jin Mo C (1994). Behavioral signs of ongoing pain and cold allodynia in a rat model of neuropathic pain. *Pain.* 59(3): 369-376.

Zhao S, Yang Y, Liu J, Liu H, Ge N, Yang H, Zhang H and Xing J (2011). Association of mitochondrial DNA content in peripheral blood leukocyte with hepatitis B virus-related hepatocellular carcinoma in a Chinese Han population. *Cancer Sci.* 102(8): 1553-1558.

Zheng H, Xiao WH and Bennett GJ (2011). Functional deficits in peripheral nerve mitochondria in rats with paclitaxel- and oxaliplatin-evoked painful peripheral neuropathy. *Exp Neurol.* 232(2): 154-161.

Zheng H, Xiao WH and Bennett GJ (2012). Mitotoxicity and bortezomib-induced chronic painful peripheral neuropathy. *Exp Neurol.* 238(2): 225-234.

Zhi WI, Chen P, Kwon A, Chen C, Harte SE, Piulson L, Li S, Patil S, Mao JJ and Bao T (2019). Chemotherapy-induced peripheral neuropathy (CIPN) in breast cancer survivors: a comparison of patient-reported outcomes and quantitative sensory testing. *Breast Cancer Res Treat.* 178(3): 587-595.

Zimmermann M (1983). Ethical guidelines for investigations of experimental pain in conscious animals. *Pain.* 16(2): 109-110.

Zylka MJ, Rice FL and Anderson DJ (2005). Topographically distinct epidermal nociceptive circuits revealed by axonal tracers targeted to Mrgprd. *Neuron.* 45(1): 17-25.